

**The BEACH domain containing protein SPIRRIG
in an interplay with TZF proteins
and the characterization of SPIRRIG in *M. polymorpha***

Inaugural-Dissertation

zur

Erlangung des Doktorgrades

der Mathematisch-Naturwissenschaftlichen Fakultät

der Universität zu Köln

vorgelegt von

Eva Koebke

aus Köln

Köln, 2021

Berichtersteller/in:

Prof. Dr. Martin Hülskamp

Prof. Dr. Ute Höcker

Prüfungsvorsitzender:

Prof. Dr. Siegfried Roth

Tag der mündlichen Prüfung:

07.12.2020

ZUSAMMENFASSUNG

Die Familie der BEACH-Domänen Proteine ist unter den Eukaryonten hochkonserviert und ihre Mitglieder wurden in den meisten bekannten Modellorganismen beschrieben. Die BEACH-Domänen Proteine entdeckte man bei der Erforschung einer schweren humanen Krankheit, die unter anderem von Symptomen wie Albinismus, Blutungsdiathese, Immunschwäche und Krebswachstum begleitet wird. Auf zellulärer Ebene sind BEACH-Domänen Proteine klassischerweise dafür bekannt, dass sie für Membrantransportprozesse, wie zum Beispiel Vesikeltransport, Autophagie, sowie Membranspaltung und -fusion wichtig sind.

Entsprechend spielt das an der Zellmorphogenese beteiligte BEACH-Domänen Protein SPIRRIG aus *Arabidopsis thaliana* ebenfalls eine Rolle in membranabhängigen Prozessen. Das Protein ist ein besonders interessanter Vertreter der Familie der BEACH-Domänen Proteine, da es bisher das einzige BEACH-Domänen Protein ist, von dem man weiß, dass es eine zusätzliche Funktion im mRNA-Stoffwechsel ausübt. In vorausgehenden Studien wurde gezeigt, dass SPIRRIG mRNA-Stabilität vermittelt und außerdem die Bildung von Processing bodies fördert. Diese Funktion von SPIRRIG ist biologisch relevant für die Salzstressreaktion von *A. thaliana*. Der exakte molekulare Wirkmechanismus von SPIRRIG ist jedoch noch nicht bekannt.

In dieser Studie wurden zur weiteren Untersuchung der Funktion von SPIRRIG zwei verschiedene Ansätze gewählt. Ein Teil dieser Arbeit zielte darauf ab, die molekulare Funktion von SPIRRIG in der Salzstressreaktion tiefergehend zu verstehen, indem ein Zusammenspiel mit Tandem zinc finger (TZF) Proteinen analysiert wurde. Während die molekularen Funktionen von pflanzlichen TZF Proteinen noch nicht vollständig verstanden sind, sind Homologe in Säugetieren dafür bekannt, dass sie eine Funktion in stress-assoziierten mRNA-Destabilisierungsprozessen haben. Dies erfolgt über die Bindung an spezifische Elemente in 3'UTRs von Ziel-mRNAs. Eine Interaktion von SPIRRIG mit TZF10 deutete stark auf eine mögliche Verbindung der beiden Proteine hin und gab Anlass zu weiteren Untersuchungen, um dieses bisher unbekanntes Wechselspiel zwischen BEACH-Domänen Proteinen und TZFs zu entschlüsseln. Bemerkenswerterweise bestätigte die vorliegende Studie die Rettung des Salzüberempfindlichkeitsphänotyps von *spirrig* Mutanten durch die Expression von *TZF10*. Umfangreiche mRNA Expressions- und Stabilitätsuntersuchungen konnten jedoch eine zuvor vermutete, biologisch relevante Rolle der *TZF10* 3'UTR im Zusammenhang mit der Rettung der *spirrig* Salzüberempfindlichkeit nicht bestätigen. Dennoch zeigte die vorliegende Arbeit überzeugend eine durch die *TZF10* 3'UTR vermittelte, allgemeine Kapazität zur mRNA-Destabilisierung. Außerdem konnte ein potentielles mRNA-Destabilisierungsmotiv isoliert werden.

Der zweite Teil dieser Arbeit verfolgte einen evolutionär-vergleichenden Ansatz, um konservierte, basale Funktionen von BEACH-Domänen Proteinen in dem Lebermoos *Marchantia polymorpha*, eine der ersten Pflanzen, die das Land besiedelten, zu entschlüsseln. Die Charakterisierung auf morphologischer und zellulärer Ebene einer *Mpspirrig*-Mutante, die aufgrund ihrer kurzen Rhizoide in einem T-DNA Screen isoliert wurde, offenbarte interessante Erkenntnisse über potenzielle Funktionen von BEACH-Domänen Proteinen in der evolutionär früh entstandenen Pflanze. Der *Mpspirrig* Phänotyp der kurzen Rhizoide, der an den Kurzwurzelhaar-Phänotyp von *Atspirrig* erinnert, erwies sich überraschenderweise als Ausdruck eines Phänotyps, der durch eine erhöhte Anzahl von gleichzeitig signifikant kleineren Zellen in Gemmae von *Mpspirrig* gekennzeichnet ist. Dieser neu entdeckte Phänotyp wies auf eine Rolle von MpSPIRRIG in Zellproliferations- und/oder Zellexpansionsprozessen hin. Außerdem unterstützte diese Arbeit nachdrücklich eine Verbindung von MpSPIRRIG mit Membrantransportwegen, indem sie die direkte Ko-Lokalisierung und Interaktion von MpSPIRRIG mit Komponenten des Endosomal sorting complex required for transport (ESCRT) nachwies. Darüber hinaus wurde gezeigt, dass MpSPIRRIG für die Salzstressreaktion von *Marchantia* relevant ist und in cytoplasmatischen mRNA-Granula lokalisiert ist. Die Doppelfunktion von SPIRRIG scheint somit in den beiden vermutlich nicht verwandten Pfaden der Salzstressreaktion und des Membrantransports evolutionär konserviert zu sein.

ABSTRACT

The BEACH domain containing proteins (BDCPs) represent a highly conserved family among eukaryotes and members have been described in most of the prominent model organisms. The BDCPs were discovered through exploration of a severe human disease comprising symptoms such as albinism, bleeding diathesis, immunodeficiency and cancer growth. On the cellular level, BDCPs are classically known to be involved in membrane trafficking processes including vesicle transport, autophagy as well as membrane fission and fusion events.

In accordance, the *Arabidopsis thaliana* cell morphogenesis and BDCP-coding gene *SPIRRIG* is implicated in membrane-dependent processes as well. The protein is a particularly interesting BDCP, as to date, it is the only member of this family known to exert an additional function in mRNA metabolism by mediating mRNA stability and promoting processing body formation biologically relevant to *A. thaliana* salt stress response. The exact molecular mechanism of *SPIRRIG*, however, remains elusive.

This study was set out to investigate *SPIRRIG* function using two different approaches. One part of this work aimed to gain further understanding of *SPIRRIG*'s molecular function in salt stress response by analyzing an interplay with tandem zinc finger (TZF) proteins. While molecular functions of plant TZF proteins are not yet fully understood, mammalian homologs are involved in stress-associated mRNA destabilization processes upon binding to specific elements in 3'UTRs of target mRNAs. An interaction of *SPIRRIG* with TZF10 strongly suggested a potential connection of the two proteins and prompted further investigations in order to unravel this so far unknown interplay between BDCPs and TZFs. Strikingly, this study confirmed TZF10 to rescue the salt hypersensitivity phenotype of *spirrig* mutants. Extensive mRNA expression and stability assays however could not confirm previously hypothesized, biologically relevant roles of the *TZF10* 3'UTR in the context of *spirrig* salt hypersensitivity rescue. Nonetheless, this work convincingly demonstrated general mRNA destabilization capacity mediated by the *TZF10* 3'UTR and isolated a potential mRNA destabilization-inducing motif.

The second part of this work utilized an evolutionarily comparative approach in order to unravel conserved, basal BDCP functions in one of the first plants colonizing the land, the liverwort *Marchantia polymorpha*. The characterization on the morphological and cellular level of a *Mpspirrig* mutant, which was identified in a T-DNA screen by its short rhizoids, revealed exciting insights on potential BDCP function in the ancient plant. The *Mpspirrig* short rhizoid phenotype, reminiscent to the short root hair phenotype of *Atspirrig*, was surprisingly shown to be an expression of a phenotype hallmarked by an increased number of at the same time

significantly smaller cells in *Mpspirrig* gemmae. This newly discovered phenotype pointed to a role of MpSPIRRIG in cell proliferation and/or cell expansion processes. Moreover, this work strongly supported a connection of MpSPIRRIG to membrane trafficking pathways by demonstrating direct co-localization and interaction of MpSPIRRIG with endosomal sorting complex required for transport (ESCRT) components. Finally, this study revealed MpSPIRRIG to be relevant to *Marchantia* salt stress response and to locate to cytoplasmic mRNA granules, providing several indications for the dual function of SPIRRIG in the two assumingly unrelated pathways of salt stress response and membrane trafficking to be evolutionarily conserved.

INDEX OF CONTENTS

| | |
|---|-----|
| ZUSAMMENFASSUNG | III |
| ABSTRACT | V |
| INDEX OF CONTENTS | VII |
| INDEX OF FIGURES | XI |
| INDEX OF TABLES | XIV |
| INDEX OF ABBREVIATIONS | XV |
| 1 INTRODUCTION | 1 |
| 1.1 BDCPs are facilitators of membrane dynamics | 1 |
| 1.2 The molecular function of BDCPs <i>in planta</i> | 3 |
| 1.2.1 The basal land plant <i>Marchantia polymorpha</i> emerged as a molecular model organism | 3 |
| 1.2.2 SPIRRIG is the best characterized BDCP in <i>Arabidopsis thaliana</i> | 4 |
| 1.3 The endosomal sorting complex required for transport (ESCRT) system and its connection to SPIRRIG | 5 |
| 1.4 SPIRRIG in cytoplasmic mRNA granules | 7 |
| 1.4.1 P-bodies and stress granules are cytoplasmic mRNA granules | 7 |
| 1.4.2 P-bodies are sites of mRNA regulation and decay | 7 |
| 1.4.3 Stress granules are sites of mRNA storage | 8 |
| 1.4.4 Arabidopsis SPIRRIG functions in salt stress response | 10 |
| 1.5 TZF proteins and their role in post-transcriptional regulation | 10 |
| 1.5.1 The family of zinc finger proteins exerts various functions | 10 |
| 1.5.2 AREs mediate mRNA destabilization | 11 |
| 1.5.3 The human TZF TTP promotes deadenylation and subsequent mRNA decay | 12 |
| 1.6 TZF proteins in <i>Arabidopsis thaliana</i> | 15 |
| 1.6.1 Association of TZF proteins with mRNA regulation has been reported | 15 |
| 1.6.2 TZF10 and TZF11 are described as regulators of salt stress response | 17 |
| 1.7 Aim of this work | 18 |
| 1.7.1 Unraveling the interplay between TZF proteins and SPIRRIG in salt stress response | 18 |
| 1.7.2 Learning about basal, conserved BDCP protein function | 18 |

| | |
|---|----|
| 2 MATERIALS AND METHODS | 20 |
| 2.1 Organisms and plant lines..... | 20 |
| 2.2 Plasmids..... | 23 |
| 2.3 Oligonucleotide sequences..... | 23 |
| 2.4 Molecular biology techniques..... | 24 |
| 2.4.1 DNA extraction for plant genotyping..... | 24 |
| 2.4.2 RNA extraction and cDNA synthesis..... | 24 |
| 2.4.3 Polymerase chain reaction (PCR)..... | 25 |
| 2.4.4 Cloning methods..... | 28 |
| 2.4.5 Plasmid purification, restriction digest and sequencing..... | 30 |
| 2.4.6 Generation of chemically competent cells..... | 31 |
| 2.4.7 Heat-shock transformation of chemically competent cells..... | 32 |
| 2.5 Biochemical techniques..... | 32 |
| 2.5.1 Protein extraction from <i>A. thaliana</i> leaf tissue..... | 32 |
| 2.5.2 SDS-PAGE..... | 32 |
| 2.5.3 Coomassie staining..... | 32 |
| 2.5.4 Semi-dry immunoblotting (western blotting)..... | 33 |
| 2.6 Plant techniques..... | 33 |
| 2.6.1 Plant growth conditions for <i>A. thaliana</i> and <i>M. polymorpha</i> | 33 |
| 2.6.2 Seed sterilization <i>A. thaliana</i> | 34 |
| 2.6.3 Crossing of <i>A. thaliana</i> and <i>M. polymorpha</i> plants..... | 34 |
| 2.6.4 Analysis of <i>M. polymorpha</i> rhizoid growth and biomass..... | 34 |
| 2.6.5 Salt stress treatments..... | 35 |
| 2.6.6 Heat stress treatment..... | 36 |
| 2.6.7 Actinomycin D treatment of <i>A. thaliana</i> seedlings..... | 36 |
| 2.6.8 Transient transformation by particle bombardment..... | 36 |
| 2.6.9 Transient transformation by infiltration of <i>N. benthamiana</i> leaves..... | 37 |
| 2.6.10 Stable transformation and selection of <i>A. thaliana</i> | 37 |
| 2.6.11 Stable transformation and selection of <i>M. polymorpha</i> | 37 |
| 2.6.12 Fluorescein diacetate staining..... | 39 |
| 2.6.13 Propidium iodide staining..... | 39 |
| 2.6.14 Microscopic analysis and confocal laser scanning microscopy (CLSM)..... | 39 |

| | |
|---|------------|
| 2.7 Protein-protein interaction assays..... | 39 |
| 2.7.1 Yeast two-hybrid pairwise interaction assay..... | 39 |
| 2.7.2 Yeast two-hybrid interaction screening..... | 41 |
| 2.8 Computational analysis | 41 |
| 3 RESULTS | 42 |
| 3.1 The interplay of TZF10 and 11 with the BDCP SPIRRIG in Arabidopsis salt stress response .. | 42 |
| 3.1.1 TZF10 localizes to cytoplasmic mRNA granules | 42 |
| 3.1.2 The mRNA of <i>TZF10</i> localizes to cytoplasmic granules..... | 43 |
| 3.1.3 <i>tzf10/tzf11</i> mutants show no salt stress phenotype..... | 45 |
| 3.1.4 <i>TZF10</i> mRNA expression responds to salt stress | 48 |
| 3.1.5 <i>TZF10</i> mRNA stability is not strikingly affected in <i>spi-4</i> | 56 |
| 3.1.6 <i>TZF10</i> rescues the salt stress phenotype of <i>spirrig</i> irrespective of its 3'UTR..... | 62 |
| 3.1.7 The salt hypersensitivity phenotype of <i>spirrig</i> is not mitigated by introduction of <i>TZF10</i> and 11 alleles with disrupted 3'UTRs | 73 |
| 3.1.8 <i>TZF10</i> rescues the salt stress phenotype of <i>spirrig</i> irrespective of its 5'UTR..... | 75 |
| 3.1.9 The 3'UTR of <i>TZF10</i> mediates mRNA destabilization effects independent from <i>spirrig</i> | 76 |
| 3.1.10 TZF10 and 11 interact with proteins of various functions in a yeast two-hybrid screen.... | 92 |
| 3.2 SPIRRIG in <i>Marchantia polymorpha</i> | 93 |
| 3.2.1 Protein and gene structure of MpSPIRRIG | 93 |
| 3.2.2 The subcellular localization of MpSPIRRIG..... | 94 |
| 3.2.3 The T-DNA mutant <i>Mpspirrig</i> | 96 |
| 3.2.4 Phenotypic characterization of <i>Mpspirrig</i> | 98 |
| 3.2.5 Unraveling the connection of MpSPIRRIG to P-bodies and the ESCRT system | 103 |
| 4 DISCUSSION | 116 |
| 4.1 The interplay of TZF10 and 11 with the BDCP SPIRRIG in Arabidopsis salt stress response | 116 |
| 4.1.1 TZF10 is associated with cytoplasmic mRNA granules and stress response | 116 |
| 4.1.2 The interplay between TZF10 and SPIRRIG is elusive | 117 |
| 4.1.3 <i>TZF10</i> function is not influenced by its UTRs in the context of <i>spirrig</i> salt hypersensitivity rescue | 119 |
| 4.1.4 The 3'UTR of <i>TZF10</i> mediates mRNA destabilizing effects independent from <i>spirrig</i> | 121 |
| 4.1.5 TZF10 and 11 interact with proteins of various functions in a yeast two-hybrid screen.... | 122 |
| 4.1.6 Outlook..... | 125 |

| | |
|--|------------|
| 4.2 SPIRRIG in <i>Marchantia polymorpha</i> | 126 |
| 4.2.1 MpSPIRRIG contains a FYVE domain | 126 |
| 4.2.2 MpSPIRRIG is associated with cell proliferation and/or cell expansion processes..... | 127 |
| 4.2.3 MpSPIRRIG is connected to P-body and ESCRT components | 128 |
| 4.2.4 Are mRNP granules continuously present in cells of <i>M. polymorpha</i> ?..... | 131 |
| 4.2.5 Outlook..... | 132 |
| 5 APPENDIX | 134 |
| 6 REFERENCES | 156 |
| 7 ACKNOWLEDGEMENTS | 170 |
| 8 DECLARATION OF ACADEMIC INTEGRITY | 172 |

INDEX OF FIGURES

| | |
|--|----|
| Figure 1: Developmental stages in the life cycle of <i>M. polymorpha</i> | 4 |
| Figure 2: Multivesicular body (MVB) formation..... | 5 |
| Figure 3: Model of the mRNP cycle..... | 9 |
| Figure 4: Model of TTP function..... | 14 |
| Figure 5: TZF10 localizes to stress granules upon heat treatment. | 43 |
| Figure 6: The mRNA of genomic <i>TZF10</i> localizes to cytoplasmic granules..... | 44 |
| Figure 7: Primary root growth of <i>tzf10/11</i> mutants on 125 mM NaCl is not significantly different compared to wild type plants. | 46 |
| Figure 8: <i>tzf10/11</i> double mutants do not show increased leaf whitening as a sign for salt hypersensitivity..... | 47 |
| Figure 9: <i>tzf10/11</i> double mutants do not show a salt hypersensitivity phenotype in the root bending assay | 48 |
| Figure 10: <i>TZF10</i> expression levels in <i>spi-4</i> compared to Col-0 under non-stress conditions.. | 51 |
| Figure 11: Relative expression of <i>RD29A</i> in salt-stressed compared to non-treated samples..... | 52 |
| Figure 12: Relative expression of <i>TZF10</i> in salt-stressed compared to non-treated samples..... | 52 |
| Figure 13: Relative expression of <i>TZF10</i> in salt-stressed compared to non-treated samples..... | 54 |
| Figure 14: Relative expression of <i>TZF10</i> in salt-stressed compared to non-treated samples..... | 55 |
| Figure 15: Relative expression of <i>TZF10</i> in Col-0 compared to <i>spi-4</i> plants under salt stress conditions | 56 |
| Figure 16: <i>RD29A</i> expression levels | 57 |
| Figure 17: Optimized experimental setup for mRNA stability assays..... | 58 |
| Figure 18: <i>RD29A</i> expression levels | 59 |
| Figure 19: <i>TZF10</i> mRNA is more stable in Col-0 than in <i>spi-4</i> | 60 |
| Figure 20: Stability of <i>TZF10</i> mRNA does not strikingly differ in Col-0 compared to <i>spi-4</i> | 61 |
| Figure 21: Stability of <i>TZF11</i> mRNA does not strikingly differ in Col-0 compared to <i>spi-4</i> | 62 |
| Figure 22: Salt stress screening on the basis of salt-induced leaf whitening in seedlings..... | 63 |
| Figure 23: Estimated portion of plants exhibiting green and white leaves of T ₂ plants subjected to salt stress screenings in different rescue scenarios. | 64 |
| Figure 24: <i>TZF10</i> rescues the salt hypersensitivity phenotype of <i>spi-4</i> | 66 |
| Figure 25: <i>TZF10</i> expression levels do not correspond to salt hypersensitivity rescue intensity | 67 |
| Figure 26: The <i>TZF10</i> 3'UTR could render <i>TZF10</i> mRNA less stable under salt stress conditions | 69 |
| Figure 27: Increased <i>TZF10</i> transcript destabilization does not correlate with the <i>spirrig</i> salt hypersensitivity rescue level. | 70 |
| Figure 28: <i>RD29A</i> expression levels. | 72 |
| Figure 29: The stably introduced disruption of the <i>TZF10</i> or <i>TZF11</i> 3'UTR does not mitigate the salt hypersensitivity phenotype of <i>spirrig</i> mutants | 74 |
| Figure 30: <i>TZF10</i> rescues the salt hypersensitivity phenotype of <i>spi-4</i> irrespective of its 5'UTR..... | 76 |
| Figure 31: The mRNA of <i>TZF10</i> localizes to stress granules..... | 78 |
| Figure 32: The mRNA of <i>TZF10</i> localizes to stress granules..... | 80 |
| Figure 33: The mRNA of <i>TZF11</i> localizes to stress granules..... | 81 |

| | |
|---|-----|
| Figure 34: Expression of <i>YFP</i> is not detectable when fused to the 3'UTRs of <i>TZF10</i> and <i>11</i> | 82 |
| Figure 35: Generated fragments of the <i>TZF10</i> and <i>11</i> 3'UTR. | 83 |
| Figure 36: Expression of <i>YFP</i> is diminished when fused to parts of <i>TZF10</i> and <i>11</i> 3'UTRs | 84 |
| Figure 37: Expression of <i>YFP</i> is diminished when fused to parts of <i>TZF10</i> and <i>11</i> 3'UTRs.. | 85 |
| Figure 38: Alignment of the 5'end parts (P1-1) of <i>TZF10</i> and <i>11</i> 3'UTRs..... | 86 |
| Figure 39: Expression of <i>YFP</i> is diminished when fused to parts of <i>TZF10</i> and <i>11</i> 3'UTRs.. | 87 |
| Figure 40: Mutated (MUT) versions of construct <i>UBQ10::YFP-3'UTR_{TZF10}(P1-1-C)</i> | 88 |
| Figure 41: Expression of <i>YFP</i> is strong when fused to mutated parts of <i>TZF10</i> 3'UTR | 89 |
| Figure 42: The localization of <i>TZF10</i> 3'UTR is not altered upon heat stress | 90 |
| Figure 43: The localization of <i>TZF10</i> 3'UTR fragments is not altered upon heat stress | 91 |
| Figure 44: Phylogeny of <i>A. thaliana</i> , <i>M. polymorpha</i> and <i>H. sapiens</i> BEACH domain proteins. | 93 |
| Figure 45: Protein structure of MpSPIRRIG and AtSPIRRIG..... | 94 |
| Figure 46: Gene structure of MpSPIRRIG and AtSPIRRIG. | 94 |
| Figure 47: Transient expression of MpSPI | 95 |
| Figure 48: Transient expression of MpSPI in Arabidopsis. | 95 |
| Figure 49: Subcellular localization of MpSPI | 96 |
| Figure 50: Gene structure of MpSPIRRIG including T-DNA insertion site | 97 |
| Figure 51: Relative expression of MpSPIRRIG in <i>Mpspirrig</i> compared to Tak-1 | 97 |
| Figure 52: <i>Mpspirrig</i> has a short rhizoid phenotype. | 98 |
| Figure 53: Time-course observation of Tak-1 and <i>Mpspirrig</i> gemmae growth..... | 99 |
| Figure 54: Length, width and thallus shape index of <i>Mpspirrig</i> and wild type plants | 100 |
| Figure 55: <i>Mpspirrig</i> thalli acquire more biomass than wild type plants | 101 |
| Figure 56: <i>Mpspirrig</i> gemmae have more and smaller cells than wild type gemmae. | 102 |
| Figure 57: <i>Mpspirrig</i> gemmae have smaller cells than wild type gemmae..... | 103 |
| Figure 58: Vacuole structure in Tak-1 and <i>Mpspirrig</i> rhizoids | 104 |
| Figure 59: Growth test of <i>M. polymorpha</i> in response to salt..... | 106 |
| Figure 60: Salt hypersensitivity of <i>Mpspirrig</i> | 106 |
| Figure 61: Representative images of Marchantia P-body marker proteins | 107 |
| Figure 62: Co-transformation of MpSPI PBW with P-body marker MpDCP2..... | 108 |
| Figure 63: Subcellular localization of ESCRT components in <i>M. polymorpha</i> | 108 |
| Figure 64: Co-localization of MpSPI PBW with ESCRT components | 109 |
| Figure 65: Co-localization of ESCRT components with MpDCP2..... | 110 |
| Figure 66: Subcellular localization of endosomal marker proteins in <i>M. polymorpha</i> | 111 |
| Figure 67: Co-expression of MpLIP5 with endosomal marker proteins..... | 111 |
| Figure 68: Co-expression of MpSPI PBW with endosomal marker proteins | 112 |
| Figure 69: MpSPI PBW localization is not affected by salt treatment. | 114 |
| Figure 70: The Arabidopsis stress granule marker AtUBP1b localizes to dot-like structures already under non-stress conditions in <i>M. polymorpha</i> | 114 |
| Figure 71: Results of pairwise yeast-two hybrid assays of MpSPI with ESCRT and P-body components..... | 115 |
| Figure 72: qPCR efficiency test standard curves of primer pairs used in this study. | 142 |

| | |
|--|-----|
| Figure 73: <i>TZF10</i> expression levels | 143 |
| Figure 74: The effect of ActD on <i>TZF10</i> expression in different transgenic lines. | 144 |
| Figure 75: <i>RD29A</i> expression levels. | 145 |
| Figure 76: The λ N22-mVENUS reporter co-expressed with Box-B repeats without an mRNA target localizes in cytoplasmic granules. | 145 |
| Figure 77: The λ N22-mVENUS reporter co-expressed with Box-B repeats without an mRNA target does not localize in cytoplasmic granules in <i>N. benthamiana</i> | 146 |
| Figure 78: The mRNA of <i>TZF10</i> sporadically localizes to stress granules | 147 |
| Figure 79: <i>TZF10</i> 3'UTR structure prediction | 148 |
| Figure 80: TZF10 protein cannot be detected in transgenic TZF10 overexpression lines. | 148 |
| Figure 81: <i>M. polymorpha</i> , stably co-transformed with 35S::MpSPI PBW-Citrine and 35S::TagRFP-MpSKD1, -MpLIP5, -MpDCP2, respectively | 149 |
| Figure 82: The RNA ligase AT3G28140 co-localizes with TZF10 and UBP1b | 153 |
| Figure 83: MYB51 localizes to stress granules under heat stress conditions | 153 |
| Figure 84: The transcripts of <i>MYB34</i> , <i>51</i> and <i>122</i> and target genes are down-regulated upon heat stress..... | 154 |
| Figure 85: MpSPI PBW/PBWF interacts with MpLIP5 in yeast | 155 |

INDEX OF TABLES

| | |
|--|-----|
| Table 1: Organisms used in this work..... | 20 |
| Table 2: T-DNA insertion lines used in this work..... | 21 |
| Table 3: Overview on transgenic <i>A. thaliana</i> TZF10, TZF11 and SWAP construct lines generated in this study..... | 22 |
| Table 4: <i>M. polymorpha</i> transgenic lines generated in this work..... | 22 |
| Table 5: General vectors used in this study..... | 23 |
| Table 6: Standard DreamTaq polymerase mixture and program..... | 25 |
| Table 7: DreamTaq Green PCR master mix and program..... | 25 |
| Table 8: Reaction mixture and program used for yeast colony PCRs..... | 26 |
| Table 9: Reaction mixture and program in preparation for PCR product sequencing at the CCG..... | 26 |
| Table 10: Reaction mixture and program used for PCRs to clone DNA fragments of interest..... | 27 |
| Table 11: qPCR reaction mixture and program..... | 27 |
| Table 12: Oligo sequences, containing overhangs complementary to sticky ends resulting from BbsI digestion, used for cloning of <i>TZF10</i> and <i>11</i> 3'UTR fragments..... | 30 |
| Table 13: Composition of the standard medium Johnson's for cultivation of <i>M. polymorpha</i> | 34 |
| Table 14: Composition of M51C medium used in transformations of <i>M. polymorpha</i> thalli..... | 38 |
| Table 15: Confocal microscopy settings for excitation and detection of fluorophores..... | 39 |
| Table 16: Software used in this study..... | 41 |
| Table 17: <i>TZF10</i> mRNA localizes to P-bodies in Col-0 and <i>spirrig</i> | 44 |
| Table 18: 18S rRNA stability as a reference gene in single and combined salt stress and actinomycin D treatments..... | 49 |
| Table 19: qPCR efficiency and correlation of primer pairs..... | 50 |
| Table 20: Transgenic lines subjected to salt stress screenings..... | 65 |
| Table 21: Transgenic lines subjected to salt stress screenings..... | 75 |
| Table 22: Overview on prey cDNA libraries implemented in the yeast two-hybrid screen..... | 92 |
| Table 23: Entry clones harboring <i>A. thaliana</i> genes/nucleic acids..... | 134 |
| Table 24: Expression clones harboring <i>A. thaliana</i> genes/nucleic acids..... | 136 |
| Table 25: Entry clones harboring <i>M. polymorpha</i> genes generated in this work..... | 139 |
| Table 26: Expression clones harboring <i>M. polymorpha</i> genes..... | 138 |
| Table 27: Genotyping-primer for <i>A. thaliana</i> T-DNA insertion lines..... | 140 |
| Table 28: Genotyping-primer pairs for <i>M. polymorpha</i> | 140 |
| Table 29: Primer pairs used for qPCR analysis..... | 140 |
| Table 30: Other primer pairs used in this work..... | 141 |
| Table 31: List of interacting proteins identified in the yeast two-hybrid screenings with TZF10 and 11 as bait proteins..... | 150 |

INDEX OF ABBREVIATIONS

| Abbreviation | Explanation |
|-------------------------|---|
| 35S CaMV | 35S promoter of the Cauliflower mosaic virus |
| A | adenosine |
| aa | amino acid |
| ABA | abscisic acid |
| ABF3 | ABSCISIC ACID RESPONSIVE ELEMENTS-BINDING FACTOR 3 |
| ABI2 | ABA INSENSITIVE 2 |
| ACT7 | ACTIN 7 |
| ActD | actinomycin D |
| AGO1 | ARGONAUTE 1 |
| ALFY | autophagy-linked FYVE protein |
| AMSH | associated molecular with SH3 domain of STAM |
| APT3 | ADENINE PHOSPHORIBOSYL TRANSFERASE 3 |
| ARE | adenylate-uridylate-rich element |
| ARP2/3 | ACTIN-RELATED PROTEIN 2/3 |
| ATP | adenosine triphosphate |
| auto | autoactive |
| bar | bialaphos resistance |
| Bchs | Blue cheese |
| BDCP | BEACH domain containing protein |
| BEACH | <i>beige</i> and Chediak-Higashi |
| BiFC | bimolecular fluorescence complementation |
| BLAST | Basic Local Alignment Search Tool |
| C | cysteine |
| CAF1 | CCR4 ASSOCIATED FACTOR 1 |
| ccdB | gene coding for a toxin known to inhibit gyrases of bacterial strains |
| CCG | Cologne Center for Genomics |
| CCR4-NOT | carbon catabolite repressor protein 4-negative on TATA-less |
| cDNA | complementary DNA |
| CDS | coding sequence |
| CFP | cyan fluorescent protein |
| CHS | Chediak-Higashi syndrome |
| Col-0 | Columbia-0 |
| COR | COLD-RESPONSIVE |
| Ct | threshold cycle |
| CPK | Ca ²⁺ -dependent protein kinase |
| CRISPR/Cas9 | clustered regularly interspaced short palindromic repeats/CRISPR-associated 9 |
| Ctrl | control |
| CYP | CYTOCHROME P450 |
| DAPI | 4',6-diamidino-2-phenylindole |
| DCP | DECAPPING |
| ddH₂O | double distilled water |
| DMSO | dimethyl sulfoxide |
| DNA | deoxyribonucleic acid |
| dNTPs | deoxyribonucleotides |
| DREB2A | DEHYDRATION-RESPONSIVE ELEMENT BINDING PROTEIN 2A |
| ds | double stranded |
| EDTA | ethylenediaminetetraacetic acid |
| EF | elongation factor |
| eIF | eukaryotic translation initiation factor |
| EMSA | electrophoretic mobility shift assay |

| | |
|-----------------|---|
| ESCRT | endosomal sorting complex required for transport |
| FDA | fluorescein diacetate |
| Fig | figure |
| FR | far-red |
| FRET-AP | Förster resonance energy transfer-acceptor photobleaching |
| FYVE | Fab-1, YGL023, Vps27, and EEA1 |
| <i>g</i> | <i>g</i> -force |
| GA | gibberellic acid |
| GAL4-AD | GAL4 activation domain |
| GAL4-BD | GAL4 binding domain |
| gDNA | genomic DNA |
| GFP | green fluorescent protein |
| GFS12 | GREEN FLUORESCENT SEED 12 |
| GK | GABI-Kat |
| GRF-GIF | GROWTH REGULATING FACTOR-GROWTH INTERACTING FACTOR |
| GRP7 | GLYCINE-RICH RBP 7 |
| GTP | guanosine triphosphate |
| GW | Gateway |
| h | hour(s) |
| H | histidine |
| HUS | hemolytic-uremic syndrome |
| Hz | hertz |
| ID | identification |
| IDR | intrinsically disordered protein |
| IG | indolic glucosinolate |
| ILV | intraluminal vesicle |
| IPCC | Intergovernmental Panel on Climate Change |
| ISRIB | integrated stress response inhibitor |
| JA | jasmonic acid |
| kb | kilo base pairs |
| kDa | kilodaltons |
| KIN1 | KINASE1 |
| L | leucine |
| LB | lysogeny broth |
| LIP5 | LYST INTERACTING PROTEIN 5 |
| LRBA | lipopolysaccharide-responsive beige-like anchor protein |
| LvsA | large volume sphere A |
| LYST | lysosomal-trafficking regulator |
| m | monomeric |
| MAPK | mitogen-activated protein kinase |
| MARD1 | MEDIATOR OF ABA-REGULATED DORMANCY 1 |
| Mb | mega base pairs |
| min | minute(s) |
| MIQE | Minimum Information for Publication of Quantitative Real-Time PCR Experiments |
| miRNA | micro RNA |
| MK2 | MAPK-activated protein kinase 2 |
| mRNA | messenger RNA |
| mRNP | messenger ribonucleoproteins |
| MS | Murashige and Skoog |
| MVB | multivesicular body |
| MYB | MYELOBLASTOSIS |
| NASC | Nottingham Arabidopsis Stock Centre |
| NBEA | neurobeachin |
| ND | not determined |

| | |
|----------------------|---|
| NDB2 | NAD(P)H DEHYDROGENASE B2 |
| NMD | nonsense-mediated mRNA decay |
| NMR | nuclear magnetic resonance |
| OCS | octopine synthase |
| OD | optical density |
| ORF | open reading frame |
| PABP | poly[A] binding protein |
| PAM | protospacer adjacent motif |
| PARN | poly[A]-specific ribonuclease |
| P-bodies, PBs | processing bodies |
| PBST | phosphate buffer saline with 0.1% Tween20 |
| PBW | PH-BEACH-WD40 |
| PBWF | PH-BEACH-WD40-FYVE |
| PCR | polymerase chain reaction |
| PH | pleckstrin homology |
| PI | propidium iodide |
| PIN | PIN-FORMED |
| PKB | protein kinase B |
| PP2A | protein phosphatase 2 |
| Psi | pound-force per square inch |
| PtdIns(3)P | phosphatidylinositol 3 phosphate |
| PVCs | pre-vacuolar compartments |
| PVDF | polyvinylidene fluoride-membrane |
| qPCR | quantitative PCR |
| RAB | Ras-related in brain |
| RBP | RNA binding protein |
| RD21A | RESPONSIVE TO DEHYDRATION 21A |
| RD29A | RESPONSIVE TO DESSICATION 29A |
| RFP | red fluorescent protein |
| RNA | ribonucleic acid |
| RNAseq | RNA sequencing |
| rpm | rounds per minute |
| RR | arginine-rich |
| RRM | RNA Recognition Motif |
| rRNA | ribosomal RNA |
| RT | room temperature |
| RT-PCR | reverse transcription polymerase chain reaction |
| SAIL | Syngenta Arabidopsis Insertion Library |
| SCAR/WAVE | SUPPRESSOR OF CYCLIC AMP RECEPTOR/WISKOTT-ALDRICH SYNDROME VERPROLIN-HOMOLOGOUS PROTEIN |
| SD | standard deviation |
| SDS-PAGE | sodiumdodecylsulfate polyacrylamide gel electrophoresis |
| Sec | seconds |
| SG | stress granule |
| SIGNAL SALK | Salk Institute Genomic Analysis Laboratory |
| SKD1 | SUPPRESSOR OF K(+) TRANSPORT GROWTH DEFECT 1 |
| SKL | serine-lysine-leucine |
| SNARE | SOLUBLE N-ETHYLMALEIMIDE-SENSITIVE-FACTOR ATTACHMENT RECEPTOR |
| SOS | SALT OVERLY SENSITIVE |
| SPI | SPIRRIG |
| STAM | signal transducing adaptor molecule |
| SZF | salt-inducible zinc finger |
| TA | annealing temperature |
| TAIR | The Arabidopsis Information Resource |

| | |
|--------------------------------|---|
| Tak-1 / -2 | Takaragaike-1 / -2 |
| T-DNA | transfer DNA |
| TFIIIA | transcription factor IIIA |
| TGG2 | β -THIOGLUCOSIDE GLUCOHYDROLASE 2 |
| TGN | trans-Golgi network |
| TIA1 | T-cell restricted intracellular antigen 1 |
| TIAR | TIA1-related |
| TIS11d | TPA-inducible sequence 11d |
| TNF-α | tumor necrosis factor alpha |
| TOL | TARGET OF MYB1-LIKE |
| TOR | Target of Rapamycin |
| TPA | 12-O-tetradecanoylphorbol-13-acetate |
| TRI | TRIsol |
| tRNA | transfer RNA |
| TTP | tristetraprolin |
| TZF | tandem zinc finger |
| U | uridine |
| UBP | OLIGOURIDYLATE BINDING PROTEIN |
| UBQ10 | UBIQUITIN10 |
| uORF | upstream open reading frame |
| UTR | untranslated region |
| VCS | VARICOSE |
| VOZ2 | VASCULAR PLANT ONE-ZINC FINGER 2 |
| Vps | Vacuolar protein sorting |
| Vta1 | Vacuolar protein sorting-associated protein 1 |
| W | tryptophan |
| WDFY | WD and FYVE zinc finger domain containing protein 4 |
| XRN | EXORIBONUCLEASE |
| YFP | yellow fluorescent protein |

1 INTRODUCTION

As plants are sessile organisms, they often have to endure and adapt to unfavorable environmental conditions. These include biotic stresses such as pathogen infections or exposition to herbivores, as well as abiotic stresses like heat, cold, drought, nutrient deficiencies and high salinity.

Especially soil salinity is an outstanding environmental threat endangering food security and crop production by causing extreme losses of yield worldwide (Kamran et al., 2020). Excess amounts of salt in fields due to saline water irrigation, application of mineral fertilizers or insufficient soil maintenance (Abdel Latef, 2010) currently affect an estimated portion of 10% of global land (Flowers et al., 2010; Kamran et al., 2020). In the light of global climate change, which comes along with warmed air and ocean temperatures additionally harming crop productivity (IPCC, 2014; Lamaoui, 2018), understanding plants' molecular mechanisms exerted by plant stress regulators is more important than ever before.

To cope with adverse growth conditions, plants have evolved several mechanisms requiring, among others, vast transcriptional reprogramming systems. Recent studies shed light on a newly discovered function of SPIRRIG (SPI), an Arabidopsis BEACH Domain Containing Protein (BDCP), classically known to be involved in membrane trafficking pathways. It was shown that SPIRRIG is involved in salt stress response via regulation of transcript stabilization and localization (Steffens et al., 2015). Strikingly, the highly conserved BDCP family has never been associated with mRNA regulation before.

1.1 BDCPs are facilitators of membrane dynamics

The BDCPs are a conserved protein family among eukaryotes and are generally known to be involved in membrane trafficking. In 1996, Nagle et al. identified the first BDCP in humans, named lysosomal-trafficking regulator (LYST). The authors characterized the corresponding disease, the Chediak-Higashi syndrome (CHS), from which patients suffer when they carry a mutation in *LYST*. Accordingly, the name for the characteristic BEACH domain was derived from *beige* and *Chediak-Higashi*, with *beige* being the mouse model for *LYST* (Barbosa et al., 1996). The disease CHS comes along with severe symptoms such as immunodeficiency, reduced pigmentation in eyes and skin, bleeding diathesis and neurological restrictions (Westbroek et al., 2007; McVey Ward et al., 2002). On the cellular level, the symptoms are, among others, reflected in abnormally enlarged lysosomes in granulocytes and other leukocytes, defects in protein sorting, exocytosis, membrane fusion/fission events, and melanosome biogenesis (McVey Ward et al., 2002; Techernev et al., 2002; Kaplan et al., 2008). In the following years, eight more human BDCPs, with the unifying function as scaffolding proteins in membrane fission and fusion, were identified (Cullinane et al., 2013). BDCPs were found to be implicated in vesicle transport, receptor signaling, apoptosis and

autophagy (Cullinane et al., 2013). Similar as mutations in *LYST*, mutations in other human BDCP encoding genes cause several diseases. Neurobeachin (*NBEA*) for example was described as a candidate gene for autism (Volders et al., 2011); lipopolysaccharide-responsive beige-like anchor protein (*LRBA*) was linked to immunodeficiency (Lopez-Herrera et al., 2012) and enhanced cell proliferation leading to cancer growth (Wang et al., 2004); and WD and FYVE zinc finger domain containing protein 4 (*WDFY4*) was connected to systemic lupus erythematosus (Han et al., 2009).

In addition, BDCP protein family members have been described in other prominent model organisms including *Saccharomyces cerevisiae*, *Dictyostelium discoideum*, *Caenorhabditis elegans*, *Drosophila melanogaster* and *Arabidopsis thaliana*. BDCP families contain two (*S. cerevisiae*), six (*D. discoideum*, *C. elegans*, *A. thaliana*, *D. melanogaster*), or up to nine (*H. sapiens*) members (De Lozanne, 2003; Teh et al., 2015; Cullinane et al., 2013). With more than 400 kDa, members of the beach domain family are extremely large proteins (De Lozanne, 2003).

BDCP domain structure is especially conserved at the C-terminal end which usually consists of a pleckstrin homology (PH) domain, the BEACH domain and subsequent WD40 repeats. PH domains, which are composed of around 100 amino acids, are generally able to bind phospholipids and to thereby associate with membranes (Cullinane et al., 2013; Lemmon, 1999). The exact molecular function of the BEACH domain is still unknown, however, an interaction of the PH domain with the BEACH domain was suggested to serve as a ligand-binding site (Jogl et al., 2002). WD40 repeats are present in numerous proteins involved in various cellular processes and were shown to mediate protein-protein interactions (reviewed in Stirnimann et al., 2010).

Interestingly, HsWDFY3/autophagy-linked FYVE protein (ALFY) is the only human BDCP containing an additional FYVE domain downstream of WD40 repeats (Cullinane et al., 2013). FYVE domains are known for their membrane targeting capacity via highly specific binding to phosphatidylinositol 3 phosphate (*PtdIns(3)P*) (Gaullier et al., 1998) and are frequently found in proteins involved in trafficking pathways (Corvera et al., 1999). HsWDFY3/ALFY was also revealed to be associated with targeting protein aggregates for autophagic degradation (Simonsen et al., 2004). In accordance with that, the *Drosophila* ortholog of HsWDFY3/ALFY, Blue cheese (*Bchs*), is involved in clearance of aggregated proteins as well (Sim et al., 2019). Strikingly, in a few other model organisms such as in *D. discoideum* or *A. thaliana*, no BDCP family member carries a FYVE domain (De Lozanne, 2003; Teh et al., 2015). Recently, FYVE domain containing proteins were identified in the ancient moss *Physcomitrella patens* (Agudelo-Romero et al., 2020). The researchers reported PpALFY1-4 to carry C-terminal FYVE domains downstream of PH, BEACH and WD40 domains. Due to the fact that BDCPs

exhibit a similar modular structure, but lack a FYVE domain in several angiosperms that were included in their study, the authors suggest the FYVE domain to have been lost during land plant evolution and to not exert essential functions (Agudelo-Romero et al., 2020).

1.2 The molecular function of BDCPs *in planta*

The exact molecular function of BDCPs in plants has not been fully elucidated yet. So far, reports on plant BDCP function are available only for the *A. thaliana* BDCPs GREEN FLUORESCENT SEED 12 (GFS12) and SPIRRIG.

GFS12 was found to be involved in vacuolar protein trafficking, as *gfs12* mutants showed defective transport of seed proteins to the protein storage vacuole (Teh et al., 2015). Furthermore, the authors describe an interaction of GFS12 with the PH domain of another Arabidopsis BDCP, BEACH-DOMAIN HOMOLOG C1 (BCHC1), and elevated avirulent bacterial growth in *gfs12/bchb1* double mutants. Consequently, the authors suggest BEACH domains in Arabidopsis to act together in mediating disease resistance and in protein trafficking (Teh et al., 2015). While there is only one report on GFS12 function, SPIRRIG function and Arabidopsis *spirrig* mutants have been characterized in more detail.

1.2.1 The basal land plant *Marchantia polymorpha* emerged as a molecular model organism

Recently, also a *Marchantia polymorpha* mutant for the BDCP SPIRRIG (*Mpspirrig*, *Mpspi*), exhibiting a short rhizoid phenotype, was isolated in a T-DNA screen (Honkanen et al., 2016). The liverwort *M. polymorpha* belongs to the bryophytes that also comprise mosses and hornworts. Bryophytes are the oldest living land plants and emerged from freshwater green algae around 450 million years ago (Mishler and Churchill, 1984; Shimamura, 2016). Common features of bryophytes, in contrast to other land plants, include the lack of a vascular system, absence of lignified cell walls, fertilization with motile sperm and dominance of the haploid gametophyte over the diploid sporophyte (Ishizaki et al., 2016). Liverworts moreover exhibit unicellular rhizoids, the first land plant rooting structures. Rhizoids are filamentous, tip-growing cells developing from ventral epidermal cells or ventral scales (Cao et al., 2014; Shimamura et al., 2016; Honkanen et al., 2016). Habitats of *M. polymorpha* are found across the globe in temperate regions (Bischler, 1989; Qiu et al., 2006; Shimamura, 2016). While researchers intensively described anatomy, morphology, physiology and development of *M. polymorpha* for the past almost 200 years (Burgeff, 1943; Ishizaki et al., 2016; Shimamura et al., 2015; Bowman, 2016), *M. polymorpha* was accessed as a molecular model organism only in recent years. Due to its advantageous phylogenetic position, *M. polymorpha* serves as an ideal model to solve essential questions regarding the evolution of land plants and the identification of basal, minimal genetics that were required for plants to adapt to conditions coming along with land colonization (Bowman et al., 2007; Ishizaki et al., 2016).

M. polymorpha meets the criteria for an ideal model system and is very suitable for laboratory work. *M. polymorpha* can be cultivated easily, vegetatively propagated and crossed. Its life phase, with approximately three months from spore to spore, is short (the main developmental stages are shown in fig. 1).

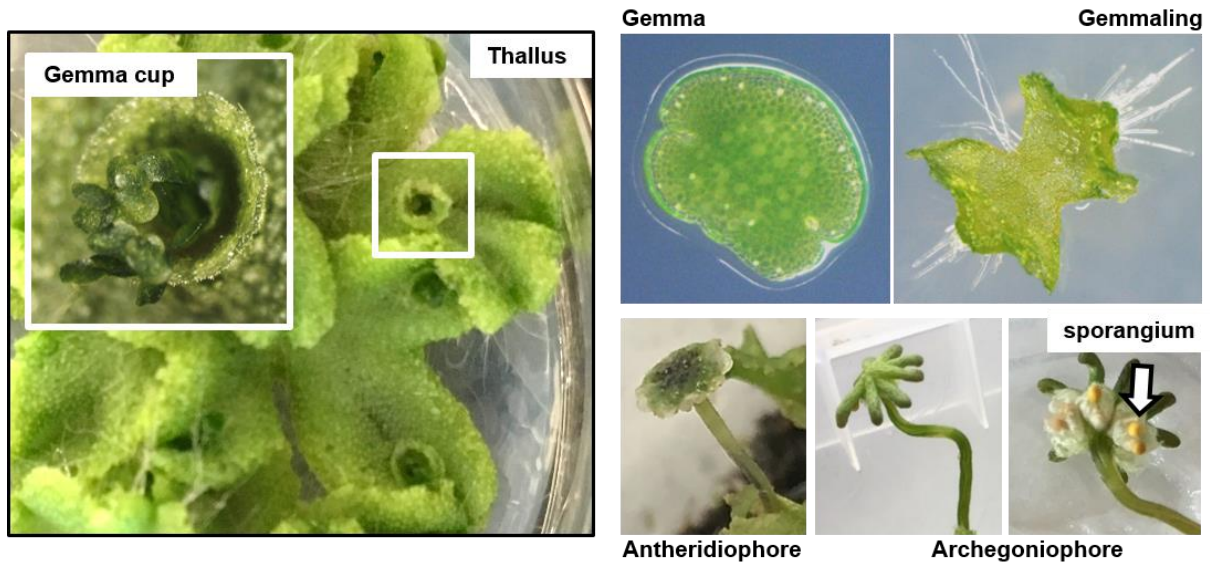


Figure 1: **Developmental stages in the life cycle of *M. polymorpha***. The thallus is the dominant, haploid gametophyte. *M. polymorpha* vegetatively propagates through emergence of gemma cups on thalli. Gemma cups give rise to numerous clonal propagules called gemmae. Gemmae stay dormant inside the cup. As soon as gemmae get dispersed, they develop to gemmalings and finally, to mature thalli. Under laboratory conditions, reproductive growth of *M. polymorpha* is induced by irradiation with far-red light and subsequently, gametangiophores emerge on mature thalli. Female, egg-harboring archegoniophores are fertilized with sperm produced by male antheridiophores. The zygote mitotically divides and develops into the diploid sporophyte. Subsequently, sporophytes produce spore-containing sporangia. Spores in turn develop from sporelings to thalli. The figure was inspired by Ishizaki et al., 2016.

The relatively small genome (approximately 280 Mb) of *M. polymorpha* has been fully sequenced and annotated and shows a low level of redundancy (Bowman et al., 2017). Together with the haploid gametophyte being dominant, *M. polymorpha* brings optimal genetic and morphological conditions for reverse and forward genetic approaches. *M. polymorpha* is susceptible to *Agrobacterium*-mediated transformation and unelaborate protocols for stable transformation of developing spores (Ishizaki et al., 2008), as well as for regenerating thallus fragments (Kubota et al., 2013) are available. Moreover, amenability to molecular genetic tools such as genome editing via homologous recombination (Ishizaki et al., 2013) and CRISPR/Cas9 (Sugano et al., 2014; Sugano et al., 2018) was reported.

1.2.2 SPIRRIG is the best characterized BDCP in *Arabidopsis thaliana*

The *A. thaliana spirrig* mutant was originally found in an EMS mutagenesis screen that aimed to identify *Arabidopsis* plants with defects in trichome cell development (Hülkamp et al., 1994). Due to its slightly curvy and twisted trichome phenotype, it was classified as a weak *distorted* mutant. Most identified plants in the *distorted* class carry mutations in genes coding for components of the ACTIN-RELATED PROTEIN 2/3 (ARP2/3) and SUPPRESSOR OF

CYCLIC AMP RECEPTOR/WISKOTT-ALDRICH SYNDROME VERPROLIN-HOMOLOGOUS PROTEIN (SCAR/WAVE) complexes, regulating actin accumulation and polymerization (e.g. reviewed in Yanagisawa et al., 2013). Strikingly, and in contrast to the other *distorted* mutants, the organization of the actin cytoskeleton in *spirrig* mutants was found to be intact. In the course of the phenotypic characterization of *spirrig*, Saedler et al. (2009) also demonstrated that trichomes of *spirrig* mutants exhibit shorter branches and reduced stalk length; that epidermal pavement cells of *spirrig* are less complex and that *spirrig* root hairs and hypocotyls are shorter than in wild type plants. At the cellular level, and as a first indication that SPIRRIG has a function in membrane integrity, fluorescein diacetate (FDA) staining revealed vacuoles in root hairs of *spirrig* to be fragmented (Saedler et al., 2009).

1.3 The endosomal sorting complex required for transport (ESCRT) system and its connection to SPIRRIG

Yeast two-hybrid cDNA library screenings with SPIRRIG as the bait protein disclosed an interaction of SPIRRIG with the ESCRT component AAA-ATPase SUPPRESSOR OF K(+) TRANSPORT GROWTH DEFECT 1 (AtSKD1; Steffens, 2014; Steffens et al., 2017).

The ESCRT system is part of the retrograde trafficking pathway starting at the plasma membrane and leading to the vacuole/lysosome via endosomes and the trans-Golgi Network (TGN). Cargo molecules, such as transmembrane proteins or cell surface receptors, are internalized via endocytosis and delivered to the TGN. From there, endosomes either recycle cargo molecules by sorting them back to the plasma membrane, or initiate degradation by sorting to the vacuole upon the most frequent degradation signal, the ubiquitination (Fig. 2).

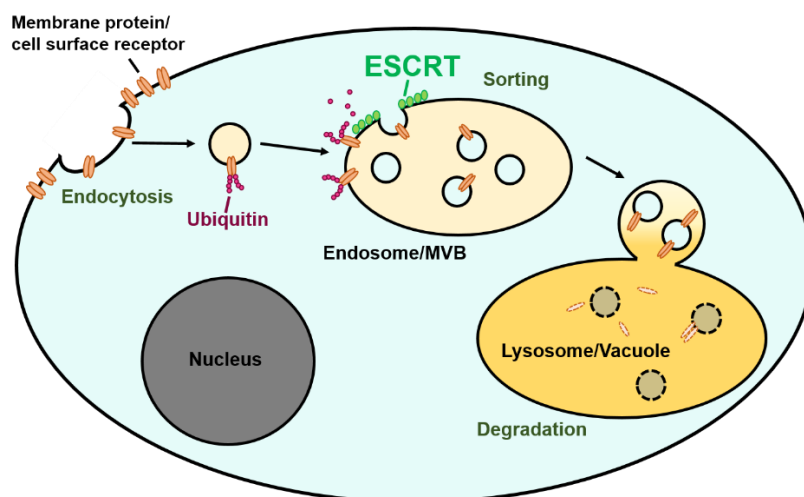


Figure 2: **Multivesicular body (MVB) formation.** Membrane proteins and cell surface receptors are internalized via endocytosis. To initiate degradation, the proteins are ubiquitinated and subsequently sorted at endosomes/MVBs. Monoubiquitinated cargo is recognized and sorted into intraluminal vesicles by the ESCRT complex. Thereafter, mature MVBs fuse with the lysosome/vacuole in which hydrolases degrade internal vesicles and cargo molecules. The scheme was recreated and modified from Schmidt and Teis, 2012.

In this process, the highly evolutionarily conserved multi-subunit ESCRT complex, is essential for the recognition and sorting of monoubiquitinated cargo into intraluminal vesicles (ILVs) of late endosomes, thereby creating multivesicular bodies (MVBs) representing pre-vacuolar compartments (PVCs, fig. 2, Schmidt and Teis, 2012).

First identification of the ESCRT machinery by analysis of vacuolar protein sorting (*vps*) mutants, corresponding *Vps* proteins, and further in-depth studies (Raymond et al., 1992, Coonrod and Stevens, 2010), led to the description of five ESCRT complexes in yeast and mammals: ESCRT-0, -I, -II, ESCRT-III core subunits and ESCRT-III accessory proteins including the SKD1/LYST INTERACTING PROTEIN 5 (SKD1/LIP5; in yeast: *Vps4*/Vacuolar protein sorting-associated protein 1 (*Vta1*)) complex (Babst et al., 2002a; Babst et al., 2002b, Katzmann et al., 2003; Hurley, 2010).

The ESCRT process starts by ESCRT-0 recognizing and capturing cargo molecules via ubiquitin binding (Bilodeau et al., 2002). ESCRT-0 components moreover bind to clathrin and PtdIns(3)*P* on endosomal membranes. Due to its ability to physically bind to ESCRT-I subunits, ESCRT-0 recruits further ESCRT complexes (Schmidt and Teis, 2012). The ESCRT-I and -II subunits share ubiquitin binding capacity and are linked to each other via protein-protein interactions (Wollert and Hurley, 2010). In the following, cargos are passed on to assembled ESCRT-III components, which are activated and recruited by ESCRT-II. ESCRT-III is responsible for membrane invagination and the scission of ILVs (Schmidt and Teis, 2012). Before sorting into ILVs, ubiquitin of cargo molecules is removed by recruited, accessory deubiquitinating enzymes (e.g. associated molecular with SH3 domain of STAM (AMSH), Henne et al., 2011). Subsequently, ESCRT-III accessory proteins recruit the SKD1/LIP5 complex. The AAA-ATPase SKD1 initiates maturation of the endosomes to MVBs as it regulates the fission of ILVs and the dissociation of the ESCRT-III complex by ATP hydrolyzation (Hurley, 2010). LIP5 in turn positively regulates SKD1 function (Fujita et al., 2003; Haas et al., 2007). Mature MVBs subsequently fuse with the vacuole/lysosome where hydrolases degrade internal vesicles and cargo molecules (Hurley, 2010).

Except for ESCRT-0, isoforms of all ESCRT components have been found and described in *A. thaliana* (Gao et al., 2017). It was suggested TARGET OF MYB1-like (TOL) proteins might take over ESCRT-0 function in plants (Gao et al., 2017), as TOL proteins were shown to carry putative clathrin-binding domains, to be able to bind ubiquitin and to regulate vacuolar sorting of the auxin efflux facilitator PIN-FORMED 2 (PIN2; Korbei et al., 2013).

An interaction of the BDCP HsLYST with HsLIP5 in yeast assays (Tchernev et al., 2002) already pointed to a potential role of BDCPs in endosomal trafficking, in particular in the ESCRT pathway. In accordance, Arabidopsis SPIRRIG was found to interact not only with the ESCRT component AtSKD1, but also with AtLIP5. Disturbance of the endosomal transport to

the lytic vacuole in *Arabidopsis spi/lip5* double mutants further demonstrated AtSPIRRIG to function in endosomal trafficking and indicated AtSPIRRIG to stimulate the activity of AtSKD1 (Steffens et al., 2017).

1.4 SPIRRIG in cytoplasmic mRNA granules

Interestingly, yeast-two hybrid cDNA library screenings with SPIRRIG as the bait protein, led to a new direction of SPIRRIG research (Steffens, 2014; M. Jakoby, personal communication). SPIRRIG interacts with *Arabidopsis* DECAPPING 1 (AtDCP1), a component of cytoplasmic mRNA granules called processing bodies (P-bodies).

1.4.1 P-bodies and stress granules are cytoplasmic mRNA granules

Upon export of transcribed and processed mRNAs from the nucleus, a highly regulated control of mRNA translation and degradation in the cytoplasm is essential for proper gene expression in eukaryotic cells. While on one hand, pools of mRNAs are directly translated, on the other hand, mRNAs are released from polysomes and can be further transported to subcellular compartments. In order to avoid accumulations of aberrant mRNA, translationally arrested, stored and stabilized mRNAs are sequestered into microscopically detectable, membrane unbound cytoplasmic foci. These complexes of mRNAs and proteins are called messenger ribonucleoproteins (mRNPs; Bailey-Serres et al., 2009). The most prominent types of mRNP granules, categorized by protein composition, are P-bodies and stress granules.

1.4.2 P-bodies are sites of mRNA regulation and decay

P-bodies store translationally stalled mRNAs and function in mRNA deadenylation, decapping and subsequent degradation (Sheth and Parker, 2003). The granules are continuously present in the cytoplasm, however, under stress conditions their occurrence increases (Xu and Chua, 2012; Motomura et al., 2015). Only in recent years, evidence was provided that P-bodies can also serve as mRNA stabilizing sites (Steffens et al., 2015; Merchante et al., 2015; Scarpin et al., 2017), which was further supported by demonstrating released mRNAs to be intact (Horvathova et al., 2017).

The main mRNA degradation pathways in eukaryotes such as mammals and yeast are initiated by rate-limiting shortening of the 3'-polyadenosine (poly[A]) tail (Chen and Shyu, 2011), mainly orchestrated by the most prominent eight subunit deadenylase carbon catabolite repressor protein 4-negative on TATA-less (CCR4-NOT) complex (Chen et al., 2002; Tucker et al., 2001; Parker and Song, 2004). Subsequently, mRNAs are either degraded 3' to 5' by the exosome or decapped by the DCP1/DCP2 decapping enzyme complex, which is followed by 5' to 3' degradation by the exoribonuclease XRN1 (Houseley and Tollervey, 2009). Components of the 5' to 3' mRNA decay pathway, including deadenylases, decapping complexes, and the 5' exonuclease, are typical P-body marker proteins in eukaryotic organisms (Maldonado-

Bonilla, 2014). In Arabidopsis, homologs for all components have been described. The Arabidopsis decapping complex is comprised of the catalytic subunit DCP2, subunits DCP1, DCP5 and VARICOSE (VCS; Xu et al., 2006; Xu and Chua, 2009). Arabidopsis XRN4, homolog to XRN1, was shown to co-localize with DCP1 and in *xrn4* mutants, accumulations of uncapped mRNAs were discovered (Weber et al., 2008). Deadenylation in Arabidopsis is catalyzed by a poly[A]-specific ribonuclease (PARN; Reverdatto et al., 2004) and the CCR4-CCR4 ASSOCIATED FACTOR 1 (CCR4-CAF1) complex (Liang et al. 2009; Walley et al., 2010; Suzuki et al., 2015). While in yeast and humans, NOT1-5 proteins were shown to regulate CCR4-CAF1 activity, no such function has yet been described in Arabidopsis (Zheng et al., 2011; Maldonado-Bonilla, 2014). However, Arae et al. (2019) recently thoroughly analyzed, identified and defined CCR4-NOT complex core components in *A. thaliana* and confirmed NOT1 to act as scaffolding protein interacting with several NOT and CAF proteins, as already known from other eukaryotic CCR4-NOT complexes. Apart from the major P-body components, the mRNA granules frequently contain additional proteins as for example the microRNA (miRNA)-dependent endonuclease ARGONAUTE1 (AGO1), components of nonsense-mediated mRNA decay (NMD), or RNA-binding proteins such as tandem zinc finger (TZF) proteins (Maldonado-Bonilla, 2014).

1.4.3 Stress granules are sites of mRNA storage

Stress granules (SGs), opposed to P-bodies, are not continuously present in the cytoplasm but especially assemble upon stress conditions and function in storage and protection of mRNAs (Anderson and Kedersha, 2008; Protter and Parker, 2016). As soon as the cells recover from stress, SGs were shown to disassemble quickly and released mRNAs can reenter the translational cycle (Merret et al., 2017). Appearance of SGs was demonstrated in yeast, animals and plants (Hoyle et al., 2007; Collier et al., 1988; Nover et al., 1983). In contrast to PBs, the main components of SGs, next to translationally stalled mRNAs, are several eukaryotic translation initiation factors (eIF, eg. eIF4A, B, C, E, G), small ribosomal subunits (40s) and various RBPs instead of mRNA decay machineries (Buchan and Parker, 2009). SG assembly is triggered by phosphorylation of eIF2 α (Kedersha et al., 1999). Formation moreover depends on for example human T-cell restricted intracellular antigen 1 (TIA1) and TIA1-related (TIAR) proteins (Gilks et al., 2004), which contain RNA recognition motifs (RRMs) next to self-aggregating prion-related domains (Waris et al., 2014; Chantarachot and Bailey-Serres, 2018). In Arabidopsis, RRM-containing members of closely related protein families RNA BINDING PROTEINS 45/47 (RBP45/47) and OLIGOURIDYLATE BINDING PROTEINS (UBP) were described as core SG components and shown to relocate to SGs upon stress conditions (Weber et al., 2008; Sorenson and Bailey-Serres, 2014; Nguyen et al., 2016; Chantarachot and Bailey-Serres, 2018).

Even though their protein composition slightly differs, P-bodies and SGs are very dynamic, often located in close proximity with each other and functionally linked (Fig. 3; Kedersha et al., 2005).

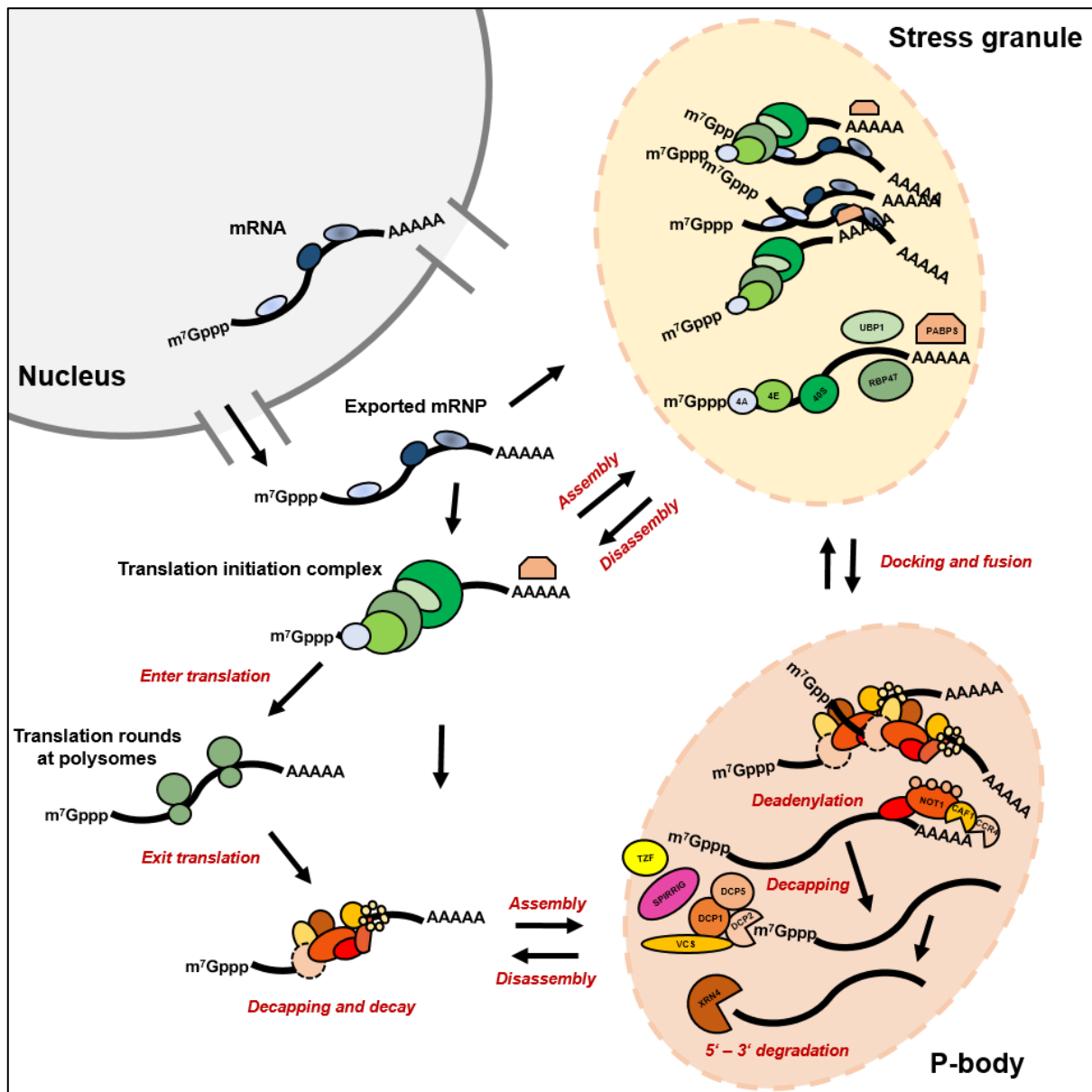


Figure 3: **Model of the mRNP cycle.** Mature mRNAs are exported out of the nucleus in nascent mRNPs containing cap-binding complexes and poly[A]-binding proteins (indicated in blue). The translation initiation complex, composed of eukaryotic initiation factors and the small ribosomal subunit 40S (indicated in green), assembles on the mature mRNA. Subsequently, mRNAs enter translation and undergo several rounds of translation at polysomes. Upon defects in translation or during stress conditions, mRNAs can exit translation and mRNA decay is induced upon recruitment of mRNA degradation complexes (indicated in red). **P-bodies** are the sites of mRNA decay, in which deadenylation (mediated by the CRR4-NOT complex) is followed by decapping (mediated by the decapping complex that consists of DCP1, 2, 5 and VCS in *A. thaliana*) and subsequent 5'-3' degradation exerted by XRN4. SPIRRIG (indicated in pink) is involved in P-body assembly, is recruited to P-bodies upon salt stress and interacts with DCP1. SPIRRIG moreover localizes the mRNA of TZF proteins to P-bodies upon salt stress and physically interacts with TZF proteins (indicated in yellow). Upon stress conditions, polysomes are disassembled. Subsequently mRNAs are sequestered in newly formed **stress granules** in which mRNAs are stored and stabilized. In contrast to P-bodies, stress granules mainly contain translation initiation factors. P-bodies and stress granules very dynamically assemble and disassemble and are supposed to dock, fuse, share and exchange proteins and mRNAs. mRNAs can reenter translation cycles from both types of mRNP granules. The scheme was recreated, unified and modified from Chantarachot and Bailey-Serres, 2018; Protter and Parker, 2016 and Buchan and Parker, 2009.

1.4.4 Arabidopsis SPIRRIG functions in salt stress response

The Arabidopsis BDCP SPIRRIG was found to interact with the P-body component AtDCP1. Moreover, further experiments revealed SPIRRIG not only to localize to P-bodies upon salt stress, but to also be involved in P-body assembly under salt stress conditions (Steffens et al., 2015). Moreover, SPIRRIG was shown to be implicated in stabilization of salt stress-regulated mRNAs and in localizing these to P-bodies, among others demonstrated for the mRNA of *TANDEM ZINC FINGER 3* (*TZF3*; Steffens et al., 2015). Finally, the results strongly suggested a biological function of SPIRRIG in Arabidopsis salt stress responses, which was further supported by the salt hypersensitivity phenotype of *spirrig* mutants (Steffens et al., 2015).

1.5 TZF proteins and their role in post-transcriptional regulation

Continuing studies demonstrated SPIRRIG to not only be involved in stabilization of *TZF* mRNAs, but to directly interact with TZF proteins as well (A. Steffens, unpublished data). TZF proteins so far are not well understood in plants, but are known to play major roles in post-transcriptional regulation in humans.

Gene expression at the post-transcriptional level is mainly regulated by numerous RNA binding proteins (RBPs) affecting mRNA translation, processing, modification, stability or localization (Hentze et al., 2018). RBPs are usually components of mRNPs and directly bind to single or double stranded RNA (Maronedze et al., 2016). Post-transcriptional control of gene expression by RBPs is known to be mediated at a variety of *cis*-regulatory elements, sequence and/or structural motifs, predominantly located in untranslated regions (UTRs) of mRNAs (Srivastava et al., 2018). Common structural RNA-binding domains found in RBPs are the RNA recognition motif (RRM), the dsRNA-binding domain or the zinc finger (Maronedze et al., 2016). Various associations and interactions of *cis*-regulatory elements with *trans*-regulatory RBPs, such as zinc finger proteins, can determine and lead to different fates of target mRNAs.

1.5.1 The family of zinc finger proteins exerts various functions

The family of zinc finger proteins is one of the most abundant protein classes in eukaryotic genomes. Any protein, containing one or more zinc ions coordinating functional, independently folded structural domains was defined as a zinc finger protein (Laity et al., 2001). Accordingly, the zinc finger protein family is comprised of members with numerous variations of structure and function, such as DNA or RNA binding, protein-protein interaction or association to membranes (Laity et al., 2001). The first report of a zinc finger protein was published with the description of the zinc finger archetype, the *Xenopus laevis* transcription factor IIIA (TFIIIA; Miller et al., 1985). Due to its ability to bind DNA and RNA, its large number of zinc domains, its extended DNA recognition sequence and poor conservation at the amino acid level among eukaryotes, TFIIIA is a somewhat unusual zinc finger protein family member (Layat et al., 2013). Generally, the zinc finger family was subdivided into the “classical” zinc fingers and the

“nonclassical” zinc fingers based on the ligand set involved in zinc ion coordination (Lee and Michel, 2014). The “classical” zinc fingers, being the first identified zinc finger family, carry a CCHH (Cys₂His₂) ligand set to bind zinc. After zinc coordination and concomitant folding to a protein structure composed of an α helix and an antiparallel β sheet, classical CCHH zinc fingers are known to act as transcription factors via binding of specific DNA sequences (Lee and Michel, 2014). “Nonclassical” zinc fingers comprise around 13 additional subclasses, varying in the ligand set required for zinc ion coordination. Some members share the function as DNA transcription factors with classical zinc fingers; however, numerous other nonclassical family members exert functions in RNA regulation or protein recognition (Lee and Michel, 2014).

One of the most prominent “nonclassical” zinc finger families, which is conserved from yeast to metazoans (Jang, 2016), are the TZF proteins. The characteristic TZF domain was found to carry two identical CCCH (C-x8-C-x5-C-x3-H) ligand sets, divided by a spacer of 18 amino acids (Blackshear et al., 2005; Jang, 2016). TZF proteins were reported to be able to bind adenosine and uridine (AU)-rich elements (AREs) and to thereby mediate decay of ARE containing mRNAs.

1.5.2 AREs mediate mRNA destabilization

AREs are distinct, *cis*-regulatory elements, typically located in 3'UTRs of mRNAs. Their presence in 5-8% of human mRNAs, coding for proteins involved in a multitude of processes such as for example proliferation, differentiation, apoptosis or metabolism (Otsuka et al., 2019; Barreau et al., 2005), highlights the biological importance of AREs. First identified AREs were found in mRNAs coding for inflammatory cytokines or lymphokines (Caput et al., 1986; Barreau et al., 2005), and were mainly reported to mark host mRNAs for degradation (Chen and Shyu, 1995). However, further studies also revealed broader connections of AREs to RNA processing, transport or translation (Otsuka et al., 2019; Garcia-Maurino et al., 2017). ARE sequences usually have a length of 50-150 nt and classically contain frequently overlapping AUUUA pentamers (Barreau et al., 2005) in uridine rich environments of 3'UTRs. The minimal and sufficient ARE sequence to induce its mRNA destabilizing property however was identified as the nonamer UUAUUUA(U/A)(U/A) (Lagnado et al., 1994). ARE-mRNAs were classified into three groups: class I containing non-overlapping, dispersed AUUUA pentamers; class II comprises mRNAs with at least two overlapping UUAUUUA(U/A)(U/A) nonamers and class III ARE-mRNAs are characterized by uridine rich regions, but are lacking AUUUA motifs at all (Uchida et al., 2019; Barreau et al., 2005). Attempts have been made to find consensus sequences and definitions of AREs within classifications, especially in connection to associated proteins and defined biological functions, however the appearance of AREs in

3'UTRs can strongly vary in combination, number and distribution (Uchida et al., 2019; Barreau et al, 2005).

The founding CCCH family member, first described and most intensely studied TZF and ARE binding protein, is human tristetraprolin (TTP). TTP belongs to a small TZF family consisting of four members in mice (Blackshear et al., 2005) and only three in humans (Sanduja et al., 2010). The description of the TTP knockout mouse, and the identification of the connection of TTP to the degradation of tumor necrosis factor alpha (TNF- α) mRNA, led to first understanding of the molecular mechanism behind TZF induced mRNA decay (Taylor et al., 1996). The knockout of TTP in mice was shown to cause a severe, systemic inflammatory syndrome; manifested in symptoms such as cachexia, arthritis, dermatitis, conjunctivitis and autoimmunity (Taylor et al., 1996; Yamasaki, 2018). Further studies could connect phenotypes of the TTP knockout mouse to an excess level of active TNF- α mRNA due to significantly increased stability connected to TTP loss (Carballo, 1998). Consistently, the TZF domain of TTP was demonstrated to directly and specifically bind to the single-stranded, simple linear ARE motif UUAUUUAUU in the 3'UTR of the TNF- α mRNA (Worthington et al., 2002; Lai et al., 2000). Strikingly, the binding to TNF- α mRNA was completely abolished, when only one of the cysteines or histidines, regardless of the position, of the TZF domain was mutated (Lai et al., 2000).

1.5.3 The human TZF TTP promotes deadenylation and subsequent mRNA decay

Upon binding to AREs, TTP promotes deadenylation and subsequent degradation of target mRNAs by recruitment of the CCR4-NOT complex (Wells et al., 2017). After TTP was shown to bind the mRNA of TNF- α , several hundreds of other mRNAs targeted by TTP were identified (Bulbrook et al., 2018; Iqbal et al., 2014; Datta et al., 2008; Stoecklin et al., 2008). Investigation of other TTP family members revealed these to act in a similar manner and additionally contributed to elucidation of the mRNA decay mechanism exerted by TTP (Brooks and Blackshear, 2013; Hudson et al., 2004). Using the nuclear magnetic resonance (NMR) structure of its TZF domain, the high affinity binding between the TZF domain and the mRNA was described with more detail at the example of human 12-O-tetradecanoylphorbol-13-acetate (TPA)-inducible sequence 11d (TIS11d). The researchers particularly showed the binding to not depend on any secondary structure of the RNA and moreover that the association of protein with RNA was the result of hydrogen bonding and interactions between hydrophobic amino acids and RNA bases (Hudson et al., 2004; Wells et al., 2017).

For both ARE-dependent mRNA decay and TTP family members, association with the 5' to 3' decay pathway in P-bodies as well as with the 3' to 5' decay pathway at exosomes was demonstrated (Brooks and Blackshear, 2013; Stoecklin et al., 2006). Research underlined 5' to 3' decay of ARE containing mRNAs induced by TTP to predominate over involvement in 3'

to 5' decay (Brooks and Blackshear, 2013; Buchan and Parker, 2009). Thus, the following elaboration refers to the current view of TTP's method of action in 5' to 3' mRNA degradation.

Upon a stress stimulus, e.g. inflammation responses, the p38 mitogen-activated protein kinase (MAPK) pathway is activated in human cells, leading to expression of TTP mRNA and protein (Mahtani et al., 2001). TTP protein generally is subject to extensive phosphorylation at several phosphorylation sites, however, phosphorylation in the p38 MAPK pathway was shown to be the main regulator of TTP function under stress conditions (Brooks and Blackshear, 2013; Cao et al., 2007; Clark et al., 2009). Therein, TTP first is phosphorylated by MAPK-activated protein kinase 2 (MK2) at two phosphorylation sites (Mahtani et al., 2001; Chrestensen et al., 2004), resulting in stabilization of TTP and promotion of TTP binding to 14-3-3 adaptor proteins (Sandler et al., 2011). TTP thereby localizes to the cytoplasm (Johnson et al., 2002; Stoecklin et al., 2004) and is prevented from recruiting the deadenylase CCR4-NOT complex (Clement et al., 2011). The ARE-binding Hu (named after the hemolytic-uremic syndrome (HUS); Popovitchenko et al., 2016) protein family, consisting of four members in humans, antagonize TTP function by stabilizing target mRNAs and/or stimulating translation initiation (Otsuka et al., 2019). Neuron-specific HuD for example was shown to mediate translation initiation by direct binding to the poly[A] tail and eIF4A (Fukao et al., 2009; Otsuka et al., 2019). Moreover, HuD recruits kinases of the protein kinase B (PKB) signaling pathway in order to phosphorylate translation initiation factor eIF4B, which in turn stimulates eIF4A activity (Rozen et al., 1990; Otsuka et al., 2019). Thus, during inflammation, stress-responsive TTP-targeted mRNAs are stabilized and subjected to translation as they are kept from deadenylation (Bulbrook et al., 2018; model of TTP function is depicted in fig. 4.

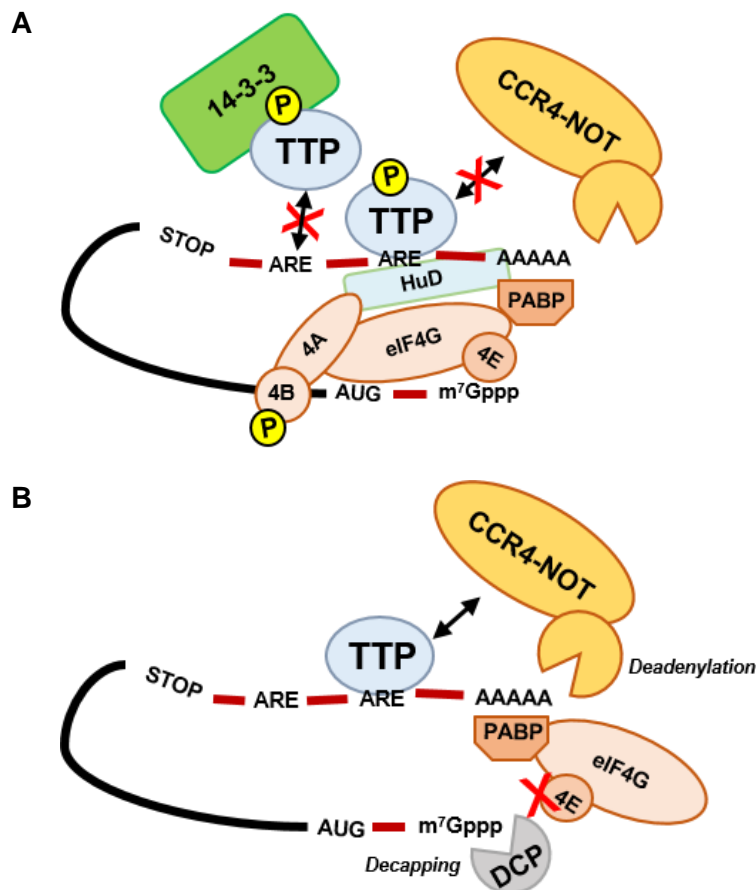


Figure 4: **Model of TTP function.** **A** Phosphorylation of TTP upon a stress stimulus results in stabilization of TTP and promotion of TTP binding to 14-3-3 adapter proteins. TTP thereby is prevented from recruiting the CCR4-NOT complex. ARE-binding Hu proteins additionally act to stabilize target mRNAs. Neuron-specific HuD directly binds to the poly[A] tail and eIF4A. Moreover, HuD promotes phosphorylation of eIF4B, which in turn stimulates eIF4A activity. Consequently, ARE-containing mRNAs are stabilized and subjected to translation. **B** Under non-stress conditions, TTP is dephosphorylated and initiates mRNA decay of ARE-containing target mRNAs by recruitment of the CCR4-NOT complex. Translation initiation factors are repressed and mRNAs are subjected to deadenylation and subsequent decapping. The scheme was recreated and modified from Otsuka et al., 2019.

As soon as the stress signaling is ceasing, TTP is activated again by dephosphorylation of the serine-threonine phosphatase PP2A (Sun et al., 2007a). Subsequently, TTP exerts its function by recruiting the CCR4-NOT complex and thereby initiates clearance by degradation of inflammatory mRNAs (Fig. 4B). In addition, TTP was shown to directly interact with the DCP complex (Lykke-Andersen and Wagner, 2005). Finally, TTP mRNA clearance and stability can be mediated by TTP itself in an auto-regulatory negative feedback loop (Brooks and Blackshear, 2013). TTP was shown to effectively bind to three dispersed AUUUA motifs in its 3'UTR to thereby promote decay of its own mRNA (Brooks et al., 2004; Tchen et al., 2004).

The recruitment of the CCR4-NOT complex by TTP is supposedly mediated by direct protein interactions, but the mechanism has not been fully elucidated yet (Bulbrook et al., 2018). The human CCR4-NOT complex consists of eight tightly associated sub-complexes with NOT1 being the scaffold protein (Lau et al., 2009; Bulbrook et al., 2018). A defined small sequence motif at the extreme C-terminal end of TTP was shown to directly bind to the NOT1 subunit (Fabian et al., 2013). However, the binding was reported to be rather weak, and removal of the

TTP C-terminal motif did not fully abrogate stimulation of TTP induced mRNA decay (Fabian et al., 2013; Blackshear and Perera, 2014). Consistently, an additional interaction between tryptophan residues in multiple regions of the TTP N- and C-terminus and the subunit NOT9 was demonstrated to be required for CCR4-NOT recruitment and subsequent mRNA decay induced by TTP (Bulbrook et al., 2018).

Blackshear and Perera (2014) investigated the conservation of the RNA-binding TZF domain and the NOT1-binding domain, throughout TZF domain containing family members in eukaryotic lineages. While both domains have been found to be present together in TZF proteins of most lineages, interestingly, the authors report absence of the C-terminal NOT1-binding domain in almost all fungi and most of plants (with exception of the three species *Chromolaena odorata*, *Selaginella moellendorffii* and *Physcomitrella patens*, Blackshear and Perera, 2014). Moreover, most plant TZF proteins contain TZF domains divergent from the classical TTP CCCH spacing pattern, frequently preceded by arginine-rich (RR) domains (Jang, 2016).

1.6 TZF proteins in *Arabidopsis thaliana*

In *A. thaliana*, a total of 68 proteins containing a CCCH zinc finger motif were identified and further divided into 11 subfamilies (Wang et al., 2008). Of 26 Arabidopsis CCCH zinc finger proteins carrying TZF domains, only two proteins, C3H14 and C3H15, contain the classical, conserved CCCH spacing pattern as it is known from TTP (Wang et al., 2008; Kim et al., 2014).

The plant-unique arginine-rich TZF (RR-TZF) CCCH zinc finger protein subfamily comprises 11 members, TZF1 to 11, carrying TZF domains preceded by RR domains. RR-TZFs are grouped according to the presence of ankyrin repeats: whereas TZF1 to 5 completely lack ankyrin protein repeats, TZF7 to 11 carry two repeats at the N-terminus, which are presumably involved in protein-protein interactions (Jang, 2016). All 11 RR-TZF members have already been described and are generally involved in plant development, hormone-mediated growth and stress responses (Jang et al., 2016; Bogamuwa and Jang, 2014). For some members, RNA binding (Pomeranz et al., 2010a), as well as localization of all members to cytoplasmic foci (Pomeranz et al., 2010b), was demonstrated. Thus, it is likely that Arabidopsis RR-TZFs affect plant growth and stress responses through regulation of gene expression via modulations in RNA metabolism (Bogamuwa and Jang, 2014).

1.6.1 Association of TZF proteins with mRNA regulation has been reported

TZF1 was first reported to localize in stress-induced cytoplasmic foci and to co-localize with P-body and SG markers such as DCP2, XRN4 and PABP8, respectively (Pomeranz et al., 2010a). At the same time, *in vitro* binding of TZF1 to RNA and DNA was demonstrated (Pomeranz et al., 2010a). TZF1 is a positive regulator for abscisic acid (ABA), sugar and salt

stress tolerance responses, and a negative regulator for gibberellic acid (GA; Lin et al., 2011; Han et al., 2014; Jang, 2016). Expression of *TZF1* mRNA was reported to be induced by ABA, salt and sugar depletion. Consistently, overexpression of *TZF1* was shown to result in an elevated tolerance to abiotic stresses, such as drought, cold and salt stress, as well as late flowering and an overall compact phenotype (Lin et al., 2011; Han et al., 2014). Ensuing research by Qu et al. (2014) specified the RNA binding capability by showing TZF1 to be able to bind poly[U] sequences and an ARE probe composed of 19 nucleosides (ARE₁₉). The interaction was shown to depend on the presence of zinc and was abrogated when the length of the ARE sequence was reduced (ARE₁₃) and when all adenosine residues were replaced with guanosine residues (Qu et al., 2014). However, binding affinity of TZF1 to ARE sequences was much weaker than between TTP and respective ARE RNA probes (Qu et al., 2014). In addition, and again in contrast to TTP RNA binding, for which only the TZF domain is necessary and sufficient, both the RR and TZF domain of TZF1 are required for RNA binding. Finally, the authors demonstrate TZF1 to be capable of triggering degradation of ARE-containing mRNAs *in vivo* using protoplast transient expression analysis (Qu et al., 2014). More recently, a direct TZF1 target was identified by proving binding and affecting the stability of the Target of Rapamycin (TOR) mRNA (Li et al., 2019).

TZF2 and TZF3 were suggested to be involved in ABA and jasmonic acid (JA) responses, as overexpression conferred ABA hypersensitivity as well as drought and salt tolerance (Huang et al., 2012; Lee et al., 2012). Positive effects on ABA responses were ascribed to the repression of the negative ABA response regulator *ABA INSENSITIVE 2 (ABI2)* in *TZF3* overexpression plants (Huang et al., 2012; Jang, 2016). No direct connection of TZF2 and TZF3 to mRNA metabolism has yet been revealed, but as the other RR-TZF members, they were shown to locate to cytoplasmic foci in maize mesophyll protoplasts (Pomeranz et al., 2010b). The seed-specific RR-TZF family members TZF4, 5 and 6 were shown to be positive regulators for ABA while being negative regulators for GA and phytochrome mediated seed germination responses (Bogamuwa and Jang 2013; Bogamuwa and Jang, 2016). Moreover, they co-localized with P-body markers DCP2 and SG markers UBP1b and PABP8 (Bogamuwa and Jang, 2013). However, in yeast two-hybrid library screens, no direct physical interaction between TZF4, 5 6 and P-body components was identified. Nonetheless, an interaction of TZF5 with the stress related proteins MEDIATOR OF ABA-REGULATED DORMANCY 1 (MARD1) and RESPONSIVE TO DEHYDRATION 21A (RD21A) was shown to be located in cytoplasmic foci (Bogamuwa and Jang, 2016). For TZF7 to 11, redundant functions in vegetative growth maintenance, activation of oxidative stress tolerance as well as negative regulation for stress-induced transition to flowering were reported (Blanvillain et al., 2011; Jang, 2016). TZF9, known to mediate pathogen-associated molecular pattern-triggered immune responses, is the only other RR-TZF, next to TZF1, which was shown to have RNA

binding capability (Maldonado-Bonilla, 2014) controlled by phosphorylation (Tabassum et al., 2020). Furthermore, association of TZF9 with P-bodies in dependence of mRNA availability, affected by inhibitor treatments, was demonstrated (Maldonado-Bonilla, 2014). TZF9 was recently shown to also physically interact with the SG marker protein POLY[A]-BINDING PROTEIN 2 (PAB2) and to even promote stress granule assembly (Tabassum et al., 2020).

1.6.2 TZF10 and TZF11 are described as regulators of salt stress response

TZF10 and TZF11 (also known as salt-inducible zinc finger (SZF) 2 and 1, respectively) were described as regulators of salt stress responses by Sun et al. (2007b). The zinc finger proteins share 68% similarity at the amino acid level and carry two tandem CCCH-type zinc finger motifs preceded by two ankyrin repeat domains at the N-terminus. In contrast to studies of Pomeranz et al. (2010b), who demonstrate localization of TZF10 and 11 in cytoplasmic foci in maize protoplasts, Sun et al. (2007b) describe TZF11 to be localized in the nucleus of epidermal onion cells after transient transformation. In a Northern blot analysis, the authors reveal an up-regulation of the generally weakly expressed *TZF10* and *11* transcripts upon salt stress. The expression peaks at 15 min and is fully recovered to precedent levels 60 min after a 200 mM NaCl treatment. Moreover, in *tzf10* and *11* single mutants, the authors registered a significant and specific up-regulation of the salt-responsive genes *RESPONSIVE TO DESSICATION 29A* (*RD29A*), *KINASE 1* (*KIN1*), *COLD-RESPONSIVE 15A* and *47* (*COR15A* and *COR47*) upon salt treatment. Whereas the single mutants did not show striking phenotypic differences compared to the wild type, the authors report a salt hypersensitivity phenotype of *tzf10/tzf11* double mutants manifested in lower germination and cotyledon greening rates as well as inhibited primary root growth of plants. Moreover, after salt irrigation of plants grown on soil, the authors report more severe wilting of *tzf10/tzf11* double mutants compared to wild type plants. Consistent to their findings, salt treatments of *TZF11* overexpression plants result in reduced expression of salt-inducible marker genes *RD29A* and *KIN1* as well as elevated tolerance to high salt concentrations. So far, no direct connection of TZF10 and TZF11 to mRNA metabolism was established.

1.7 Aim of this work

The exact molecular function of SPIRRIG remains elusive. The protein is a particularly interesting BDCP, as it was the first and so far only BDCP demonstrated to be associated with mRNA metabolism (Steffens et al., 2015), biologically relevant to *A. thaliana* salt stress response. This work aims to gain further understanding of SPIRRIG's molecular function in salt stress response by analyzing an interplay with TZF proteins, known to be associated with mRNA regulation processes. Moreover, an evolutionary comparative approach was implemented in order to elucidate the conserved set of SPIRRIG function in a basal land plant.

1.7.1 Unraveling the interplay between TZF proteins and SPIRRIG in salt stress response

Previous experiments strongly hinted to a novel connection between the BDCP SPIRRIG and TZF proteins in *A. thaliana*. Not only direct protein co-localization and interaction between SPIRRIG and TZFs were uncovered, but also indications that TZF10, known to be implicated in salt stress response, rescues the salt hypersensitivity phenotype of *spirrig*. Interestingly, the rescue of this phenotype was not observable when the 3'UTR of *TZF10* was present downstream of the CDS in the introduced construct (A. Steffens, unpublished). The results strongly suggested a self-regulating mechanism of TZF10 binding to its 3'UTR to initiate its own mRNA decay. While a self-regulating mechanism and general involvement of the human TZF TTP in mRNA decay is already known and well described, the mechanisms exerted by plant TZFs are far from understood. Thus, this study was set out to investigate the role of TZF in mRNA decay with a special focus on the yet unknown interplay of TZFs with SPIRRIG. Understanding this interplay will contribute to the elucidation of the general role of BDCPs in mRNA metabolism.

Rescue experiments, expression and stability assays were performed in this work in order to shed light on the underlying function of *TZF10* and its 3'UTR in mRNA decay and how the salt hypersensitivity rescue of *spirrig* might be affected by it. The study was complemented with experiments tackling *TZF10* 3'UTR destabilizing capacity independent from SPIRRIG. Furthermore, a yeast two-hybrid screening was conducted in order to broaden the view on TZF function in *A. thaliana*.

1.7.2 Learning about basal, conserved BDCP protein function

The dual function of SPIRRIG in mRNA metabolism and membrane trafficking suggests SPIRRIG to act in two unrelated, independent pathways. While morphological phenotypes of *spirrig* might be connected to membrane dynamics linked to the ESCRT pathway, the *spirrig* salt hypersensitivity phenotype could likely be explained by defects in salt stress-dependent mRNA regulation. Due to the fact that so far no other BDCP was connected to mRNA decay

before, it is conceivable that the function is specific to *A. thaliana* salt stress response and was acquired by plants at later stages during land plant evolution.

In 2016, Honkanen et al. isolated the *Mpspirrig* mutant in a T-DNA screen looking for rhizoid mutants. The analysis of this mutant depicts an excellent opportunity to elucidate basal BDCP function and its relevance to one of the first plants colonizing the land. In this work, phenotypic description of *Mpspirrig* was carried out at the morphological and cellular level to find differences or communalities to the *Arabidopsis spirrig* mutant. In order to reveal a potential function in salt stress response, gemmaling growth on salt-containing medium was evaluated. Furthermore, protein-protein co-localization and interaction assays were conducted in order to address the question if connections of SPIRRIG to mRNA metabolism and membrane trafficking are evolutionarily conserved and belong to the basal set of BDCP function.

2 MATERIALS AND METHODS

2.1 Organisms and plant lines

The organisms used in this study are listed in table 1.

Table 1: Organisms used in this work.

| Species | Name of ecotype/strain | Genotype/attributes | Reference |
|----------------------------------|------------------------|---|-----------------------------|
| <i>Arabidopsis thaliana</i> | Columbia (Col-0) | Wild type | - |
| <i>Marchantia polymorpha</i> | Takaragaike-1 (Tak-1) | Wild type male | Okada et al., 2000 |
| | Takaragaike-2 (Tak-2) | Wild type female | Okada et al., 2000 |
| <i>Nicotiana benthamiana</i> | - | Wild type | - |
| <i>Escherichia coli</i> | DH5 α | F-, ϕ 80 <i>lacZ</i> Δ M1, Δ (<i>lacZYA-argF</i>), U169, <i>deoR</i> , <i>recA1</i> , <i>endA1</i> , <i>hsdR17</i> , (rk-, mk+), <i>phoA</i> , <i>supE44</i> , <i>thi-1</i> , <i>gyrA96</i> , <i>relA1</i> , - λ | Hanahan, 1983 |
| | DB3.1 | <i>gyrA462</i> , <i>endA1</i> , Δ (<i>sr1 recA</i>), <i>mcrB</i> , <i>mrr</i> , <i>hsdS20</i> , <i>glnV44</i> , <i>ara14 galk2</i> , <i>lacY1</i> , <i>proA2</i> , <i>rpsL20</i> , <i>xyl5</i> , <i>leuB6</i> , <i>mtl1</i> | Bernard and Couturier, 1992 |
| <i>Agrobacterium tumefaciens</i> | GV3101::pMP90 | pTiC58 Δ T-DNA; rifampicin and gentamicin resistance | Koncz et al., 1989 |
| | GV3101::pMP90RK | pTiC58 Δ T-DNA; rifampicin, gentamicin and kanamycin resistance | Koncz et al., 1989 |
| <i>Saccharomyces cerevisiae</i> | AH109 | <i>MATa</i> , <i>trp1-901</i> , <i>leu2-3, 112</i> , <i>ura3-52</i> , <i>his3-200</i> , <i>gal4D</i> , <i>gal80D</i> , <i>LYS2::GAL1UASGAL1TATA-HIS3</i> , <i>GAL2UAS-GAL2TATA-ADE2</i> , <i>URA3::MEL1UAS-MEL1TATA-lacZ</i> | James et al., 2002 |

Table 2 shows *A. thaliana* and *M. polymorpha* T-DNA insertion lines generated or used in this study. *A. thaliana* T-DNA insertion mutants were obtained from the Nottingham Arabidopsis Stock Centre (NASC).

Table 2: T-DNA insertion lines used in this work. Single T-DNA insertion mutants were obtained from the Nottingham Arabidopsis Stock Centre (NASC).

| Name of mutant line | Ecotype | Targeted gene(s) | Site of insertion | SIGNAL SALK Identifier(s) | Reference |
|--------------------------------|---------|-------------------------------------|---------------------|---|--|
| <i>M. polymorpha</i> | | | | | |
| Mpspirrig, Mpspi-2, ST17-11 | Tak-1 | Mp2g15800 | CDS | - | Honkanen et al., 2016, this study |
| <i>A. thaliana</i> | | | | | |
| <i>spi-4</i> | Col-0 | AT1G03060 | CDS | GK_420D09 | Steffens et al., 2015 |
| <i>spi-3</i> | Col-0 | AT1G03060 | CDS | SALK_065311 | Steffens et al., 2015 |
| <i>tzf10-1</i> | Col-0 | AT2G40140 | CDS | SALK_024800 | Sun et al., 2007b (designated as <i>atszf2-1</i>) |
| <i>tzf10-2</i> | Col-0 | AT2G40140 | 3'UTR | SAIL_207G08 | This study |
| <i>tzf11-1</i> | Col-0 | AT3G55980 | 5'UTR | SALK_141550 | Sun et al., 2007b (designated as <i>atszf1-1</i>) |
| <i>tzf11-2</i> | Col-0 | AT3G55980 | CDS | GK_158E10 | A. Steffens, this study |
| <i>tzf11-3</i> | Col-0 | AT3G55980 | 3'UTR | SAIL_191G05 | This study |
| <i>tzf10-1 / tzf11-1</i> | Col-0 | AT2G40140 AT3G55980 | CDS/ 5'UTR | SALK_024800/ SALK_141550 | Sun et al., 2007b (designated as <i>atszf2-1/atszf1-1</i>), this study |
| <i>tzf10-1 / tzf11-2</i> | Col-0 | AT2G40140 AT3G55980 | CDS/ CDS | SALK_024800/ GK_158E10 | A. Steffens, this study |
| <i>tzf10-2 / tzf11-3</i> | Col-0 | AT2G40140 AT3G55980 | 3'UTR/ 3'UTR | SAIL_207G08/ SAIL_191G05 | This study |
| <i>spi-3/ tzf10-1/ tzf11-2</i> | Col-0 | AT1G03060 AT2G40140 AT3G55980 | CDS/ CDS/ CDS | SALK_065311/ SALK_024800/ GK_158E10 | This study |
| <i>spi-4/tzf10-1/ tzf11-2</i> | Col-0 | AT1G03060 AT2G40140 AT3G55980 | CDS/ CDS/ CDS | GK_420D09/ SALK_024800/ GK_158E10 | This study |
| <i>spi-3/ tzf10-2</i> | Col-0 | AT1G03060 AT2G40140 | CDS/ 3'UTR | SALK_065311/ SAIL_207G08 | This study |
| <i>spi-3/ tzf11-3</i> | Col-0 | AT1G03060 AT3G55980 | CDS/ 3'UTR | SALK_065311/ SAIL_191G05 | This study |
| <i>spi-4/ tzf10-2</i> | Col-0 | AT1G03060 AT2G40140 | CDS/ 3'UTR | GK_420D09/ SAIL_207G08 | This study |
| <i>spi-4/ tzf11-3</i> | Col-0 | AT1G03060 AT3G55980 | CDS/ 3'UTR | GK_420D09/ SAIL_191G05 | This study |

An overview on transgenic *A. thaliana* lines is given in table 3.

Table 3: **Overview on transgenic *A. thaliana* TZF10, TZF11 and SWAP construct lines generated in this study.** All constructs carry the glufosinate resistance gene *bar*.

| Nucleic acid | Clone ID | Plasmid | Background |
|--|----------|---------------|---------------------|
| TZF10 | | | |
| 5'UTR _{TZF10} +CDS _{TZF10} +3'UTR _{TZF10} | EK0042 | UBQ pAM-PAT | <i>spi-4; spi-3</i> |
| CDS _{TZF10} +3'UTR _{35SCaMV} | EK0003 | UBQ pAM-PAT | <i>spi-4; spi-3</i> |
| CDS _{TZF10} +3'UTR _{TZF10} | EK0004 | UBQ pAM-PAT | <i>spi-4; spi-3</i> |
| 5'UTR _{TZF10} -YFP-CDS _{TZF10} +3'UTR _{TZF10} | EK0018 | UBQ pENSG-YFP | <i>spi-4; spi-3</i> |
| YFP-CDS _{TZF10} +3'UTR _{35SCaMV} | AST1022 | UBQ pENSG-YFP | <i>spi-4; spi-3</i> |
| YFP-CDS _{TZF10} +3'UTR _{TZF10} | AST1300 | UBQ pENSG-YFP | <i>spi-4; spi-3</i> |
| TZF11 | | | |
| 5'UTR _{TZF11} +CDS _{TZF11} +3'UTR _{TZF11} | EK0043 | UBQ pAM-PAT | <i>spi-4; spi-3</i> |
| CDS _{TZF11} +3'UTR _{35SCaMV} | EK0044 | UBQ pAM-PAT | <i>spi-4; spi-3</i> |
| CDS _{TZF11} +3'UTR _{TZF11} | EK0053 | UBQ pAM-PAT | <i>spi-4; spi-3</i> |
| 5'UTR _{TZF11} -YFP-CDS _{TZF11} +3'UTR _{TZF11} | EK0057 | UBQ pENSG-YFP | <i>spi-4; spi-3</i> |
| YFP-CDS _{TZF11} +3'UTR _{35SCaMV} | AST1014 | UBQ pENSG-YFP | <i>spi-4; spi-3</i> |
| YFP-CDS _{TZF11} +3'UTR _{TZF11} | EK0046 | UBQ pENSG-YFP | <i>spi-4; spi-3</i> |
| SWAP | | | |
| 5'UTR _{TZF10} +CDS _{ABF3} +3'UTR _{ABF3} | EK0005 | UBQ pAM-PAT | <i>spi-4; spi-3</i> |
| 5'UTR _{ABF3} +CDS _{ABF3} +3'UTR _{TZF10} | EK0007 | UBQ pAM-PAT | <i>spi-4; spi-3</i> |
| 5'UTR _{ABF3} +CDS _{TZF10} +3'UTR _{TZF10} | EK0006 | UBQ pAM-PAT | <i>spi-4; spi-3</i> |
| 5'UTR _{TZF10} +CDS _{TZF10} +3'UTR _{ABF3} | EK0056 | UBQ pAM-PAT | <i>spi-4; spi-3</i> |
| 5'UTR _{TZF10} -YFP-CDS _{ABF3} +3'UTR _{ABF3} | EK0055 | UBQ pENSG-YFP | <i>spi-4; spi-3</i> |
| 5'UTR _{ABF3} -YFP-CDS _{ABF3} +3'UTR _{TZF10} | EK0052 | UBQ pENSG-YFP | <i>spi-4; spi-3</i> |
| 5'UTR _{ABF3} -YFP-CDS _{TZF10} +3'UTR _{TZF10} | EK0019 | UBQ pENSG-YFP | <i>spi-4; spi-3</i> |
| 5'UTR _{TZF10} -YFP-CDS _{TZF10} +3'UTR _{ABF3} | EK0047 | UBQ pENSG-YFP | <i>spi-4; spi-3</i> |

Table 4 shows all *M. polymorpha* transgenic lines generated in this work.

Table 4: ***M. polymorpha* transgenic lines generated in this work.**

| Nucleic acid | Clone ID | Plasmid | Resistance | Background |
|-------------------|----------|-----------|---------------|------------|
| MpSPI PBW-Citrine | EK257 | pMpGWB406 | G418 | Tak-1 |
| MpSPI PBW-Citrine | EK257 | pMpGWB406 | G418 | Tak-1 |
| TagRFP-MpDCP2 | EK266 | pMpGWB335 | Chlorsulfuron | |
| MpSPI PBW-Citrine | EK257 | pMpGWB406 | G418 | Tak-1 |
| TagRFP-MpLIP5 | EK316 | pMpGWB335 | Chlorsulfuron | |
| MpSPI PBW-Citrine | EK257 | pMpGWB406 | G418 | Tak-1 |
| TagRFP-MpSKD1 | EK270 | pMpGWB335 | Chlorsulfuron | |

2.2 Plasmids

An overview on all general vectors used in this work is given in table 5. Specific entry and expression clones generated and used in this study can be found in table 23 and 24 (respectively, *A. thaliana*) and in table 25 and 26 (respectively, *M. polymorpha*) in the appendix.

Table 5: General vectors used in this study. All plasmids are Gateway-compatible.

| Name | Description/Purpose | Resistance in <i>E. coli</i> | Reference/Origin |
|---------------|---|------------------------------|--|
| pDONR201 | Entry vector for Gateway cloning | Kanamycin | Invitrogen |
| pDONR207 | Entry vector for Gateway cloning | Gentamicin | Invitrogen |
| UBQ pAM-PAT | <i>UBQ10</i> driven plant expression | Ampicillin/ Carbenicillin | This study; pAM-PAT GenBank ID AY436765.1 |
| UBQ pENSG-YFP | <i>UBQ10</i> driven plant expression, N-terminal fusion of YFP | Ampicillin/ Carbenicillin | M. Jakoby |
| pENSG-C/YFP | <i>35S CaMV</i> driven plant expression, N-terminal fusion of YFP or CFP | Ampicillin/ Carbenicillin | Feys et al., 2005 |
| pEXSG-C/YFP | <i>35S CaMV</i> driven plant expression, C-terminal fusion of YFP or CFP | Ampicillin/ Carbenicillin | Feys et al., 2005 |
| pAMARENA | <i>35S CaMV</i> driven plant expression, N-terminal fusion of mCherry | Ampicillin/ Carbenicillin | M. Jakoby, GenBank ID: FR695418 |
| pAUBERGINE | <i>35S CaMV</i> driven plant expression, C-terminal fusion of mCherry | Ampicillin/ Carbenicillin | M. Jakoby, GenBank ID: FR695418 |
| pAS | Yeast expression, N-terminal fusion of GAL4-BD, tryptophan ORF | Ampicillin/ Carbenicillin | Clontech |
| pACT | Yeast expression, N-terminal fusion of GAL4-BD, leucine ORF | Ampicillin/ Carbenicillin | Clontech |
| pMpGWB406 | <i>35S CaMV</i> driven plant expression, C-terminal fusion of Citrine | Spectinomycin | Ishizaki et al., 2015 |
| pMpGWB335 | <i>35S CaMV</i> driven plant expression, N-terminal fusion of TagRFP | Spectinomycin | Ishizaki et al., 2015 |
| pSCJ232 | <i>35S CaMV</i> driven plant expression, N-terminal fusion of 16 Box-B-repeats | Kanamycin | Schönberger et al., 2012 |
| pSCJ351 | <i>UBQ10</i> driven plant expression Δ N22 C-terminally fused to mVenus | Kanamycin | Schönberger et al., 2012 |

2.3 Oligonucleotide sequences

Tables containing oligonucleotide sequences used in this work for genotyping, qPCR analysis and other purposes, can be found in the appendix (Tables 27-30).

2.4 Molecular biology techniques

2.4.1 DNA extraction for plant genotyping

Small pieces (approximately 1 cm²) of *Marchantia* thallus tissue or *Arabidopsis* leaves were transferred to 2 ml reaction tubes containing glass (*Arabidopsis*, \varnothing 2.7 mm) or ceramic (*Marchantia*, mixture of \varnothing 1.4-1.6 mm and 2.7-3.3 mm) beads. After addition of 300 μ l of Magic Buffer (50 mM Tris/HCl pH 7.2, 300 mM NaCl, 10% sucrose), the samples were homogenized using a tissue lyzer (Qiagen) for 1:30 min at 30 Hz. If the plant material was not yet fully disrupted, homogenization was repeated. The plant extracts were kept at 4°C for short term storage and at -20°C for long term storage.

2.4.2 RNA extraction and cDNA synthesis

For *Arabidopsis* samples, RNA extraction was done utilizing the RNeasy Kit (Qiagen) according to the manufacturer's protocol.

For *Marchantia* samples, RNA extraction was done utilizing TRI reagent (Ambion Life Technologies) according to the following protocol: 50-100 mg of plant material were transferred to 2 ml safe lock reaction tubes containing 4-6 ceramic beads (mixture of \varnothing 1.4-1.6 mm and 2.7-3.3 mm). The material was frozen in liquid N₂ and either directly processed or stored at -80°C. Before extraction, the samples were shredded in a tissue lyzer (Qiagen) for 1 min at 30 Hz and quickly frozen again in liquid N₂. Subsequently, 300 μ l of TRI reagent was added and samples were vortexed shortly. The samples were then shaken again in the tissue lyzer for 2 min at 30 Hz. Another 700 μ l of TRI reagent was added and the samples were incubated for 3 min at RT. To induce phase separation, 200 μ l chloroform was added, vortexed shortly and centrifuged for 15 min, 4°C, at 13000 rpm. The upper, translucent phase was carefully pipetted into fresh 1.5 ml reaction tubes and mixed with 550 μ l isopropanol. The samples were vortexed and incubated at RT for 10 min and subsequently centrifuged at 15°C with 13000 rpm for 20 min. The supernatant was carefully removed to not disturb the RNA pellet. The RNA pellet was washed in subsequent steps using 70% and 100% EtOH (addition of 500 μ l EtOH followed by centrifugation for 5 min at 13000 rpm). For RNAseq, each washing step was done twice to secure removal of all remaining TRI reagent in the samples. The RNA pellets were dried at 37°C for at least 30 min and then eluted in 30 μ l RNase free ddH₂O at 37°C for 10 min. To remove remaining DNA, 1 μ l DNaseI and 2 μ l 10x DNaseI buffer were added and incubated for 1 h at 37°C. The reaction was stopped by addition of 2.5 μ l 25 mM EDTA and incubation at 65°C for 15 min. DNA free RNA was kept at -80°C for long term storage.

Synthesis of cDNA was executed with the RevertAid H Minus First Strand cDNA Synthesis Kit™ (Thermo Scientific) for *Arabidopsis* samples, or the SuperScript™ III First-Strand cDNA Synthesis Kit (Thermo Scientific) for *Marchantia* samples, both using oligo(dT)₂₀ primers. 500 ng RNA was used for synthesis of the *Arabidopsis* cDNA for measurement of expression

levels and stability assays. 1 µg RNA was used for synthesis of *Marchantia* cDNA. Before application in quantitative real-time PCR (qPCR), the generated cDNA was tested by PCR for contamination of genomic DNA with primers amplifying *ELONGATION FACTOR1α* (*EF1α*; Arabidopsis, table 29, appendix) or *ADENINE PHOSPHORIBOSYL TRANSFERASE 3* (Mp*APT3*; *Marchantia*, Saint-Marcoux et al., 2015, table 29, appendix) and for uniformity of concentration with primers amplifying 18S rRNA (Arabidopsis, table 29, appendix) or Mp*APT3* (*Marchantia*, Saint Marcoux et al., 2015, table 29, appendix).

2.4.3 Polymerase chain reaction (PCR)

For amplification of DNA regions of interest, different PCR programs and reaction mixtures were used.

2.4.3.1 Standard PCRs for genotyping and cDNA testing

For genotyping PCRs, standard DreamTaq™ polymerase (Thermo Scientific) was utilized. Reaction mixture and program for respective PCRs can be found in table 6.

Table 6: **Standard DreamTaq polymerase mixture and program.** TA=annealing temperature of used primer pair.

| Reaction | Program |
|-----------------------------|---------------------------|
| 1-2 µl DNA | 95°C 2 min |
| 0.5 µl 10 mM Primer forward | 95°C 30 sec |
| 0.5 µl 10 mM Primer reverse | TA 30 sec |
| 0.5 µl 10 mM dNTPs | 72°C 1 min for up to 2 kb |
| 3 µl 10x buffer | 72°C 10 min |
| 0.3 µl DreamTaq | 4°C ∞ |
| ad 30 µl ddH ₂ O | |

The DreamTaq™ Green PCR master mix (Thermo Scientific) was mainly used in this work for cDNA testing, since the ready-to-use master mix already contains buffer, dNTPs and loading dye. Thus, pipetting errors potentially decreasing the accuracy of results can thereby be circumvented. The reaction mixture and program is shown in table 7.

Table 7: **DreamTaq Green PCR master mix and program.** TA=annealing temperature of used primer pair.

| Reaction | Program |
|---------------------------------------|---------------------------|
| 1-2 µl DNA | 95°C 2 min |
| 0.5 µl 10 mM Primer forward | 95°C 30 sec |
| 0.5 µl 10 mM Primer reverse | TA 30 sec |
| 12.5 µl DreamTaq Green PCR master mix | 72°C 1 min for up to 2 kb |
| ad 25 µl ddH ₂ O | 72°C 10 min |
| | 4°C ∞ |

2.4.3.2 Yeast colony PCR and sequencing

Yeast colony PCRs were performed with a DreamTaq polymerase (Thermo Scientific) reaction mixture and program (Table 8). Sequences for primers AD3XL and AD5XXL can be found in table 30 (appendix).

Table 8: Reaction mixture and program used for yeast colony PCRs.

| Reaction | Program |
|---|------------------------------|
| 3.25 μ l 50 mM MgCl ₂ | 95°C 4 min |
| 1 μ l 10 mM Primer AD3XL | 95°C 45 sec 1 |
| 1 μ l 10 mM Primer AD5XXL | 62°C 30 sec 40 cycles |
| 1 μ l 10 mM dNTPs | 72°C 2:30 min 1 |
| 5 μ l 10x buffer | 72°C 5 min |
| 0.8 μ l DreamTaq | 4°C ∞ |
| ad 50 μ l ddH ₂ O | |

After successful amplification, 5 μ l of the PCR mixtures were incubated with 0.5 μ l ExoI and 1 μ l FastAP (Thermo Scientific) for 15 min at 37°C followed by 15 min at 85°C. Preceding to Sanger sequencing performed at the Cologne Center for Genomics (CCG), the following reaction with BigDye v3.1 and 5x BigDye BDT sequencing buffer (1 M Tris, 1 M MgCl₂, ad 100 ml ddH₂O, pH 9, store at 4°C) was performed:

Table 9: Reaction mixture and program in preparation for PCR product sequencing at the CCG.

| Reaction | Program |
|---|-----------------------------|
| 1 μ l PCR product (digested with ExoI/ FastAP) | |
| 0.25 μ l BigDye v3.1 | 96°C 10 sec 1 |
| 2.25 μ l 5x BigDye BDT sequencing buffer | 55°C 5 sec 32 cycles |
| 0.25 μ l 10 μ M Primer AD5XXL | 60°C 4 min 1 |
| 5 μ l 10x buffer | |
| ad 10 μ l ddH ₂ O | |

2.4.3.3 PCR for cloning of DNA fragments of interest

Coding sequences of interest were amplified using the Phusion™ High-Fidelity DNA Polymerase (Thermo Scientific) due to its proof-reading capacity and thus significantly lower error rates than that of ordinary Taq polymerases. Used reaction mixture and program for Phusion PCRs in this study are presented in table 10.

Table 10: Reaction mixture and program used for PCRs to clone DNA fragments of interest. TA=annealing temperature of used primer pair.

| Reaction | Program |
|----------------------------------|---------------------|
| 1 μ l cDNA | 98°C 30 sec |
| 1 μ l 10 mM Primer forward | 98°C 10 sec 1 |
| 1 μ l 10 mM Primer reverse | TA 30 sec 35 cycles |
| 1 μ l 10 mM dNTPs | 72°C 15-30 sec/kb J |
| 10 μ l 5x HF buffer | 72°C 10 min |
| 0.8 μ l Phusion polymerase | 4°C ∞ |
| ad 50 μ l ddH ₂ O | |

2.4.3.4 Site-directed mutagenesis

Site-directed mutagenesis was employed in this work in order to delete a sequence from a plasmid of interest (Clone IDs: EK035 derived from AST666, table 24, appendix). Towards this, primers were designed with an overlapping region of 25 bp and a PCR was subsequently conducted with Phusion reaction mixture and program (table 10). After successful amplification of the DNA sequence of interest, 1 μ l DpnI (Thermo Scientific) was added to 10 μ l of PCR reaction. The mixture was incubated for 1 h at 37°C and afterwards, 2 μ l of the mixture was used to transform 50 μ l *E. coli* DH5 α .

2.4.3.5 Quantitative real-time PCR (qPCR)

Quantitative real-time PCRs using the double-strand intercalating, fluorescent dye SYBRTM Green (Thermo Scientific), was employed in this work in order to detect and quantify the amplification of gene fragments of interest in real-time. Reaction mixtures (Table 11) were pipetted into 96-well plates suitable for qPCR (BIOplastics BV), which were sealed with designated cover foils (Opti-Seal Optical Disposable Adhesive, BIOplastics BV). qPCR using the program presented in table 11, was executed by a QuantStudio 5 System and subsequent analysis was conducted with the QuantStudio TM Design and Analysis Software version 1.4.1 (ABI/Life Technologies).

Table 11: qPCR reaction mixture and program. Data was collected at the time points indicated by the asterisk.

| Reaction | Program |
|----------------------------------|-----------------------|
| 1 μ l cDNA | 50°C 2 min |
| 0.2 μ l 10 mM Primer forward | 95°C 10 min 1 |
| 0.2 μ l 10 mM Primer reverse | 95°C 15 sec 40 cycles |
| 5 μ l SYBR Green | 60°C 1 min * J |
| ad 10 μ l ddH ₂ O | 95°C 15 sec |
| | 60°C 1 min |
| | 95°C 1 sec * |

qPCR primer design and efficiency testing

Primer pairs implemented in qPCR analysis were designed with GenScript.com. Subsequent testing in two steps secured sufficient quality of primer pairs. First, a normal PCR on wild type cDNA samples (2.4.3.1, table 7) was conducted in order to see if primer pairs amplify a single DNA fragment without primer dimers. Second, qPCR analysis was performed in order to evaluate qPCR primer efficiency. Towards this, average Ct values of two technical and three biological replicates of cDNA dilution series comprising 1:10, 1:20, 1:40, 1:80, 1:160 and 1:320 dilutions of wild type samples were determined.

Subsequent data analysis was conducted manually with Microsoft Excel 2016. The slope of standard curves (average Ct values (y-axis) plotted against the log [10] of the dilutions (x-axis)), was calculated. In order to calculate the efficiency (E), the slope was subsequently deployed in the formula $E = -1 + 10^{(-1/\text{slope})}$. Furthermore, the correlation of the values was determined. Desired qPCR efficiency of reference genes ranges between 90-110% with a correlation between -1 and -0.99. qPCR efficiency of genes of interest is sufficient in the range of 80-120% with a correlation between -1 and -0.99 (Bustin et al., 2009; Stephan et al., 2019). In addition, qPCR melting curves were checked in order to exclude disturbing effects of primer dimers.

Stability of reference genes

Reference gene stability under stress conditions was evaluated using the software BestKeeper (Pfaffl et al., 2004) and geNorm (Vandesompele et al., 2002).

Analysis of relative gene expression

To determine relative gene expression and normalization against one reference gene, qPCR data was analyzed with the $2^{-\Delta\Delta Ct}$ method (Livak and Schmittgen, 2001). For normalization against two reference genes, geometric averaging was employed (Vandesompele et al., 2002).

2.4.3.6 Gel electrophoresis

Amplified DNA fragments were visualized on a 1% agarose gel supplemented with ethidium bromide using 6X DNA loading dye (Thermo Scientific) and 1 kb DNA ladder (Thermo Scientific). Gels were monitored with the Universal Hood II and Quantity One Software version 4.5.0 (BioRad).

2.4.4 Cloning methods**2.4.4.1 Gateway cloning system**

In this work, most of the cloning procedures were executed with the Gateway™ cloning system (Invitrogen), which is easier and more time efficient compared to classical cloning methods (Hartley et al., 2000). The Gateway system is based on the two recombination reactions used by the bacteriophage λ for integration and excision of its DNA into and out of the genome of

E. coli via specific *att* recombination sites (Landy, 1989). The first part of the *in vitro* adaptation is the BP reaction, in which the BP Clonase II enzyme mix, consisting of the λ phage integrase and integrase host factor, catalyzes the transfer of a DNA fragment of interest into a donor vector. In a preceding PCR, the DNA fragment of interest gets amplified and flanked with *attB* sites. The *attB* sites can recombine with *attP* sites carried by Gateway donor vectors (pDONR). After successful recombination, the resulting entry clone (pENTR) now contains the DNA fragment of interest flanked by *attL* sites. In BP reactions of this study, 1.75 μ l PCR product (diluted 1:5 in ddH₂O), 0.25 μ l donor vector (pDONR201 or pDONR207) and 0.5 μ l BP Clonase II enzyme mix were used. The reactions were incubated at RT for 1 h - overnight and subsequently transformed in *E. coli* DH5 α . In the second reaction of the Gateway system, the LR reaction, entry clones are the substrate for generation of expression clones via catalysis by the LR Clonase II enzyme mix consisting of the λ phage integrase, integration host factor and excisionase. The LR Clonase II enzyme mix enables the transfer of the DNA fragment of interest, flanked by *attL* sites in the entry vector, into several destination vectors carrying *attR* sites. The *attL* sites recombine with *attR* sites and thereby an expression vector carrying the DNA fragment of interest can be created, now flanked again by *attB* sites. In LR reactions of this study, 0.5 μ l entry vector, 0.25 μ l destination vector, 0.5 μ l LR Clonase II enzyme mix and 1.75 μ l ddH₂O were used. The reactions were incubated at RT for 1 h - overnight and subsequently transformed in *E. coli* DH5 α . To enable easy selection of successfully recombined clones, donor and destination vectors carry antibiotic resistances and a gene cassette, positioned between *att* recombination sites. The cassette consists of a chloramphenicol resistance and the *ccdB* gene encoding a toxic gene product known to inhibit gyrases. As the *E. coli* strain DB3.1 is insensitive to the toxin, cells of this strain were used to duplicate empty donor and destination vectors. An overview of general donor and destination vectors used in this study can be found in table 5.

2.4.4.2 Cloning of *TZF10* and *11* 3'UTR fragments

The protocol for cloning of *TZF10* and *11* 3'UTR fragments (3.1.9.3) was adapted from Schiml et al. (2016). At first, a DONR201 vector containing a *CFP* (as a placeholder) flanked by BbsI recognition sites, was generated by PCR amplification (primer pair amplifying *CFP* with BbsI sites, table 30, appendix) and subsequent BP reaction (resulting clone ID: EK179). The following LR reaction transferred the module BbsI-*CFP*-BbsI (with BbsI being the recognition sites) into the destination vector UBQ pENSG-YFP resulting in UBQ BbsI-*CFP*-BbsI-ENSG-YFP (clone ID: EK180). 3'UTR fragments were subsequently ordered as oligo sequences (table 12, Sigma) with overhangs complementary to sticky ends resulting from BbsI digestion (F: 5'-ATTG; R: 5'-AAAC, respectively), and annealed (2 μ l of each oligo (50 μ M), ad 50 μ l ddH₂O) for 5 min at 95°C. The mixture was cooled for 20 min at RT.

Table 12: Oligo sequences, containing overhangs complementary to sticky ends resulting from BbsI digestion, used for cloning of *TZF10* and 11 3'UTR fragments.

| Name | Oligo sequences |
|--------------------------------------|---|
| 3'UTR _{TZF10} (P1-1) | F CTCAGAAGCAGAAAGAAAGATGTGGGATTTATATTGCTTTTGTCTTCTGGGCC TCTCTACACAGAATCTAACAAATCTG R ACTACAGATTTGTTAGATTCTGTGTAGAGAGGCCCCAGAAGACAAAAGCAATAT AAATCCCACATCTTTCTTTCTGCTTC |
| 3'UTR _{TZF10} (P1-2) | F CTCAGCAATAATTCTTTGATTTGTGTTTGACCCATAGTTTGGTTACTAGTATAT GTTTTTTTATGTTCTTTTTTCTTTG R ACTACAAAGAAAAAAGAACATAAAAAACATATACTAGTAACCAAATATGGG TCAAACACAAATCAAAGAATTATTGC |
| 3'UTR _{TZF11} (P1-1) | F CTCAACACACACAAAGATGGTTTCTTATATATATTGCTTTTGGGCCATC TCTGCAAA R ACTATTTGCAGAGATGGCCCAAAAGCAATATATAAGAAACCATCTT TGTGTGTGT |
| 3'UTR _{TZF11} (P1-2) | F CTCATTTGATTCTTTAATTTTTGTGACTTTCTTTAGTTGTTACTGTTAT TAGTAGTAT R ACTAATACTACTAATAACAGTAACAACAAAGAAAGTCACAAAAATTA GAATCAAA |
| 3'UTR _{TZF10} (P1-1-1) | F CTCAGAAGCAGAAAGAAAGATGTGGGATTTATATTGCTTTTGTG R ACTAGACAAAAGCAATATAAATCCCACATCTTTCTTTCTGCTTC |
| 3'UTR _{TZF10} (P1-1-2) | F CTCATTCTGGGCCTCTCTACACAGAATCTAACAAATCTG R ACTACAGATTTGTTAGATTCTGTGTAGAGAGGCCCCAGAA |
| 3'UTR _{TZF10} (P1-1-C) | F CTC AATTTATATTGCTTTTGTCTTCTGGGCCTCTCTACACA R ACTATGTGTAGAGAGGCCCCAGAAGACAAAAGCAATATAAAT |
| 3'UTR _{TZF11} (P1-1-1) | F CTC AACACACACAAAGATGGTTTCTTATATATATTGCTTTTGTG R ACTACAAAAGCAATATATAAGAAACCATCTTTGTGTGTGT |
| 3'UTR _{TZF11} (P1-1-C) | F CTC AATATATATTGCTTTTGGGCCATCTCTGCAAA R ACTATTTGCAGAGATGGCCCAAAAGCAATATATAT |
| 3'UTR _{TZF10} (P1-1-C) MUT1 | F CTC AAGGGAGAGGGCGGGGGTCTTCTGGGCCTCTCTACACA R ACTATGTGTAGAGAGGCCCCAGAAGACCCCGCCCTCTCCCT |
| 3'UTR _{TZF10} (P1-1-C) MUT2 | F CTC AAGGGAGAGGGCGGGGGTCTTCTGGGCCGCGCGGCGCG R ACTACGCGCCGCGCGGCCCCAGAAGACCCCGCCCTCTCCCT |

The destination vector UBQ BbsI-*CFP*-BbsI-*ENSG*-YFP was digested with BbsI (10 µl vector, 2 µl Buffer Green, 1 µl BbsI (Thermo Scientific), 7 µl ddH₂O) for at least 1 h at 37°C. After purification of the restriction digest (using elution buffer and columns from the GeneJET Gel Purification Kit, Thermo Scientific, according to the manual), a ligation (2µl digested vector, 3 µl annealed oligos, 1 µl T4 ligase, 1 µl 10x ligase buffer (Thermo Scientific), 9 µl ddH₂O) was performed and incubated for 1 h at RT. 5 µl of the reaction was subsequently used to transform *E. coli* DH5α.

2.4.5 Plasmid purification, restriction digest and sequencing

Selective LB medium (5 ml) was inoculated with a single colony of transformed *E. coli* and grown overnight under constant shaking at 220 rpm at 37°C. The culture was centrifuged for 2 min at 8000 rpm and plasmid purification was subsequently performed with the GeneJET

Plasmid Miniprep Kit (Thermo Scientific) according to the manufacturer's protocol. The plasmid DNA was eluted in 50 μ l elution buffer, resulting in a usual concentration of 150-400 ng/ μ l. Plasmid DNAs were further digested with suitable restriction enzymes (most often used and suitable for Gateway clones: BsrGI (Thermo Scientific) reaction mix with 2 μ l plasmid DNA, 2 μ l 10x buffer, 0.3 μ l enzyme and 15.7 μ l ddH₂O, 37°C, 1 h) and subjected to 1% agarose gel electrophoresis. If band patterns showed expected sizes, plasmid DNA was sequenced at GATC (LightRun, Eurofins Genomics) using suitable primers for sequencing (2.5 μ l DNA, 2.5 μ l 10 mM primer, 5 μ l ddH₂O). Most frequently, a standard primer pair (SelA/SelB, table 30, appendix) was used to sequence inserts in Gateway-compatible plasmids. If insert lengths exceeded the reading limit of Sanger sequencing (800-1000 bp), appropriate gene-specific primers were designed.

2.4.6 Generation of chemically competent cells

To assure sterile environment, all steps during the generation of competent cells were performed under a laminar flow hood.

For the generation of chemically competent *E. coli* (DH5 α , DB3.1) cells, 5 ml of LB medium without antibiotics was inoculated with 50 μ l of competent *E. coli* cells and grown overnight at 37°C under constant shaking (220 rpm). 1 ml of the pre-culture was used to inoculate 200 ml of LB medium without antibiotics. The main culture was grown at 37°C under constant shaking (220 rpm) until it reached an OD₆₀₀ of 0.4 (approximately 2 h). The cells were centrifuged at 1600g for 7 min at 4°C and pellets were subsequently resuspended in a total of 40 ml sterile CaCl₂ solution (60 mM CaCl₂, 10 mM PIPES, 15% glycerol, pH 7). The cultures were centrifuged at 1100g for 5 min at 4°C. Afterwards, the pellets were resuspended in a total of 40 ml sterile CaCl₂ solution and incubated on ice for 30 min. Again, cultures were centrifuged at 1100g for 5 min at 4°C and pellets were resuspended in a total of 8 ml of sterile CaCl₂ solution. Aliquots of 50 and 100 μ l competent cells were quickly pipetted at 4°C, frozen in liquid N₂ and stored at -80°C.

For the generation of chemically competent *A. tumefaciens* (GV3101 pMP90RK, pMP90) cells, 5 ml of YEB medium containing 20 mg/l rifampicin was inoculated with 50 μ l of competent *A. tumefaciens* cells and grown overnight at 28°C under constant shaking (200 rpm). 2.5 ml of the overnight culture was used to inoculate 250 ml of YEB medium containing 20 mg/l rifampicin and the culture was grown until an OD₆₀₀ of 0.5 - 0.6 was reached. The culture was centrifuged at 4000 rpm for 15 min, pellets were resuspended in a total of 25 ml ice-cold, sterile 0.15 M NaCl₂ solution and incubated for 15 min on ice. Subsequently, the culture was again centrifuged at 4000 rpm for 15 min and pellets were resuspended in a total of 5 ml ice-cold, sterile 20 mM CaCl₂. Aliquots of 50 and 100 μ l competent cells were quickly pipetted at 4°C, frozen in liquid N₂ and stored at -80°C.

2.4.7 Heat-shock transformation of chemically competent cells

For transformation of chemically competent *E. coli* (DH5 α , DB3.1) cells, 0.5 μ l plasmid DNA or 2.5 μ l BP/LR reactions were incubated with 50 μ l of cells for 10-20 min on ice. Subsequently, a heat-shock of 42°C for 1:30 min was applied. 300 μ l of LB medium without antibiotics was added and the transformed cells were incubated for 30-60 min at 37°C under constant shaking (650 rpm). The cells were centrifuged for 2 min at 8000 rpm and the supernatant was discarded. The cells were resuspended in remaining LB medium, plated on selective LB agar and incubated overnight at 37°C.

Transformation of chemically competent *A. tumefaciens* (pMP90RK, pMP90) cells was done according to the described protocol with slight modifications. 2 μ l plasmid DNA was used, 700 μ l YEB without antibiotics was added after heat-shock and cells were incubated for 1:30 h at 28°C before plating 100 μ l without centrifugation on selective YEB agar. The agrobacteria were grown for 2-3 days at 28°C.

2.5 Biochemical techniques

2.5.1 Protein extraction from *A. thaliana* leaf tissue

A defined weight (around 100 mg) of leaf tissue was transferred to 2 ml safe lock reaction tubes containing 3-4 glass beads (\varnothing 2.7 mm). The material was frozen in liquid N₂ and either directly processed or stored at -80°C. Before extraction, the samples were shredded in a tissue lyzer (Qiagen) for 1 min at 30 Hz and quickly frozen again in liquid N₂. This step was repeated once. Subsequently, the tissue was mixed 1:1 with SDS sample buffer (50 mM Tris/HCl pH 6.8, 10% Glycerol, 2% SDS, 0.1% Bromophenol Blue; freshly supplemented with 100 mM DTT) and incubated for at least 10 min at 99°C. Protein extracts were stored short-term at RT or 4°C and long-term at -20°C.

2.5.2 SDS-PAGE

For SDS-PAGE, 15-20 μ l of protein extracts were run in 8% SDS separation gels (for 1 gel (5 ml): 2.3 ml ddH₂O, 1.3 ml acrylamide mix (Rotiphorese Gel 30, Roth), 1.3 ml 1.5 M Tris/HCl pH 8.8, 50 μ l 10% SDS, 50 μ l 10% ammoniumpersulfate (APS), 3 μ l tetramethylethylenediamine (TEMED)) and stacking gels (for 1 gel (1ml): 0.68 ml ddH₂O, 0.17 ml acrylamide mix, 0.13 ml 1.5 M Tris/HCl pH 6.8, 10 μ l 10% SDS, 10 μ l 10% APS, 1 μ l TEMED) for 60-90 min at 20 mA per gel in fresh 1X SDS-electrophoresis buffer (3.03 g Tris, 18.1 g glycine, 10 ml 10%SDS, up to 1 l with ddH₂O).

2.5.3 Coomassie staining

To visualize the protein content of total protein extracts, SDS gels were stained with a Coomassie solution (80 mg Coomassie Brilliant Blue G-250, 35 mM HCl, ad 1 l ddH₂O, overnight shaking in darkness before first usage). The gels were boiled for 3 min in ddH₂O,

subsequently soaked in Coomassie solution and again cooked for a few minutes. The Coomassie solution was discarded afterwards. Additional boiling steps in ddH₂O followed until the gels showed adequate staining intensity.

2.5.4 Semi-dry immunoblotting (western blotting)

Semi-dry immunoblotting (western blotting) was employed in this work in order to detect proteins of interest using specific antibodies.

For the electrophoretic transfer of proteins, SDS gels were quickly washed in cathode buffer (1 l: 100 ml Roti®Blot 2K (Roth), 50 ml methanol, 850 ml ddH₂O) and subsequently placed onto a methanol-activated polyvinylidene fluoride-membrane (PVDF, Roth). The gel and membrane in turn were placed between two Whatman papers soaked in cathode or anode buffer (1 l: 100 ml Roti®Blot 2A (Roth), 50 ml methanol, 850 ml ddH₂O). The transfer of proteins from gels onto membranes was conducted with 40 mA for 17 h at 4°C. Afterwards, the PVDF membranes were blocked in phosphate buffer saline with 0.1% Tween-20 (PBST, 1 l: 8 g NaCl, 0.2 g KCl, 1.44 g Na₂HPO₄, 0.24 g KH₂PO₄, 1 ml Tween-20, ad 1 l ddH₂O) supplemented with 5% milk for 1h. Detection of YFP and YFP-tagged proteins of interest was performed by subsequent incubation of membranes with a mouse α -GFP antibody (Roche), diluted 1:2000 in 5 ml PBST + 5% milk under constant rotation for 1h. Afterwards, the membranes were washed three times with 20 ml PBST for 10 min, and incubated with a second goat α -mouse antibody (Merck) diluted 1:10000 in 5 ml PBST under constant rotation for 1 h. Chemiluminescence of coupled horseradish peroxidase was detected with the West Femto Maximum Sensitivity Kit (Thermo Scientific) at a LAS4000 (Amersham).

2.6 Plant techniques

2.6.1 Plant growth conditions for *A. thaliana* and *M. polymorpha*

Seeds of *A. thaliana* were either sown on soil or cultivated axenically on half strength Murashige and Skoog medium (½ MS; Duchefa; 2.15 g/l, 0.8% plant agar, adjust pH to 5.7 with 1 M KOH, autoclave; Murashige and Skoog, 1962) supplemented with 0.8% plant agar. The plants were grown under long day conditions (16 h light/8 h darkness cycle) at 21°C and 120 $\mu\text{mol m}^{-2} \text{s}^{-1}$ light intensity.

For axenic vegetative propagation, gemmae of *M. polymorpha* were put out on Johnson's medium (Table 13) supplemented with 0.8 % plant agar and grown under long day conditions (16 h light/8 h darkness cycle) and white light irradiation (60 $\mu\text{mol m}^{-2} \text{s}^{-1}$) at 21°C.

Table 13: Composition of the standard medium Johnson's for cultivation of *M. polymorpha*.

| Johnson's medium (Johnson et al., 1957) |
|--|
| 20 ml Stock A (30.3 g/l KNO ₃ ; 6.15 g/l MgSO ₄) |
| 20 ml Stock B (47.2 g/l Ca(NO ₃) ₂ *4 H ₂ O) |
| 100 mg Inositol |
| 1 ml Stock C (1.864 g/l KCl; 0.773 g/l H ₃ BO ₄ ; 0.223 g/l MnSO ₄ *4 H ₂ O; 0.288 g/l ZnSO ₄ *7 H ₂ O; 0.0624 g/l CuSO ₄ *5 H ₂ O; 0.309 g/l (NH ₄) ₆ Mo ₇ O ₂₄ *4 H ₂ O) |
| 1 ml Stock D (6.95 g/l FeSO ₄ *7 H ₂ O; 9.365 g/l Na ₂ EDTA) |
| 535.2 mg/l (NH ₄) ₂ SO ₄ |
| 69 mg/l NH ₄ H ₂ PO ₄ |
| 533 mg 2-(<i>N</i> -morpholino)ethanesulfonic acid (MES) |
| 10 g/l sucrose |
| 0.8% plant agar |
| ad 1 l with ddH ₂ O; adjust pH to 5.6 with 1 M KOH; autoclave |

To induce the reproductive growth phase of *M. polymorpha*, three- to four-week-old, axenically grown thalli were transferred into semi-sterile, soil containing microboxes (SacO₂, Belgium). Plants were grown under long day conditions (16 h light/8 h darkness cycle) and white light irradiation (60 $\mu\text{mol m}^{-1} \text{s}^{-1}$) supplemented with far-red (FR) light (700-880 nm; 15 $\mu\text{mol m}^{-1} \text{s}^{-1}$) at 21°C for at least four weeks.

2.6.2 Seed sterilization *A. thaliana*

Before axenic cultivation, seeds of *A. thaliana* were surface-sterilized. The seeds were transferred to 2 ml reaction tubes, placed into a desiccator, and set out to the vapor of an approximately 5:1 mixture of NaOCl and HCl for at least 3 h.

2.6.3 Crossing of *A. thaliana* and *M. polymorpha* plants

For crossing of *A. thaliana* plants, the pollen receiving plant was emasculated by removal of the anthers. Subsequently, the stigma was pollinated with pollen of the other crossing partner. All steps were executed with forceps under the binocular microscope.

For crossing of *M. polymorpha* plants, drops of sterile ddH₂O were placed onto fully developed antheridiophores and incubated for several minutes. The ddH₂O containing sperm, visible by its opaque color, was afterwards collected into a 1.5 ml reaction tube and subsequently distributed on mature archegoniophores. If the crossing procedure was successful, sporangia developed after approximately four weeks.

2.6.4 Analysis of *M. polymorpha* rhizoid growth and biomass

To assess rhizoid growth defects, the measurement of maximum rhizoid length was performed. Gemmae were grown vertically for seven days on solid Johnson's under normal conditions. For each of the $n \geq 10$ gemmalings, the 10 longest rhizoids were measured. For biomass

measurements, the fresh weight of $n \geq 10$ 14-day-old gemmalings, grown horizontally on solid Johnson's under normal conditions, was determined after careful removal of residual agar in rhizoids. To assure even growth conditions and nutrient availability, mutant and wild type plants were grown on the same plate. The plates were regularly shuffled in the growth cabinet in order to exclude effects of different exposure to light.

2.6.5 Salt stress treatments

2.6.5.1 Analysis of primary root growth rates

Surface-sterilized *A. thaliana* seeds were sown on solid $\frac{1}{2}$ MS, stratified for at least four days, and subsequently grown vertically for eight days under normal conditions. Afterwards, the seedlings were carefully transferred onto solid $\frac{1}{2}$ MS supplemented with and without 125 mM NaCl, respectively. For each genotype and condition, two to three plates with 12-15 plants each were prepared. The plants were allowed to further grow vertically under normal conditions. The day after transfer (day 0), the end points of primary roots were marked clearly. At day 5, pictures of the plants were taken and primary root lengths were determined with ImageJ. Primary root growth (cm/day) of plants grown on salt-containing medium was calculated and set in relation to primary root growth of plants grown on control medium.

2.6.5.2 Root bending assay

Surface-sterilized *A. thaliana* seeds were sown on solid $\frac{1}{2}$ MS, stratified for at least four days, and subsequently grown vertically for seven days under normal conditions. Afterwards, the seedlings were carefully transferred onto solid $\frac{1}{2}$ MS, supplemented with and without 125 mM NaCl, respectively. For each genotype and condition, three plates with 12-15 plants each were prepared. The plants were allowed to further grow vertically, but this time with roots upside down, under normal conditions. The root bending was documented after another seven days.

2.6.5.3 Salt stress treatments preceding *TZF10* expression analysis

For salt stress timeline experiments, seeds of plant lines of interest were surface-sterilized, stratified for at least four days and vertically grown on solid $\frac{1}{2}$ MS under normal conditions. After 14 days, the seedlings were carefully transferred to liquid $\frac{1}{2}$ MS. To allow acclimation, the seedlings were at first constantly shaken under normal conditions for 1 h. Afterwards, NaCl was added to a final concentration of 200 mM. Control plants were treated with addition of respective amounts of ddH₂O. At designated time points (3.1.4), three biological replicates of seedlings in pools of 2-3 plants each were harvested. The samples were frozen in liquid N₂ and either directly further processed in RNA isolations or stored at -80°C.

2.6.5.4 Analysis of *M. polymorpha* rhizoid growth and biomass on salt-containing medium

To examine potential salt hypersensitivity, gemmae were grown on solid Johnson's supplemented with and without 50 mM NaCl. The determination of maximum rhizoid length and fresh weight after 7 and 14 days, respectively, was performed as described above (2.6.4). Average reductions of rhizoid length and biomass on salt-containing medium were calculated and were set in relation to length and biomass acquired on control medium.

2.6.5.5 Salt stress screening of T₂ plants

For salt stress screenings, transgenic *A. thaliana* lines of the T₂ generation (3.1.6) were sown on round plates (diameter: 15 cm, height: 2 cm) filled with 70 ml ½ MS supplemented with 125 mM. Three lines were sown in separate areas on one plate with 40-50 surface-sterilized seeds each, and stratified for three days at 4 °C. Afterwards, the plants were horizontally grown under normal conditions for four weeks.

2.6.6 Heat stress treatment

For heat stress treatment and induction of stress granule formation, transiently transformed leaves of *A. thaliana* or *N. benthamiana* were subjected to 40°C for 50 min. Leaves were kept on ½ MS plates in order to keep them moist during the treatment.

2.6.7 Actinomycin D treatment of *A. thaliana* seedlings

Preceding to mRNA stability assays, surface-sterilized seeds of plant lines of interest were either sown on solid ½ MS (control lines) or on solid ½ MS supplemented with 10 µg/ml Basta® (Aventis; transgenic lines, table 3) and stratified for at least three days at 4°C. Afterwards, the plants were vertically grown under normal conditions for 14 days. The plants were transferred to 6-well plates and incubated in liquid ½ MS (2 ml and up to 12 seedlings per well) under constant rotation and normal conditions. After 1 h, NaCl was added to half of the samples to a final concentration of 200 mM. Control plants were treated with addition of respective amounts of ddH₂O. After another 1 h of incubation under constant rotation and normal conditions, actinomycin D (ActD, stock: 10 mg/ml in 100% dimethyl sulfoxide (DMSO)) was added to again half of the samples to a final concentration of 150 µg/ml (an overview on the experimental setup is given in fig. 17, 3.1.5.2). Control samples were treated with respective amounts of DMSO. At designated time points (Fig. 17, 3.1.5.2), three biological replicates of seedlings in pools of 2-3 plants each were harvested. The samples were frozen in liquid N₂ and either directly further processed in RNA isolations or stored at -80°C.

2.6.8 Transient transformation by particle bombardment

Plant materials used for transient transformation by particle bombardment were either *Marchantia* thallus fragments of two- to three-week-old plants or *Arabidopsis* leaves of three-

to four-week-old plants placed on ½ MS plates. For DNA preparation of a single shot, approximately 300 ng of vector DNA were mixed with microcarriers (30 mg/ml gold, 1 µm), CaCl₂ (2.5 M), spermidine (0.1 M) and ddH₂O (ad 25 µl). After vigorous shaking (1300 rpm, at least 3 min), microcarriers were washed in subsequent steps using 70% and 100% EtOH. The DNA-coated microcarriers were resuspended in 100% EtOH and applied onto macrocarriers. Biolistic transformation was carried out with a PDS-1000 / He Biolistic® Particle Delivery System (Bio-Rad). Upon application of a vacuum of 25 in Hg vac, DNA-coated gold particles were shot at 900 psi into the plant tissue. The bombarded material recovered overnight in darkness.

2.6.9 Transient transformation by infiltration of *N. benthamiana* leaves

25 ml YEB medium containing appropriate antibiotics was inoculated with colonies of transformed Agrobacteria and grown overnight on 200 rpm at 28°C. The cultures were centrifuged (4000 rpm, 15 min) and pellets were resuspended in 1x Agromix (90 ml 10x Agromix (100 mM MgCl₂ x 6 H₂O, 100 mM MES, set pH on 5.6), 10 ml 3,5-dimethoxy-4-hydroxyacetophenon (3 mg/ml in 100% EtOH), 900 ml ddH₂O).

2.6.10 Stable transformation and selection of *A. thaliana*

5 ml YEB medium containing appropriate antibiotics were inoculated with colonies of transformed agrobacteria and grown overnight on 200 rpm at 28°C. The next day, 500 µl of that culture was used to inoculate 200 ml selective YEB medium. The mixture was grown again overnight - 24 h on 200 rpm at 28°C. Afterwards, 10 g of sucrose and 40 µl of Silwet L-77 were added to the culture and incubated under constant shaking (200 rpm) for another 10 min. Designated plants were dipped into the culture to allow full coverage of flowers with bacterial suspension. The transformed plants were kept in a wet and dark environment overnight before they were grown again under greenhouse conditions until the ripening of seeds.

After floral dipping, seeds of the transformed T₀ generation, giving rise to the T₁ generation, were sown on soil and as soon as seedlings started to germinate, sprayed with a 0.1% Basta solution supplemented with 0.001% Tween-20. After one to two weeks, surviving T₁ plants were screened for expected fluorescence and further cultivated on soil and in greenhouse conditions.

2.6.11 Stable transformation and selection of *M. polymorpha*

Stable transformation of *M. polymorpha* thalli was conducted with modifications according to Kobuta et al. (2013). Gemmae were grown on medium M1 (1X Gamborg B5, 0.5 g/l MES, 0.8% plant agar, pH 5.7). After growth of two to three weeks under normal conditions, thalli were cut into four pieces and thereby apical notches were removed. The thallus fragments

were allowed to regenerate for three days on medium M2 (1X Gamborg B5, 10 g/l sucrose, 0.8% plant agar, pH 5.7).

The day before transformation, 5 ml of selective YEB medium were inoculated with colonies of transformed agrobacteria and grown overnight on 200 rpm at 28°C. On transformation day, the culture was centrifuged (4000 rpm, 15 min) and the pellet was resuspended in 5 ml M51C medium (Table 14) containing 2% sucrose and 100 µM 3,5-dimethoxy-4-hydroxyacetophenon. After growth of 5-8 h at 28°C, 200 rpm, 1 ml of the agrobacteria culture was used to inoculate 50 ml M51C medium containing 2% sucrose and 100 µM 3,5-dimethoxy-4-hydroxyacetophenon. Approximately 100 regenerated thallus fragments were added and co-cultivated with agrobacteria for three days under constant shaking in long day conditions (16 h light/8 h darkness cycle) and white light irradiation (60 µmol m⁻¹ s⁻¹) at 21°C. Afterwards, the thallus fragments were washed in 1 g/l cefotaxime under constant shaking for 45 min. The fragments were then put out on selective medium M3 (1X Gamborg B5, 0.8% plant agar, pH 5.7) containing appropriate antibiotics (10 µg/ml G418 or 5 µM chlorsulfuron, respectively) and 100 µg/ml cefotaxime to eliminate growth of remaining agrobacteria.

Table 14: **Composition of M51C medium used in transformations of *M. polymorpha* thalli.**

| M51C medium (Ono et al., 1979; Ishizaki et al., 2008) |
|--|
| 2 g/l KNO ₃ |
| 0.4 g/l NH ₄ NO ₃ |
| 0.37 g/l MgSO ₄ *7 H ₂ O |
| 0.3 g/l CaCl ₂ *2 H ₂ O |
| 0.275 g/l KH ₂ PO ₄ |
| 0.04 g/l EDTA-NaFe(III) |
| B5 micronutrients (0.25 mg NAMoO ₄ *2 H ₂ O; 0.025 mg CuSO ₄ *5 H ₂ O; 0.025 mg CoC ₂ *6 H ₂ O; 2 mg ZnSO ₄ *7 H ₂ O; 10 mg MnSO ₄ *7 H ₂ O; 3 mg H ₃ BO ₃) |
| B5 vitamins (100 mg Inositol; 1 mg Nicotinic Acid; 1 mg Pyridoxine-HCl; 10 mg Thiamine-HCl) |
| 0.75 mg/l KI |
| 20 g/l sucrose |
| 0.3 g/l L-Glutamine |
| 1 g/l Casamino-Acids |
| ad 1 l with ddH ₂ O; autoclave |

As transformants emerging on the first selective medium could still be genetically chimeric, gemmae deriving from first transformants (G₁) were grown again on respective selective medium. Experiments were not performed earlier than with isogenic gemmae/gemmalings/thalli deriving from this (G₂) or later generations (according to Ishizaki et al., 2016).

2.6.12 Fluorescein diacetate staining

For fluorescein diacetate (FDA) staining of *M. polymorpha*, young (two- to five-days-old) gemmae were put onto depression slides and covered with an FDA solution (5 mg/l FDA in ddH₂O, diluted from a stock solution of 5 mg/ml FDA in acetone) for 5-10 min. Subsequently, samples were rinsed in ddH₂O (Westermann et al., 2020).

2.6.13 Propidium iodide staining

For propidium iodide (PI) staining of *M. polymorpha*, young (two- to five-days-old) gemmae were put onto depression slides and covered with a PI solution for 10 min (10 mg/l in ddH₂O). Afterwards, samples were rinsed with ddH₂O (Westermann et al., 2020).

2.6.14 Microscopic analysis and confocal laser scanning microscopy (CLSM)

Microscopic observation of *A. thaliana* and *M. polymorpha* samples was executed with a Leica MZ 16 F fluorescence binocular or a Leica TCS SP8 CLSM using an HC PL APO 20x/0.75 IMM CORR CS2 objective. CLSM images were captured at a digital gain of 100%, a resolution of 1024x1024 pixels and bidirectional scanning with a speed of 700 Hz. Multiple fluorophores were scanned with different detectors, sequentially by line. To reduce noise or optimize signal intensities, line/frame averaging and/or accumulation were applied. Table 15 shows fluorescence excitation and detection of emission according to wave-length spectra of used fluorophores.

Table 15: Confocal microscopy settings for excitation and detection of fluorophores.

| Fluorophore | Excitation | Detection with HyD |
|-------------|---------------------------|--------------------|
| CFP | 458 nm (Argon laser, 20%) | 470 nm – 480 nm |
| YFP | 514 nm (Argon laser, 20%) | 524 nm – 530 nm |
| mCherry | 561 nm (DPSS561) | 607 nm – 618 nm |
| mVenus | 514 nm (Argon laser, 20%) | 520 nm – 535 nm |
| Citrine | 514 nm (Argon laser, 20%) | 520 nm – 535 nm |
| TagRFP | 561 nm (DPSS561) | 570 nm – 590 nm |
| FDA | 514 nm (Argon laser, 20%) | 500 nm – 540 nm |
| PI | 561 nm (DPSS561) | 610 nm – 630 nm |

2.7 Protein-protein interaction assays

2.7.1 Yeast two-hybrid pairwise interaction assay

The yeast two-hybrid system was introduced in 1989 by Fields and Song as a novel method for detection of protein-protein interactions. The method is based on the properties of the GAL4 protein of *Saccharomyces cerevisiae*. The proteins of interest are fused to GAL4-binding (GAL4-BD) and activation (GAL4-ACT) domains by integration of the genes into the yeast expression vectors pAS (GAL4-BD) and pACT (GAL4-ACT). For co-transformation, the yeast

strain AH109 is used as it is incapable of biosynthesis of the essential amino acids histidine (H), tryptophan (W) and leucine (L).

10 ml YPAD medium (8 g Difco peptone, 4 g yeast extract, 40 mg adenine, 380 ml ddH₂O, pH 5, autoclaved; 2% glucose) were inoculated with AH109 cells and grown overnight at 30°C under constant shaking (200 rpm). The next day, 1 ml of the pre-culture was used to inoculate 50 ml YPAD (sufficient for 10-15 transformations) and grown for approximately 3-4 h at 30°C under constant shaking until an OD₆₀₀ of 0.8 was reached. The cultures were centrifuged (4000 rpm, 5 min) and pellets were resuspended in 0.1 M LiAc. The cells were again centrifuged (4000 rpm, 5 min), the supernatant was discarded, and cells were resuspended in remaining LiAc. For each transformation, 240 µl PEG3350, 36 µl 1 M LiAc, 10 µl ssDNA (10 mg/ml, heated at 99°C for 10 min) and 65 µl ddH₂O were added to the cells, and the mixture was vigorously vortexed for 30 sec. 350 µl of the yeast suspension were added to 1 µl of each plasmid DNA (1 µl pAS with integrated gene of interest and 1 µl pACT with integrated gene of interest) in 1.5 ml reaction tubes, shortly vortexed and subsequently incubated at 42°C for 40 min. Afterwards, the cells were centrifuged (6000 rpm, 30 sec) and resuspended in 100 µl ddH₂O before plating them on SD-LW medium (0.68 g yeast nitrogen base w/o amino acids and (NH₄)₂SO₄, 2 g (NH₄)₂SO₄, 0.24 g DO Supplement -LWH, 8 mg histidine, 40 mg adenine, 7.2 g agar, 380 ml ddH₂O, pH 5.8, autoclaved, 2% glucose). As the yeast expression vectors pAS and pACT harbor the genes for biosynthesis of W and L, respectively, it enables AH109 to grow on medium lacking W and L after successful co-transformation of both plasmids. The yeast was grown for five to seven days on SD-LW at 30°C. Colonies of the yeast were then picked, pooled (at least five colonies per transformation) and resuspended in 100 µl ddH₂O. Subsequently, the yeast was stamped on SD-LWH medium (0.68 g yeast nitrogen base w/o amino acids and (NH₄)₂SO₄, 2 g (NH₄)₂SO₄, 0.24 g DO Supplement -LWH, 40 mg adenine, 7.2 g agar, 380 ml ddH₂O, pH 5.8, autoclaved, 2% glucose) containing ascending concentrations (5, 15, 30 mM) of 3-AT (42.04 g 3-amino 1,2,4-triazole, ad 500 ml ddH₂O, sterile filtrated). Protein interactions can be detected on medium lacking L, W and H as AH109 is only able to grow if the GAL4-BD and GAL4-ACT come in spatial proximity via interaction of the two proteins of interest, and thereby can activate the expression of a H biosynthesis gene that is stably transformed in AH109. Growth of yeast on SD-LWH was documented three, five and seven days after stamping. An interaction between two proteins of interest was considered as positive, when growth of yeast was observed in at least three independent transformations and when the negative control (pAS with integrated gene of interest + pACT-GFP) did not show growth on the same plate at the same day.

2.7.2 Yeast two-hybrid interaction screening

In order to screen for interaction partners of proteins of interest in this work, a yeast two-hybrid interaction screening was performed.

Yeast AH109 transformation with proteins of interest as bait proteins (integrated into pAS (GAL4-BD)) was performed as described above (2.7.1). Afterwards, 200 ml SD-W medium (0.68 g yeast nitrogen base w/o amino acids and $(\text{NH}_4)_2\text{SO}_4$, 2 g $(\text{NH}_4)_2\text{SO}_4$, 0.24 g DO Supplement -LH, 8 mg histidine, 40 mg adenine, 7.2 g agar, 380 ml ddH₂O, pH 5.8, autoclaved, 4% glucose) were inoculated with transformed yeast (per bait and library), and grown overnight at 30°C under constant shaking (200 rpm). The next day, libraries of interest (Table 22, 3.1.10) were thawed in the water bath at 42°C. Subsequently, 8 ml of each library was added to 12 ml YPAD (=1 OD/ml) and incubated for 1 h at 30°C under constant shaking (200 rpm). The OD₆₀₀ of all cultures was measured and 10 OD of bait culture were mixed with 10 OD of each library. The mixture was centrifuged at 4000 rpm for 5 min at RT, the supernatant was discarded and the pellet was resuspended in 10 ml YPAD + 10% PEG6000. The dissolved pellets were incubated overnight under constant shaking at 80 rpm and 30°C. The next day, the cultures were centrifuged at 4000 rpm for 5 min at RT. The supernatant was discarded and each pellet was dissolved in 15 ml SD-LWH + 3 mM 3-AT + 100 µg/ml ampicillin + 0.05 % Gelrite® (Serva), and subsequently unified with in total 500 ml of the same medium. The mixture was distributed to round petri dishes (diameter: 9 cm) and incubated for 5-10 days at 30°C. Subsequently, colonies were picked (in 10 µl Gelrite medium) and pipetted into 100 µl SD-LWH in microtiter plates. The colonies were afterwards stamped onto plates containing SD-LWH + 3mM 3-AT and incubated overnight at 30°C. Information on reaction mixture, program, and sequencing of yeast colony PCRs performed the next day can be found in 2.4.3.2, table 8.

2.8 Computational analysis

Computational analysis in the course of this work was conducted with the software listed in table 16. Other software used in this study is directly mentioned in respective chapters.

Table 16: Software used in this study.

| Software | Application |
|--|--|
| Microsoft Office 2016 | Processing of texts and figures; statistical analysis |
| Inkscape vector graphics editor 0.92.3 | Figure composition and creation |
| ImageJ 1.52i | Image processing, measurements of root- and rhizoid length / gemmae- and cell area / mean gray intensity |
| CLC DNA Workbench 5.6.1 | Sequence analysis, <i>in silico</i> cloning, alignments and phylogenetic tree construction |
| Leica Application Suite X 3.4.2 | Confocal image examination |

3 RESULTS

The results gained in the course of this work are presented in two separate parts. While the first part focusses on the investigation of the interplay between TZF proteins and the BDCP SPIRRIG in *A. thaliana*; results obtained by the characterization of SPIRRIG in *M. polymorpha* are presented in the second part.

3.1 The interplay of TZF10 and 11 with the BDCP SPIRRIG in Arabidopsis salt stress response

In yeast two-hybrid interaction screenings with the C-terminal part of SPIRRIG as the bait protein, TZF10 and 11 were identified as SPIRRIG interaction partners (M. Jakoby, A. Steffens, unpublished data). The interactions were confirmed in pairwise yeast two-hybrid assays, co-immunoprecipitation experiments of bacterially expressed proteins and bimolecular fluorescence complementation (BiFC) experiments in transiently transformed *N. benthamiana* leaves (A. Steffens, unpublished data).

This result strongly hinted to a newly discovered connection between the TZF proteins known to induce mRNA decay at P-bodies in humans (Sanduja et al., 2010), and the BDCP SPIRRIG, which was found to be associated with P-bodies and mRNA regulation as well (Steffens et al., 2015). In plants, the involvement of TZF proteins in mRNA regulation and the mechanism, by which TZF proteins in plants potentially affect mRNA decay, is not nearly as well understood as in humans.

In order to elucidate the interplay of SPIRRIG and TZFs, with a special focus on potential regulatory mechanisms mediated by the *TZF* 3'UTR, a variety of different approaches was applied in this work. Results gained from localization assays, rescue experiments, analysis of mRNA expression and stability in salt stress response and interaction studies are presented in the following. If not stated otherwise, all proteins and genes mentioned below refer to *A. thaliana*; therefore, respective prefixes have been omitted.

3.1.1 TZF10 localizes to cytoplasmic mRNA granules

The human zinc finger protein TTP is securely established as a component of stress granules and P-bodies, not only by its prominent function in mRNA regulation, but also by co-localization with SG and PB marker proteins (Rigby et al., 2005; Kedersha et al., 2005). In contrast, the connection of plant TZFs to mRNA granules has not been fully elucidated yet. All 11 Arabidopsis RR-TZF family members have been shown to localize to cytoplasmic foci in maize protoplasts (Pomeranz et al., 2010b). However, the study did not include co-localization analysis with mRNA granule marker proteins. Only for TZF1 and TZF9, direct co-localization with both SG and PB markers was demonstrated so far (Pomeranz et al., 2010a; Tabassum et al., 2020, respectively).

Preceding experiments revealed co-localization of TZF10 with the PB marker DCP1 under non-stress conditions (A. Steffens, unpublished data). In addition, co-localization of TZF10 with the Arabidopsis SG marker UBP1b upon stress conditions was tested in this study. As heat stress is particularly efficient and feasible for plant material, the transformed leaves were treated with 40°C for 50 min to induce stress responses.

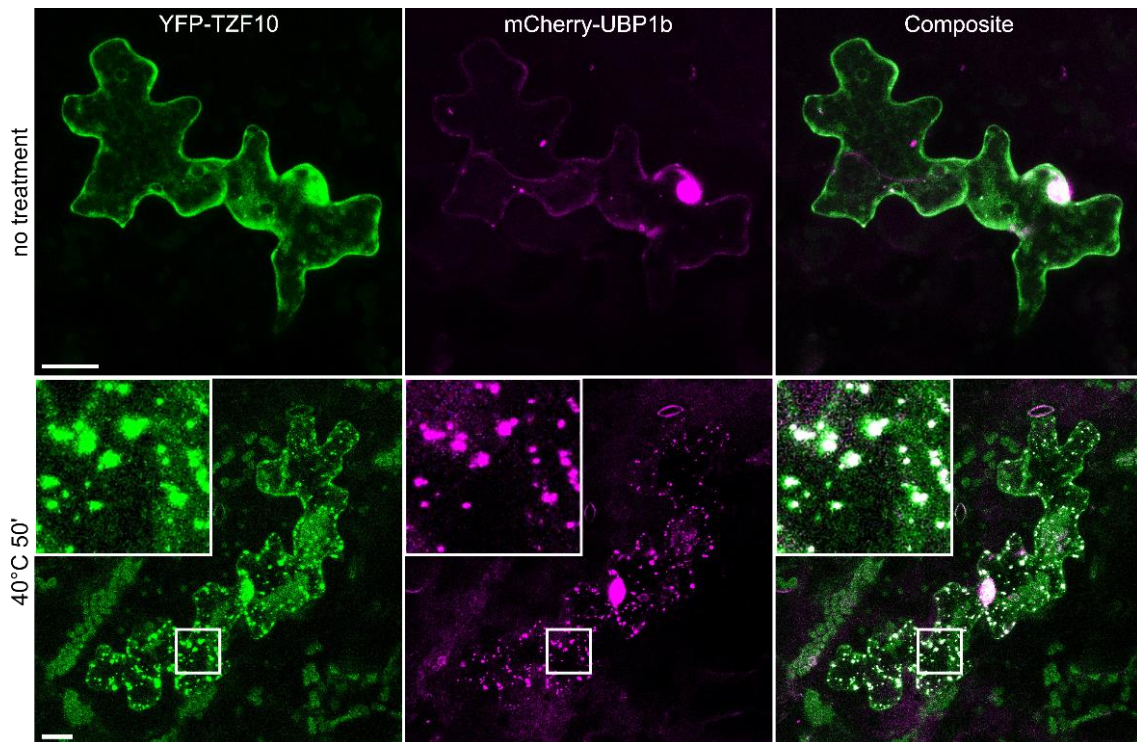


Figure 5: **TZF10 localizes to stress granules upon heat treatment.** *35S::YFP-TZF10* was transiently co-expressed with *35S::mCherry-UBP1b* in epidermal cells via particle bombardment of *A. thaliana* leaves. An exemplary picture before and after heat treatment (40°C, 50 min) is shown. YFP-TZF10 strongly accumulated in UBP1b-labeled SGs under stress conditions, highlighted by the zoom-in. The scale bar depicts 20 μm .

Under non-stress conditions, nuclear-cytoplasmic localization with occasional occurrence of cytoplasmic dots was found for both TZF10 and UBP1b (Fig. 5, upper row). After heat treatment, strong accumulation of mRNPs and co-localization of TZF10 with UBP1b-labeled SGs was observable (Fig. 5, lower row).

3.1.2 The mRNA of *TZF10* localizes to cytoplasmic granules

In order to visualize the mRNA of *TZF10* in *A. thaliana* and *N. benthamiana* cells, the λN22 system (Schönberger et al., 2012) was utilized. The system makes use of the viral RBP λN22 , a peptide from the lambda phage, consisting of 22 amino acids and fused to a fluorescent protein (Daigle and Ellenberg, 2007). λN22 is able to recognize and bind a 15-nt RNA stem loop, known as the Box-B element. In the Gateway-compatible system, applicable to plants, an mRNA of interest is fused to Box-B elements in the target RNA construct. The reporter construct carries λN22 fused to a fluorescent protein (here: mVenus). When the constructs are

co-transformed, λ N22 binds to the Box-B elements and thereby indirectly visualizes the mRNA of interest.

The analysis revealed that the mRNA of *TZF10* including both UTR sequences (genomic *TZF10*; g*TZF10*) distinctively localizes to cytoplasmic granules in Col-0 and *spi-4* (Fig. 6). Table 17 shows the portion of g*TZF10* mRNA signals overlapping with the P-body marker DCP1-mCherry.

Table 17: ***TZF10* mRNA localizes to P-bodies in Col-0 and *spirrig***. Utilization of the λ N22-system revealed the mRNA of genomic *TZF10* (g*TZF10*) to form cytoplasmic granules overlapping with P-bodies (DCP1-mCherry) under non-stress conditions. Average values [%] of $n=14$ cells are shown. Unpaired Student's *t*-testing revealed no significant difference between the genotypes.

| Genotype | <i>TZF10</i> mRNA granules |
|--------------|----------------------------|
| Col-0 | 83.2 (SD +/- 29.6) |
| <i>spi-4</i> | 91.2 (SD +/- 18.4) |

The mRNA of g*TZF10* strongly co-localizes with DCP1 already under non-stress conditions and with no difference between the genotypes Col-0 and *spi-4*. Exemplary pictures of the co-localization are shown in fig. 6.

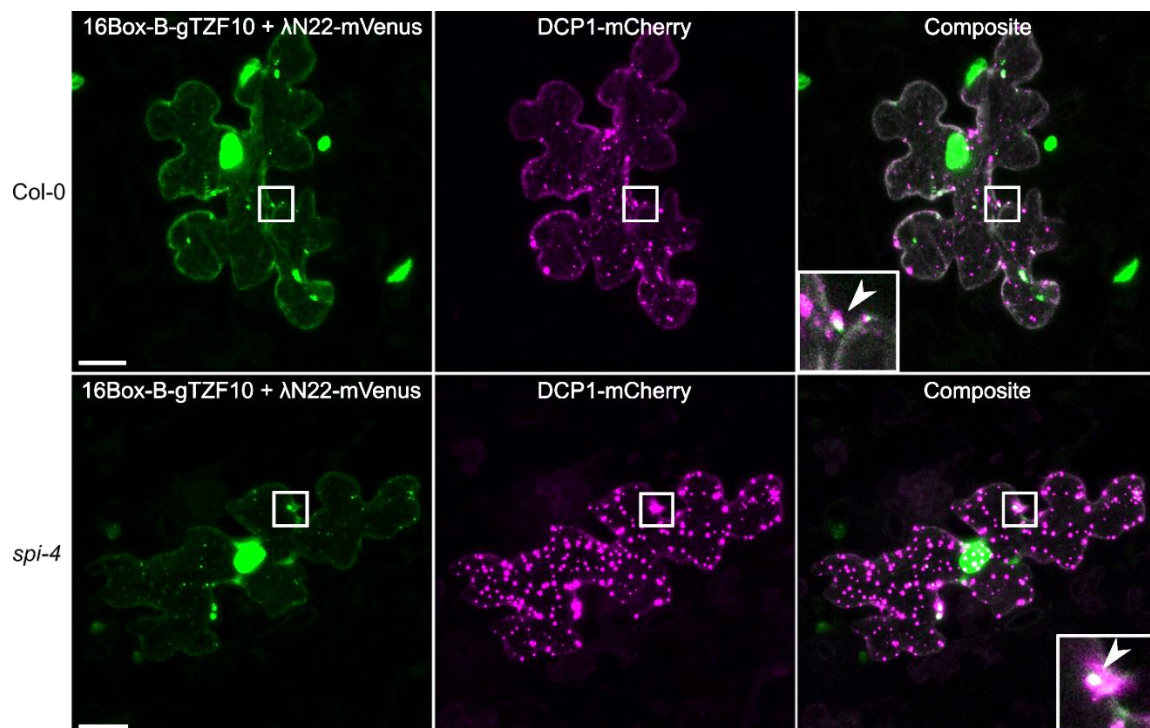


Figure 6: **The mRNA of genomic *TZF10* localizes to cytoplasmic granules.** The λ N22-system was applied to transiently visualize the mRNA of genomic *TZF10* (g*TZF10*) in Col-0 and *spi-4* via particle bombardment on *A. thaliana* leaves. Exemplary pictures of cells under non-stress conditions are shown. The arrows highlight overlapping *TZF10* mRNA signals with the P-body marker DCP1-mCherry. Scale bars indicate 20 μ m.

Respective control experiments corresponding to *TZF10* mRNA localization revealed predominant localization of the λ N22-mVenus reporter in the nucleus and less frequent, in the cytoplasm (Steffens et al., 2015; controls comprised: 1, the λ N22-mVENUS reporter co-

expressed with Box-B repeats without the mRNA target; 2, target constructs without Box-B repeats but with an N-terminally fused mCherry co-expressed with the reporter construct; 3, the λ N22-mVENUS reporter co-expressed with genomic *ABSCISIC ACID RESPONSIVE ELEMENTS-BINDING FACTOR 3 (ABF3)*, a transcript unaffected in its stability in *spirrig*. Cytoplasmic granules were almost absent (Steffens et al., 2015).

3.1.3 *tzf10/tzf11* mutants show no salt stress phenotype

Sun et al. (2007b) described *tzf10/tzf11* double mutants to be salt hypersensitive and thus to interestingly exhibit phenotypic overlap to *spirrig* mutants. The phenotype appeared to be reflected in lower germination and cotyledon greening rates as well as inhibited primary root growth of plants. In contrast, *tzf10* and *tzf11* single mutants were described to be phenotypically similar to wild type plants under non-stress as well as under salt stress conditions.

The double mutant characterized by Sun et al. (2007b) was generated and re-analyzed in this study. Therefore, *tzf10-1* and *tzf11-1* single mutants, obtained from the Nottingham Arabidopsis Stock Center (SALK_024800 and SALK_141550, table 2), were crossed. Homozygous mutants were isolated and insertion sites were confirmed by genotyping as well as by subsequent sequencing of the flanking genomic DNA regions. As the T-DNA insertion in the *tzf11-1* mutant (SALK_141550) is located in the 5'UTR, 300 bp upstream of the ATG, another *tzf10/tzf11* double mutant with a T-DNA insertion in the CDS of *TZF11* (further referred to as *tzf11-2*, GK_158E10) was included in the analysis. The double mutant *tzf10-1/tzf11-2* (SALK_024800/GK_158E10) was obtained by crossing respective single mutants (crossing performed by A. Steffens, re-confirmation of insertion sites by genotyping and sequencing in this study). The salt response of both generated *tzf10/tzf11* mutants was thoroughly examined again in this study.

At first, possible alterations in primary root growth on salt-containing medium were investigated. Therefore, surface-sterilized seeds were sown on ½ MS and grown vertically for eight days under normal conditions. The seedlings were subsequently transferred onto ½ MS with and without supplementation of 125 mM NaCl. After five days, primary root growth of plants grown on NaCl-containing medium was determined and set in relation to primary root growth of plants grown on control medium.

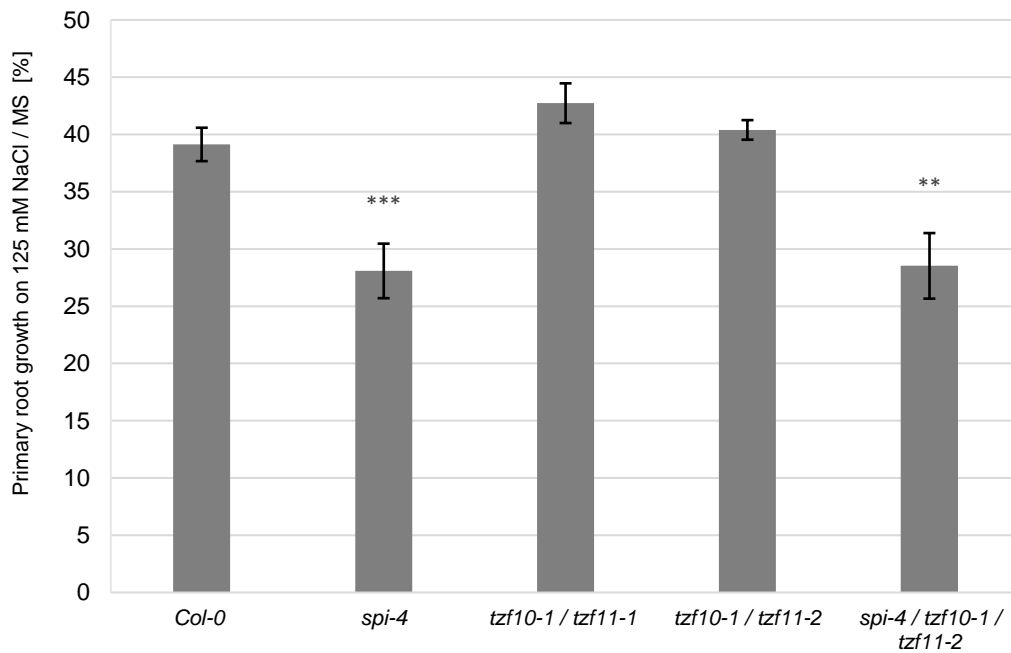


Figure 7: **Primary root growth of *tzf10/11* mutants on 125 mM NaCl is not significantly different compared to wild type plants.** Seeds were sown on $\frac{1}{2}$ MS agar plates and grown for 13 days under normal conditions. Afterwards, seedlings of each genotype were transferred to three fresh $\frac{1}{2}$ MS agar control plates and $\frac{1}{2}$ MS agar plates supplemented with 125 mM NaCl, respectively. Primary root growth was assessed after five days for $n \geq 33$ plants. Asterisks indicate significant differences in primary root growth between the mutant plants and the wild type Col-0; ***= $p < 0.001$; **= $p < 0.01$. Significance was tested with unpaired, two-tailed Student's *t*-tests. Error bars represent the standard error.

As a positive control for hypersensitive salt response, *spi-4* was included in the analysis. Accordingly, *spi-4* showed a significantly stronger reduction in primary root growth on salt-containing medium compared to Col-0 (Fig. 7). Both of the *tzf10/tzf11* mutants did not show significant differences in primary root growth compared to the wild type (Fig. 7). In order to evaluate potential additional effects of *tzf10/tzf11* mutations in the *spirrig* background, the triple knockout mutant *spi-4/tzf-10-1/tzf11-2* was generated by crossing and included in the analysis. However, the *tzf10/tzf11* mutations did not augment the salt hypersensitivity phenotype of *spi-4* (Fig. 7).

Apart from primary root growth inhibition, Sun et al. (2007b) reported cotyledons of *tzf10-1/tzf11-1* seedlings to show significantly stronger whitening upon growth on salt-containing medium than wild type plants. Thus, whitening of leaves as a sign for salt hypersensitivity was assessed next. Seeds were directly sown and grown horizontally on solid $\frac{1}{2}$ MS medium supplemented with or without 125 mM NaCl. After four weeks, plants showing green or white leaves were scored and the percentage of plants with completely green leaves was determined. As plants grown on $\frac{1}{2}$ MS without salt entirely showed green leaves (100%), only results of plants grown on salt-containing medium are presented in fig. 8. The percentage of plants with green leaves among *spi-4* seedlings was dramatically decreased compared to Col-0; thus matching the expectations for a salt hypersensitive mutant. Conversely, and also

again contrary to results of Sun et al. (2007b), the percentage of plants with green leaves among both *tzf10/tzf11* mutants was on the same level (between 80-90%) as among wild type plants.

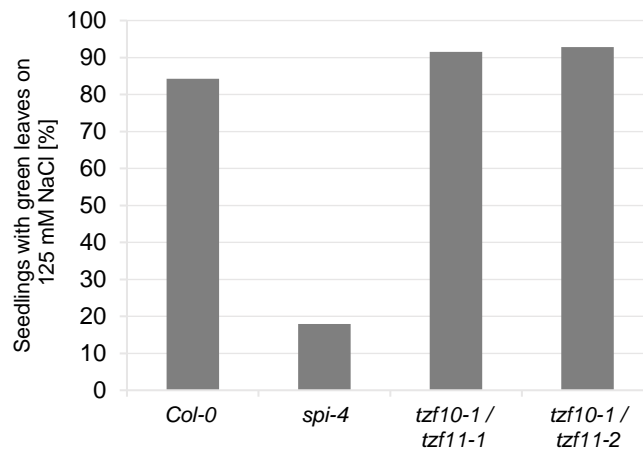


Figure 8: ***tzf10/11* double mutants do not show increased leaf whitening as a sign for salt hypersensitivity.** Surface-sterilized seeds were sown and directly grown on $\frac{1}{2}$ MS supplemented with 125 mM NaCl. After four weeks, plants showing green or white leaves were scored ($n \geq 26$) and the percentage of plants with completely green leaves was determined.

As the result gained by the leaf whitening assay (Fig. 8) was already conclusive and in line with previous results, no further repetitions of this experiment were conducted to enable statistical analysis.

To demonstrate inhibition of *tzf10-1/tzf11-1* primary root growth on salt-containing medium, Sun et al. (2007b) make use of the qualitative root-bending assay. The root-bending assay was previously implemented for the identification of salt hypersensitive mutants in mutagenesis screens and led to the isolation of the *salt overly sensitive* (*sos*) mutants (Wu et al., 1996; Zhu, 2000; Shi et al., 2002). In the assay, seedlings first are grown vertically in absence of stress, before they are transferred on salt-containing medium and control medium. The plants are subsequently grown vertically again, but this time with roots upside down. Due to gravitropism, continued growth of the roots results in bending, which is supposed to be lacking in salt hypersensitive mutants (Wu et al., 1996). The advantage of this assay for mutagenesis screens is to thereby being able to discriminate between stress hypersensitive mutants and agravitropic mutants (Wu et al., 1996). For the salt hypersensitive *sos* mutants, arrested primary root growth and swollen root tips upon salt stress were demonstrated in root-bending assays (Shi et al., 2002).

In this study, the root-bending assay was used to test the potential salt hypersensitivity phenotype of *tzf10/tzf11* mutants.

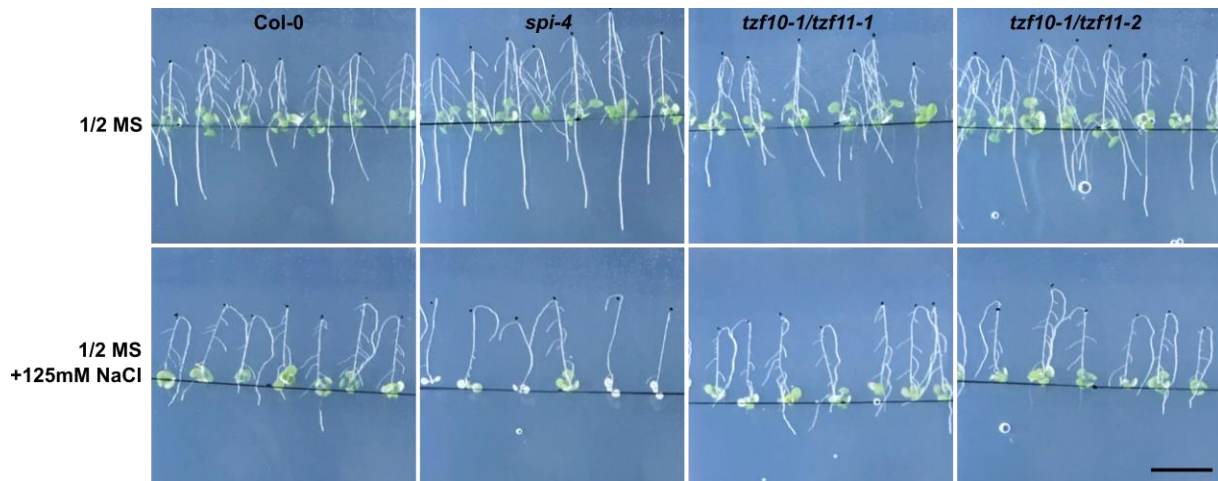


Figure 9: *tzf10/11* double mutants do not show a salt hypersensitivity phenotype in the root-bending assay. The figure shows exemplary pictures of 14-day-old plants. The seedlings were vertically grown for seven days on $\frac{1}{2}$ MS. Afterwards, they were transferred on $\frac{1}{2}$ MS supplemented with and without 125 mM NaCl and were further grown vertically, this time with roots upside down, for another seven days. The scale bar displays 2 cm.

As a salt hypersensitive mutant, *spi-4* showed clear phenotypical differences on salt-containing medium compared to Col-0 in the root-bending assay. A stronger whitening of cotyledons and increased inhibition of *spi-4* primary root growth was distinctively visible. However, slight bending of roots still took place in some of the *spi-4* plants (Fig. 9). In contrast, both *tzf10/tzf11* double mutants did not show obvious phenotypical differences on salt-containing medium compared to Col-0. Primary root growth did not appear to be more inhibited in *tzf10/tzf11* double mutants than in the wild type, and root-bending was clearly observable.

In summary, the published phenotype of the *tzf10-1/tzf11-1* mutant by Sun et al. (2007b), who stated growth of *tzf10-1/tzf11-1* to be significantly inhibited under salt stress conditions, could not be verified in this study. Results obtained by the performed salt stress assays clearly show *tzf10/tzf11* double mutants not to be salt hypersensitive. Nonetheless, this result does not fully exclude relevance of TZF10 and 11 in salt stress responses of *A. thaliana*.

3.1.4 TZF10 mRNA expression responds to salt stress

TZF10 expression levels were analyzed in wild type and *spi-4* under non-stress and stress conditions. Preceding these measurements, all qPCR primer pairs were (re-)evaluated to ensure adequate performance.

3.1.4.1 Re-evaluation of a primer pair amplifying 18S rRNA as a reference gene for qPCR

Ribosomal 18S RNA (18S rRNA) is frequently used as a reference gene to normalize expression values of genes of interest (Bogdanović et al., 2012; Steffens et al., 2015; Zhang et al., 2012). However, application of 18S rRNA for normalization in qPCR experiments can be regarded critically concerning two aspects: first, as there is no poly[A] tail present in 18S, reverse transcription is frequently primed with specific primers or random hexamers; second and subsequently, 18S rRNA is heavily abundant and cDNA has to be strongly diluted in order

to be comparable to cDNA of genes of interest. Nonetheless, Bogdanović et al. (2012) did prove that 18S rRNA of *A. thaliana* can be successfully, non-specifically, transcribed with poly[dT] primers regardless of the lacking poly[A] tail. As transcription of 18S rRNA with poly[dT] primers is not as efficient as with specific primers or random hexamers; extensive dilution can thus often conveniently be circumvented and 18S rRNA expression levels can directly be compared with expression values of genes of interest (Bogdanović et al., 2012).

To allow comparability of results, a primer pair for 18S rRNA from previous experiments (Steffens et al., 2015; AT3G41768) was implemented to normalize expression values in this study. To assure adequate primer performance with present conditions and equipment, primer efficiency, as well as 18S rRNA stability in salt stress and upon actinomycin D treatments, was examined in this work.

A suitable reference gene for qPCR experiments is characterized by robust and stable expression. Moreover, depending on the experimental setup, at most marginal variation in different developmental stages, tissues and/or upon different growth/stress conditions is acceptable. The Minimum Information for Publication of Quantitative Real-Time PCR Experiments (MIQE) guidelines provide a directory for scientifically reliable performance and evaluation of qPCR experiments and results. According to the guidelines, primers optimally amplify 80 to 200 bp of a reference gene and should act at 90-110% PCR efficiency showing linear calibration curves with correlation coefficients (r^2) \leq -0.99 (Bustin et al., 2009; Stephan et al., 2019).

qPCR efficiency testing revealed the used 18S rRNA primers, amplifying a fragment of 102 bp, to perform at **93%** efficiency with an r^2 of **-0.998** (standard curve fig. 72A, appendix). Analysis of melting curves moreover did not identify any disturbing impact of primer dimers (data not shown). Next, the stability level of 18S rRNA upon single and combined salt and actinomycin D treatments was assessed using the statistical algorithms BestKeeper (Pfaffl et al., 2004) and geNorm (Vandesompele et al., 2002). On that account, combined data of treated and untreated Col-0 samples from two independent experiments were analyzed. Table 18 shows the stability values resulting from BestKeeper and geNorm calculations.

Table 18: **18S rRNA stability as a reference gene in single and combined salt stress and actinomycin D treatments.** Values were calculated with the statistical algorithms geNorm (Vandesompele et al., 2002) and BestKeeper (Pfaffl et al., 2004). Combined data of treated and untreated Col-0 samples ($n=30-60$) from two independent experiments were analyzed.

| | geNorm | BestKeeper | | |
|------------------------------------|---------------|----------------------|----------|--------------------------------|
| | Stability (M) | Stability (SD[± CP]) | CV [%CP] | Coefficient of correlation [R] |
| Salt stress | 0.81 | 0.45 | 2.9 | 0.696 |
| Actinomycin D | 0.78 | 0.46 | 2.95 | 0.634 |
| Salt stress + Actinomycin D | 0.68 | 0.29 | 1.92 | 0.547 |

The three most relevant values concerning stability and expression levels for reference genes determined by the BestKeeper software are the standard deviation (stability value, SD), the coefficient of variation (CV) and the coefficient of correlation (R; Pfaffl et al., 2004). A stably expressed reference gene is supposed to give low SD ($SD < 1$) and CV, and high R values (Zhang et al., 2016). For example, Zhang et al. (2016) considered a reference gene for *Halostachys caspica* with $R = 0.632$, $SD = 0.35$ and $CV = 2.00$ to be the most suitable of several tested candidates. As BestKeeper calculations for 18S rRNA resulted in values on a comparable level, and most importantly in SD values < 1 (Table 18), it can be regarded suitable for the analyzed treatments. Calculation with the algorithm geNorm gives the stability value M. The threshold for stability is $M = 1.5$; thus if it is $M < 1.5$, a reference gene is considered to be stably expressed under given conditions (Zhang et al., 2016). In the applied treatments, the stability value M for 18S rRNA ranged between 0.68-0.81 (Table 18). According to the geNorm and BestKeeper calculations, 18S rRNA can therefore be regarded as stable and suitable for qPCR experiments with single or combined salt stress and actinomycin D treatments.

3.1.4.2 Evaluation of primer pairs amplifying TZF and a salt-stress responsive target gene

All primer pairs amplifying genes of interest used in this study were tested for adequate primer efficiency first. Primer pairs amplifying a genomic fragment of *TZF10* and *TZF11*; and moreover a primer pair specifically amplifying a fragment of the construct carrying *TZF10* in transgenic lines (lines presented in table 3), were implemented. A primer pair amplifying a fragment of the *A. thaliana* salt stress-inducible gene *RD29A* was used to control the effectivity of salt treatment in respective experiments. Table 19 shows the results of the qPCR efficiency test. Primer sequences, primer origin and standard curves of efficiency tests are given in table 29 and fig. 72 in the appendix.

Table 19: qPCR efficiency and correlation of primer pairs.

| Gene | Efficiency [%] | Correlation (r^2) |
|-----------------------------------|----------------|-----------------------|
| <i>TZF10</i> | 108% | -0.998 |
| <i>TZF11</i> | 96% | -0.999 |
| <i>TZF10</i> (construct-specific) | 88% | -0.998 |
| <i>RD29A</i> | 93% | -0.997 |

With adequate qPCR efficiencies above 80% and below 120%, all primer pairs matched the criteria of the MIQE guidelines for genes of interest (Bustin et al., 2009) and were subsequently applied in qPCR experiments.

3.1.4.3 *TZF10* expression levels do not differ in *spirrig* compared to wild type plants under non-stress conditions

An initial experiment preceding to this work interestingly demonstrated the stable introduction of *TZF10* to rescue the salt hypersensitivity phenotype of *spirrig* mutants (A. Steffens, unpublished) and thus pointed to an interplay between *TZF10* and *SPIRRIG*. The finding prompted an investigation on how *TZF10* expression might be affected in *spirrig* mutants.

Previous qPCR analysis data indicated *TZF10* expression levels to be significantly reduced by 2.3-2.9 fold in *spirrig* mutants compared to wild type plants under non-stress conditions (A. Steffens, unpublished data).

However, these results could not be confirmed in this study. Expression levels of *TZF10* were repeatedly determined under non-stress conditions and were always found to be on a similar level with no significant differences in *spi-4* compared to the wild type (exemplarily shown in fig. 10).

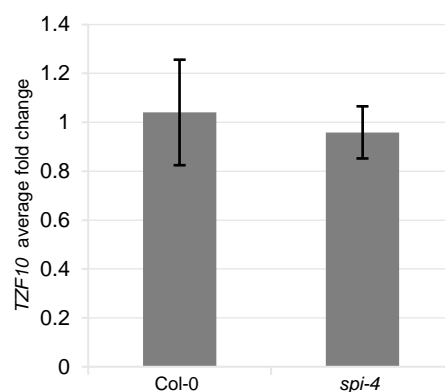


Figure 10: *TZF10* expression levels in *spi-4* compared to Col-0 under non-stress conditions. 14-day-old seedlings were incubated in liquid ½ MS for 1 h under constant shaking. Expression levels were determined in three biological replicates by qPCR analysis, normalized to reference gene 18S rRNA and compared to wild type plants. Error bars indicate the standard error. Significance was tested with a Mann-Whitney-U test ($p < 0.10$).

3.1.4.4 The expression of *TZF10* is induced by salt stress

Sun et al. (2007b) examined the expression of *TZF10* and *11* mRNA under salt stress conditions by Northern blot analysis. According to their results, *TZF10* and *11* mRNA is strongly salt-induced and peaked already at 15 minutes after a 200 mM NaCl treatment. After 60 min, the expression of both mRNAs was fully recovered to pre-treatment levels (Sun et al., 2007b). To thoroughly re-analyze the salt-induced expression pattern of *TZF10* and *11* mRNA in Col-0 and in *spirrig* mutants, salt stress timeline experiments were conducted in this work. Therefore, seedlings, grown for 14 days on solid ½ MS, were shaken in liquid ½ MS supplemented with or without 200 mM NaCl and subsequently harvested at different time points. In a first approach, *TZF10* expression was analyzed upon **15**, **60** and **180** min of salt stress. In order to

confirm an effect of the salt, the expression of the *A. thaliana* salt stress-inducible gene *RD29A* (Msanne et al., 2011; Lee et al., 2016) was determined beforehand (Fig. 11).

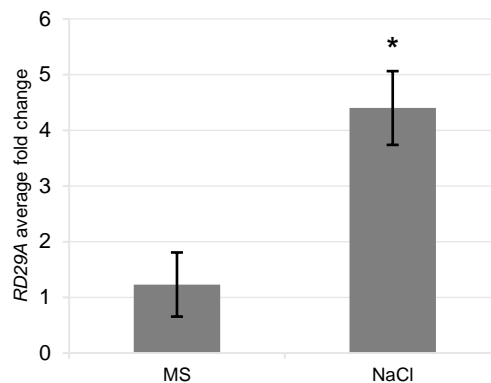


Figure 11: **Relative expression of *RD29A* in salt-stressed compared to non-treated samples**, normalized to reference gene 18S rRNA. Expression levels were determined in Col-0 samples, treated or not treated with 200 mM NaCl for 180 min. $n=3$. Error bars indicate the standard error. Significance, indicated by the asterisk, was tested with a Mann-Whitney-U test ($p<0.10$).

As the expression of *RD29A* was strongly and significantly up-regulated in NaCl-treated samples compared to control samples (Fig. 11), the salt stress treatment in the experiment was considered effective. Next, *TZF10* expression was assessed (Fig. 12).

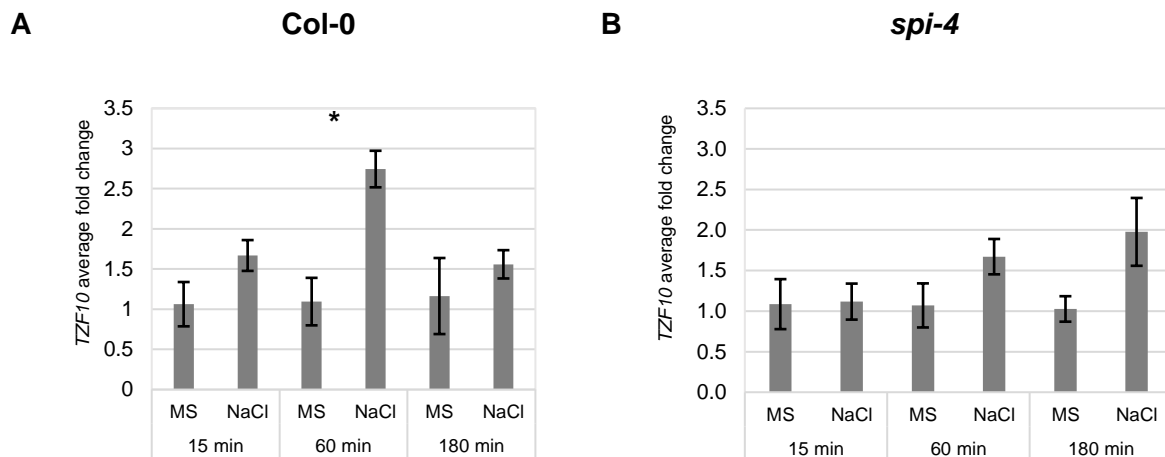


Figure 12: **Relative expression of *TZF10* in salt-stressed compared to non-treated samples**, normalized to reference gene 18S rRNA. Expression levels were determined in Col-0 (A) and *spi-4* (B) samples, treated or not treated with 200 mM NaCl for designated time periods. $n=3$. Error bars indicate the standard error. Significance, indicated by the asterisk, was tested with a Mann-Whitney-U test ($p<0.10$).

In contrast to results of Sun et al. (2007b), the expression level of *TZF10* was only slightly increased in Col-0 samples treated with NaCl compared to control samples after 15 min (Fig. 12A). After 60 min however, a significant elevation of *TZF10* expression was observable in NaCl-treated compared to control Col-0 samples. That significant, salt-induced increase of *TZF10* expression was absent after 180 min of treatment. In *spi-4*, weak tendencies for *TZF10* to be up-regulated upon 60 and 180 min of salt treatment were detectable; but the effect was not significant (Fig. 12B).

To elucidate and cover the salt-induced expression pattern of *TZF10* more closely, a second approach and repetition of the experiment with more harvesting points was performed. *TZF10* expression was thus analyzed upon **15, 30, 60, 90, 120, 180** and **240** min of salt stress (Fig. 13).

Whereas *TZF10* expression was not yet elevated upon 15 and 30 min of salt stress, a first significant salt-induced up-regulation was again visible after 60 min (Fig. 13A). While a high expression was still significantly present at 120 min of salt treatment, it was only tendentially maintained at 180 min. At 240 min, *TZF10* expression was back at the pre-treatment level and not significantly different compared to control samples anymore. Even though a slight elevation of *TZF10* expression in NaCl-treated *spi-4* plants was detectable at 60 to 120 min, the up-regulation was not significantly different compared to control samples throughout the whole time of salt treatment. Already 180 min upon salt stress, *spi-4* samples did not show any salt-induced *TZF10* up-regulation tendencies anymore (Fig. 13B).

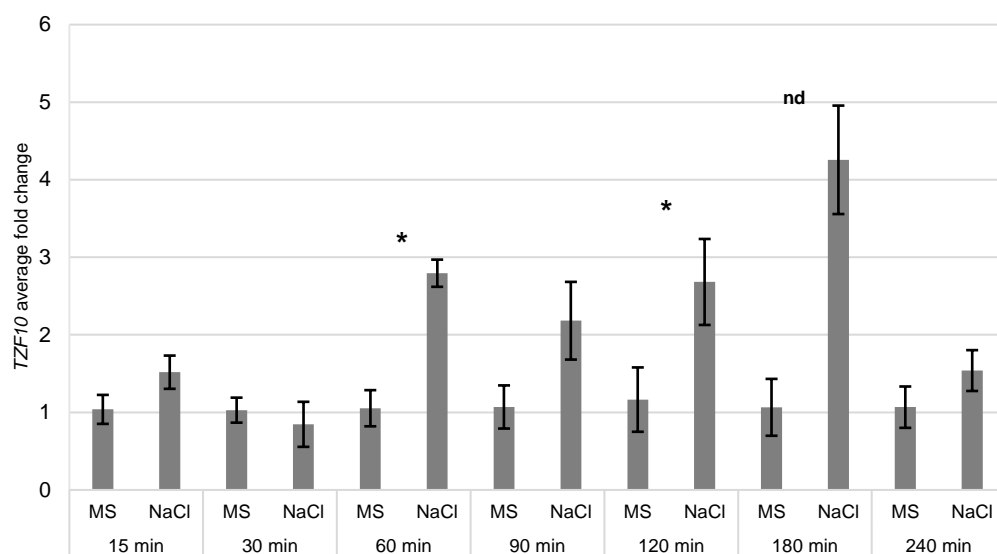
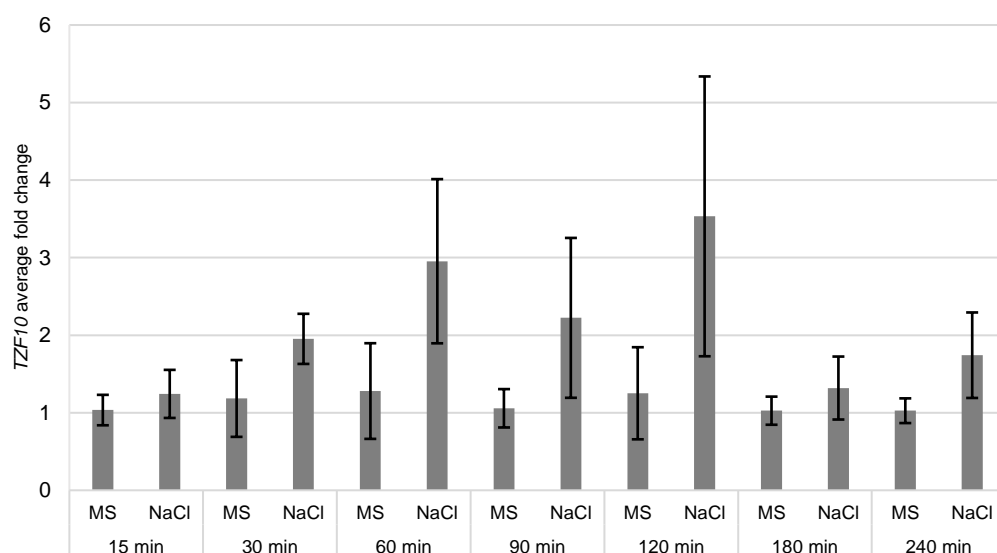
A Col-0**B *spi-4***

Figure 13: **Relative expression of *TZF10* in salt-stressed compared to non-treated samples**, normalized to reference gene 18S rRNA. Expression levels were determined in Col-0 (**A**) and *spi-4* (**B**) samples, treated or not treated with 200 mM NaCl for designated time periods. $n=2$ (Col-0, 180 min) - 3. Error bars indicate standard errors. Significance, indicated by the asterisks, was tested with a Mann-Whitney-U test ($p<0.10$). nd= significance could not be determined, as only two replicates for Col-0, MS, 180 min were available.

As the above presented experiments and the experiments described in 3.1.5 were conducted equally, the data of four independent experiments were next analyzed in combination. In line with the results of the single examinations, the analysis in combination clearly revealed that in Col-0, *TZF10* was significantly up-regulated after 180 min of salt stress (Fig. 14A). However, *TZF10* expression was only marginally elevated upon 60 min of salt treatment in Col-0. In *spi-4*, no significant up-regulation was detectable (Fig. 14B).

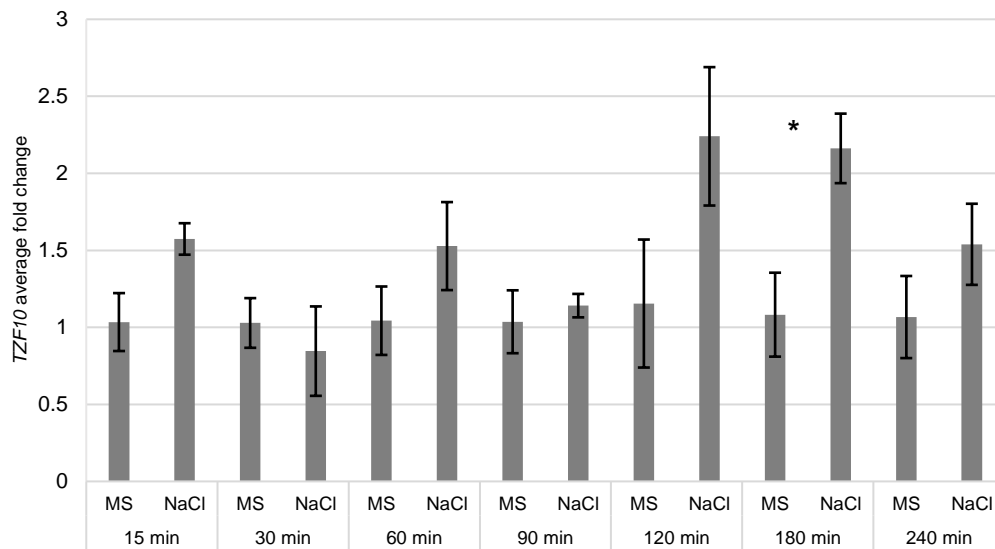
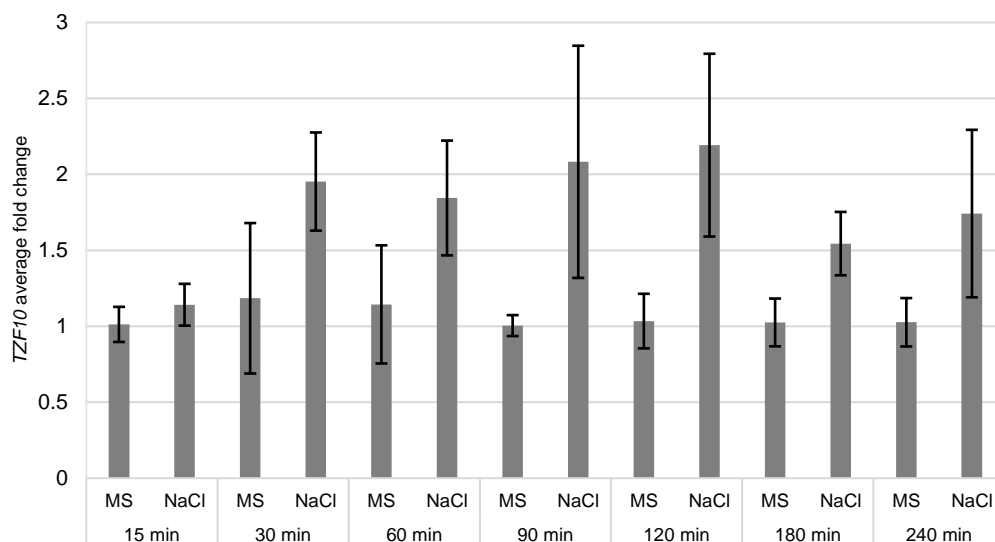
A Col-0**B spi-4**

Figure 14: **Relative expression of *TZF10* in salt-stressed compared to non-treated samples**, normalized to reference gene 18S rRNA. Expression levels were determined in Col-0 (**A**) and *spi-4* (**B**) samples, treated or not treated with 200 mM NaCl for designated time periods. Data from four independent experiments were combined and analyzed; $n=12$ (60 min), 9 (90 min), 6 (15 min, 120 min, 180 min), 3 (30 min, 240 min). Error bars depict standard errors. Significance, indicated by asterisks, was tested with a Mann-Whitney-U test ($p<0.10$).

3.1.4.5 *TZF10* expression levels do not differ in *spirrig* compared to wild type plants under stress conditions

In order to address the question if *TZF10* expression levels generally differ between wild type and *spi-4* plants under salt stress conditions, the combined data were directly compared among the genotypes next without normalization to control conditions. No significant differences in *TZF10* expression could be determined (Fig. 15).

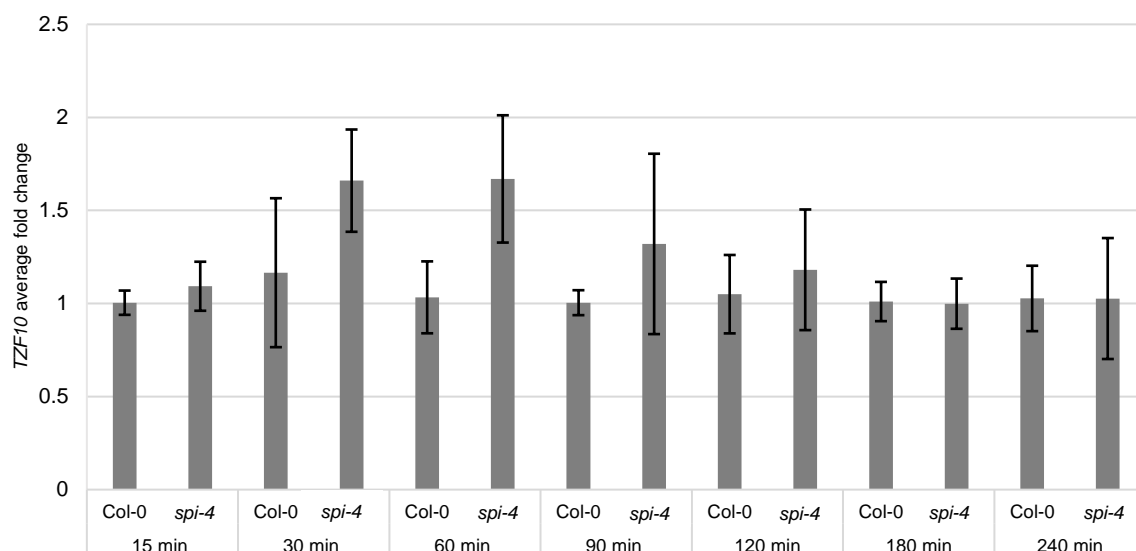


Figure 15: **Relative expression of *TZF10* in Col-0 compared to *spi-4* plants under salt stress conditions**, normalized to reference gene 18S rRNA. Expression levels were determined in samples treated with 200 mM NaCl, for designated time periods and compared between the genotypes. Data from four independent experiments were combined and analyzed; $n=12$ (60 min), 9 (90 min), 6 (15 min, 120 min, 180 min), 3 (30 min, 240 min). Error bars depict standard errors. Significance was tested with a Mann-Whitney-U test ($p<0.10$).

3.1.5 *TZF10* mRNA stability is not strikingly affected in *spi-4*

Since no differences in *TZF10* expression under non-stress and stress conditions were detectable in *spirrig* mutants compared to wild type plants, *TZF10* mRNA stability in both genotypes was investigated next.

In order to assess the stability of the *TZF10* mRNA upon salt stress and control conditions, seedlings were treated with ActD and subsequently, expression levels were determined by qPCR. ActD is an intercalating antibiotic and a known inhibitor of DNA transcription. Particularly by binding a double-stranded DNA conformation within the transcriptional complex, ActD effectively blocks transcription and prevents RNA chain elongation (Sobell, 1985). Since 1954, ActD is widely used as an anticancer drug (Koba and Konopa, 2005). In *Arabidopsis*, ActD is frequently applied to block transcription and to determine stability of mRNAs of interest (Shen et al., 2016; Narsai et al., 2007; Mishiba et al., 2013).

3.1.5.1 The experimental setup of a first mRNA stability assay has to be optimized

For a first mRNA stability assay, the experimental setup previously used by Steffens et al., 2015, was adapted. 12-day-old seedlings of plant lines of interest were incubated under constant shaking in either liquid $\frac{1}{2}$ MS or liquid $\frac{1}{2}$ MS supplemented with 125 mM NaCl for four hours. Afterwards, ActD was added to a final concentration of 150 $\mu\text{g/ml}$ to all of the samples. Samples were taken before ($=0$ h ActD), as well as six hours after ActD treatment (pools of 2-3 seedlings, 3 biological replicates).

General effectivity of the salt treatment was tested first by analyzing the expression level of salt-induced *RD29A*. An almost 10-fold increase of *RD29A* in salt-treated, compared to control Col-0 samples, confirmed the induced salt response in the plants (Fig. 16A).

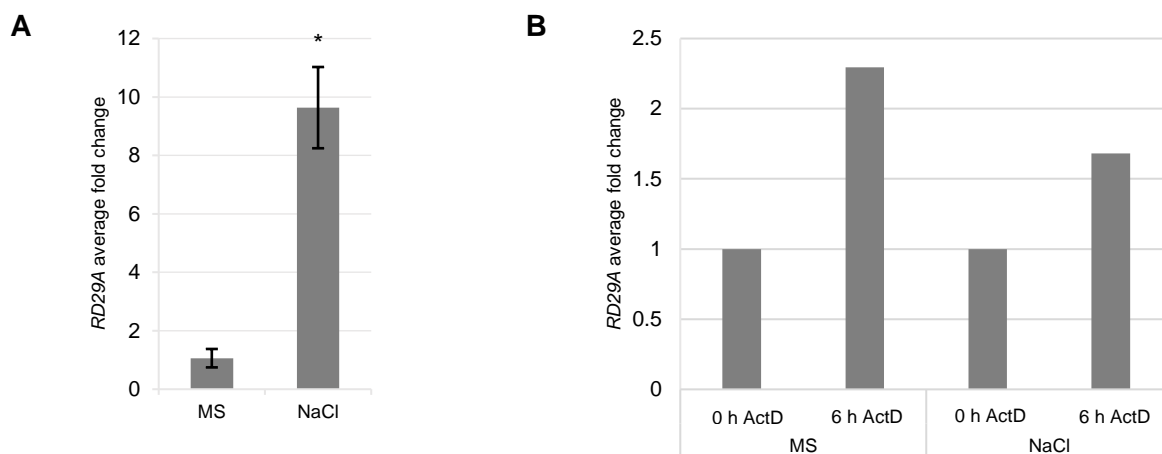


Figure 16: ***RD29A* expression levels.** **A** Relative expression of *RD29A* in salt-stressed compared to control samples, normalized to reference gene 18S rRNA. Expression levels were determined in Col-0 samples either incubated in liquid ½ MS or liquid ½ MS supplemented with 125 mM NaCl for four hours. $n=3$. Error bars depict standard errors. Significance, indicated by the asterisk, was tested with a Mann-Whitney-U test ($p<0.10$). **B** Relative expression of *RD29A* in samples treated with 150 µg/ml ActD for 6 h, compared to control samples, normalized to reference gene 18S rRNA. Expression levels were determined in Col-0 samples either incubated in liquid ½ MS or liquid ½ MS supplemented with 125 mM NaCl for four hours before the addition of ActD solution. $n=1$.

Narsai et al. (2007) confirmed inhibition of transcription by demonstrating ActD to be able to prevent the up-regulation of a transcript (*NAD(P)H DEHYDROGENASE B2 (NDB2)*) normally induced by salicylic acid. Upon ActD treatment, followed by addition of salicylic acid, a typically four- to five-fold induction of the *NDB2* transcript failed to appear. In a similar manner, effectivity of ActD was tested in this study. The expression level of the salt stress-inducible gene *RD29A* was analyzed in Col-0 samples incubated with 150 µg/ml ActD for 6 h after pre-treatment with or without 125 mM NaCl for 4 h. After addition of ActD, no substantial further increase of the *RD29A* expression level would thus be expected. However, in both samples, pre-treated with or without NaCl, a distinct elevation of *RD29A* expression was observable (Fig. 16B). Furthermore, the increased expression of *RD29A* in control samples (Fig. 16B) might indicate the plants to have been stressed even when they were incubated in liquid ½ MS only. The results did not confirm an efficient block of transcription but also did not fully exclude it, as it is conceivable that the effect of ActD not directly sets in as soon as ActD is added to the samples. In the meantime, between addition of ActD and the potential onset of the ActD effect on transcription, *RD29A* expression could have been elevated first, but arrested later. To circumvent this problem, control samples should have been taken at each time point to enable direct comparison between expression levels in samples with and without ActD treatment. Further analysis moreover revealed it was not possible to draw any conclusion on differences in *TZF10* mRNA stability in plant lines of interest (Fig. 73 and fig. 74, appendix).

Thus, these results highlighted a striking weakness of the here applied experimental design. Consequently, to obtain more reliable results, it was decided to develop a more suitable, new experimental design including necessary control samples.

3.1.5.2 An optimized experimental setup allows conclusions on mRNA stability

The experimental setup for the mRNA stability assays conducted next was adapted as described in the following. First, the timing and duration of salt stress and ActD addition was modified. Second, control samples not treated with ActD were drawn at each harvesting time point. In the experiment described above (3.1.5.1) no significant long-term up-regulation of *TZF10* was determinable after 10 h of salt stress in Col-0 and *spi-4* (Fig. 73A, appendix). Moreover, previous experiments showed the expression level of *TZF10*, if at all, to be elevated 1 h after salt treatment and maintained up to 3 h afterwards in Col-0 (3.1.4). Therefore, the plants were incubated in liquid $\frac{1}{2}$ MS with or without 200 mM NaCl for only 45 minutes before ActD addition. Samples were subsequently taken 15 min, 45 min and 75 min after ActD addition. An overview on the applied setup is given in fig. 17. Two experiments were successively conducted and results from both assays are presented in the following.

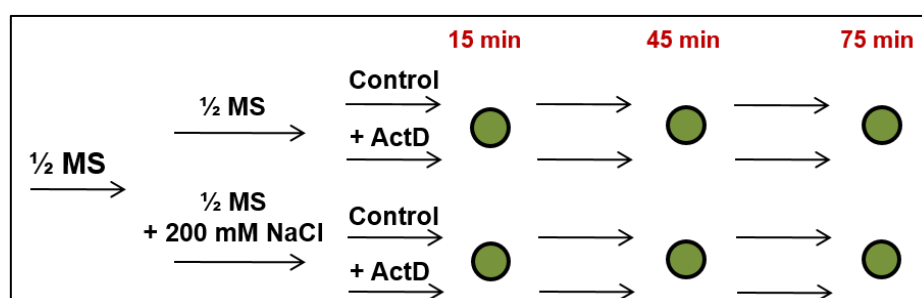


Figure 17: **Optimized experimental setup for mRNA stability assays.** Plant lines of interest were incubated under constant shaking in liquid $\frac{1}{2}$ MS for 1 h. Afterwards, NaCl was added to half of the samples to a final concentration of 200 mM. Upon 45 min of incubation, 150 μ g/ml ActD solved in DMSO was added to again half of the samples. Respective amounts of DMSO were applied to control samples. Samples were subsequently harvested after 15 min, 45 min and 75 min of ActD treatment.

The efficiency of salt treatment and transcriptional block was analyzed using the example of *RD29A* expression in both experiments. The testing in the course of the first conducted assay revealed a 3.5-fold elevation of *RD29A* expression in a salt-treated compared to a control sample, suggesting the salt treatment to have been effective (Fig. 18A). Direct comparison of ActD-treated samples to control samples showed a down-regulation of *RD29A* expression, likely due to transcriptional block induced by ActD (exemplarily shown for 45 min ActD treatment, fig. 18B). The *RD29A* expression level was down-regulated more strongly in ActD treated samples incubated without NaCl (fold change: 0.02) than in ActD treated samples supplemented with NaCl (fold change: 0.8), indicating the mRNA of *RD29A* to presumably be stabilized under salt stress conditions (Fig. 18B). Results from the subsequently conducted assay were similar (Fig. 75, appendix). Thus, the modified experimental setup proved to be successful and allowed conclusions on mRNA stability.

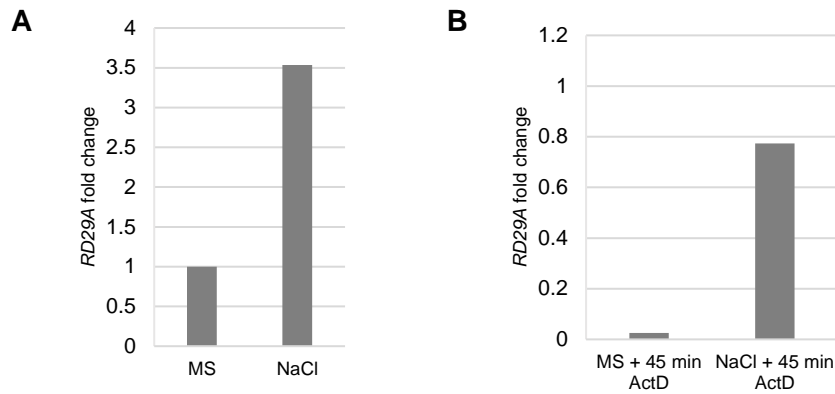


Figure 18: ***RD29A* expression levels.** The effect of salt treatment (**A**) and transcriptional block induced by ActD (**B**) was exemplarily tested in single Col-0 replicates. **A** Relative expression of *RD29A* in samples incubated in liquid ½ MS containing 200 mM NaCl for 90 min, compared to control samples incubated in liquid ½ MS only, normalized to reference gene 18S rRNA. $n=1$. **B** Relative expression of *RD29A* in samples incubated in liquid ½ MS with or without 200 mM NaCl and treated with 150 µg/ml ActD for 45 min. The expression was compared to respective control samples not treated with ActD. The expression was normalized to reference gene 18S rRNA. $n=1$.

3.1.5.3 *TZF10* mRNA stability does only slightly differ in *spi-4* compared to Col-0

TZF10 mRNA stability data analysis first focused on investigating if *TZF10* mRNA stability generally is affected in *spirrig* mutants. Conclusions concerning *TZF10* mRNA stability were drawn from the influence of ActD on *TZF10* expression levels under non-stress and stress conditions in Col-0 and *spi-4*.

In the first experiment, the expression levels did not significantly change upon 15 min, 45 min and 75 min ActD treatment in Col-0 under non-stress conditions (Fig. 19A). In contrast, under salt stress conditions, the *TZF10* expression level was significantly decreased in samples treated with ActD for 45 min compared to the control, represented by a fold change of 0.37. However, after 75 min ActD treatment, no significant influence of ActD was determinable anymore (Fig. 19A). In summary, the results indicate a general stabilization of the *TZF10* mRNA in the wild type, with the exception of one sampling point (45 min ActD) depicting slight instability.

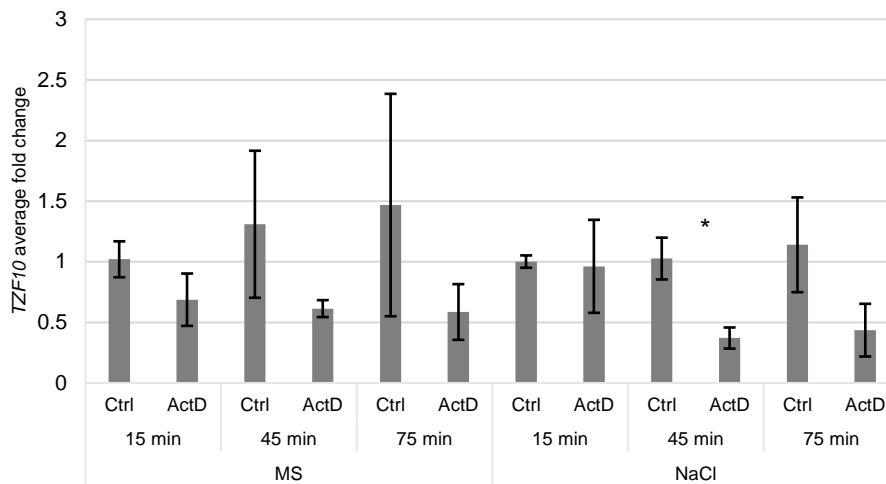
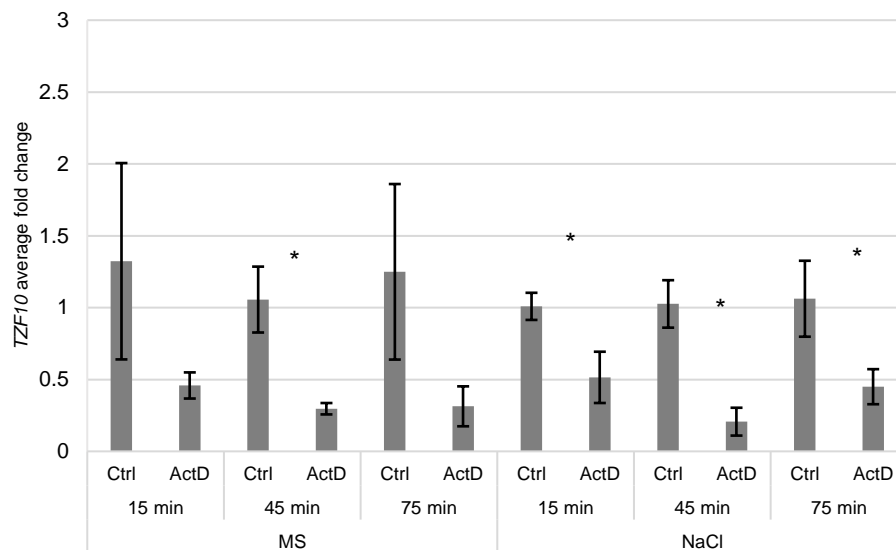
A Col-0**B spi-4**

Figure 19: ***TZF10* mRNA is more stable in Col-0 than in *spi-4***. The effect of transcriptional block induced by ActD is displayed by relative expression of *TZF10* in Col-0 (A) and *spi-4* (B) samples incubated in liquid $\frac{1}{2}$ MS with or without 200 mM NaCl and treated with 150 μ g/ml ActD for designated time periods, compared to control samples (Ctrl) incubated in liquid $\frac{1}{2}$ MS with or without 200 mM NaCl only, normalized to reference gene 18S rRNA. $n=3$. Error bars depict standard errors. Significance was tested with a Mann-Whitney-U test ($p<0.10$).

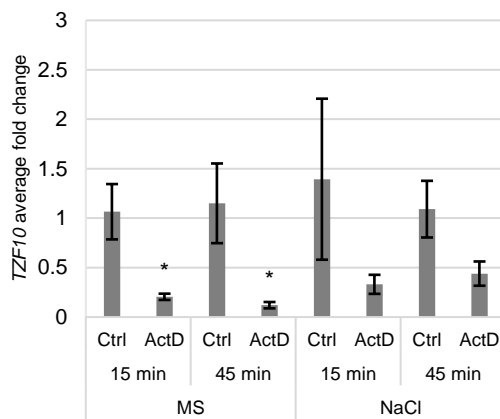
The impact of ActD in *spi-4* however was more severe. Under non-stress conditions, *TZF10* expression levels were significantly reduced in samples treated with ActD for 45 min, represented by a fold change of 0.3. The effect was still strong in samples treated with ActD for 75 min. Under salt stress conditions, the *TZF10* expression levels were significantly decreased already after 15 min of ActD treatment. The effect was similarly strong after 45 min and 75 min of ActD treatment (Fig. 19B).

Taken together, the results of the first experiment pointed to an overall increased *TZF10* mRNA decay especially under stress conditions, but also under non-stress conditions, in *spi-4*

compared to Col-0. As the effect of ActD was already determinable after 15 and 45 min, samples were not again analyzed after 75 min of ActD treatment in the repeated experiment.

In contrast to above described results, a significant effect of ActD on the expression level of *TZF10* was detectable in Col-0 control samples after 15 and 45 min after transcriptional block under non-stress conditions (Fig. 20A) in the second experiment. The effect was less pronounced and not significant in NaCl-treated samples, potentially indicating the transcript of *TZF10* to have slightly been more stable under salt stress conditions. In *spi-4*, unlike presented in fig. 12., the mRNA of *TZF10* was not significantly destabilized upon ActD treatment in control and NaCl-treated samples, with the single exception of non-stressed samples treated with ActD for 45 min (Fig. 20B). Hence, the results of the preceding mRNA stability assay suggesting *TZF10* transcripts to generally be more stable in Col-0 compared to in *spi-4*, could not be confirmed.

A Col-0



B *spi-4*

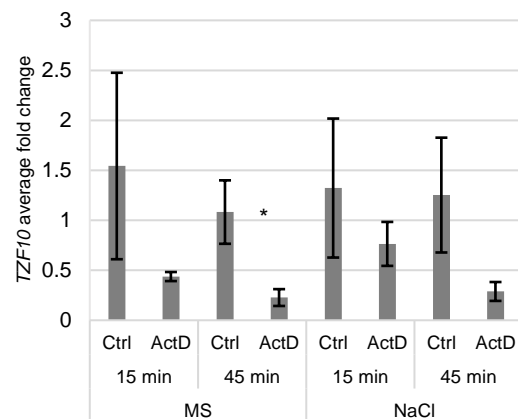


Figure 20: **Stability of *TZF10* mRNA does not strikingly differ in Col-0 compared to *spi-4*.** The effect of transcriptional block induced by ActD is displayed by relative expression of *TZF10* in Col-0 (A) and *spi-4* (B) samples incubated in liquid ½ MS with or without 200 mM NaCl and treated with 150 µg/ml ActD for designated time periods, compared to control samples (Ctrl) incubated in liquid ½ MS with or without 200 mM NaCl only, normalized to reference gene 18S rRNA. $n=3$. Error bars depict standard errors. Significance was tested with a Mann-Whitney-U test ($p < 0.10$).

3.1.5.4 *TZF11* mRNA stability does not differ in *spi-4* compared to Col-0

As no striking differences in *TZF10* mRNA stability in Col-0 compared to *spi-4* were determinable, it was next asked if *TZF11* mRNA stability instead might be affected in *spi-4*. To get a first and quick impression, samples, collected after 45 min of ActD treatment, were analyzed (Fig. 21).

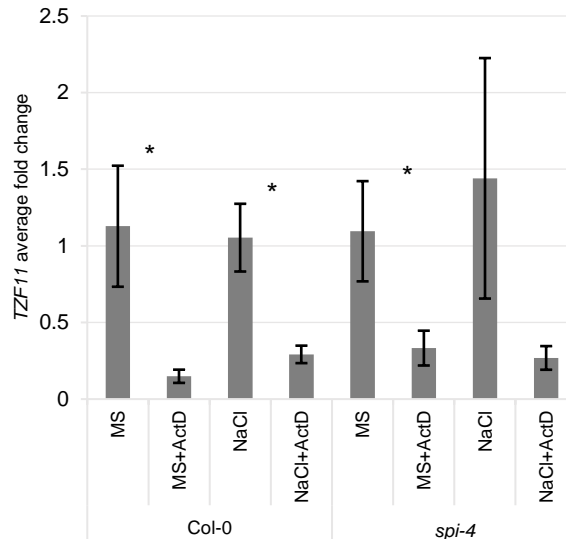


Figure 21: **Stability of *TZF11* mRNA does not strikingly differ in Col-0 compared to *spi-4*.** The effect of transcriptional block induced by ActD is displayed by relative expression of *TZF10* in Col-0 (A) and *spi-4* (B) samples incubated in liquid ½ MS with or without 200 mM NaCl for 90 min and treated with 150 µg/ml ActD for 45 min (45+45), compared to control samples incubated in liquid ½ MS with or without 200 mM NaCl only, normalized to reference gene 18S rRNA. $n=3$. Error bars depict standard errors. Significance was tested with a Mann-Whitney-U test ($p<0.10$).

The analysis however demonstrated that also *TZF11* mRNA is similarly destabilized in *spi-4* and Col-0 under non-stress and stress conditions (Fig. 21).

3.1.6 *TZF10* rescues the salt stress phenotype of *spirrig* irrespective of its 3'UTR

An initial experiment indicated that the introduction of *TZF10* rescued the salt hypersensitivity phenotype of *spirrig* mutants (A. Steffens, unpublished data). In this experiment, the salt response phenotype of the different transgenic lines was tested on the basis of primary root growth. Interestingly, the effect was especially obvious when only the CDS of *TZF10* was introduced, but not distinctively apparent when the 3'UTR was added to the CDS. The used constructs were driven by different promoters (*UBQ10* and *35S CaMV*, respectively) and carried different plant selection markers (glufosinate (phosphinothricin, Basta) and glyphosate resistance genes, respectively). Consequently, the transgenic lines were treated with different herbicides. As both promoter and herbicide treatment could have a significant impact on primary root growth; a new, uniform construct set was composed and subsequently, a set of transgenic lines was generated in this work (Table 3). Moreover, to circumvent herbicide treatment of transgenic lines but not of control plants, a new salt stress screening method was established.

3.1.6.1 Establishment of a salt stress screening method

To examine and screen the salt response of *spi-4* lines, transformed with *TZF10*, leaf whitening as a sign for salt hypersensitivity was evaluated. The seeds were directly sown and grown horizontally on solid ½ MS medium supplemented with 125 mM NaCl. After four weeks, plants

showing green or white leaves were scored and the percentage of plants with completely green leaves was determined. In order to allow estimations on when a transgenic line can be regarded as either salt hypersensitive or rescued, the method was applied to Col-0 and *spirrig* mutants first.

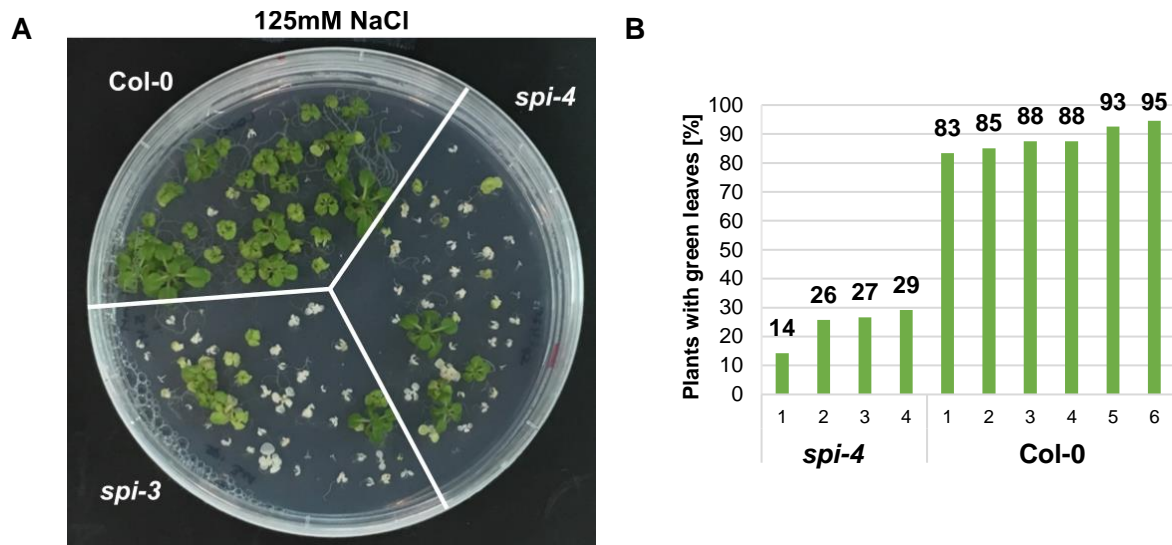


Figure 22: **Salt stress screening on the basis of salt-induced leaf whitening in seedlings.** **A** Exemplary picture of Col-0, *spi-4* and *spi-3* plants, directly sown and grown horizontally on solid $\frac{1}{2}$ MS medium supplemented with 125 mM NaCl for four weeks. **B** Scored percentages of *spi-4* and Col-0 plants with completely green leaves grown on four to six different plates (of in total 11-35 plants each), containing solid $\frac{1}{2}$ MS medium supplemented with 125 mM NaCl for four weeks.

Whereas among Col-0 seedlings only a few plants showed salt-induced whitening of leaves and on average, 88% of Col-0 plants exhibited green leaves; growth of *spirrig* mutants was strongly compromised and leaves showed severe salt-induced whitening (Fig. 22A+B). On average, only 24% of *spi-4* plants exhibited green leaves upon salt treatment (Fig. 22B).

In the subsequent testing of transgenic lines, plants of the T₂ generation are subjected to the salt stress screenings. Because the screening goes without herbicide treatments, the plants are not selected on the basis of construct integration. Thus, untransformed *spi-4* mutants are still present among the tested plants. If it is assumed that the constructs were not inserted multiple times, segregation of constructs occurs 1:2:1. If it is moreover assumed that the construct acts dominant, the following predictions for levels of salt hypersensitivity rescue, visualized in fig. 23, can be postulated.

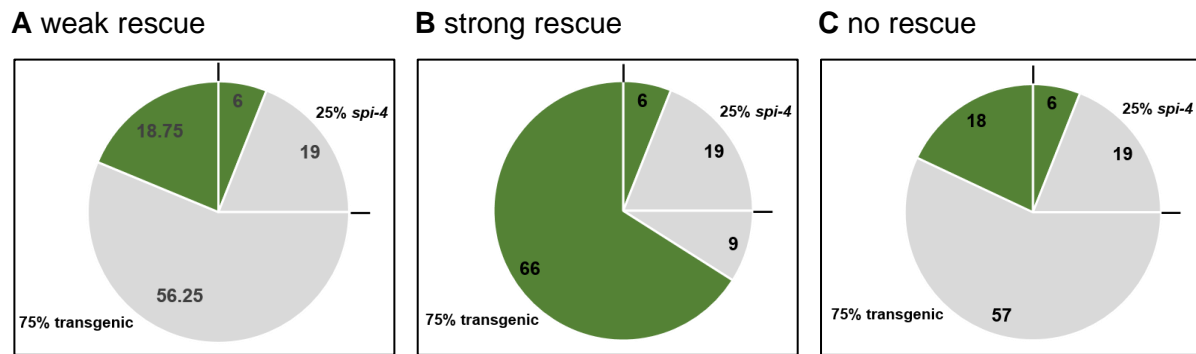


Figure 23: Estimated portion of plants exhibiting green and white leaves of T_2 plants subjected to salt stress screenings in different rescue scenarios. Scenarios of weak (A), strong (B) and no (C) rescue are shown. Values are given in %. Green color indicates the amount of plants with green leaves. Grey color indicates the portion of plants with white leaves.

25% of the tested plants are non-transformed *spirrig* mutants. They are salt hypersensitive. In order to not miss a salt hypersensitivity rescue line, all ensuing calculations were based on the averaged results presented above (Fig. 22B). Thus, approximately 24% of the non-transformed *spirrig* plants are expected to exhibit green leaves anyway. 24% of 25% amount to 6% of the tested plants in total (Fig. 23A-C).

The other 75% of all tested plants are transgenic and either hetero- or homozygous for the introduced construct. At least 25% and at most 88% of these plants are expected to exhibit green leaves in order to be regarded as a candidate for a salt hypersensitivity rescue line. 25% of 75% would represent 18.75% of the tested plants in total (weak rescue, fig. 23A). 88% of 75% of plants amount to 66% of the tested plants in total (strong rescue, fig. 23B).

If only 24% or less of the 75% plants carrying the construct exhibit green leaves, it can be assumed that introduction of the construct did not cause rescue of the *spirrig* salt hypersensitivity phenotype. 24% of 75% of plants amount to 18% of the tested plants in total (no rescue, fig. 23C).

Taken together, the threshold for a transgenic line to be a candidate for salt hypersensitivity rescue is set to 25% (6% of *spirrig* mutants exhibiting green leaves anyways + 18.75% of transgenic lines in case of a weak rescue, fig. 23A, rounded up). Thus, if 25% or more of the plants exhibit green leaves, the salt hypersensitivity of *spirrig* mutants is regarded as rescued.

3.1.6.2 The 3'UTR of *TZF10* has no impact on *spi-4* salt hypersensitivity rescue

An overview of the whole construct/transgenic line set generated in the course of this work, as well as more detailed information concerning used plasmids, can be found in table 3. Table 20 lists the transgenic lines that were selected for salt stress screenings first. Lines transformed with constructs harboring the *TZF10* CDS only and constructs harboring the *TZF10* CDS+3'UTR were chosen. The transcription in lines transformed with constructs without the 3'UTR of *TZF0* is terminated by the construct-own terminator sequence 3'UTR_{35SCaMV}. For the sake of clarity, respective designations have been omitted in the following chapters.

Table 20: **Transgenic lines subjected to salt stress screenings.** Constructs with or without *YFP*, and either carrying only the CDS of *TZF10* or the CDS with the addition of the 3'UTR, were introduced into *spi-4*. Transcription in lines without the 3'UTR_{*TZF10*} is terminated by the construct-own terminator sequence 3'UTR_{35S*CaMV*}. For the sake of clarity, respective designations have been omitted.

| Introduced construct | Background | Selection |
|--|--------------|--|
| <i>UBQ10::YFP-TZF10 CDS</i> | <i>spi-4</i> | Glufosinate resistance gene <i>bar</i> |
| <i>UBQ10::YFP-TZF10 CDS+3'UTR</i> | <i>spi-4</i> | Glufosinate resistance gene <i>bar</i> |
| <i>UBQ10::TZF10 CDS</i> | <i>spi-4</i> | Glufosinate resistance gene <i>bar</i> |
| <i>UBQ10::TZF10 CDS+3'UTR</i> | <i>spi-4</i> | Glufosinate resistance gene <i>bar</i> |

The constructs were introduced into *spirrig* mutants via floral dipping. Subsequently, T₁ plants were Basta-selected and successfully transformed lines were further cultivated. Additional selection on the basis of fluorescence was not possible, as YFP could not be detected in all of the examined plant lines. Seeds of Basta-selected T₁ plants, giving rise to T₂ plants, were subjected to the above described salt stress screening. Successful integration of constructs was exemplarily confirmed by genotyping of T₂ plants. If possible or available, up to 20 T₂ lines for each construct were tested. However, due to low transformation efficiencies, low germination or plate contamination, the number of lines taken into account had to be reduced. On each plate, containing solid ½ MS supplemented with 125 mM NaCl, three different lines with 50 seeds each were grown simultaneously.

According to the predictions presented in 3.1.6.1, the screening revealed 69% of all the tested transformed *spi-4* lines, harboring the *TZF10* CDS only, with or without addition of *YFP*, show a potential rescue of salt hypersensitivity (Fig. 24A).

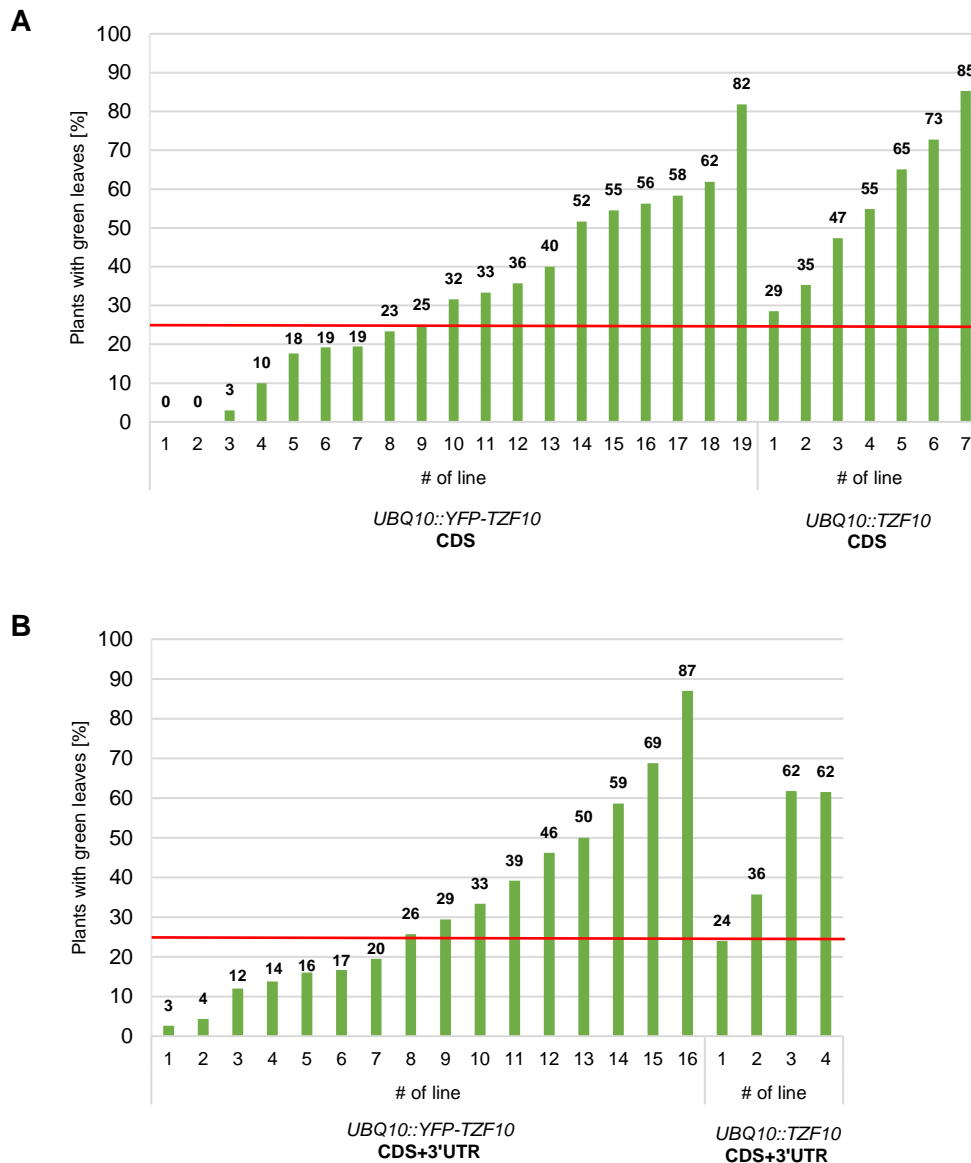


Figure 24: ***TZF10* rescues the salt hypersensitivity phenotype of *spi-4*.** *TZF10* was transformed into *spi-4* plants with or without the addition of the 3'UTR and/or *YFP*. Transgenic *spi-4* T₂ lines harboring either the *TZF10* CDS (A) or the *TZF10* CDS+3'UTR (B) were subjected to salt stress screening. Therefore, seeds were directly sown (three lines with 50 seeds each on plates, due to low germination or contamination: total $n=11-43$) and horizontally grown on 125 mM NaCl. After four weeks of growth, percentages of plants with green leaves were scored. The red line indicates the threshold, above which plants were regarded as salt hypersensitivity rescue lines.

Of the transgenic lines, carrying the *TZF10* CDS + 3'UTR, with or without addition of *YFP*, 60% exhibited increased numbers of plants with green leaves, indicating a potential rescue (Fig. 24B).

Conclusively, the presented results demonstrate that *TZF10* indeed rescues the *spirrig* salt hypersensitivity phenotype. The results however do not indicate that this effect is abrogated when the 3'UTR is present downstream of the *TZF10* CDS. Even if the threshold of 25% of plants with green leaves, above which plants were regarded as salt hypersensitivity rescue lines, would have been set distinctively higher, rescue of *spirrig* transformed with the *TZF10* CDS+3'UTR would still have been determinable. 50% of all plants transformed with the *TZF10*

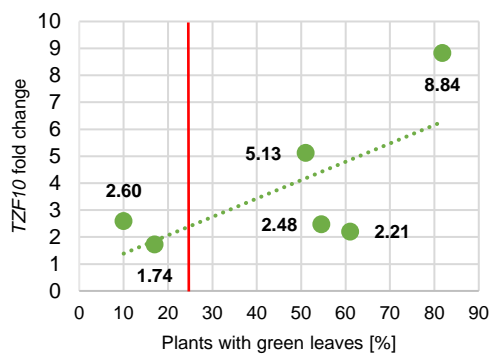
CDS+3'UTR exhibited 30% or more plants with green leaves (Fig. 24B).

The following hypothesis were subsequently postulated and tested:

1) A high *TZF10* expression level could compensate for a potentially increased *TZF10* mRNA decay in lines harboring the 3'UTR. It was therefore tested, if the salt hypersensitivity rescue in *spi-4* lines harboring the *TZF10* CDS+3'UTR can be explained by elevated *TZF10* expression levels.

2) *TZF10* expression levels might generally correlate with the intensity of salt hypersensitivity rescue. Thus, *TZF10* expression levels were exemplarily tested in 12 of the transformed lines. Six lines, of which two exhibited no, and four exhibited clear salt hypersensitivity, were chosen for each construct. Figure 25 shows the result of the analysis.

A *UBQ10::YFP-TZF10* CDS



B *UBQ10::YFP-TZF10* CDS+3'UTR

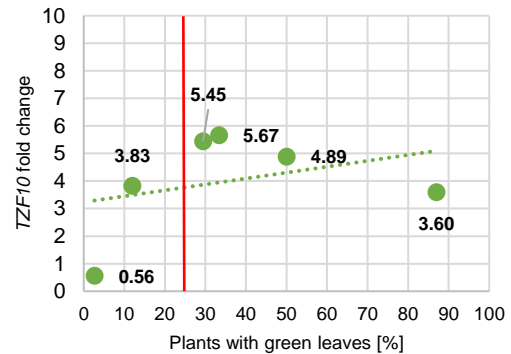


Figure 25: ***TZF10* expression levels do not correspond to salt hypersensitivity rescue intensity** in transgenic *spi-4* lines harboring either the *TZF10* CDS (A) or the *TZF10* CDS+3'UTR (B). *TZF10* expression levels were determined by qPCR analysis (leaf pools of \geq five plants horizontally grown on solid $\frac{1}{2}$ MS supplemented with 125 mM NaCl for four weeks, $n=2$). Expression levels were normalized to reference gene 18S rRNA. *TZF10* fold changes, compared to *TZF10* relative expression levels in Col-0, are shown. The red line marks the threshold above which lines were regarded as salt hypersensitivity lines. The green lines represent the trend lines with the coefficients of determination $r^2 = 0.47$ (A) and $r^2 = 0.112$ (B).

With the exception of one line with a fold change of 0.56, all the tested transgenic lines were identified as *TZF10* overexpression lines (Fig. 25). The results however did not indicate that *TZF10* expression levels were substantially higher in lines transformed with the *TZF10* CDS+3'UTR, than in lines transformed with the *TZF10* CDS only. The underlying hypothesis that a high *TZF10* expression level would compensate for a potentially increased *TZF10* mRNA decay in lines harboring the 3'UTR, has to therefore be neglected. Plant lines with comparably lower *TZF10* fold change showed relatively strong rescue (e.g. fold change 2.21 with 61% of plants with green leaves, fig. 25A) while plant lines with similar *TZF10* fold change showed no rescue (e.g. fold change 2.6 with 10% of plants with green leaves, fig. 25A). At the same time, the intensity of salt hypersensitivity rescue in plant lines with comparably high *TZF10* expression levels (fold change of around 5) varied strongly as well (29-51% of plants with green leaves). Even though a trend of higher expression in strong rescue plants might be

observable (trend line, fig. 25A+B), a general direct correlation of *TZF10* expression levels with the level of salt hypersensitivity rescue could not be detected, further supported by low coefficients of determination ($r^2 = 0.47$ (Fig. 25A) and $r^2 = 0.112$ (Fig. 25B)).

3.1.6.3 *TZF10* mRNA destabilization, induced by its 3'UTR, cannot be correlated to salt hypersensitivity rescue of *spirrig*

Even though it was shown that a high *TZF10* expression level did not compensate for a potentially increased *TZF10* mRNA decay in transgenic *spi-4* salt hypersensitivity rescue lines harboring the *TZF10* CDS+3'UTR (3.1.6.2); a general influence of the 3'UTR on *TZF10* mRNA stability has not been excluded yet.

It can be hypothesized that a low intensity of salt hypersensitivity rescue exhibited by transgenic *spi-4* lines expressing the *TZF10* CDS+3'UTR might be due to increased *TZF10* mRNA decay induced by the 3'UTR. In order to investigate this notion, *TZF10* mRNA stability in plant lines transformed with the *TZF10* CDS has to be assessed and compared to mRNA stability in plant lines transformed with the *TZF10* CDS+3'UTR. Towards this, data derived from experiments presented in 3.1.5.2, were analyzed. In total six transgenic *spi-4* lines either transformed with the *TZF10* CDS or the *TZF10* CDS+3'UTR (3.1.6.2; three for each construct) with similar *TZF10* expression levels (fold change: 2.21 - 5.67) were selected. While *TZF10* CDS expression lines with relatively strong salt hypersensitivity rescue phenotype were picked (50-61% plants with green leaves), *TZF10* CDS+3'UTR expression lines with no or weak salt hypersensitivity rescue phenotype were chosen (12-33% plants with green leaves). Single site insertion and thus heterozygosity of T₂ lines was confirmed beforehand.

Fig. 26 depicts the results of *TZF10* mRNA stability analysis in three independent *TZF10* overexpression lines for each construct with *spi-4* background.

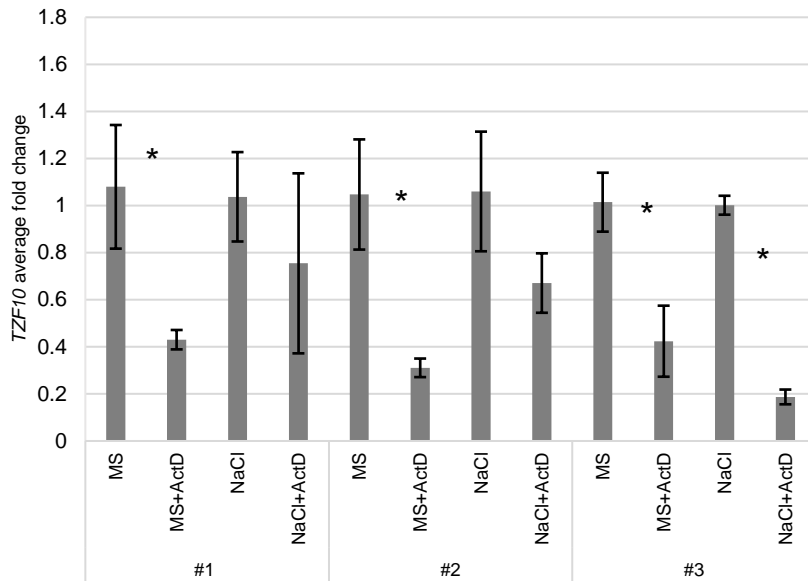
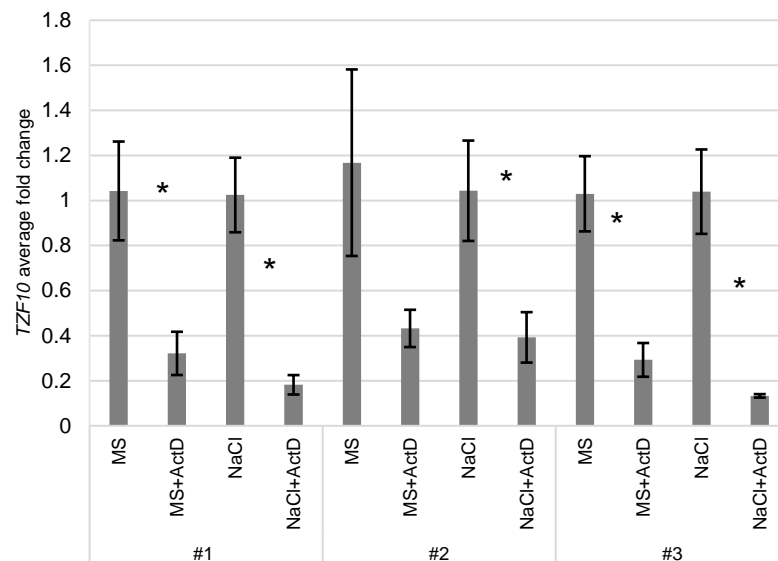
A *TZF10* CDS in *spi-4* (three independent lines, #1-3)**B *TZF10* CDS+3'UTR in *spi-4* (three independent lines, #1-3)**

Figure 26: **The *TZF10* 3'UTR could render *TZF10* mRNA less stable under salt stress conditions.** The effect of transcriptional block induced by ActD is displayed by relative expression of *TZF10* in three different transgenic *spi-4* lines either transformed with the *TZF10* CDS (A) or the *TZF10* CDS+3'UTR (B). Samples were incubated in liquid ½ MS with or without 200 mM NaCl and treated with 150 µg/ml ActD for 15 min, compared to control samples incubated in liquid ½ MS with or without 200 mM NaCl only, and normalized to reference gene 18S rRNA. $n=3$. Error bars depict standard errors. Significance was tested with a Mann-Whitney-U test ($p<0.10$).

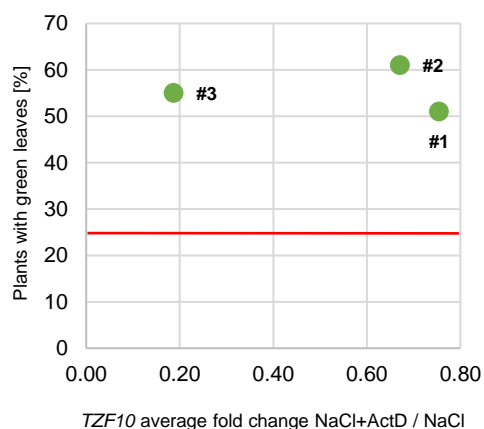
All the lines transformed with the *TZF10* CDS showed significant destabilization of the *TZF10* transcript under non-stress conditions, represented by significantly lower *TZF10* expression levels upon ActD treatment compared to control samples (Fig. 26A). While in two of the lines clear stabilization of *TZF10* transcript was detectable upon salt treatment (no significant difference of *TZF10* average fold change upon ActD treatment in #1 and #2), one line showed

significantly lower expression levels of *TZF10*, induced by ActD, suggesting the *TZF10* mRNA to here be destabilized under salt stress conditions as well.

The lines transformed with the *TZF10* CDS+3'UTR overall displayed *TZF10* transcript destabilization under control and salt stress conditions, depicted by significant differences in *TZF10* average fold changes of ActD-treated compared to control samples (Fig. 26B). No significant difference, but clear tendency, was solely determinable in one line (#2) under control conditions (Fig. 26B).

While the results on one hand imply that the addition of the 3'UTR to the CDS of *TZF10* generally causes increased destabilization of the *TZF10* transcript in the overexpression lines especially under salt stress conditions, on the other hand, the results cannot be correlated to the overexpression lines' salt hypersensitivity rescue phenotype. Fig. 27 visualizes the level of *TZF10* mRNA destabilization with corresponding levels of salt hypersensitivity rescue in the analyzed transgenic lines. Line #3, transformed with the *TZF10* CDS, exhibited increased *TZF10* transcript destabilization under salt stress conditions compared to line #1 and #2. However, the level of salt hypersensitivity rescue phenotype of line #3 (Fig. 27A, 55% plants with green leaves, 3.1.6.2) was comparable to those of line #1 (Fig. 27A, 51% plants with green leaves, 3.1.6) and line #2 (Fig. 27A, 61% plants with green leaves, 3.1.6.2).

A *UBQ10::YFP-TZF10* CDS



B *UBQ10::YFP-TZF10* CDS+3'UTR

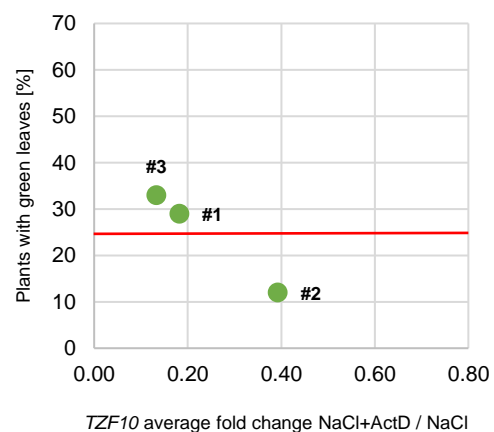


Figure 27: **Increased *TZF10* transcript destabilization does not correlate with the *spirrig* salt hypersensitivity rescue level.** *TZF10* average fold changes (samples treated with 200 mM NaCl and 150 μ g/ml ActD for 15 min, compared to control samples treated with 200 mM NaCl without ActD, and normalized to reference gene 18S rRNA) were plotted against the level of salt hypersensitivity rescue (plants with green leaves in %) of respective transgenic lines (three independent lines for each construct #1-#3, harboring the *TZF10* CDS only (A) or the *TZF10* CDS+3'UTR (B)). $n=3$. Error bars have been omitted for the sake of a better overview, but are given in the corresponding figure 26. The red line marks the threshold above which lines were regarded as salt hypersensitivity lines.

In agreement with an overall increased *TZF10* transcript destabilization under salt stress conditions, the level of salt hypersensitivity phenotype rescue in the tested *spi-4* lines transformed with the *TZF10* CDS+3'UTR, was generally lower (Fig. 27B, #3 = 33% and #1 = 29% plants with green leaves, 3.1.6.2). Nonetheless, while line #2 exhibited no salt

hypersensitivity phenotype rescue (Fig. 27B, 12% plants with green leaves, 3.1.6.2), *TZF10* transcript destabilization was slightly less pronounced in line #2 compared to the other two lines displaying a clear salt hypersensitivity rescue phenotype. Taken together, the results suggest that *TZF10* transcript destabilization induced by the *TZF10* 3'UTR does not affect the level of salt hypersensitivity rescue of stably transformed *spirrig* mutants.

3.1.6.4 *RD29A* is strongly up-regulated in a *TZF10* overexpression line, but is not affected in its mRNA stability

Examination of salt-inducible *RD29A* expression levels in *spi-4*, and *spi-4* transformed with *TZF10* CDS or *TZF10* CDS+3'UTR, interestingly revealed an extreme up-regulation of *RD29A* (fold change 59.3) in one of the two tested lines transformed with the *TZF10* CDS after 60 min of salt treatment (Fig. 28A). Up-regulation of *RD29A* upon salt stress was strikingly lower in *spi-4* (fold change 17.9, fig. 28A) and the other tested transgenic lines, transformed with *TZF10* CDS or *TZF10* CDS+3'UTR (fold changes from 14.5 - 23, fig. 28A). The result raised the question, if *RD29A* mRNA generally is more stable in *spi-4* lines expressing *TZF10* CDS under salt stress conditions.

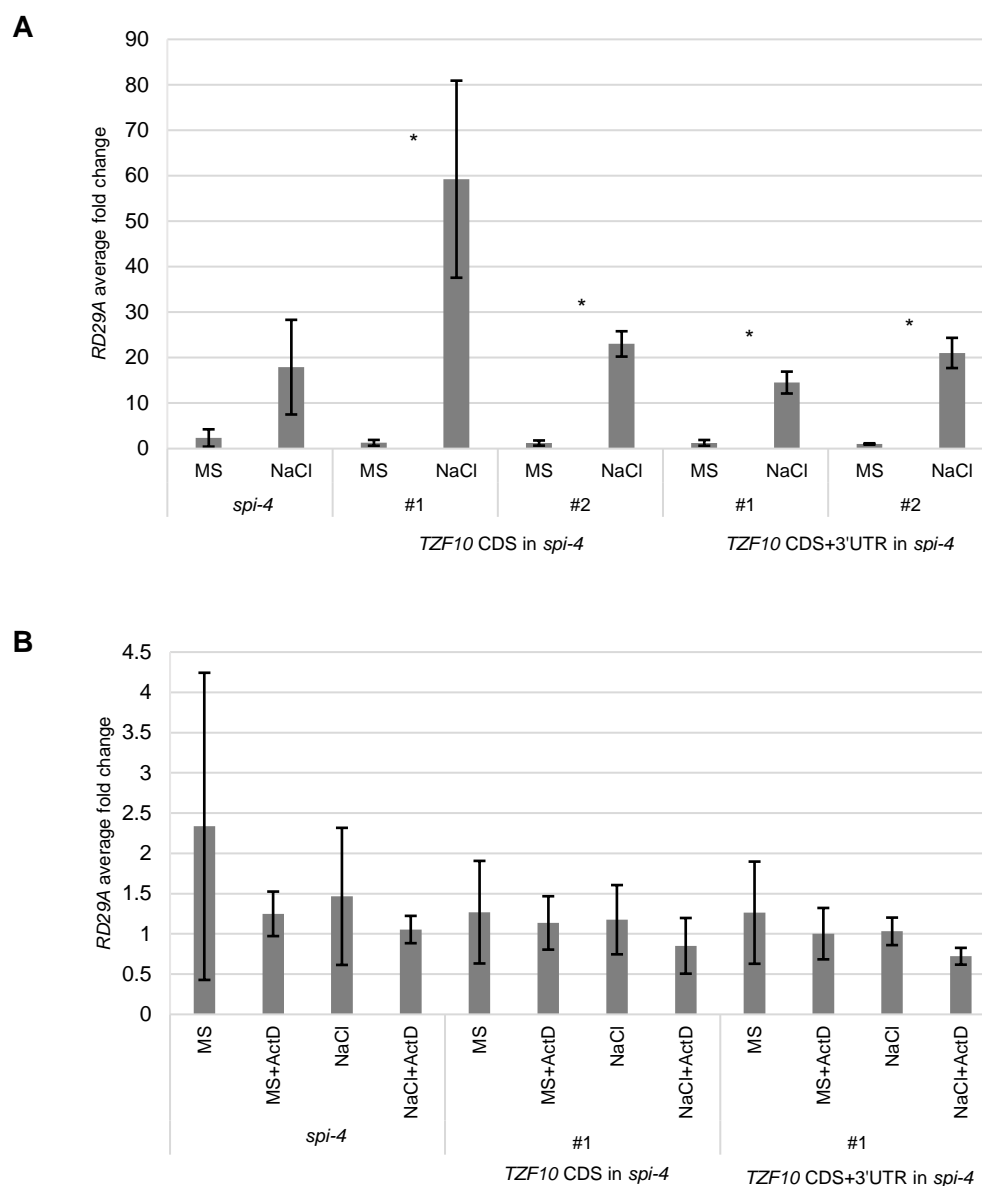


Figure 28: **RD29A expression levels.** The effect of salt treatment (**A**) and transcriptional block induced by ActD (**B**) was tested in *spi-4* and transgenic *spi-4* lines transformed with indicated constructs. **A** Relative expression of *RD29A* in samples incubated in liquid $\frac{1}{2}$ MS containing 200 mM NaCl for 60 min, compared to control samples incubated in liquid $\frac{1}{2}$ MS only, normalized to reference gene 18S rRNA. $n=3$. Error bars depict standard errors. Significance was tested with a Mann-Whitney-U test ($p<0.10$). **B** Relative expression of *RD29A* in samples incubated in liquid $\frac{1}{2}$ MS with or without 200 mM NaCl for 60 min and treated with 150 μ g/ml ActD for 15 min compared to respective control samples, normalized to reference gene 18S rRNA. $n=3$. Error bars depict standard errors. Significance was tested with a Mann-Whitney-U test ($p<0.10$).

Analysis of the samples treated with ActD (60 min salt including treatment with 150 μ g/ml ActD for 15 min, fig. 28B), however did not indicate stronger stabilization of *RD29A* mRNA in the transgenic lines. *RD29A* mRNA appeared to be evenly stable in *spi-4* and the overexpression lines, as *RD29A* expression levels were not reduced upon ActD treatment under non-stress as well as salt stress conditions in all the samples (Fig. 28B).

3.1.7 The salt hypersensitivity phenotype of *spirrig* is not mitigated by introduction of *TZF10* and *11* alleles with disrupted 3'UTRs

Initial experiments indicated that the salt hypersensitivity phenotype of *spirrig* mutants can be rescued by the introduction of the *TZF10* CDS (A. Steffens, unpublished data). However, when the 3'UTR was added to the CDS, this effect was not apparent. The results strongly suggested that *TZF10* destabilizes its own mRNA by binding of its own 3'UTR. Accordingly, this study investigated, in parallel to experiments presented in 3.1.6, if stably introduced versions of *TZF10* and *11*, with disrupted 3'UTRs, could rescue or mitigate the salt hypersensitivity phenotype of *spirrig* mutants. For both *TZF10* and *11*, insertion lines with the T-DNA directly located in the 3'UTR, were available and obtained from the Nottingham Arabidopsis Stock Center (SAIL_207G08 and SAIL_191G05, respectively, for more details see table 2). Homozygous mutants (further referred to as *tzf10-2* and *tzf11-3*) were isolated, insertion sites were confirmed by genotyping as well as subsequent sequencing of the flanking genomic DNA regions, and *spirrig/tzf* (*spi-3/tzf10-2* and *spi-4/tzf11-3*) double mutants were generated by crossing.

The salt response of the single and double mutants was tested by examination of primary root growth and leaf whitening. The *spirrig* alleles *spi-4* and *spi-3* were included in the analysis as positive controls for salt hypersensitivity.

As expected, primary root growth reduction of *spi-4* and *spi-3* was significantly lower than that of wild type plants on 125 mM NaCl (Fig. 29A). Likewise, leaf whitening, as a sign for salt hypersensitivity, was severely enhanced in *spirrig* mutants compared to Col-0 (Fig. 29B). Primary root growth of *tzf10* and *tzf11* single mutants with disrupted 3'UTRs did not significantly differ compared to Col-0 (Fig. 29A). Similarly, leaf whitening was not altered compared to wild type plants (Fig. 29B). The introduction of the *tzf10* and *tzf11* single 3'UTR mutations into *spirrig* mutants did not lead to a rescue or mitigation of the salt hypersensitivity phenotype, as results for both, primary root growth reductions and percentages of green leaves, were on the same level as in *spi-4* and *spi-3* plants, respectively.

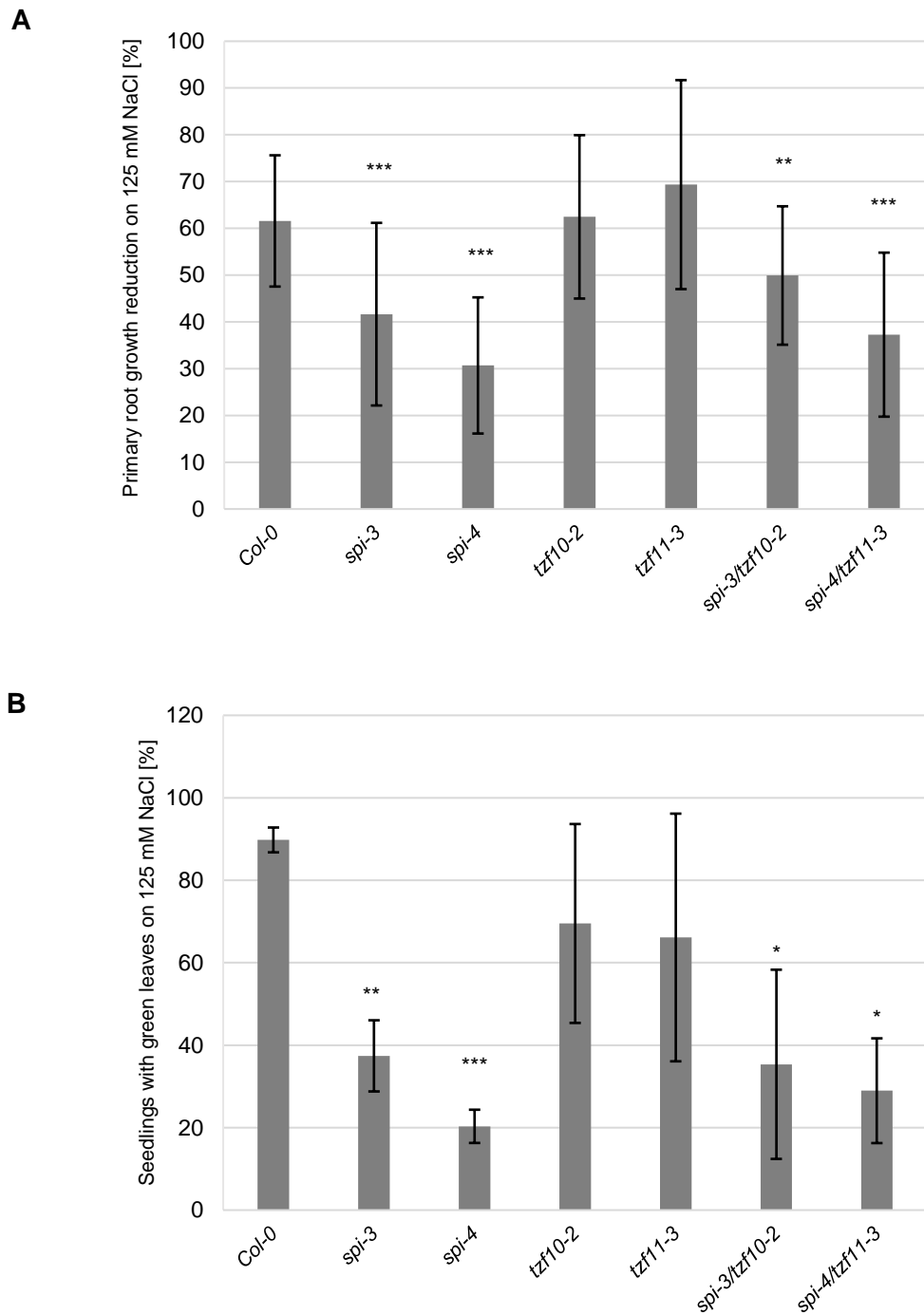


Figure 29: **The stably introduced disruption of the *TZF10* or *TZF11* 3'UTR does not mitigate the salt hypersensitivity phenotype of *spirrig* mutants. A Primary root growth reductions.** Seeds were sown on $\frac{1}{2}$ MS agar plates and grown for seven days under normal conditions. Afterwards, seedlings of each genotype were transferred to two fresh $\frac{1}{2}$ MS agar control plates and $\frac{1}{2}$ MS agar plates supplemented with 125 mM NaCl, respectively. Primary root growth reduction was assessed after five days for $n \geq 19$ plants. **B Percentages of plants with green leaves.** Seeds were sown and directly grown on $\frac{1}{2}$ MS plates supplemented with 125 mM NaCl. After four weeks, plants showing green or white leaves were scored and the percentage of plants with completely green leaves was determined. For each genotype, $n \geq 11$ plants each were grown on three different plates. Average percentages are shown. Asterisks indicate significant differences in primary root growth reductions or percentages of plants with green leaves between the mutant plants and the wild type Col-0; ***= $p < 0.001$; **= $p < 0.01$; *= $p < 0.05$. Significance was tested with unpaired, two-tailed Student's *t*-tests. Error bars represent the standard deviation.

These results, and the results presented in 3.1.6, do not hint towards an effect of the *TZF10* 3'UTR on the salt stress phenotype of *spirrig* as it was hypothesized before.

3.1.8 *TZF10* rescues the salt stress phenotype of *spirrig* irrespective of its 5'UTR

Similar to 3'UTRs, also 5'UTRs can contain several linear or structural regulatory elements strongly contributing to gene expression and/or translation. While the 5' m⁷GpppG cap can already determine efficiency of translation, also secondary structural elements (reviewed in Leppek et al., 2017), upstream open reading frames (uORFs; Lin et al., 2019), Kozak sequences improving ATG recognition (Kozak, 1986) or regulatory RBPs binding to the 5'UTR (Wilkie et al., 2003), can enhance or repress translation. Moreover, it was shown that introns in 5'UTRs generally can affect gene expression. For example, 5'UTR intron length of the *A. thaliana* *ELONGATION FACTOR 1 α -A3* (*EF1 α -A3*) gene was demonstrated to determine the level of gene expression (Chung et al., 2006).

The 3'UTR was not proven to influence the salt hypersensitivity rescue phenotype of *spi-4* by the introduction of *TZF10*. Therefore, it was asked next, if the *TZF10* 5'UTR might have a regulatory effect on *TZF10* gene expression or translation in *spirrig* mutants in general or even has an impact on salt hypersensitivity rescue of *spirrig* mutants.

While the CDS of *TZF10* consists of a single exon, one intron is located in its 5'UTR. Two intron splicing models, with a length difference of 4 bp, are available (arabidopsis.org). It would be conceivable, to find one gene model predominant over the other in *spi-4*, dependent on salt stress or not. Thus, qualitative RT-PCR on salt-treated and control *spi-4* and Col-0 cDNA and subsequent sequencing were performed. However, no indication for a different pattern of *TZF10* splicing variants in *spi-4* was found (data not shown).

To evaluate potential effects induced by the *TZF10* 5'UTR on salt hypersensitivity rescue of *spirrig* mutants, it was investigated next, if salt hypersensitivity is also rescued by introduction of constructs containing the *TZF10* 5'UTR in addition to its CDS+3'UTR. An overview of the generated transgenic lines is given in table 21. In addition to lines harboring the *TZF10* 5'UTR, with or without *YFP* tag, transformants containing a swap construct with the 5'UTR of *ABF3* were generated. *ABF3* was regarded as a suitable control, as its transcript was shown to not be affected in its stability in *spirrig* mutants under non-stress and stress conditions (Steffens et al., 2015).

Table 21: **Transgenic lines subjected to salt stress screenings.** Constructs with or without *YFP*, and either carrying only the CDS of *TZF10* or the CDS with the addition of the 3'UTR, were introduced into *spi-4*.

| Introduced construct | Background | Selection |
|--|--------------|--|
| <i>UBQ10::5'UTR_{TZF10}- CDS+3'UTR_{TZF10}</i> | <i>spi-4</i> | Glufosinate resistance gene <i>bar</i> |
| <i>UBQ10::5'UTR_{TZF10}-YFP- CDS+3'UTR_{TZF10}</i> | <i>spi-4</i> | Glufosinate resistance gene <i>bar</i> |
| <i>UBQ10::5'UTR_{ABF3}-YFP- CDS+3'UTR_{TZF10}</i> | <i>spi-4</i> | Glufosinate resistance gene <i>bar</i> |

The generation, selection and salt stress screening of transgenic lines was performed as described in chapter 3.1.6.

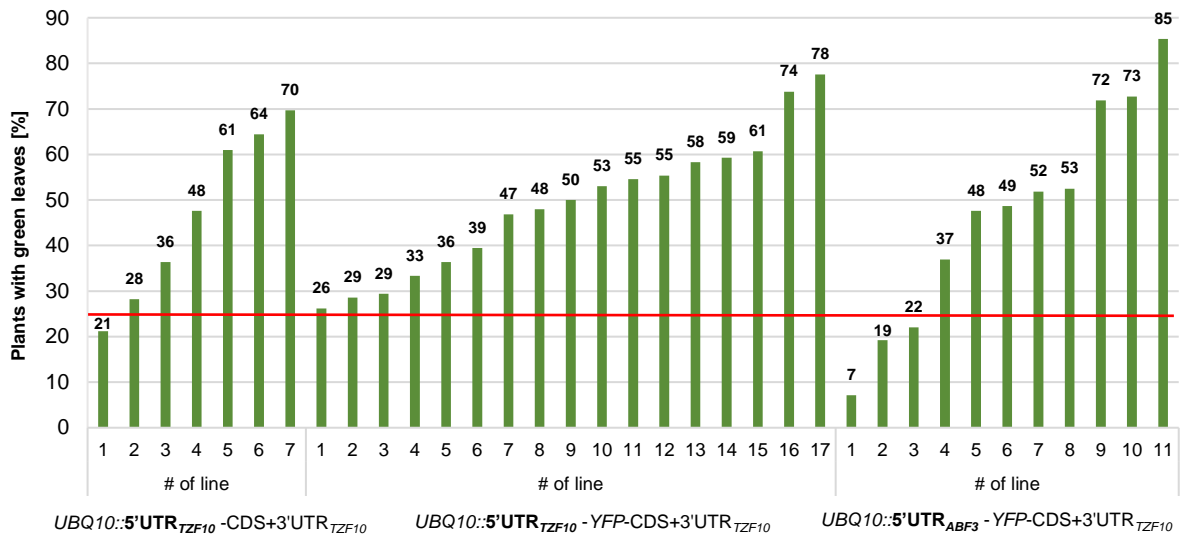


Figure 30: ***TZF10* rescues the salt hypersensitivity phenotype of *spi-4* irrespective of its 5'UTR.** *TZF10* was transformed into *spi-4* plants with or without the addition of the *TZF10* or *ABF3* 5'UTR and/or *YFP*. The transgenic T₂ lines were subjected to salt stress screening. Therefore, seeds were directly sown (three lines with approximately 60 seeds each on plates, due to low germination or contamination: total $n=11-64$) and horizontally grown on 125 mM NaCl. After four weeks of growth, percentages of plants with green leaves were scored. The red line indicates the threshold, above which plants were regarded as salt hypersensitivity rescue lines.

96% of the 24 tested lines containing the *TZF10* 5'UTR, with or without *YFP*, displayed clear rescue of salt hypersensitivity, represented by more than 25% of plants with green leaves upon salt treatment for four weeks. Of 11 lines containing the *ABF3* 5'UTR, eight (=73%) exhibited rescue of the *spirrig* salt hypersensitivity phenotype (Fig. 30). The results thus do not hint to an impact of the *TZF10* 5'UTR; rescue of *spi-4* salt hypersensitivity by introduction of *TZF10* not only occurs irrespectively of 3'UTR presence, but also of 5'UTR presence.

3.1.9 The 3'UTR of *TZF10* mediates mRNA destabilization effects independent from *spirrig*

The fact that all the *spi-4* lines, stably transformed with a construct containing the *TZF10* CDS+3'UTR and analyzed in the stability assay exhibited increased overall *TZF10* mRNA stabilization under salt stress conditions, indicated that the 3'UTR generally might have a destabilizing capacity independent from *spirrig*. This notion was investigated in three different approaches, presented in the following.

3.1.9.1 The 3'UTR has no substantial impact on *TZF10* and 11 mRNA localization

As the *TZF10* 3'UTR was shown to have a destabilizing effect on the mRNA of *TZF10* upon salt stress (3.1.6, fig. 26B), it was reasoned that the 3'UTR might alter mRNA localization under stress conditions. To evaluate a potential impact, general localization behavior of *TZF10* and 11 mRNA with and without the addition of the 3'UTR was investigated in wild type plants next.

Therefore, respective reporter and mRNA target constructs were transiently expressed in leaves of *A. thaliana* (via particle bombardment) and *N. benthamiana* (via leaf infiltration). The transcription of constructs without the 3'UTR of *TZF10* is terminated by the construct-own *A. tumefaciens* octopine synthase (OCS) terminator sequence 3'UTR_{OCS}. For the sake of clarity, respective designations have been omitted in the following. mRNA localization was qualitatively assessed under non-stress and stress conditions. As heat stress is particularly efficient and feasible for plant material, the transformed leaves were treated with 40°C for 50 min to induce stress responses.

Figure 31 shows the transient visualization of the *TZF10* mRNA (CDS) with and without addition of the 3'UTR by particle bombardment of *A. thaliana* Col-0 leaves. Irrespective of the addition of the 3'UTR, the mRNA of *TZF10* mainly showed nuclear-cytoplasmic localization with occasional occurrence of cytoplasmic granules. The stress granule marker UBP1b (Nguyen et al., 2016) was chosen as a stress marker and co-transformed. Upon heat treatment, a strong increase of UBP1b labeled cytoplasmic dots demonstrated the substantial impact of heat stress on the leaves. However, the appearance of *TZF10* mRNA labeled dots co-localizing with UBP1b, was only slightly increased, with or without the addition of the *TZF10* 3'UTR (Fig. 31, row 2, mRNA of *TZF10* CDS).

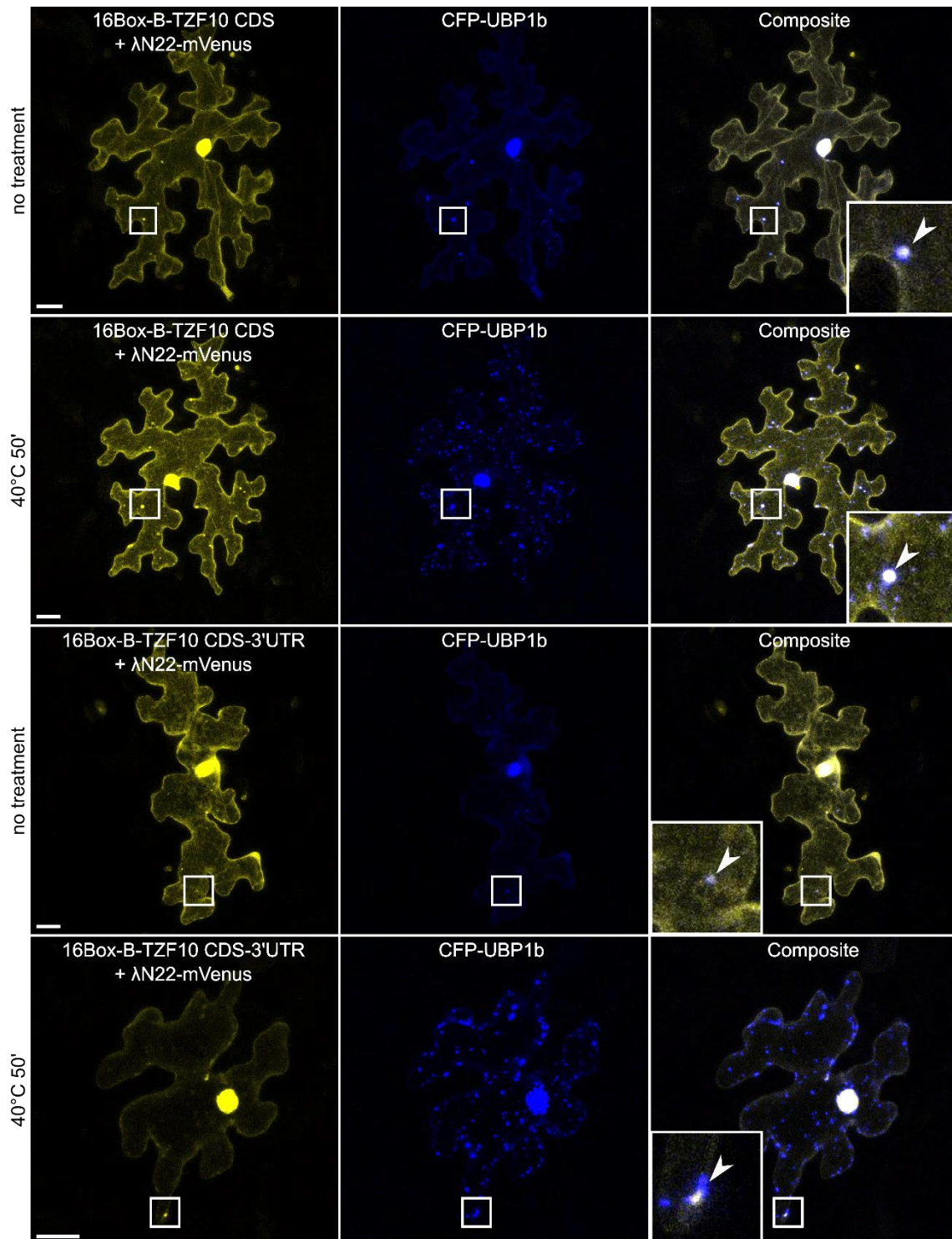


Figure 31: **The mRNA of *TZF10* localizes to stress granules.** The λ N22-system was applied to transiently visualize the mRNA of *TZF10* CDS with or without the addition of the 3'UTR in *Col-0* via particle bombardment in *A. thaliana* epidermal leaf cells. Exemplary pictures of cells under non-stress and stress (40°C, 50 min) conditions are shown. The arrows highlight overlapping *TZF10* mRNA signals with the stress granule marker CFP-UBP1b. Scale bars indicate 20 μ m.

The here presented experiments were conducted to get a general impression on *TZF* mRNA localization under non-stress and stress conditions. Therefore, thorough evaluation of potential negative controls (e.g. as performed in Steffens et al. (2015), details given in 3.1.2) has been omitted in these first attempts. However, a λ N22-mVENUS reporter co-expressed with Box-B

repeats without an mRNA target, but still containing the GW-cassette, was included in the analysis and monitored under non-stress and stress conditions. Upon transient expression in *A. thaliana* epidermal leaf cells, the λ N22-mVENUS reporter was located in the nucleus and the cytoplasm, but also in distinct cytoplasmic granules (Fig. 76, row 1, appendix). After heat treatment, the amount of granules even increased (Fig. 76, row 2, appendix). This result confirms the finding of Schönberger et al. (2012), who reported perpetual presence of cytoplasmic “transport” foci independent of the RNA type (foreign, TagRFP or plant mRNA) upon utilization of the λ N22-system. However, when the λ N22-mVENUS reporter was co-expressed with Box-B repeats fused to the GW-cassette in tobacco epidermal leaf cells, almost none of such cytoplasmic foci were observed before and after heat treatment (Fig. 77, row 1+2, appendix). This might indicate that transient *N. benthamiana* expression could be more suitable for utilization of the λ N22-system and could allow acquisition of more reliable results.

Thus, the constructs and combinations for evaluation of *TZF10* mRNA localization were transiently expressed in *N. benthamiana* (Fig. 32) by infiltration of leaves next. In line with previous results, the mRNA of *TZF10*, with or without added 3'UTR, showed nuclear-cytoplasmic and occasional dot-like localization under non-stress conditions (Fig. 32, rows 1+3). Upon heat stress, the localization of the *TZF10* CDS mRNA did not noticeably change (Fig. 32, row 2). In contrast, the mRNA of the *TZF10* CDS+3'UTR accumulated in an increased number of cytoplasmic granules frequently co-localizing with the stress granule marker UBP1b (Fig. 32, row 4). However, it was not possible to reproduce this result in several further repetitions of the experiment and the mRNA of the *TZF10* CDS+3'UTR did not repeatedly show altered localization behavior upon heat treatment. Sporadically, the *TZF10* CDS+3'UTR mRNA could be observed in cytoplasmic granules, co-localizing with UBP1b, in a similar manner as the mRNA of the *TZF10* CDS only (exemplarily shown in fig. 78, appendix).

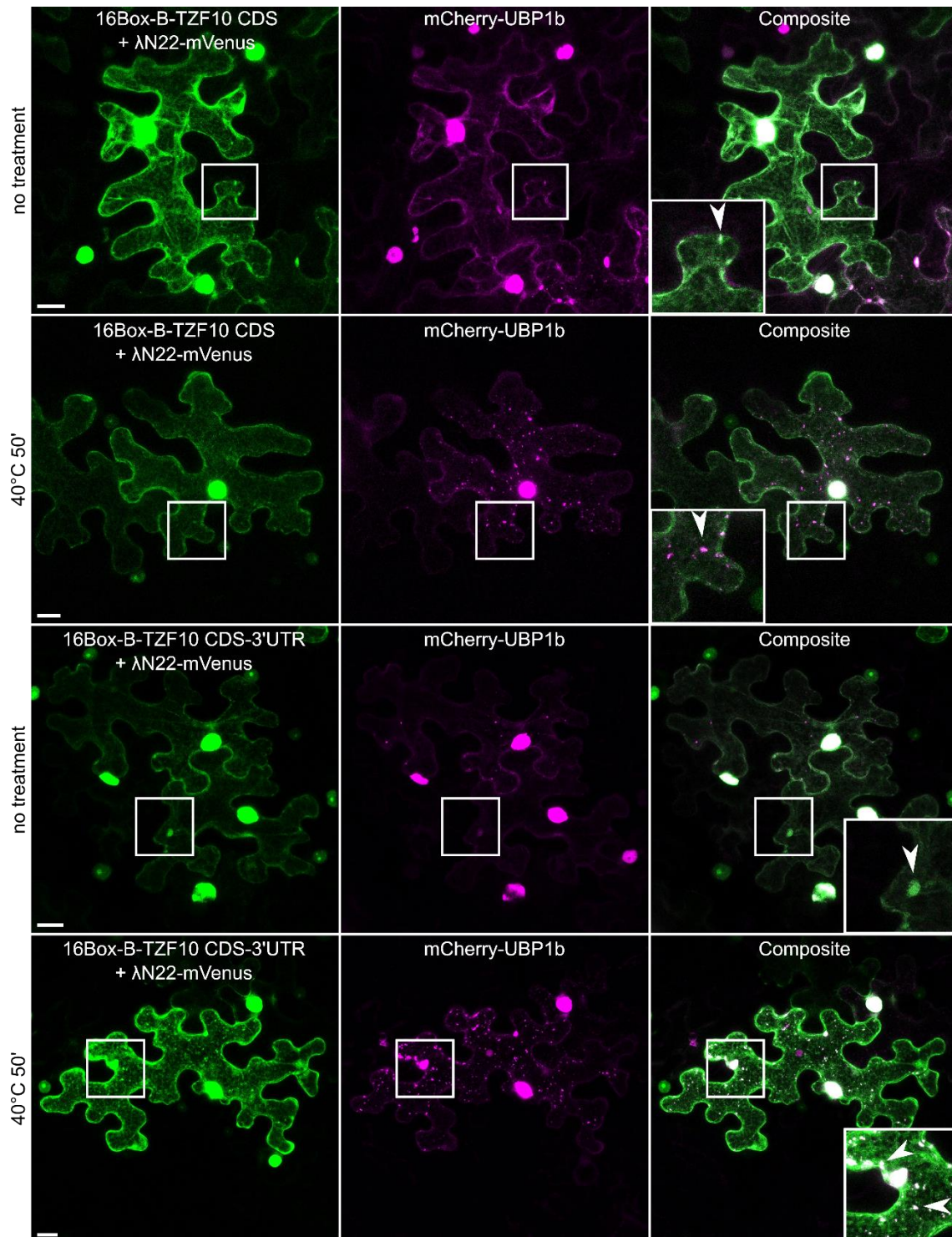


Figure 32: **The mRNA of *TZF10* localizes to stress granules.** The Δ N22-system was applied to transiently visualize the mRNA of *TZF10* CDS with or without the addition of the 3'UTR via infiltration of *N. benthamiana* leaves. Exemplary pictures of epidermal cells under non-stress and stress (40°C, 50 min) conditions are shown. The arrows highlight overlapping *TZF10* mRNA signals with the stress granule marker CFP-UBP1b. Scale bars indicate 20 μ m.

To assess the localization of the mRNA of *TZF11* as well, respective reporter and mRNA target constructs with and without fused 3'UTR were infiltrated in *N. benthamiana* leaves and subjected to heat stress without a stress marker protein first. Under non-stress conditions, and irrespective of the 3'UTR, the mRNA of *TZF11* was located in the nucleus and cytoplasm of the tobacco epidermal cells with almost no occurrence of cytoplasmic granules (Fig. 33, left

row). Upon heat stress and in contrast to the localization of the *TZF10* mRNA, a strong accumulation of *TZF11* mRNA labeled cytoplasmic dots could be observed with or without addition of the 3'UTR (Fig. 33, right row).

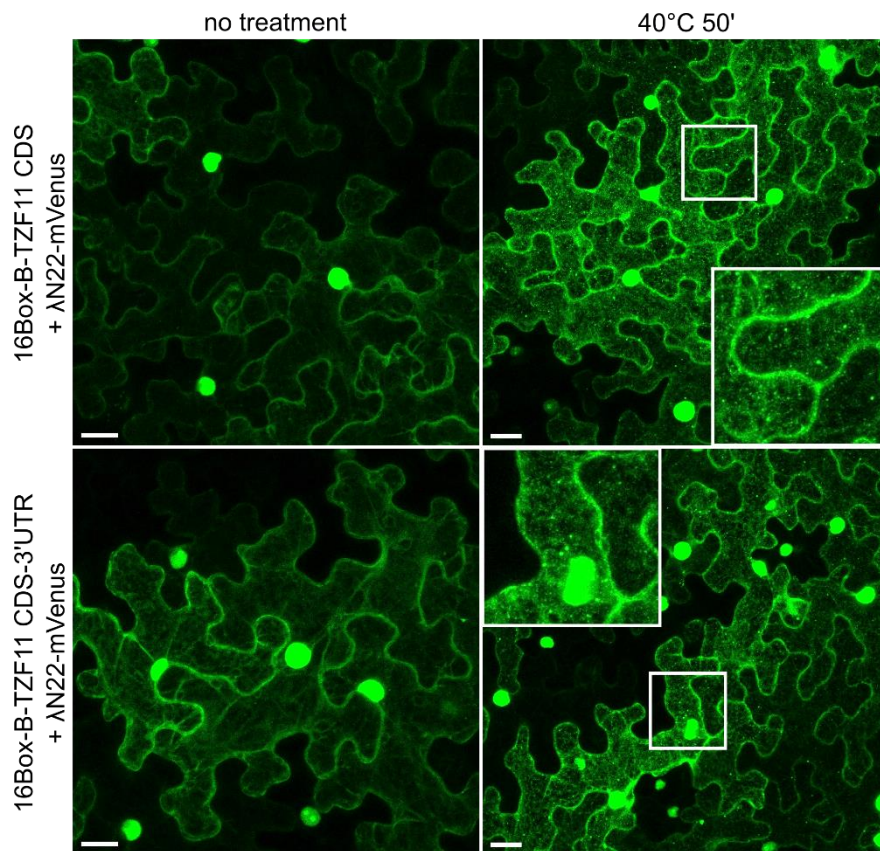


Figure 33: **The mRNA of *TZF11* localizes to stress granules.** The ΔN22-system was applied to transiently visualize the mRNA of *TZF11* CDS with or without the addition of the 3'UTR via infiltration of *N. benthamiana* leaves. Exemplary pictures of epidermal cells under non-stress and stress (40°C, 50 min) conditions are shown. The arrows highlight overlapping *TZF10* mRNA signals with the stress granule marker CFP-UBP1b. Scale bars indicate 20 μm.

In summary, the here presented results did not provide consistent evidence for a potential impact of the 3'UTR on the mRNA localization of *TZF10* and *11*. Localization behavior under non-stress conditions and stress conditions did not particularly differ when the 3'UTR was absent or present downstream of the *TZF10* and *11* CDS mRNA. Therefore, the experiments were not further pursued.

3.1.9.2 The 3'UTR of *TZF10* destabilizes mRNA of *YFP*

In order to investigate the subcellular localization guided by the 3'UTR of *TZF10* and *11*, the 3'UTRs of both genes were fused to *YFP* under the control of a *UBQ10* promoter. The constructs were transiently expressed in *A. thaliana* Col-0 epidermal cells via particle bombardment. Surprisingly, *YFP* expression was hardly detectable in transformed cells when *YFP* was fused to either the 3'UTR of *TZF10* or *TZF11* (Fig. 34, row 1+2) implying the 3'UTRs to be able to induce *YFP* mRNA destabilization. Parallel expression of a peroxisome marker (*35S::CFP-SKL*) proved successful transformation of the observed cells.

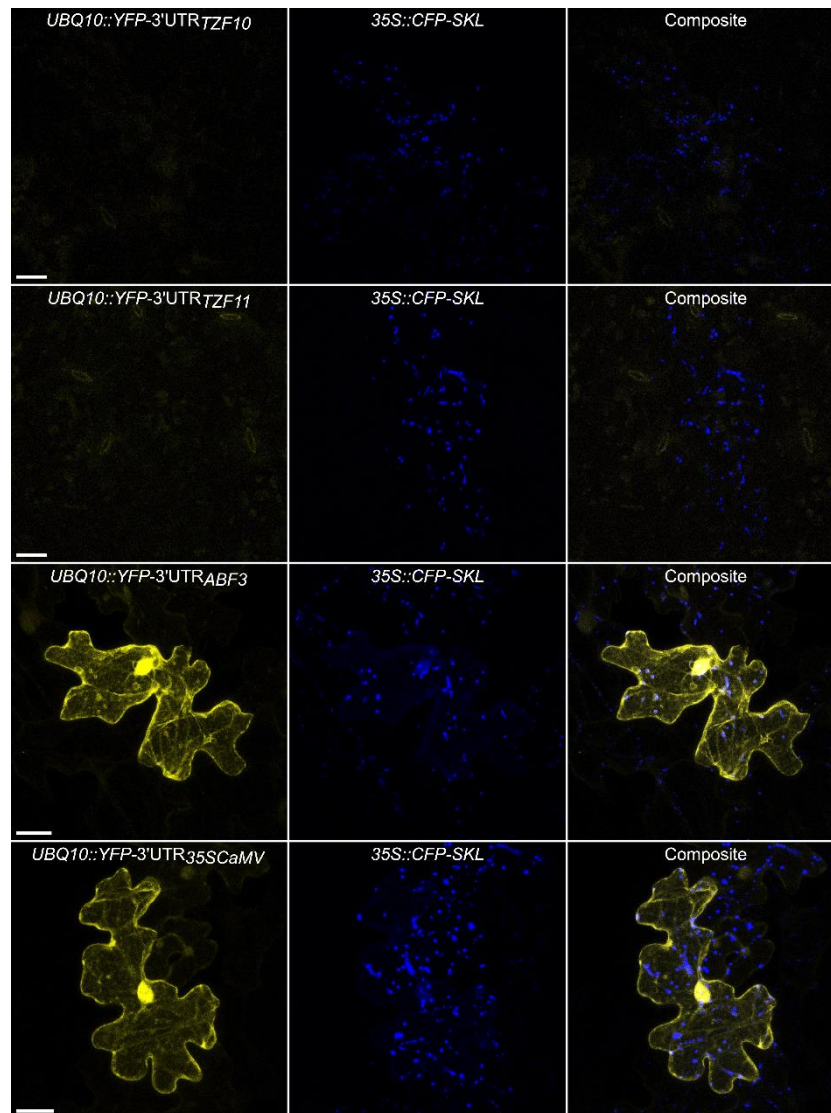


Figure 34: **Expression of YFP is not detectable when fused to the 3'UTRs of TZF10 and 11.** The figure shows exemplary pictures of transient expression of indicated constructs via particle bombardment of *A. thaliana* epidermal cells. Whereas no or very weak YFP fluorescence was detectable when fused to the 3'UTRs of TZF10 and 11 (row 1+2), YFP expression upon transformation of control constructs (row 2 +3) was very strong. The pictures were taken at an argon laser intensity of 20%. YFP was excited with the 512 nm laser line, set to a high intensity (15-18%) for 3'UTR constructs to detect any fluorescence and was set low (1-2%) for control constructs. Apart from that, the exact same settings (same digital gain and offset, no line or frame averaging/accumulation) were applied to all scans. No modifications to single pictures were made. The peroxisomal marker 35S::CFP-SKL served as a control for transformation. The scale bar depicts 20 μ m.

As positive controls, a construct containing YFP only (*UBQ10::YFP* + construct-own 3'UTR_{35SCaMV}) and a construct containing YFP fused to the 3'UTR of *ABF3* (*UBQ10::YFP-3'UTR_{ABF3}*) were chosen. The transcript of *ABF3* on one hand was shown to not be affected in its stability in *spirrig* mutants under non-stress and stress conditions (Steffens et al., 2015). On the other hand, literature research indicated its 3'UTR to have never been shown to be implicated in regulating mRNA stability. Confocal microscopy of positive control samples demonstrated strong and expected expression of YFP (Fig. 34, row 3+4).

The expression of YFP is diminished when fused to parts of TZF10 and 11 3'UTRs

The human TZF protein TTP was not only demonstrated to induce mRNA decay by binding ARE sequences in 3'UTRs of target transcripts (Wells et al., 2017), but also of its own mRNA (Brooks et al., 2004; Tchen et al., 2004). Therefore, it was reasoned that the 3'UTRs of *TZF10* and *11* might also contain ARE sequences or other mRNA destabilizing motifs. To identify and to elucidate the mRNA destabilizing capacity, fragments of both *TZF10* and *11* 3'UTRs were consecutively generated mainly on the basis of sequence. Folding structure was additionally evaluated with the Software for Statistical Folding of Nucleic Acids and Studies of Regulatory RNAs (Sfold, <http://sfold.wadsworth.org>; job mode: batch; minimum free energy structure diagram), but was only considered when otherwise potentially folded parts would have been heavily disrupted (exemplarily shown for *TZF10*, fig. 79, appendix). Sequence analysis using RegRNA2.0 (Chang et al., 2013) did not identify any classical ARE sequence in the 3'UTRs of *TZF10* and *11*. An overview on the generated 3'UTR fragments is presented in fig. 35.

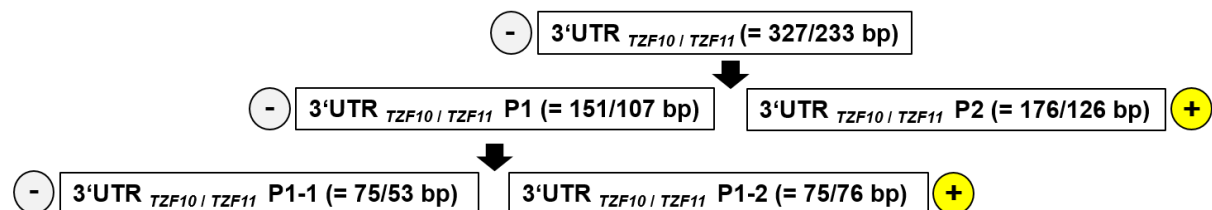


Figure 35: **Generated fragments of the *TZF10* and *11* 3'UTR.** The 3'UTRs of *TZF10* and *11* were consecutively split into fragments. The minus (grey) indicates the fragments leading to no or low fluorescence; the plus (yellow) indicates the fragments leading to strong fluorescence upon fusion to *YFP* and subsequent biolistic, transient transformation of *A. thaliana* epidermal cells. P=part.

Fig. 36 shows the results of the transient expression of constructs containing two parts (resulting from the first split) of the *TZF10* and *11* 3'UTR, respectively, fused to *YFP*. Whereas the constructs harboring the 3'UTRs' 5'end parts (P1) showed no or very weak *YFP* fluorescence, transformation of constructs harboring the 3'end parts (P2) resulted in very strong expression of *YFP* (Fig. 36).

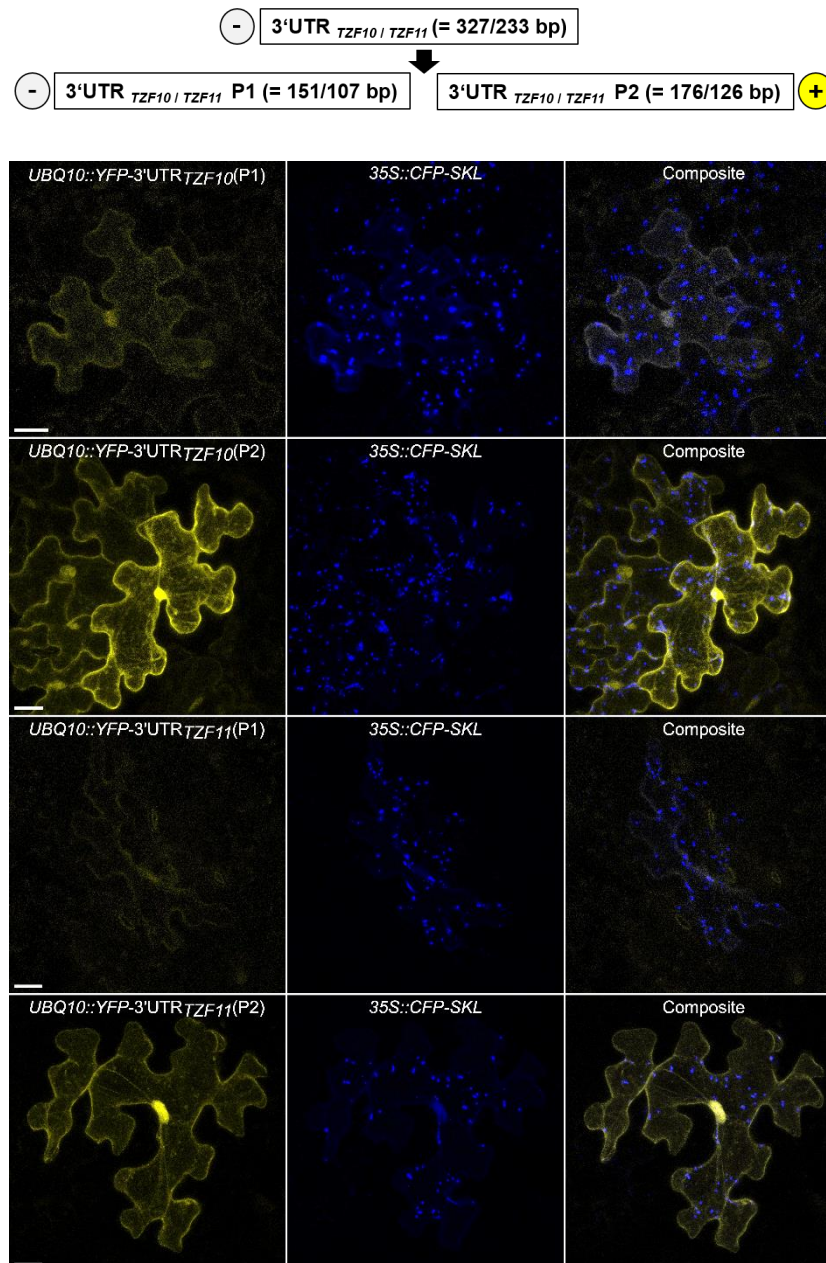


Figure 36: **Expression of YFP is diminished when fused to parts of *TZF10* and *11* 3'UTRs.** The figure shows exemplary pictures of transient expression of indicated constructs via particle bombardment of *A. thaliana* epidermal cells. Whereas no or very weak YFP fluorescence was detectable when fused to the P1 of *TZF10* and *11* 3'UTRs (row 1+3), YFP expression upon transformation of constructs containing P2 (row 2+4) was very strong. The pictures were taken at an argon laser intensity of 20%. YFP was excited with the 514 nm laser line, that was set to a high intensity (15-18%) for P1 constructs to detect any fluorescence and was set low (1-2%) for P2 constructs. Apart from that, the exact same settings (same digital gain and offset, no line or frame averaging/accumulation) were applied to all scans. No modifications to single pictures were made. The peroxisomal marker *35S::CFP-SKL* served as a control for transformation. P=part. The scale bar depicts 20 μ m.

Consequently, P1 fragments of *TZF10* and *TZF11* 3'UTRs were further split into two parts (see overview provided in fig. 35 and fig. 37).

Strikingly, transformation of constructs containing 5'end parts (P1-1) again led to no or very weak expression of YFP, while there was strong expression of YFP upon transformation of constructs containing 3'end parts (P1-2, fig. 37).

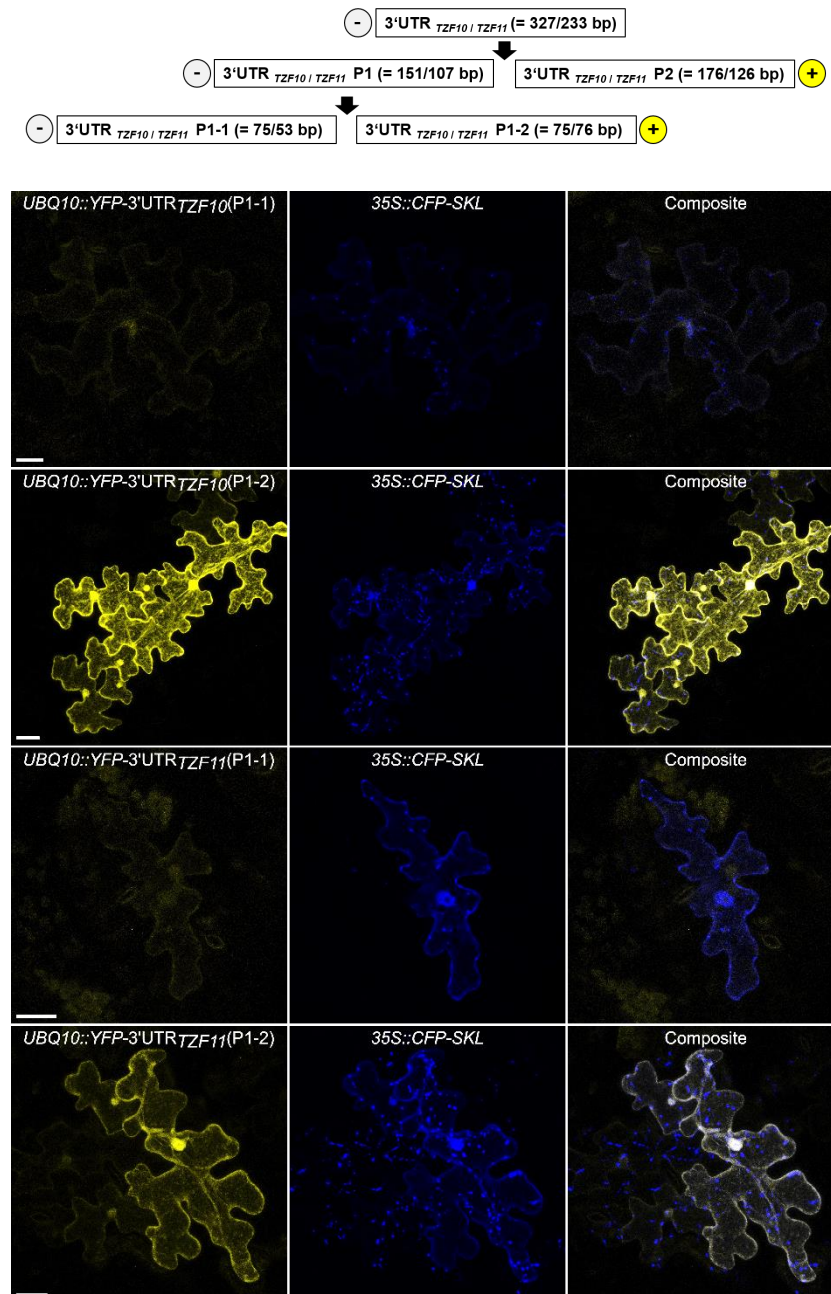


Figure 37: **Expression of YFP is diminished when fused to parts of TZF10 and 11 3'UTRs.** The figure shows exemplary pictures of transient expression of indicated constructs via particle bombardment of *A. thaliana* epidermal cells. Whereas no or very weak YFP fluorescence was detectable when fused to the P1-1 of TZF10 and 11 3'UTRs (row 1+3), YFP expression upon transformation of constructs containing P1-2 (row 2+4) was very strong. The pictures were taken at an argon laser intensity of 20%. YFP was excited with the 512 nm laser line, that was set to a high intensity (15-18%) for P1-1 constructs to detect any fluorescence and was set low (1-2%) for P1-2 constructs. Apart from that, the exact same settings (same digital gain and offset, no line or frame averaging/accumulation) were applied to all scans. No modifications to single pictures were made. The peroxisomal marker 35S::CFP-SKL served as a control for transformation. P=part. The scale bar depicts 20 μ m.

An AU-rich, conserved region of the TZF10 and 11 3'UTRs likely harbors a motif mediating mRNA destabilization

The subsequent creation of fragments from both TZF10 and 11 3'UTR parts P1-1 was based on the alignment provided in fig. 38. As indicated, five fragments were generated in total, with respect to a conserved region of 31/37 bp (Fig. 38).

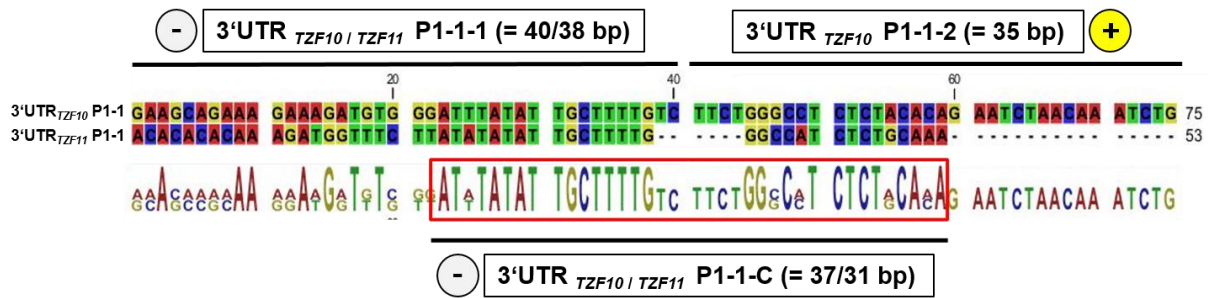


Figure 38: **Alignment of the 5' end parts (P1-1) of *TZF10* and 11 3'UTRs.** Creation of fragments P-1-1, P-1-2 and P1-1-C (P=part; C=conserved region) was based on the provided alignment generated with CLC DNA Workbench 5.6.1. P1-1-2 was solely generated for *TZF10*. The minus (grey) indicates the fragments leading to no or low fluorescence; the plus (yellow) indicates the fragments leading to strong fluorescence upon fusion to *YFP* and subsequent biolistic, transient transformation of *A. thaliana* epidermal cells. The red box highlights a conserved region of the *TZF10* and *11* 3'UTR.

When 3'UTR_{*TZF10*}(P1-1-1) and (P1-1-C), containing both the 5' end of the conserved region, were fused to *YFP* and transiently expressed in *A. thaliana*, only very weak expression of *YFP* was detectable (Fig. 39). Likewise, the C-terminal fusion of the two *TZF11* 3'UTR parts P1-1-1 and P1-1-C strongly diminished *YFP* fluorescence (Fig. 39). Strong expression of *YFP* was solely detectable when fused to 3'UTR_{*TZF10*}(P1-1-2), containing the 3' end of the conserved region (Fig. 39).

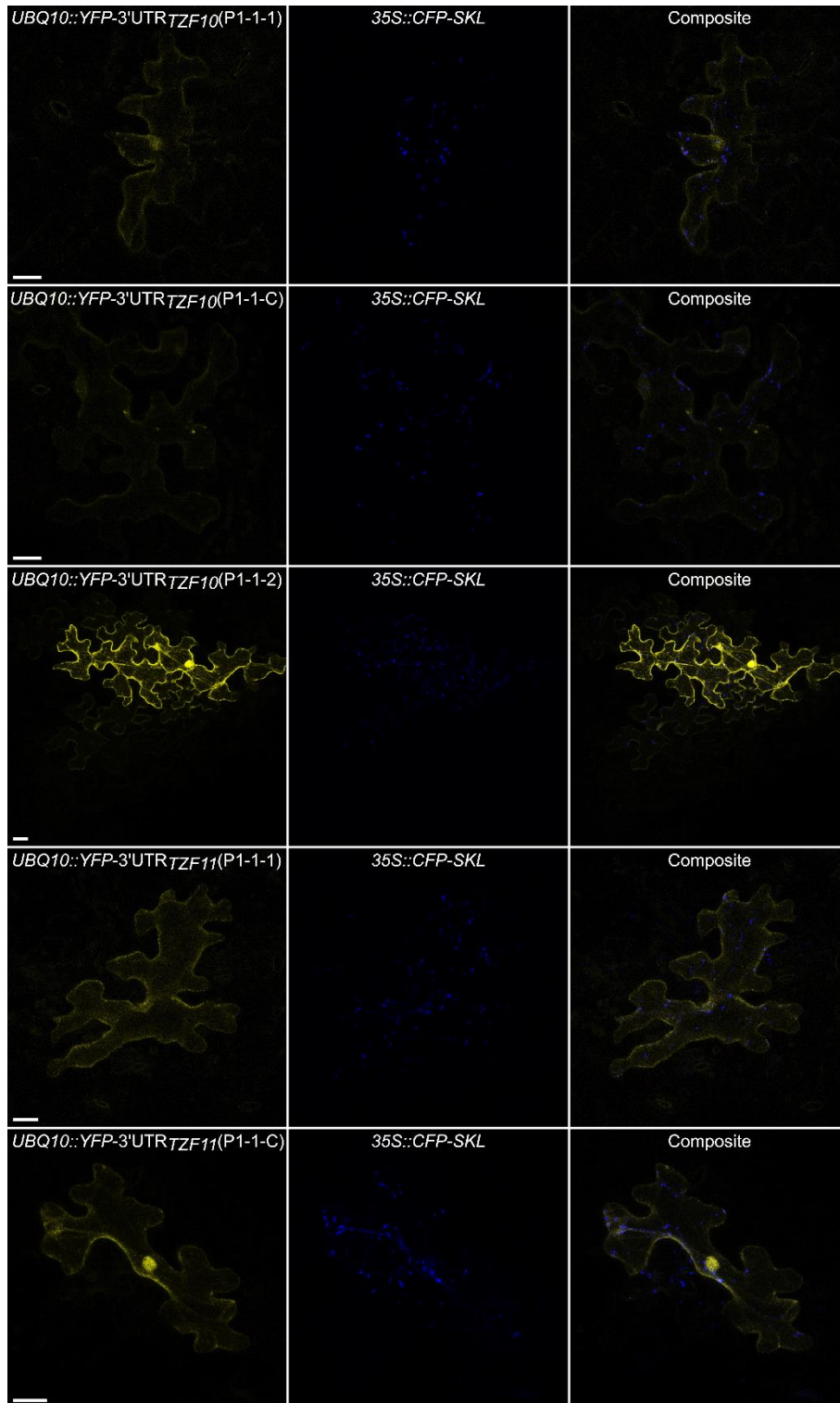


Figure 39: **Expression of YFP is diminished when fused to parts of *TZF10* and *11* 3'UTRs.** The figure shows exemplary pictures of transient expression of indicated constructs via particle bombardment of *A. thaliana* epidermal cells. Whereas no or very weak YFP fluorescence was detectable when fused to the P1-1-1 and P1-1-C (P=part; C=conserved) of *TZF10* 3'UTR (row 1+2), YFP expression upon transformation of a construct containing P1-1-2 (row 3) was very strong. Weak YFP fluorescence was detectable when fused to the P1-1-1 and P1-1-C (P=part; C=conserved) of *TZF11* 3'UTR. The pictures were taken at an argon laser intensity of 20%. YFP was excited with the 514 nm laser line that was set to a high intensity (15-18%) for P1-1-1/-C constructs to detect any fluorescence and was set low (1-2%) for the *TZF10* P1-1-2 construct. Apart from that, the exact same settings (same digital gain and offset, no line or frame averaging/accumulation) were applied to all scans. No modifications to single pictures were made. The peroxisomal marker 35S::CFP-SKL served as a control for transformation. The scale bar depicts 20 μ m.

The results demonstrate that the potential mRNA decay inducing region was successfully narrowed down to the approximately first 80 bp of both the *TZF10* and *11* 3'UTR. As the shared sequence between the parts P1-1-1 and P1-1-C (compare alignment provided in fig. 38) presumably induced *YFP* mRNA decay, indicated by diminished YFP fluorescence (Fig. 39), a potential motif mediating mRNA destabilization most likely is located in the first 15 bp, **AUUUAUAUUGC UUUG**, of the conserved region within these 80 bp.

The expression of YFP is strong when fused to mutated parts of the TZF10 3'UTR

To support this finding and to evaluate the possible role of this AU-rich region, 3'UTR_{*TZF10*}(P1-1-C) was mutated next. Qu et al. (2014) reported Arabidopsis TZF1 to bind to AREs. In order to demonstrate specific binding, the authors used mutated ARE probes, disrupted by replacements of A by G residues. Similarly, U or A residues were replaced in two different mutated versions of 3'UTR_{*TZF10*}(P1-1-C; fig. 40).

| | |
|--|--|
| <i>UBQ10::YFP-3'UTR_{TZF10}(P1-1-C)</i> | A T T T A T A T T G C T T T T G T C T T C T G G G C C T C T C T A C A C A |
| <i>UBQ10::YFP-3'UTR_{TZF10}(P1-1-C) MUT1</i> | A G G G A G A G G G C G G G G T C T T C T G G G C C T C T C T A C A C A |
| <i>UBQ10::YFP-3'UTR_{TZF10}(P1-1-C) MUT2</i> | A G G G A G A G G G C G G G G T C T T C T G G G C C G C G C G G C G C G |

Figure 40: Mutated (MUT) versions of construct *UBQ10::YFP-3'UTR_{TZF10}(P1-1-C)*. P=part; C=conserved.

Compared to the non-mutated version of the construct, expression of *YFP* was substantially enhanced when fused to the mutated 3'UTR parts (Fig. 41). The effect was already visible when only the 5' end part of the sequence was mutated (MUT1) and not particularly intensified when the 3' end part of the sequence was additionally altered (MUT2; fig. 41).

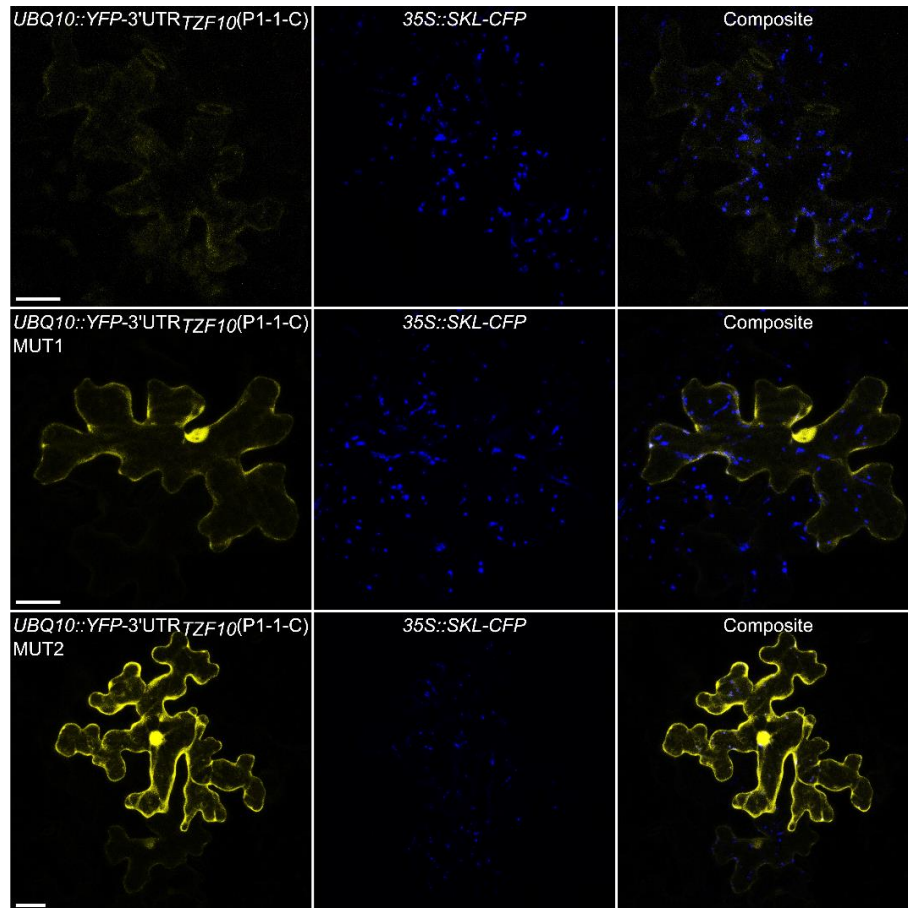


Figure 41: **Expression of YFP is strong when fused to mutated parts of *TZF10* 3'UTR.** The figure shows exemplary pictures of transient expression of indicated constructs via particle bombardment of *A. thaliana* epidermal cells. Whereas no or very weak YFP fluorescence was detectable when fused to the P1-1-C (P=part; C=conserved) of *TZF10* 3'UTR (row 1), YFP expression upon transformation of constructs containing mutated versions (row 2+3) was very strong. The pictures were taken at an argon laser intensity of 20%. YFP was excited with the 514 nm laser line, which was set to a high intensity (18%) for P1-1-C construct to detect any fluorescence. At the same intensity (18%) expression of YFP fused to mutated versions (row 2+3) was substantially stronger. The exact same settings (same digital gain and offset, no line or frame averaging/accumulation) were applied to all scans. No modifications to single pictures were made. The peroxisomal marker *35S::CFP-SKL* served as a control for transformation. The scale bar depicts 20 μm .

The result supports the hypothesis that the potential mRNA destabilization inducing motif is located in the first 15 bp of the *TZF10* 3'UTR and that an intact AU residue array is possibly required. In another approach, the potential motif **AUUUAUAUUGCUUUG** was introduced into the 3'UTR of *ABF3*. However, in the context of a foreign 3'UTR, not known to be implicated in mRNA decay, diminished YFP expression mediated by the motif was not observable. The intensity of YFP fluorescence was on a comparable level as when native *ABF3* 3'UTR was fused to YFP (data not shown, compare fig. 34).

3.1.9.3 Localization of the *TZF10* 3'UTR is not altered upon heat stress

In order to investigate the localization of the *TZF10* 3'UTR itself under non-stress and stress conditions, the mRNA was indirectly visualized using the λN22 system (Schönberger et al., 2012; introduced in 3.1.2). Respective constructs were transiently expressed in

N. benthamiana via leaf infiltration. Localization behavior was observed before and after heat treatment of 40°C for 50 min. Co-localization with the SG marker UBP1b was examined.

Under non-stress conditions, the 3'UTR of *TZF10* was nuclear-cytoplasmically localized with occasional occurrence in dot-like structures (Fig. 42, row 1). Likewise, UBP1b fluorescence was detected in the nucleus and evenly in the cytoplasm before heat stress. Strong formation of SGs labeled by UBP1b was detectable upon heat treatment as expected (Fig. 42, row 2). In contrast, no alteration of the *TZF10* 3'UTR localization was observable. The 3'UTR was found in the nucleus, cytoplasm and was rarely co-localizing with SGs marked by UBP1b under stress conditions (Fig. 42, row 2).

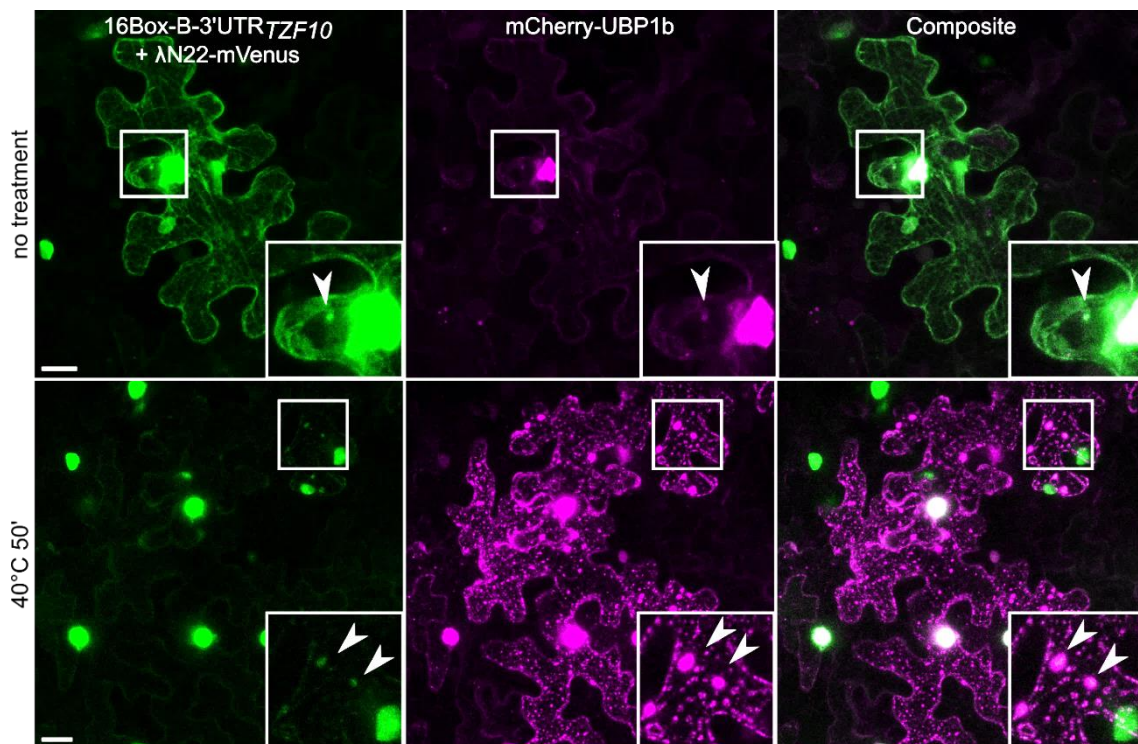


Figure 42: **The localization of *TZF10* 3'UTR is not altered upon heat stress.** The λ N22-system was applied to transiently visualize the *TZF10* 3'UTR via infiltration of *N. benthamiana* leaves. Exemplary pictures of epidermal cells under non-stress and stress (40°C, 50 min) conditions are shown. The arrows highlight overlapping *TZF10* mRNA signals with the stress granule marker mCherry-UBP1b. Scale bars indicate 20 μ m.

Next, fragments of the *TZF10* 3'UTR were visualized. In preceding experiments (3.1.9.3), part 1 (P1) of *TZF10* 3'UTR (3.1.9.3, fig. 36) was identified to presumably destabilize the mRNA of *YFP*, indicated by strongly diminished fluorescence when fused to *YFP*. In contrast, fusion of *TZF10* 3'UTR part 2 (P2) to *YFP* and subsequent transient expression in *A. thaliana*, resulted in strong *YFP* fluorescence (3.1.9.3, fig. 36).

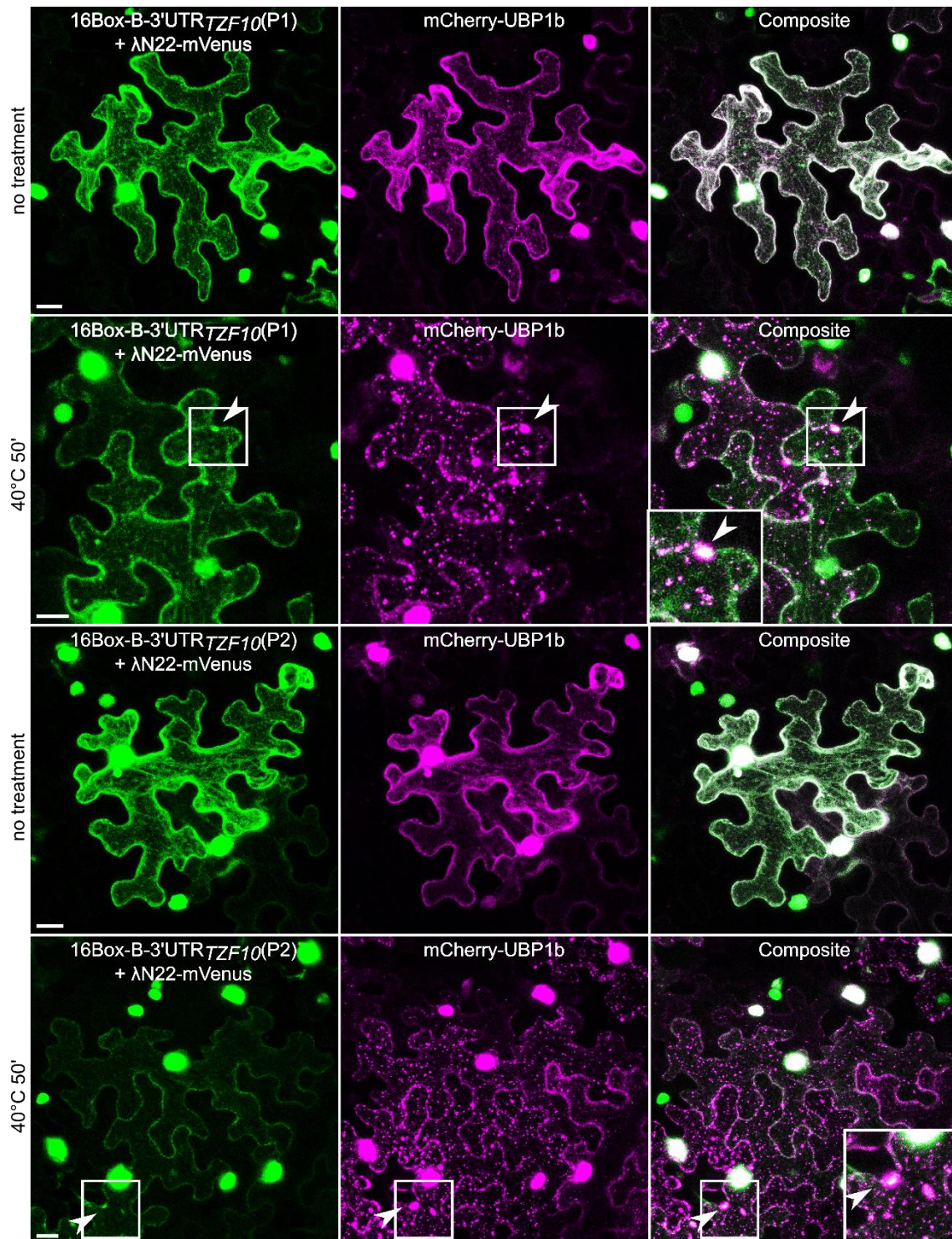


Figure 43: **The localization of *TZF10* 3'UTR fragments is not altered upon heat stress.** The Δ N22-system was applied to transiently visualize *TZF10* 3'UTR fragments (P1 and P2) via infiltration of *N. benthamiana* leaves. Exemplary pictures of epidermal cells under non-stress and stress (40°C, 50 min) conditions are shown. The arrows highlight overlapping *TZF10* mRNA signals with the stress granule marker mCherry-UBP1b. P=part. Scale bars indicate 20 μ m.

However, both parts of the *TZF10* 3'UTR localized equally. Furthermore, the localization behavior of 3'UTR parts was not different from full-length 3'UTR under non-stress and stress conditions. Before and after heat treatment, the 3'UTR parts were found to be localized in the cytoplasm and nuclei of the transformed cells. Occasional dot-like localization was detectable

irrespective of heat treatment. Strong accumulation of UBP1b in SGs demonstrated the impact of heat stress on the cells (Fig. 43).

3.1.10 TZF10 and 11 interact with proteins of various functions in a yeast two-hybrid screen

To broaden the view on TZF function in *A. thaliana*, a yeast two-hybrid screening was performed. TZF10 and 11 as bait proteins were mated with four cDNA libraries derived from different Arabidopsis tissues/cultures grown under varying conditions (Table 22).

Table 22: Overview on prey cDNA libraries implemented in the yeast two-hybrid screen.

| Library | Tissue/culture | Vector | Generated by | Reference |
|---------|---|--------|---|-----------------------------------|
| CLON | Vegetative tissue; Three-week-old, green leaf material | pGAD10 | Clontech (Takara Bio, USA) | Clontech (Takara Bio, USA) |
| SAL | Suspension culture | pACT2 | Dr. Klaus Salchert (working group of Dr. Csaba Koncz, MPI Cologne) | Nemeth et al., 1998 |
| FLG+ | Col-0, grown in liquid culture, treated with flg22 | pACT2 | Dr. Denise Altenbach | Altenbach and Robatzek, 2007 |
| ETIO | Whole Col-0 seedlings; seeds were stratified for two days and then transferred to darkness for 48 h at 22°C | pACT2 | Dr. Chenggang Liu (working group of Dr. Alan Jones, University of North Carolina) | Klopffleisch <i>et al.</i> , 2011 |

The screening in total revealed 313 positive interactions with identified proteins of various function. Some of the proteins were roughly grouped into the following categories: Calcium/calmodulin-binding proteins, NAD(P)-binding or NADPH-producing proteins, lipid droplet- or lipid transfer-associated proteins, SOLUBLE N-ETHYLMALIMIDE-SENSITIVE-FACTOR ATTACHMENT RECEPTOR (SNARE) proteins or ESCRT components. Interestingly, among the other interactors, MYELOBLASTOSIS (MYB) transcription factors (MYB101, MYB34) were found. Moreover, an interaction with the myrosinase β -THIOGLUCOSIDE GLUCOHYDROLASE 2 (TGG2) that, together with MYB34, is being part of the glucosinolate-myrosinase system in Arabidopsis, was identified. No proteins associated with mRNA regulation or core components of mRNP granules were identified, except for GLYCINE-RICH RBP 7 (GRP7), an RBP involved in mRNA metabolism and abiotic stress responses (Köster et al., 2014; Kim et al., 2008). A list of all the interacting proteins can be found in the appendix (Table 31).

3.2 SPIRRIG in *Marchantia polymorpha*

The description of the BDCP SPIRRIG in *A. thaliana* revealed an implication not only in membrane dynamics and trafficking (Saedler et al., 2009, Steffens et al., 2017), but also in salt stress-related mRNA regulation (Steffens et al., 2015). The characterization of a *M. polymorpha spirrig* (Mp*spirrig*, Mp*spi*) mutant is an excellent opportunity to unravel ancient functions and mechanisms exerted by BDCPs in a basal land plant. In this work, the T-DNA mutant Mp*spirrig* was phenotypically described on a morphological and cellular level. Moreover, co-localization and interaction studies were implemented to tackle the connection of MpSPIRRIG to both mRNA regulation and membrane trafficking. In this paragraph and all chapters following, the prefixes 'Mp' and 'At' are used to discriminate between genes and proteins either referring to *M. polymorpha* or *A. thaliana*, respectively. According to the guidelines for gene nomenclature in Marchantia (Bowman et al., 2016), the prefixes for *M. polymorpha* are not written in italic letters (regardless of gene, mutated gene, protein etc.).

3.2.1 Protein and gene structure of MpSPIRRIG

BLAST analysis (marchantia.info, MpTak1v5.1) led to the identification of five BDCPs in *M. polymorpha*. Phylogenetic tree construction further confirmed MpSPIRRIG (Mp2g15880) as the closest homolog to AtSPIRRIG (AT1G03060) and the closely related, but not yet described, Arabidopsis BEACH-DOMAIN HOMOLOG A2 (AtBCHA2, AT4G02660; fig. 44).

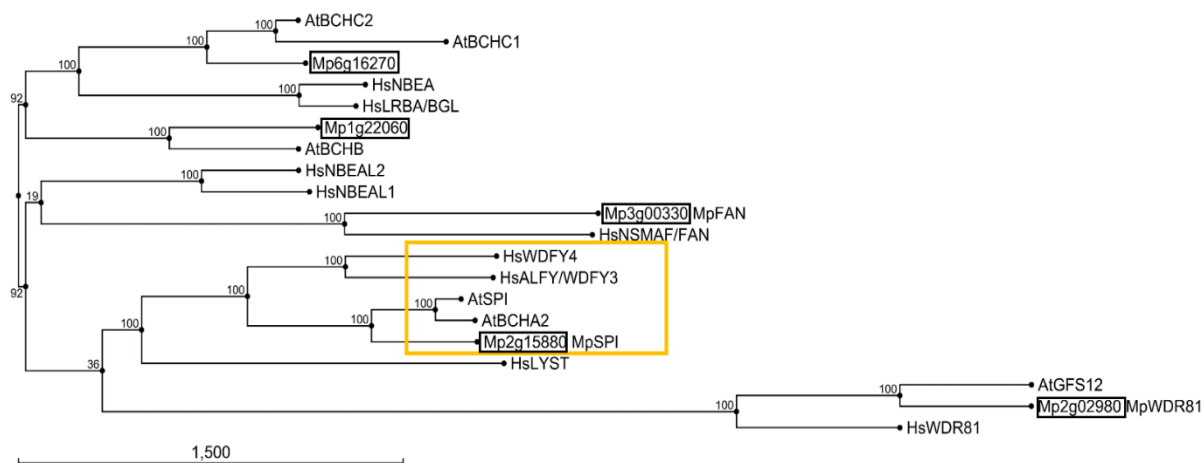


Figure 44: **Phylogeny of *A. thaliana*, *M. polymorpha* and *H. sapiens* BEACH domain proteins.** The tree was constructed based on whole protein sequences with the Neighbor Joining algorithm using CLC DNA Workbench 5.6.1. Bootstrap values are shown at nodes. The yellow box, which highlights group A of BDCPs including SPIRRIG, was subsequently added and adapted from Saedler et al., 2009; Teh et al., 2014.

Figure 45 shows the protein structure of SPI in Marchantia and Arabidopsis. The overall sequence identity of the proteins is 52%, whereas the PBW (PH domain, BEACH domain and WD40 repeats) domains share an identity of 66%. The BEACH domains themselves are 79% identical on the amino acid level. In contrast to AtSPIRRIG, MpSPIRRIG interestingly contains an additional FYVE domain at the C-terminal end (Fig. 45).

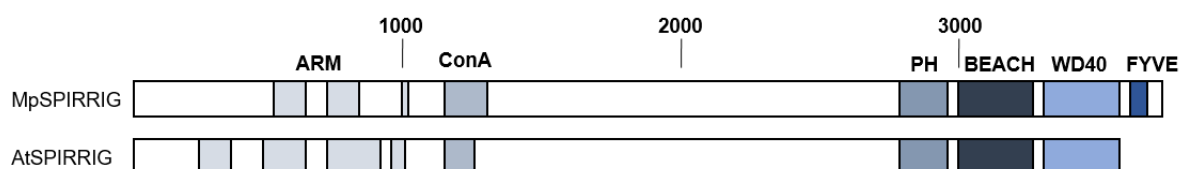


Figure 45: **Protein structure of MpSPIRRIG and AtSPIRRIG.** Sizes are indicated in amino acid (aa) number. MpSPIRRIG has a total number of 3766 aa; AtSPIRRIG 3601 aa. ARM = Armadillo repeats. ConA = Concanavalin A-like lectin domain. PH = pleckstrin homology domain. BEACH = *beige* and Chediak-Higashi domain. WD40 = WD40 repeats. FYVE = FYVE domain.

The corresponding gene structure of MpSPIRRIG and AtSPIRRIG is shown in fig. 46. Both genes carry 20 exons with a total length of 11298 bp (Marchantia) and 10803 bp (Arabidopsis).

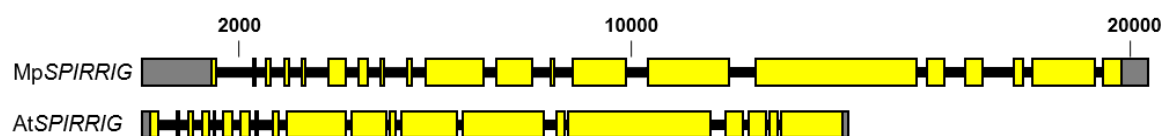


Figure 46: **Gene structure of MpSPIRRIG and AtSPIRRIG.** Sizes are indicated in base pair (bp) number. Gray boxes show UTRs, black lines depict introns, yellow boxes represent exons.

3.2.2 The subcellular localization of MpSPIRRIG

With a CDS of around 11 kb, and thus significantly above the average Arabidopsis gene length of approximated 2.2 kb (Wortman et al., 2003), SPIRRIG is an extraordinarily large gene. During the course of experiments describing Arabidopsis SPIRRIG, the gene turned out to be very difficult to amplify and to work with due to its massive size (M. Jakoby, personal communication). As subcellular localization of AtSPIRRIG was not altered when the protein was reduced to the C-terminus including functional PH, BEACH and WD40 domains (further referred to as PBW; Steffens et al., 2015), subsequent experiments in Marchantia were conducted with the PBW construct.

Accordingly, the PBW fragment of MpSPIRRIG was created and subcellular localization was observed. As MpSPIRRIG carries an additional FYVE domain at the C-terminal end, the PBW-FYVE (further referred to as PBWF) fragment was generated as well. It was included in the experiments in order to detect potential effects of the FYVE domain on localization and/or interaction behavior.

First, MpSPI PBW and PBWF were transiently expressed in three- to four-week-old male wild type plants, Takaragaike-1 (Tak-1) thalli via biolistic transformation.

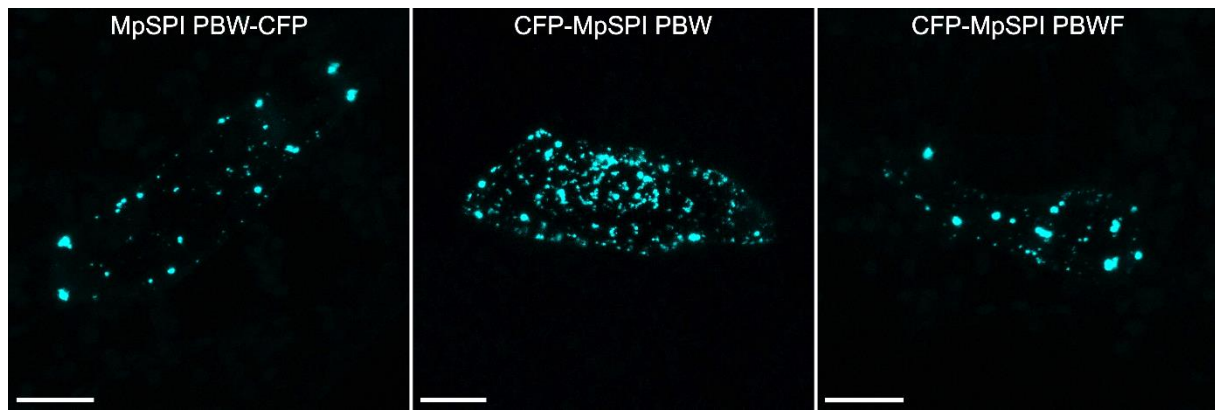


Figure 47: **Transient expression of MpSPI.** MpSPI PBW and PBWF, driven by a 35S CaMV promoter, were transiently expressed via biolistic transformation in three- to four-week-old thalli of *M. polymorpha*. PBW=pleckstrin homology, BEACH and WD40 domain. PBWF= pleckstrin homology, BEACH, WD40 and FYVE domain. The scale bars depict 20 μ m.

In Arabidopsis, a nuclear-cytoplasmic localization of AtSPI PBW was described (Steffens et al., 2015). Only upon salt stress, AtSPI PBW was found to relocate to P-bodies, resulting in a cytoplasmic dot-like localization (Steffens et al., 2015). Interestingly, MpSPI PBW shows a cytoplasmic dot-like localization already under normal, non-stressed conditions (Fig. 47) in *M. polymorpha* cells. This localization behavior is not influenced by the position of the fluorescent tag (Fig. 47). Furthermore, the FYVE domain does not alter the cytoplasmic dot-like localization of MpSPI PBW.

In order to find out if the environment in *M. polymorpha* cells causes the dot-like localization of MpSPI PBW, or if the protein itself induces the localization, MpSPI PBW was transiently expressed in leaves of two-week-old Arabidopsis plants via particle bombardment.

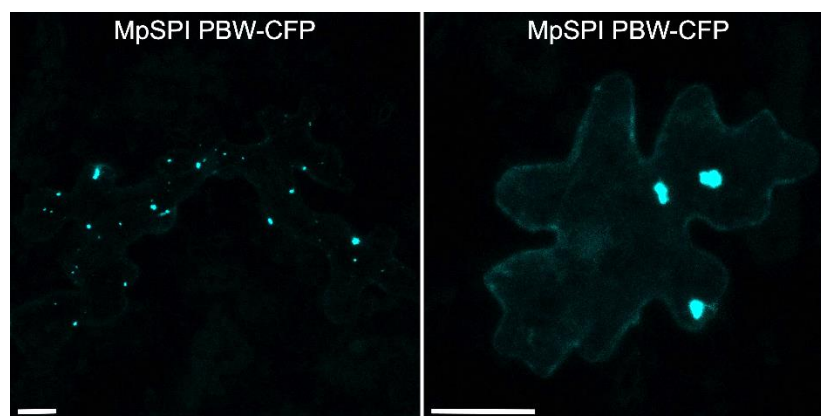


Figure 48: **Transient expression of MpSPI in Arabidopsis.** 35S::MpSPI PBW was transiently expressed in leaves of two-week-old *A. thaliana* plants via biolistic transformation. PBW=pleckstrin homology, BEACH and WD40 domain. The scale bars depict 20 μ m.

In Arabidopsis, MpSPI PBW localizes in cytoplasmic dots under non-stress conditions as well (Fig. 48). The transformed cells showed ranges from fewer to higher dot number, exemplarily shown in fig. 48.

To confirm observed localization behavior of MpSPIRRIG in transient expression, MpSPI PBW was stably expressed via transformation of regenerating Tak-1 thalli. Fluorescence was observed in five-day-old gemmae derived from the isogenic, stable line.

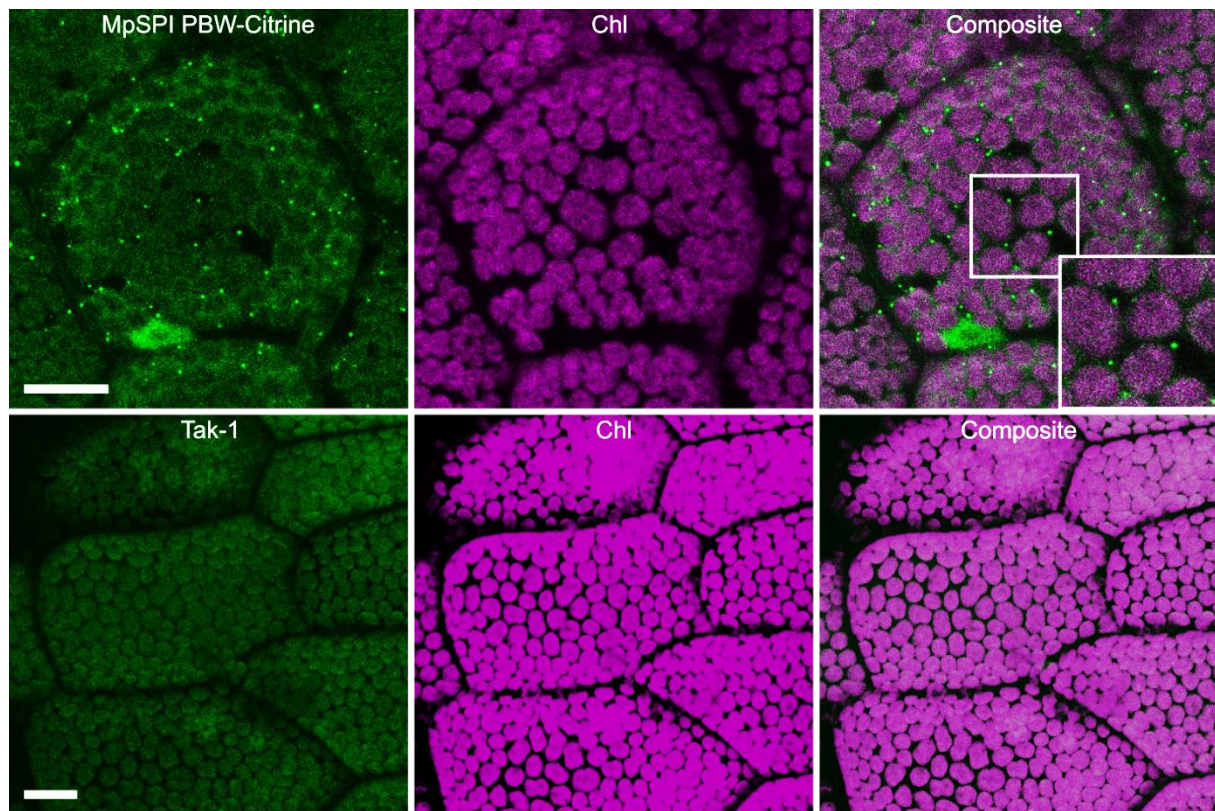


Figure 49: **Subcellular localization of MpSPI.** 35S::MpSPI PBW was stably transformed into regenerating Tak-1 thalli. The upper row shows five-day-old gemmae derived from the stable line. The lower row shows excitation and detection of untransformed Tak-1 gemmae with identical confocal settings used for the Citrine fluorophore. Chl=Chlorophyll autofluorescence, detected at 690-700 nm. PBW=pleckstrin homology, BEACH and WD40 domain. The scale bars indicate 20 μ m.

In line with previous results, stable transformation revealed MpSPI PBW to be localized in nuclei and cytoplasmic dots under non-stressed conditions (Fig. 49). The weaker background fluorescence of chloroplasts most likely derives from autofluorescence, as caption of untransformed Tak-1 gemmae shows comparable chlorophyll fluorescence upon excitation and detection with identical confocal imaging settings as for the Citrine fluorophore. Same observations have been made by Kanazawa et al. (2020), who also report strong chlorophyll autofluorescence upon detection of Citrine.

3.2.3 The T-DNA mutant *Mpspirrig*

The *Mpspirrig* mutant analyzed in this study was isolated in a T-DNA screen that was set out to identify genes involved in *Marchantia* rhizoid development (Honkanen et al., 2016). The insertion site of the T-DNA in the 15th exon of MpSPIRRIG is displayed in fig. 50. Corresponding designations for the mutant allele are *Mpspi-2* and ST17-11 (Honkanen, 2015; Honkanen et al., 2016), further referred to as *Mpspirrig* or *Mpspi*.

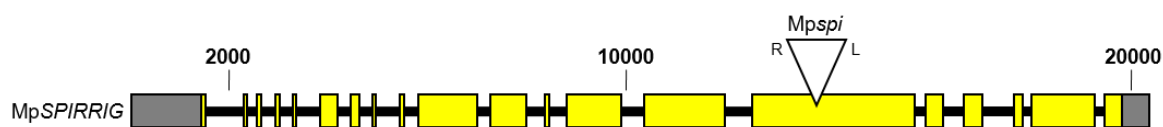


Figure 50: **Gene structure of MpSPIRRIG including T-DNA insertion site**, depicted by the triangle. R and L show right and left borders of the T-DNA, respectively. Sizes are indicated in bp number. Gray boxes show UTRs, black lines depict introns, yellow boxes represent exons.

The T-DNA insertion site was confirmed via PCR with a gene-specific primer and a primer binding at the left border of the T-DNA (pCAMBIA1300, primer in table 28, appendix) and subsequent sequencing. PCR with sex-specific primer pairs amplifying male (*rbm27*) and female (*rhf73*) DNA markers (Table 28, appendix; Westermann, 2018; Fujisawa et al., 2001) revealed the *Mpspirrig* mutant line to be male. This was further confirmed by the emergence of antheridiophores.

To test how the T-DNA insertion affects the expression of the *Mpspirrig* transcript, a primer pair suitable for qPCR, located downstream of the insertion site, was designed (Table 29, appendix). After sufficient qPCR efficiency of the primer pair was verified (100.6 %, correlation -0.994; standard curve fig. 72B, appendix), qPCR was performed on cDNA of 14-day-old, whole thalli. As *Mpspirrig* is a male *Marchantia* line, the experiment was carried out with the corresponding male wild type, Tak-1, as the control.

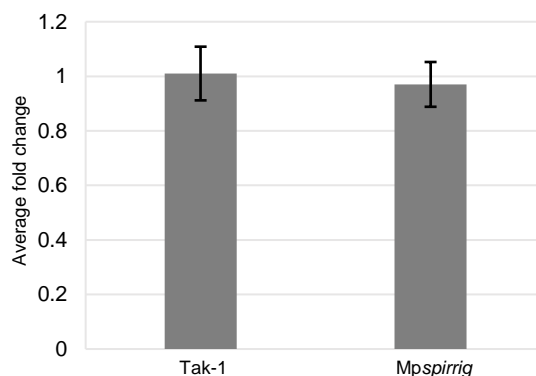


Figure 51: **Relative expression of MpSPIRRIG in Mpspirrig compared to Tak-1**, normalized to reference genes *MpAPT3* and *MpACTIN7* (*MpACT7*) (Saint-Marcoux et al., 2015). $n=3$. Significance was tested with a Mann-Whitney-U test ($p<0.10$).

The qPCR analysis revealed *MpSPIRRIG* to generally be expressed on a rather low level in Tak-1 thalli. This was reflected by an average Ct value of $26.33 \pm \text{SD } 0.23$. The qPCR analysis moreover showed the expression of *MpSPIRRIG* to not be significantly up- or down-regulated in the mutant line (Fig. 51). The T-DNA does not harbor a promoter sequence towards the left boarder (pCAMBIA1300; Honkanen et al., 2016), thus downstream effects on transcription induced by the T-DNA on the *MpSPIRRIG* transcript are not likely. A qualitative RT-PCR employing a primer pair spanning the T-DNA insertion site (Table 30) in the course of this study however already indicated absence of a full-length transcript in *Mpspirrig* (data not shown).

3.2.4 Phenotypic characterization of *Mpspirrig*

In order to thoroughly assess morphological and cellular differences between *Mpspirrig* and wild type plants, several measurements and observations were conducted during gemmaling growth. All experiments were carried out with the corresponding male wild type, Tak-1, as controls in parallel.

3.2.4.1 *Mpspirrig* has a short rhizoid phenotype

The T-DNA mutant *Mpspirrig* was described to develop shorter rhizoids than *Marchantia* wild type plants (Honkanen et al., 2016). Rhizoid growth of *Mpspirrig* and Tak-1 was tracked in order to confirm this phenotype.

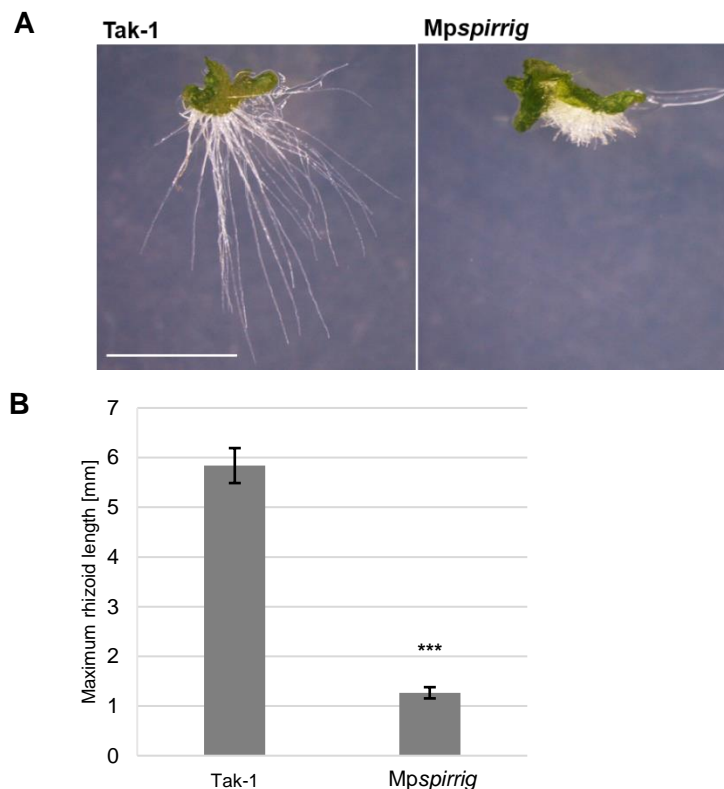


Figure 52: ***Mpspirrig* has a short rhizoid phenotype.** **A** Seven-day-old gemmalings grown vertically on Johnson's. The scale bar represents 2 mm. **B** Maximum rhizoid length of seven-day-old gemmalings. $n=10$. Significance was tested with a two-tailed, unpaired Student's t -test, ***= $p<0.001$.

The short rhizoid phenotype of *Mpspirrig* can be clearly observed and was statistically confirmed with the measurement of maximum rhizoid length of seven-day-old gemmalings (Fig. 52A+B).

3.2.4.2 *Mpspirrig* gemmalings acquire more biomass during early development

In order to examine differences in development of *Mpspirrig* compared to Tak-1, a time-course observation of gemmae growth and measurements of gemmae area were carried out. Therefore, gemmae were taken out of gemmae cups (day 0) and grown on solid Johnson's medium for another five days. Each day, images of gemmae were taken and gemmae area was measured.

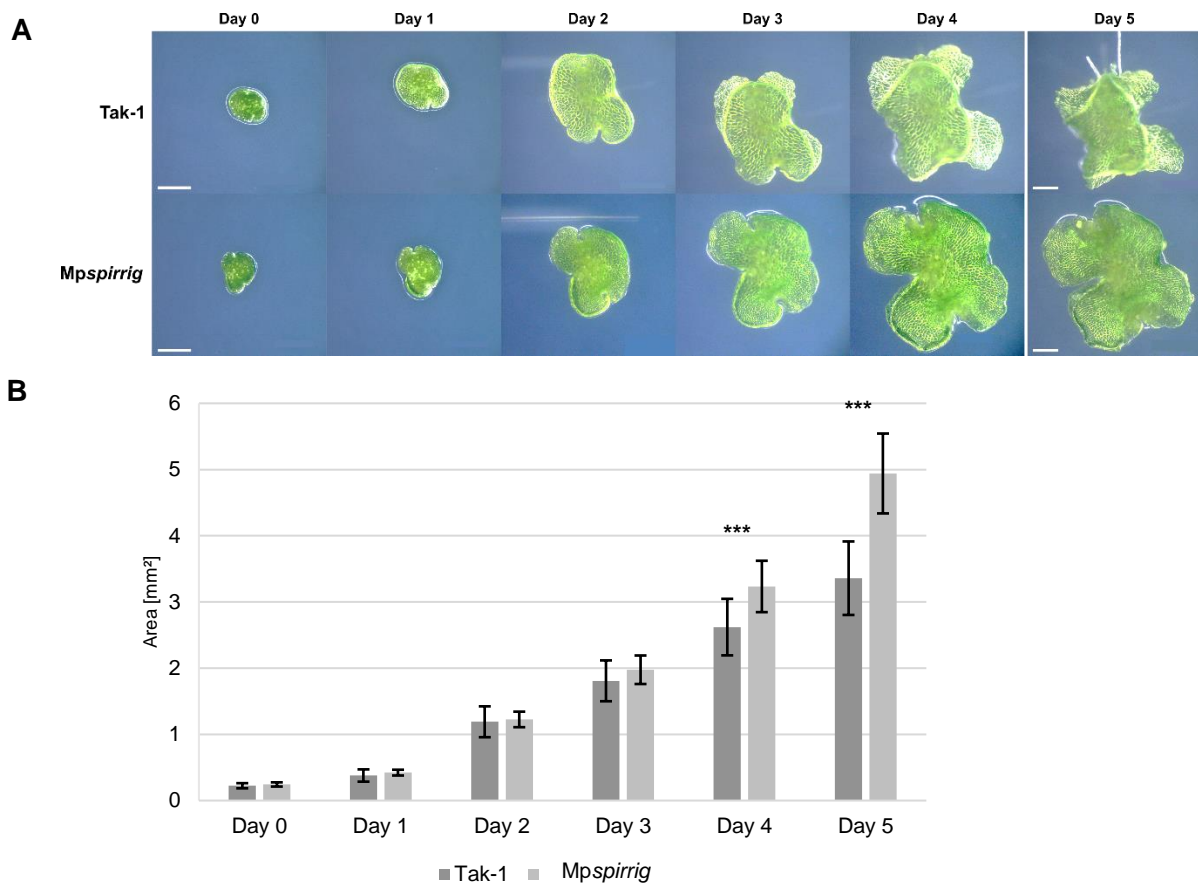


Figure 53: **Time-course observation of Tak-1 and Mpspirrig gemmae growth.** The development of gemmae was tracked for six days, starting from the day on which gemmae were taken out of gemmae cups (day 0) to grow on solid Johnson's medium for another five days. **A** Representative images of Tak-1 and Mpspirrig gemmae used for area measurements. The scale bars indicate 500 μm . **B** Measurements of gemmae area. $n=11$. Significance was tested with a two-tailed, unpaired Student's t -test, ***= $p<0.001$.

From day 0 to day 3, no differences in growth and development of gemmae were observable (Fig. 53A+B). From day 4 on, Mpspirrig gemmae showed a significant increase of size compared to Tak-1 gemmae, which was most pronounced on day 5 (Fig. 53B).

Furuya et al. (2018) presented parameters for describing the shape of Marchantia gemmalings. To examine the shape of *Mpangustifolia* mutants, the authors defined and measured the length (distance between apical notches, fig. 54A), the width (distance from the trace of stalk to the opposite site, crossing the length at 90°; fig 54A) and the gemma/thallus-shape index (ratio of width to length). In this study, the same measures were applied for characterization of Mpspirrig gemmae shape. Therefore, two-day- and five-day-old gemmae, grown on solid Johnson's, were observed.

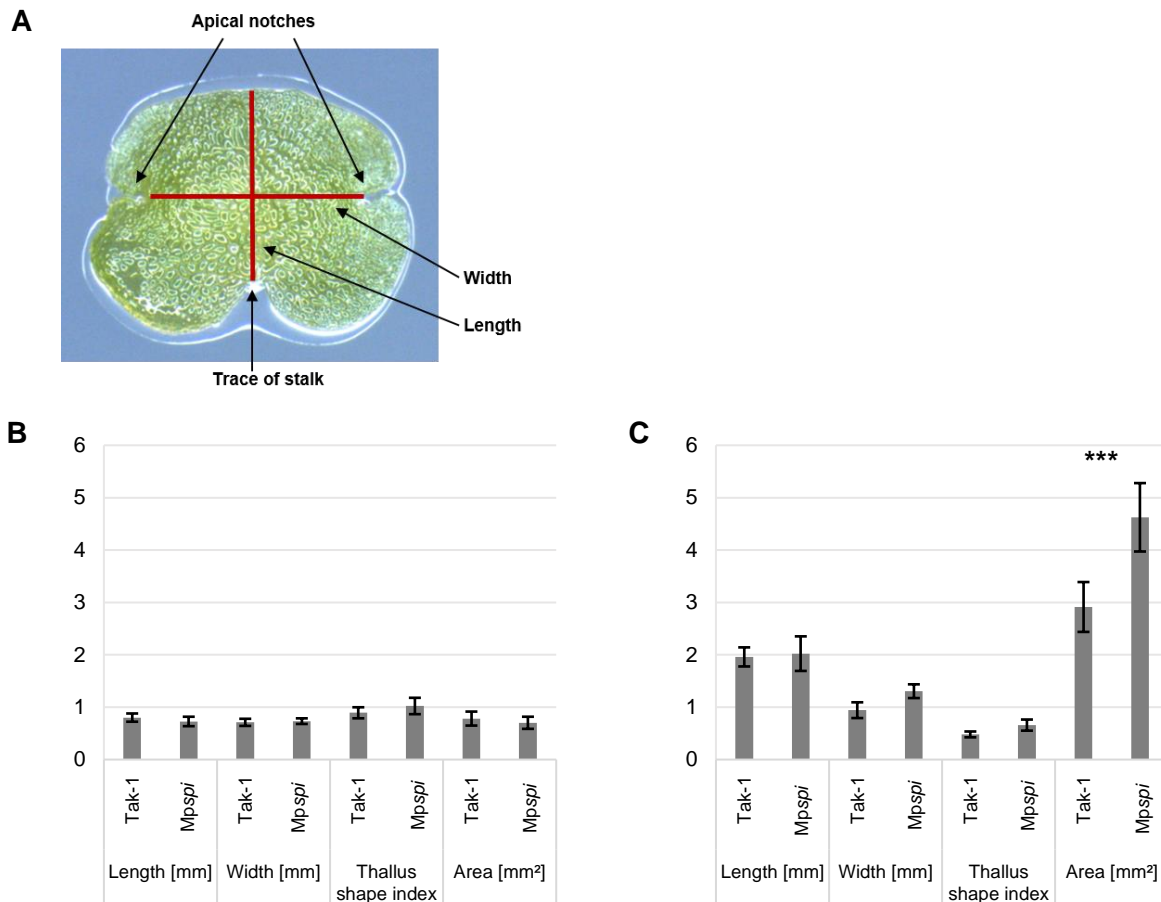


Figure 54: **Length, width and thallus shape index of *Mpspirrig* and wild type plants.** **A** Representative image of a *Marchantia* gemma with marked apical notches, trace of stalk, length and width axis. Adapted from Furuya et al., 2018. **B** Length, width, thallus shape index and area measurements of two-day-old gemmae. $n=10$. No significant difference of parameters between the genotypes was determined. **C** Length, width, thallus shape index and area measurements of five-day-old gemmae. $n=10$. Significance was tested with a two-tailed, unpaired Student's *t*-test, ***= $p<0.001$.

The analysis of length, width and gemma/thallus shape index revealed no significant differences in general gemma shape between *Mpspirrig* and Tak-1 (Fig. 54C+D). Consistent with previous results, area measurements confirmed a significant increase in size of five-day-old, but not of two-day-old, *Mpspirrig* gemmae.

To analyze if size differences of gemmae are reflected in the phenotype and in differences of biomass of older plants, morphology and fresh weight of 14-day-old thalli were explored next.

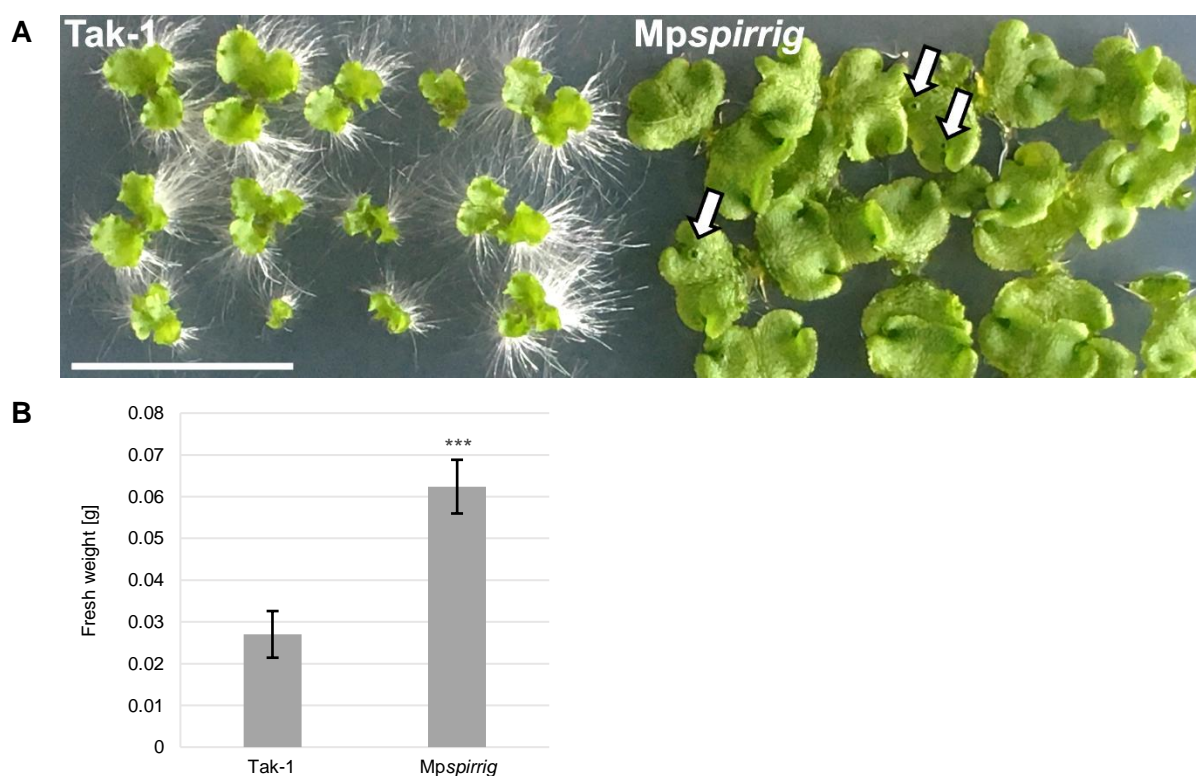


Figure 55: **Mpspirrig thalli acquire more biomass than wild type plants.** **A** Representative image of Tak-1 and Mpspirrig thalli grown on the same Johnson's agar plate for 14 days. Arrows indicate gemmae cups. The scale bar displays 2 cm. **B** Fresh weight of 14-day-old Tak-1 and Mpspirrig thalli. $n=16$. Significance was tested with a two-tailed, unpaired Student's t -test, ***= $p<0.001$.

Images and fresh weight clearly showed a significant, approximately 3 fold, increase of biomass in 14-day-old Mpspirrig thalli in comparison to Tak-1 (Fig. 55A+B). Whereas no gemmae cups have yet emerged on Tak-1 thalli, already a few have been developed in Mpspirrig after 14 days of growth (indicated by arrows in fig. 55A).

3.2.4.3 Mpspirrig gemmae have more and smaller cells

In order to explain the size difference between Mpspirrig and Tak-1, gemmae were studied in depth on a cellular level. To clearly visualize cell walls, gemmae were stained with propidium iodide (PI). PI is a red-fluorescent cell dye not able to pass the cell wall of viable cells. PI is only able to penetrate damaged cell membranes and due to its intercalating property stains the nuclei of dead cells. As it gets excluded from living cells, while maintaining its fluorescent property, PI can be readily used to stain and visualize cell walls. In this study, cells of PI-stained Mpspirrig and Tak-1 gemmae were counted and cell size was measured.

Figure 56 shows the analysis of cells of one-day-old gemmae. Cells along the width axis (compare fig. 54A) were counted, showing a significant increase of cell number in Mpspirrig compared to Tak-1 (Fig. 56B). The area of cells generally increases towards the center of Marchantia gemmae. Therefore, cell sizes were measured separately in each one of six outer cell layers (Fig. 56C). To allow comparability of results, location of the parts in all examined gemmae (opposite of the trace of stalk, far enough from apical notches) in which cells were

analyzed, was chosen equally (exemplarily shown in fig. 56A). The analysis revealed cells of *Mpspirrig* to be significantly smaller in all cell layers compared to cells of Tak-1 (Fig. 56D).

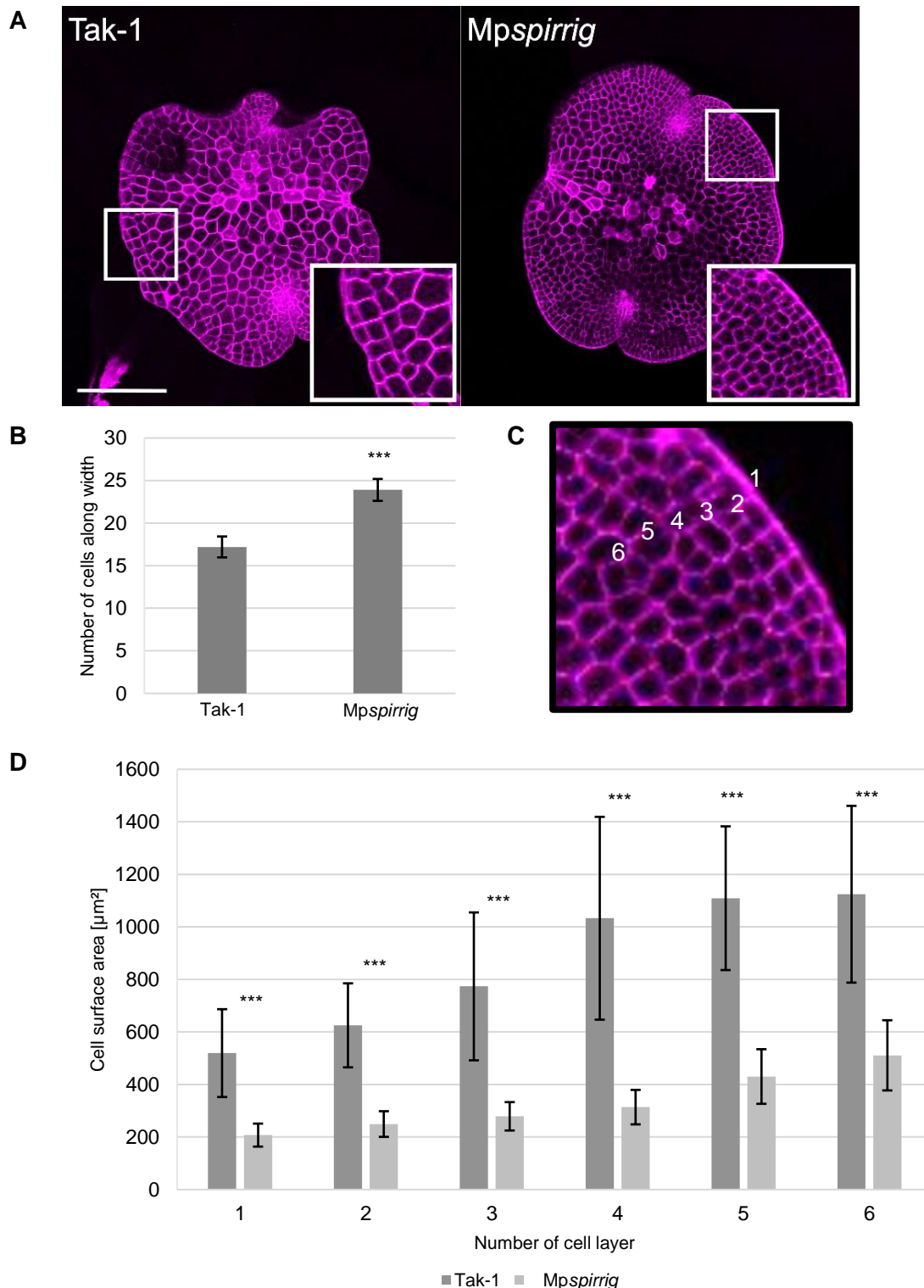


Figure 56: ***Mpspirrig* gemmae have more and smaller cells than wild type gemmae.** Cell size and number was determined in one-day-old *Mpspirrig* and Tak-1 gemmae. **A** Representative confocal images of PI-stained gemmae. The scale bar indicates 250 µm. **B** Number of cells along the width axis. $n=10$. Significance was tested with a two-tailed, unpaired Student's t -test, ***= $p<0.001$. **C** Exemplary gemmae area for cell size measurements. In each of the six outer cell layers, ten cells were analyzed. **D** Cell area of Tak-1 and *Mpspirrig* in six cell layers, with layer one being the outermost layer of the gemmae. $n=10$ gemmae with 10 individual cells per layer. Significance was tested with a two-tailed, unpaired Student's t -test, ***= $p<0.001$.

As one-day-old *Mpspirrig* gemmae do not yet show an overall increase in gemmae size (Fig. 53B), cell measurements were repeated with four-day-old gemmae.

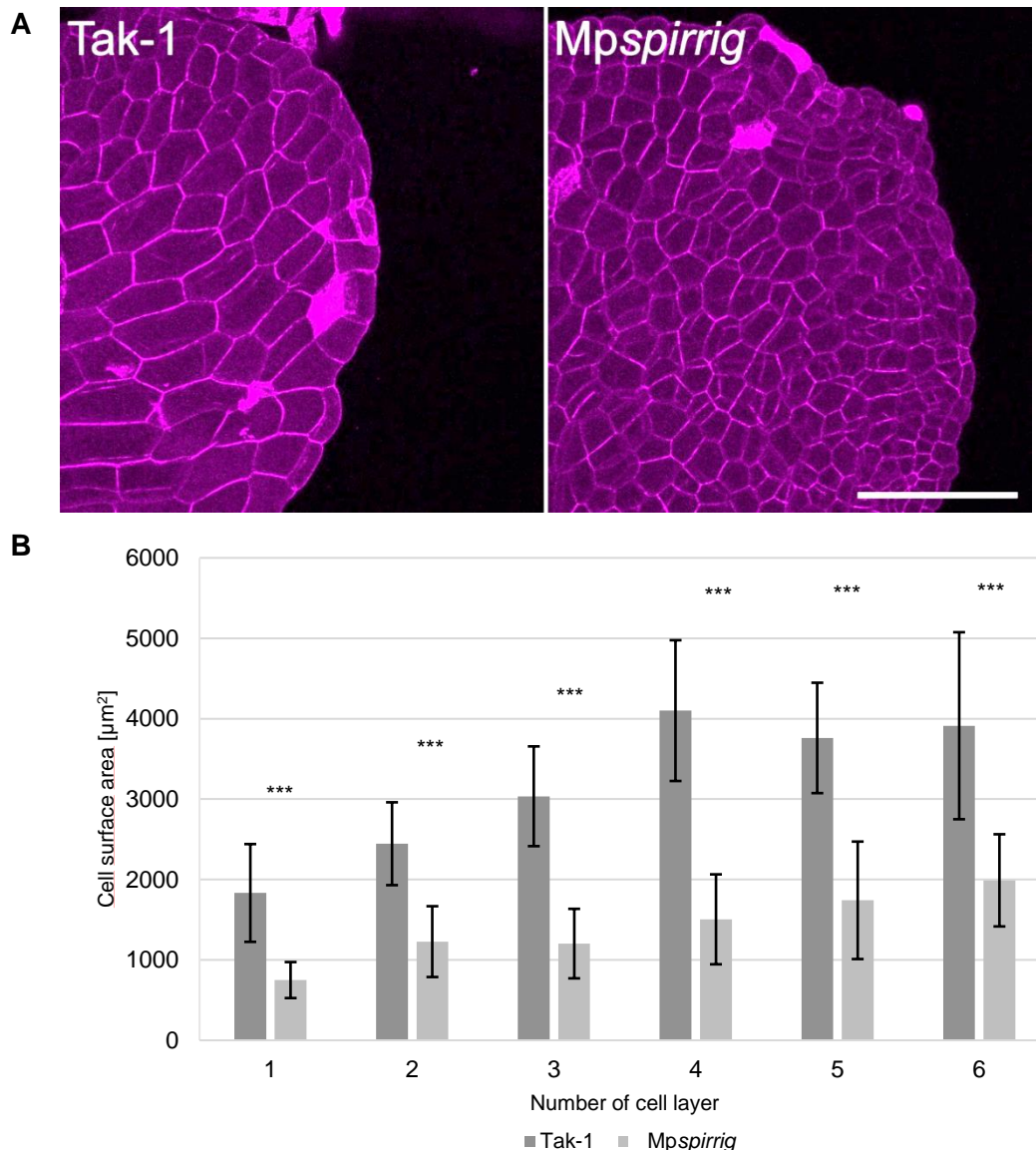


Figure 57: ***Mpspirrig* gemmae have smaller cells than wild type gemmae.** Cell size was determined in four-day-old *Mpspirrig* and Tak-1 gemmae. **A** Representative confocal images of PI-stained, four-day-old gemmae. The scale bar indicates 200 µm. **B** Cell area of Tak-1 and *Mpspirrig* in six cell layers, with layer one being the outermost layer of the gemmae. $n=10$ gemmae with ten individual cells per layer. Significance was tested with a two-tailed, unpaired Student's *t*-test, ***= $p<0.001$.

Consistent with the previous result, the cell size of four-day-old gemmae in *Mpspirrig* compared to Tak-1, was significantly decreased in all cell layers (Fig. 57B).

3.2.5 Unraveling the connection of MpSPIRRIG to P-bodies and the ESCRT system

Studies on AtSPIRRIG uncovered unexpected functions in salt stress response, including salt stress dependent P-body formation, co-localizations and interactions with P-body components, as well as stabilization of salt stress regulated mRNAs (Steffens et al., 2015). Apart from that, a connection of AtSPIRRIG to the ESCRT system was detected as interactions with the ESCRT components AtSKD1 and AtLIP5 were described. Moreover, it was found that the

endosomal transport route of soluble proteins to the vacuole is disturbed in *spi/lip5* Arabidopsis double mutants (Steffens et al., 2017).

An analysis of the connection between SPIRRIG, P-bodies and the ESCRT system in *M. polymorpha* could unravel if already reported functions belong to the primary, evolutionarily conserved set of BDCP functions in basal land plants. Prominent phenotypes of *Atspirrig* were linked to either functions and were analogously investigated in *Mpspirrig*.

3.2.5.1 Vacuoles of *Mpspirrig* are not fragmented

Vacuoles of root hairs in Arabidopsis *spirrig* mutants have been found to be fragmented (Saedler et al., 2009). The result was the first indication that SPIRRIG could have a function in membrane integrity and trafficking. Analogously, in this work, vacuole structure in rhizoids of *Mpspirrig* was analyzed upon staining with fluorescein diacetate (FDA).

FDA is a non-fluorescent, cell-permeable dye and serves as an esterase substrate. Once entering the cytoplasm, FDA is directly hydrolyzed and converted into a green-fluorescent, negatively charged fluorescein (Rotman and Papermaster, 1966). After conversion, FDA is not able to pass the plasma membrane or the tonoplast anymore. Due to these properties, FDA can be used as a negative stain for the vacuole as it solely stains the cytoplasm of viable cells.

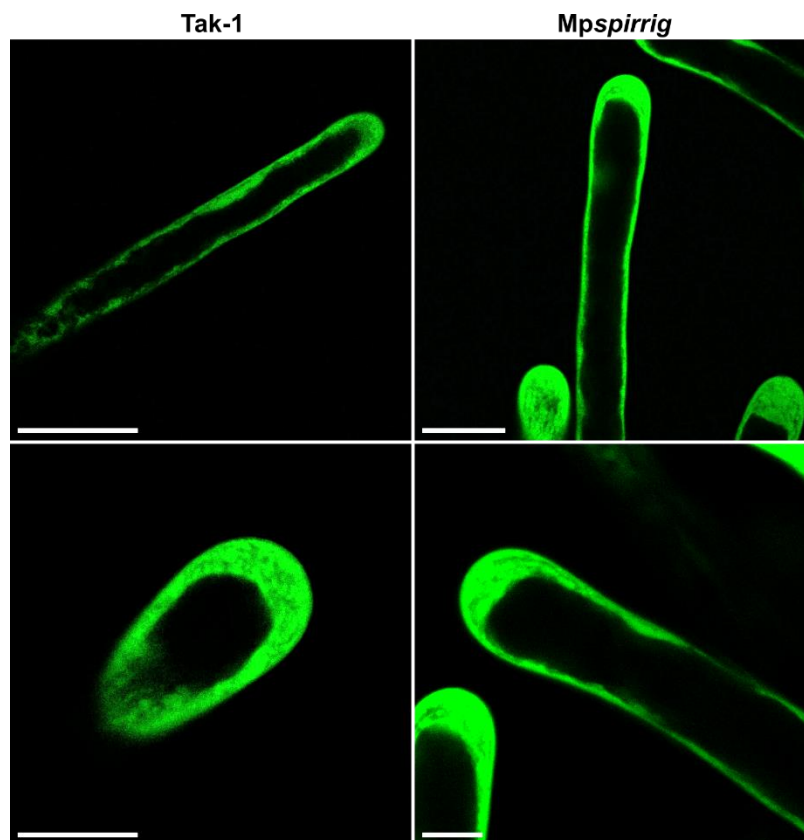


Figure 58: **Vacuole structure in Tak-1 and *Mpspirrig* rhizoids.** Rhizoids of five-day-old gemmalings were stained with FDA. The scale bar indicates 50 μm .

FDA staining of five-day-old Tak-1 and *Mpspirrig* gemmalings demonstrated that vacuoles in rhizoids of *Mpspirrig*, unlike those in root hairs of *Arabidopsis spirrig*, do not show a fragmentation phenotype (Fig. 58). The finding suggests MpSPIRRIG to not be essential for vacuolar integrity in rhizoids. To a small percentage, fragmentation of vacuoles also occurs in root hairs of *Arabidopsis* wild type plants (Saedler et al., 2009). Likewise, rare fragmentation was observed in *Marchantia* Tak-1 rhizoids (data not shown).

3.2.5.2 *Mpspirrig* has a salt hypersensitivity phenotype

Arabidopsis SPIRRIG was found to interact with P-body components, to associate with and regulate the assembly of P-bodies upon salt stress (Steffens et al., 2015). In accordance, *Arabidopsis spirrig* mutants show a salt hypersensitivity phenotype and thus demonstrate a biological relevance of SPIRRIG in salt stress response. The salt hypersensitivity phenotype is reflected in decreased primary root growth, strong cotyledon whitening and restricted overall growth under transpiring conditions when subjected to high salt concentrations (Steffens et al., 2015).

Tanaka et al. (2018) reported one of the first studies investigating salt stress response in *M. polymorpha*. The authors conducted a growth test on NaCl, finding growth of *M. polymorpha* to be completely repressed on 250 mM NaCl and inhibited on 50 mM NaCl. Consequently, they picked 50 mM NaCl to be their working concentration for performance of RNA sequencing in salt stressed gemmalings. The researchers identified several salinity-stress responsive transcription factors.

In this study, *Mpspirrig* was tested for a possible salt hypersensitivity phenotype by quantification of rhizoid growth and biomass upon growth on solid Johnson's supplemented with NaCl. To confirm results for general salinity response of *Marchantia* by Tanaka et al. (2018), and to find ideal conditions for further experiments, gemmaling growth on 50 mM and 100 mM NaCl was qualitatively tested first.

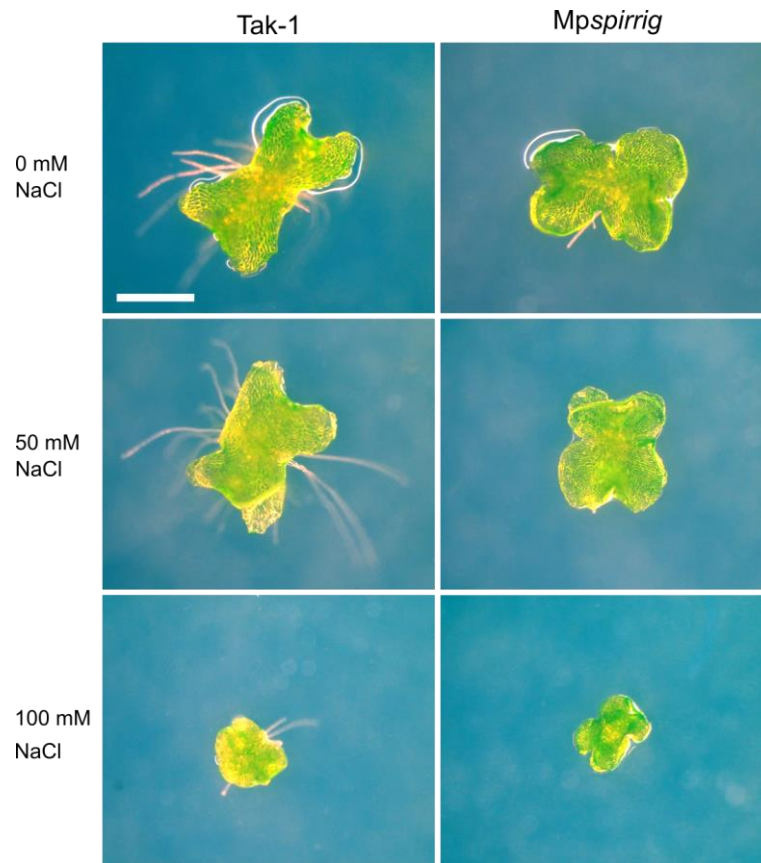


Figure 59: **Growth test of *M. polymorpha* in response to salt.** Exemplary images of four-day-old Tak-1 and *Mpspirrig* gemmalings grown on solid Johnson's supplemented with either 0, 50 or 100 mM NaCl. The scale bar indicates 1 mm.

Consistent with results of Tanaka et al. (2018), 50 mM NaCl already had a slight, inhibitory effect on growth of *M. polymorpha* after four days (Fig. 59). On 100 mM NaCl, growth of gemmalings was severely restricted (Fig. 59). Accordingly, quantification of rhizoid growth and biomass was determined after growth on 50 mM NaCl.

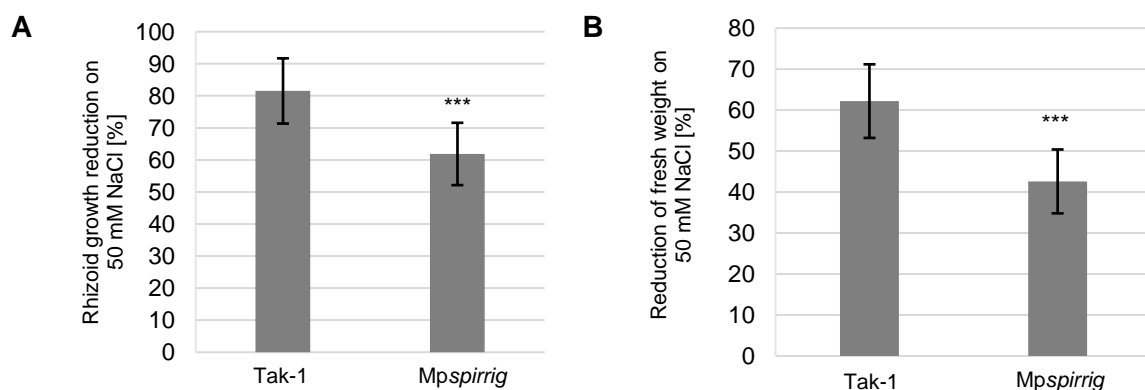


Figure 60: **Salt hypersensitivity of *Mpspirrig*** manifested in stronger reduction of rhizoid growth and biomass compared to Tak-1 upon growth on solid Johnson's supplemented with 50 mM NaCl. **A** Rhizoid growth reduction of seven-day-old Tak-1 and *Mpspirrig* gemmalings upon growth on 50 mM NaCl compared to growth on Johnson's without salt. Based on determination of maximum rhizoid length. $n=18$. Significance was tested with a two-tailed, unpaired Student's t -test, ***= $p<0.001$. **B** Reduction of fresh weight of 14-day-old Tak-1 and *Mpspirrig* gemmalings upon growth on 50 mM NaCl compared to growth on Johnson's without salt. $n=16$. Significance was tested with a two-tailed, unpaired Student's t -test, ***= $p<0.001$.

The determination of rhizoid growth reduction was based on the measurement of maximum rhizoid length of seven-day-old Tak-1 and *Mpspirrig* gemmalings grown vertically on solid Johnson's. The analysis revealed that upon growth on 50 mM NaCl, Tak-1 rhizoids still acquired approximately 82% of their length, whereas rhizoids of *Mpspirrig* reached only approximately 62% of their length (Fig. 60A). Similarly, the fresh weight of 14-day-old Tak-1 gemmalings was reduced to approximately 62% of biomass on NaCl, compared to growth on Johnson's without NaCl, whereas biomass of *Mpspirrig* gemmalings was reduced to approximately 43% (Fig. 60B). The relative reduction of rhizoid length and fresh weight in *Mpspirrig* was significantly different from Tak-1. The results thus point to a salt hypersensitivity phenotype of *Mpspirrig* and suggest biological relevance of MpSPIRRIG in *Marchantia* as well.

3.2.5.3 MpSPI PBW co-localizes with P-body and ESCRT components

Whereas findings gained by phenotypic description of *Mpspirrig* clearly suggest a relevance of MpSPIRRIG in *Marchantia* salt stress response, the results do not imply a role of MpSPIRRIG in membrane integrity at least in vacuoles of rhizoids. In order to further elucidate association of MpSPIRRIG with both processes, co-localization with P-body and ESCRT components was investigated next.

Co-localization studies of MpSPI PBW with P-body and ESCRT components were performed using biolistic, transient double transformations of two- to three-week-old Tak-1 thalli.

As P-body components were not yet studied in *M. polymorpha* the protein localization of P-body markers MpDCP1 and MpDCP2 (cloning and construct generation in this study, Westermann et al., 2020) was checked in single bombardments first.

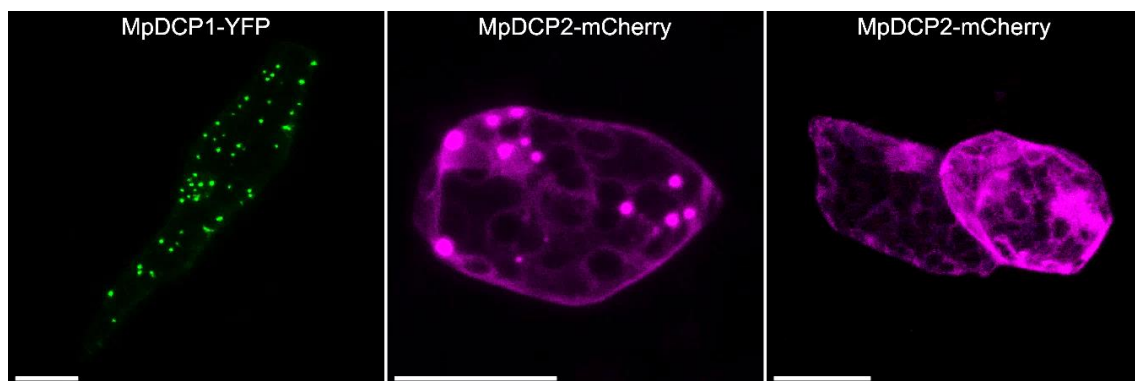


Figure 61: **Representative images of *Marchantia* P-body marker proteins.** 35S::MpDCP1 and 35S::MpDCP2 were transiently expressed in two- to three-week-old *M. polymorpha* thalli via particle bombardment. The scale bars represent 20 μ m.

MpDCP1 localizes in punctate structures throughout the cytoplasm of transformed cells, likely representing P-bodies (Fig. 61 left). MpDCP2 occasionally localizes to cytoplasmic dots as well, exemplarily shown in fig. 61 (middle). However more often, MpDCP2 was expressed evenly in the cytoplasm and weakly in the nucleus (Fig. 61 right). In *Arabidopsis*, AtDCP2 only

is recruited to P-bodies upon stress conditions while under normal conditions it shows cytoplasmic localization (Motomura et al., 2014). Thus, the observed localization behavior of MpDCP2 was anticipated.

In former experiments, AtDCP1 was shown to recruit various proteins of different, often unrelated pathways, to P-bodies in a non-conclusive manner (L. Stephan, D. Gagliardi, personal communication). Therefore, MpDCP2 was chosen for co-localization analysis with MpSPI.

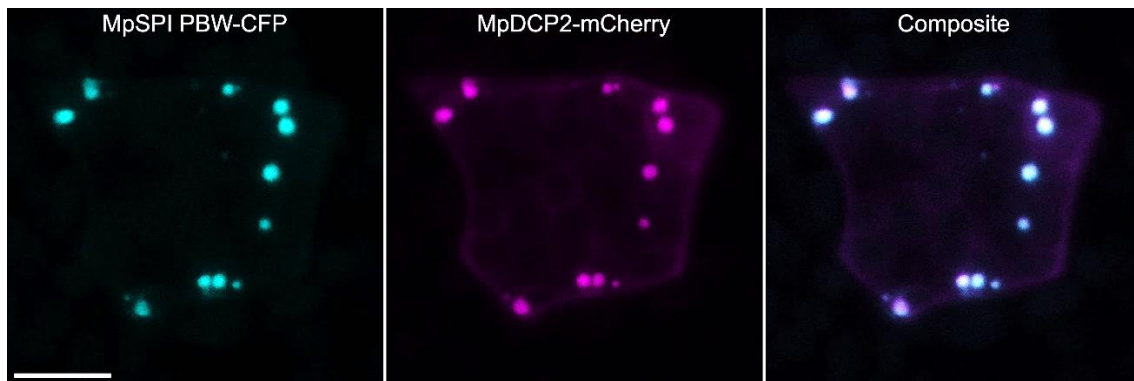


Figure 62: **Co-transformation of MpSPI PBW with P-body marker MpDCP2.** 35S::MpSPI PBW and 35S::MpDCP2 were transiently expressed in two- to three-week-old *M. polymorpha* thalli via particle bombardment. The scale bar indicates 20 μ m.

The co-bombardment of MpSPI PBW and MpDCP2 showed clear and strong co-localization of the proteins under non-stressed conditions (Fig. 62).

In Arabidopsis, the ESCRT components AtSKD1 and AtLIP5 are known interactors of AtSPIRRIG (Steffens et al., 2017). Thus, the Marchantia homologs MpSKD1 and MpLIP5 (cloning and construct generation in this study) were chosen for co-localization studies. As both proteins have not yet been described in *M. polymorpha*, their localization behavior was analyzed in single bombardments first. The transformations revealed both MpSKD1 and MpLIP5 to be localized in the nucleus as well as in cytoplasmic, dot-like structures (Fig. 63).

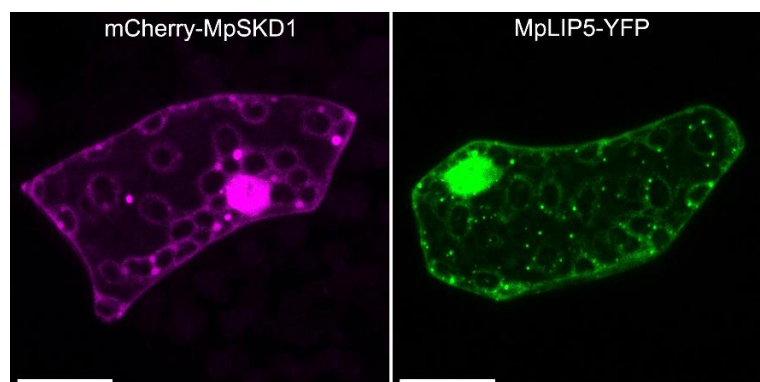


Figure 63: **Subcellular localization of ESCRT components in *M. polymorpha*.** 35S::MpSKD1 and 35S::MpLIP5 were transiently expressed in two- to three-week-old *M. polymorpha* thalli via particle bombardment. The scale bar indicates 20 μ m.

Upon subsequent co-transformation with MpSPI PBW, strong co-localization with MpLIP5 and MpSKD1 was detected (Fig. 64). The localization pattern of MpLIP5 and MpSKD1 in double transformations clearly resembles the dot-like structures in single transformations indicating fluorescent signals to be authentic.

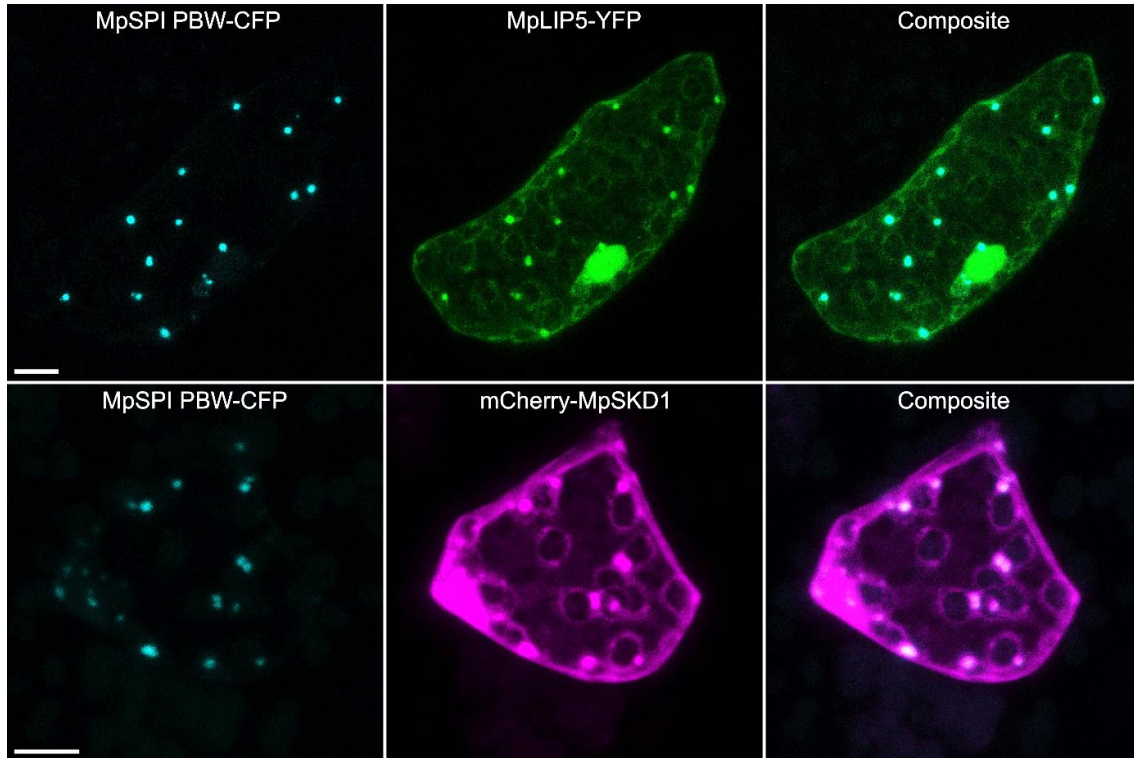


Figure 64: **Co-localization of MpSPI PBW with ESCRT components.** *35S::MpSKD1*, *35S::MpLIP5* and *35S::MpSPI PBW* were transiently expressed in two- to three-week-old *M. polymorpha* thalli via particle bombardment. The scale bars indicate 20 μm .

Recent studies demonstrated AtSKD1 to partially associate with stress granules and P-bodies in *A. thaliana*, especially under stress conditions (Wolff, 2018). Likewise, transient co-expression of MpSKD1 or MpLIP5 with MpDCP2 showed partial co-localization of the ESCRT members with the P-body component (Fig. 65) indicating that also in *M. polymorpha*, MVB biogenesis and mRNP granule formation might be associated.

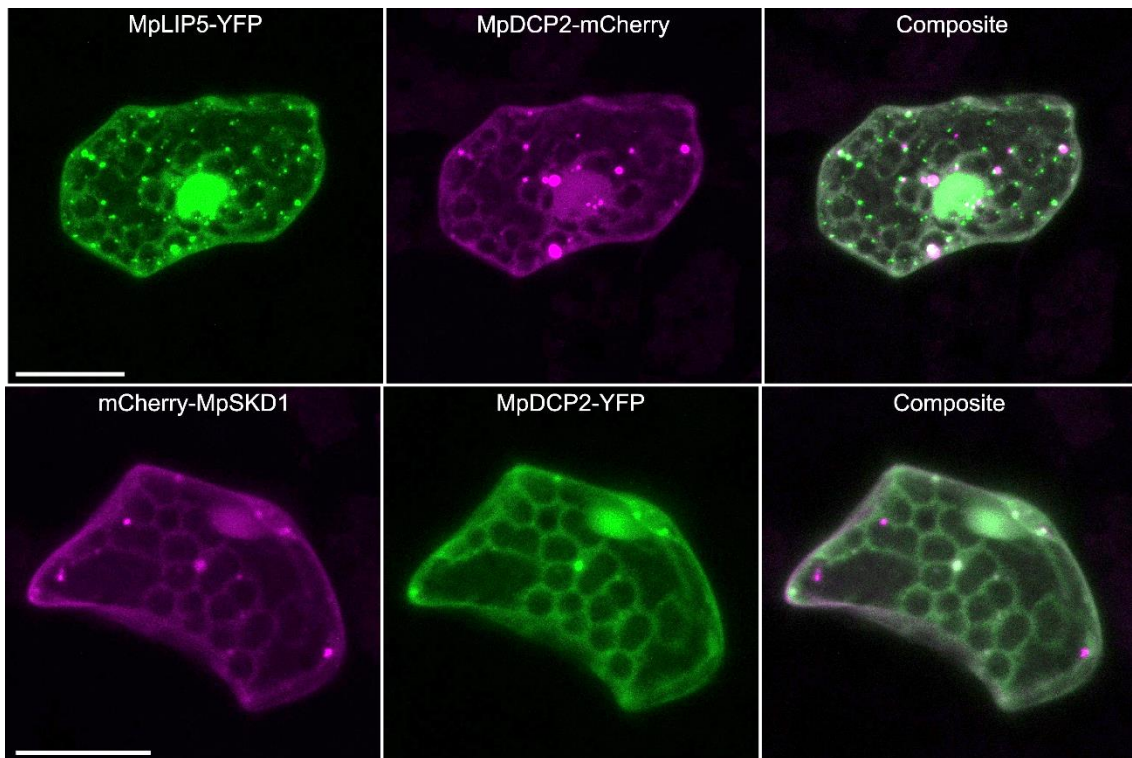


Figure 65: **Co-localization of ESCRT components with MpDCP2.** *35S::MpSKD1*, *35S::MpLIP5* and *35S::MpDCP2* were transiently expressed in two- to three-week-old *M. polymorpha* thalli via particle bombardment. The scale bars indicate 20 μm .

The assays, which analyzed MpSPI PBW co-localization with ESCRT and P-body components, showed very strong co-localization close to a complete overlap of fluorescent signals (Fig. 62; fig. 64). Strong co-localizations and high protein concentrations due to the particle bombardment method always raise the question, if proteins form artificial aggregates (Bolognesi and Lehner, 2018). In order to support observed co-localizations to not be due to aggregation, additional marker proteins were included in the analysis. The endosomal marker proteins and Ras-related in brain 5 (RAB5) related small GTPases AtARA6 and AtARA7 were described to only partially co-localize with AtLIP5, AtSKD1 and AtSPI PBW (Steffens et al., 2017). The *Marchantia* homologs of AtARA6 and AtARA7, MpARA6 and MpRAB5, were already identified and proven to be localized in endosomal structures by co-staining with FM1-43 in stable lines (Minamino et al., 2017). Single transient transformations of MpARA6 and MpRAB5 (cloning and generation of constructs performed in this study; Westermann et al., 2020) confirmed reported localization in punctate structures, likely representing endosomes (Fig. 66).

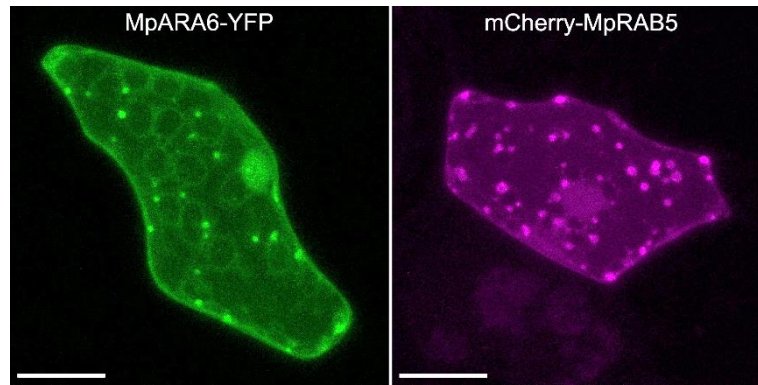


Figure 66: **Subcellular localization of endosomal marker proteins in *M. polymorpha*.** *35S::MpARA6* and *35S::MpRAB5* were transiently expressed in two- to three-week-old *M. polymorpha* thalli via particle bombardment. The scale bar indicates 20 μm .

Co-transformation of *MpARA6* and *MpRAB5* with *MpLIP5* resulted in partial co-localization of the proteins (Fig. 67). Non-overlapping fluorescent signals next to co-localization of both proteins are clearly visible (zoom-ins, fig. 67).

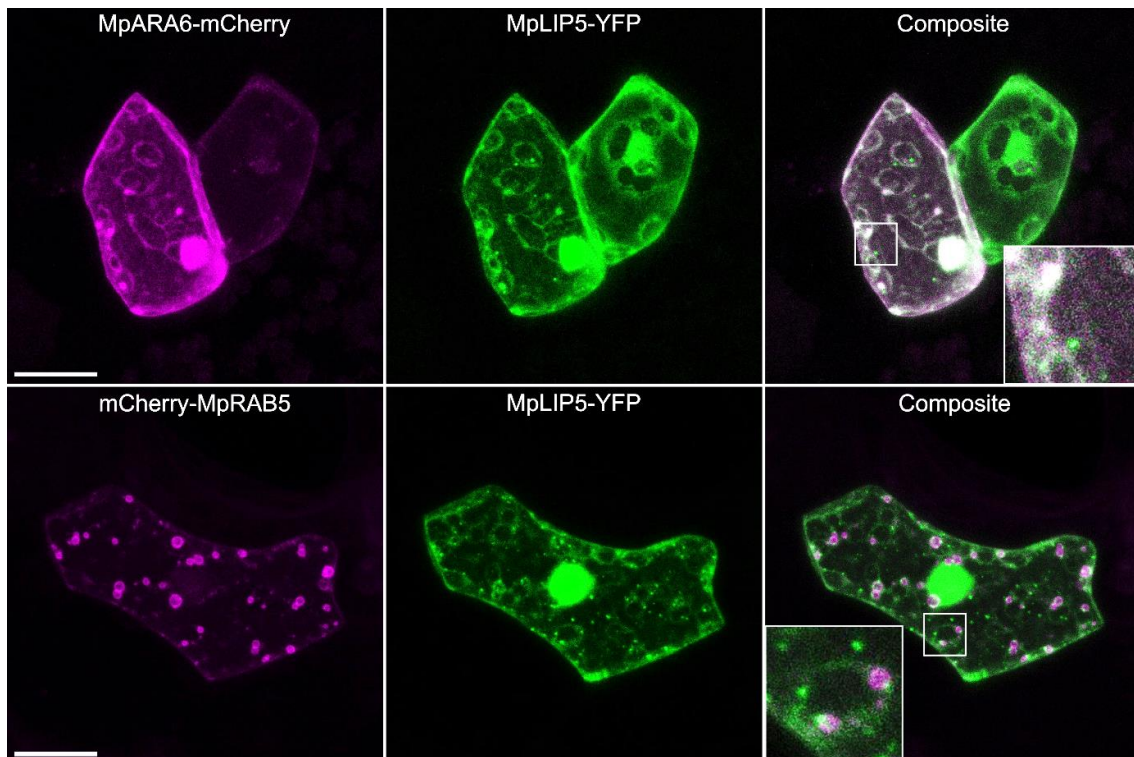


Figure 67: **Co-expression of *MpLIP5* with endosomal marker proteins.** *35S::MpLIP5*, *35S::MpARA6* and *35S::MpRAB5* were transiently expressed in two- to three-week-old *M. polymorpha* thalli via particle bombardment. The scale bar indicates 20 μm .

The same result was obtained from co-transformation of *MpSPI* PBW with *MpARA6* and *MpRAB5*. Fluorescent *MpSPI* PBW signals, not overlapping with *MpARA6* and *MpRAB5* signals, or vice versa, were detectable (Fig. 68).

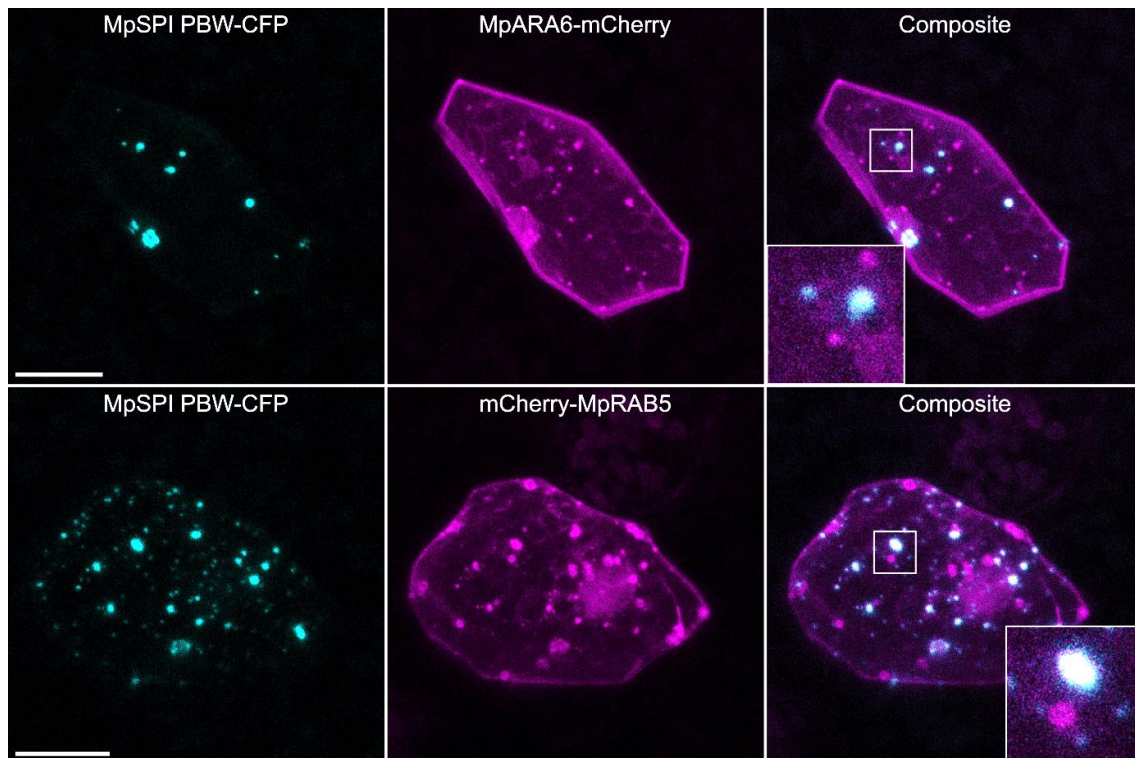


Figure 68: **Co-expression of MpSPI PBW with endosomal marker proteins.** *35S::MpSPI PBW*, *35S::MpARA6* and *35S::MpRAB5* were transiently expressed in two- to three-week-old *M. polymorpha* thalli via particle bombardment. The scale bar indicates 20 μm .

In summary, co-expression analysis showed MpSPI PBW to co-localize with P-body and ESCRT components in transiently transformed cells of Marchantia thalli. As expected, MpLIP5 and MpSPI PBW partially co-localize with the endosomal markers MpARA6 and MpRAB5. This result likely rules out aggregation capacity of MpLIP5 and MpSPI PBW and thus supports biological meaning of immediate proximity of MpSPIRRIG with P-bodies and the ESCRT system in cells of *M. polymorpha*.

3.2.5.4 Co-localization of MpSPI PBW with p-Body/ESCRT marker proteins cannot be analyzed in transgenic lines

In theory, stable genomic transformation of Marchantia thallus fragments (Ishizaki et al., 2008) or spores (Kubota et al., 2013) is supposed to be efficient and easy to conduct. However, during the experimental procedures, several problems were faced in the course of this study. Stable transformation of spores was not possible as either the crossing or spore production was rarely successful. Moreover, during the selection process of transformed thalli, treatment with only two herbicides (G418, chlorsulfuron) turned out to be effective. Selection with kanamycin, gentamycin or glufosinate was not possible as growth of Marchantia thalli was not even restricted upon respective treatments (data not shown). Therefore, the choice of constructs was limited. Constructs used for transient expression studies (3.2.5.3) could not be employed as they harbor the bialaphos (bar) resistance gene for plant selection. Ishizaki et al. (2015) provided a Gateway-compatible binary vector series containing a variety of plasmids

applicable to *M. polymorpha* transformation. As transient expression of genes of interest proved to be strong under the control of 35S *CaMV* promoters (3.2.5.3), and selection with G418 and chlorsulfuron was particularly promising; respective constructs were selected from the vector series (pMpGWB406 containing Citrine as the fluorescent tag and G418 resistance; pMpGWB335 containing TagRFP as the fluorescent tag and chlorsulfuron resistance; Ishizaki et al., 2015) and employed for stable *Marchantia* co-transformation.

After several unsuccessful transformation procedures, due to either no emergence of transformants or due to emergence of non-fluorescent transformants; stably transformed, transgenic *Marchantia* lines co-expressing MpSPI PBW-Citrine with TagRFP-MpSKD1, TagRFP-MpLIP5 and TagRFP-MpDCP2 (all under control of the 35S *CaMV* promoter), respectively, were generated by subsequent thallus transformations of the MpSPI PBW-Citrine line presented in 3.2.2, fig. 49. However not only MpSPI PBW-Citrine fluorescence was strongly diminished and much weaker than in single expression lines, but also expression of the other marker proteins was very faint and hardly detectable (Fig. 81, appendix). Therefore, unfortunately co-localizations presented above could not be confirmed and no further stress-related studies could be conducted in stably expressing *Marchantia* lines.

3.2.5.5 The localization of MpSPI PBW is not affected by MpDCP2 co-expression and salt treatment

As AtSPIRRIG was shown to localize to P-bodies upon salt stress (Steffens et al., 2015), localization behavior of MpSPIRRIG in salt-treated, transiently transformed *Marchantia* thalli, was investigated next. Comparable dot-like localization of MpSPI PBW was observable before and after incubation in liquid Johnson's supplemented with 150 mM NaCl for 60 min (Fig. 69A). Moreover, MpSPI PBW granules co-localize with MpDCP2 under non-stress and stress conditions (Fig. 69B). Scoring of granules confirmed no significant increase or decrease of MpSPI PBW dots upon salt treatment in single or co-bombardments with MpDCP2 (Fig. 69C). Furthermore, co-expression of MpDCP2 does not affect MpSPI PBW granule number (Fig. 69C).

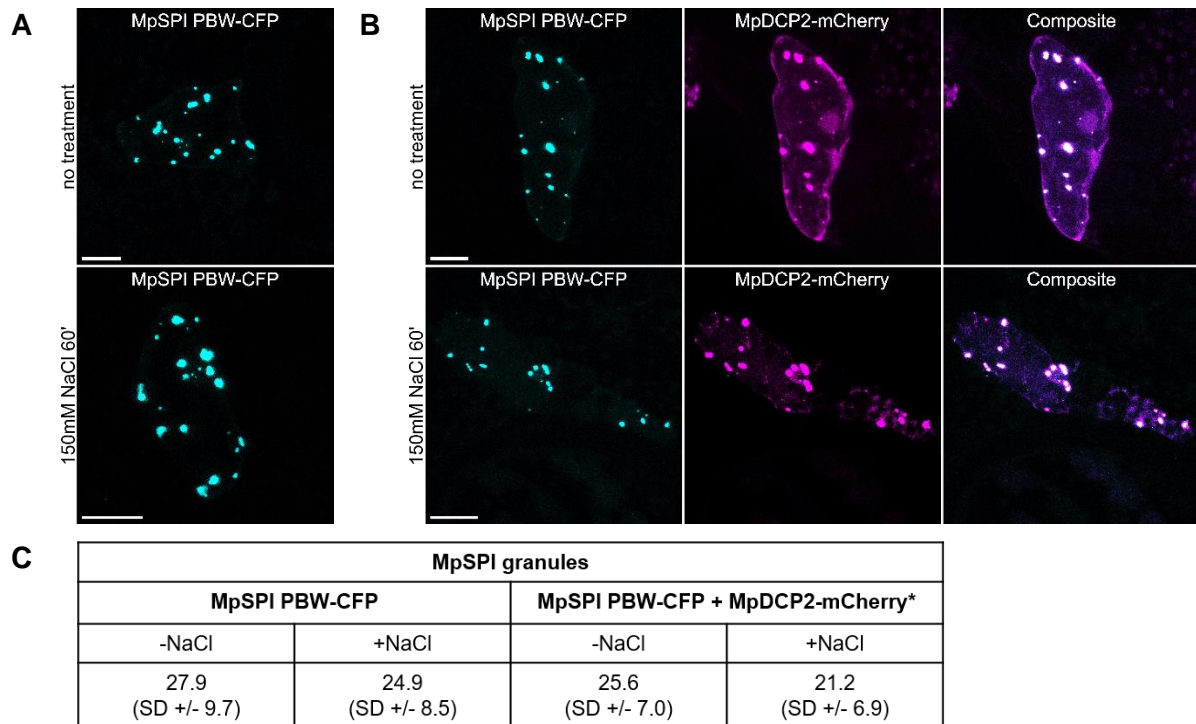


Figure 69: **MpSPI PBW localization is not affected by salt treatment.** Marchantia thallus fragments, transiently transformed with *35S::MpSPI PBW* (**A**) or *35S::MpSPI PBW + 35S::MpDCP2* (**B**), were subjected to liquid Johnson's containing 150 mM NaCl for 60 min. Localization was observed before and after salt treatment. The number of MpSPI PBW granules was scored in single and co-bombardments with MpDCP2 (**C**). $n=13-16$. Significance was tested with a two-tailed, unpaired Student's *t*-test. * MpSPI-PBW nearly showed a complete overlap (assessed qualitatively) with MpDCP2 and vice versa.

The Arabidopsis SG marker AtUBP1b is known to be evenly localized in the cytoplasm and nuclei in cells of *A. thaliana* under normal conditions. Assembly of cytoplasmic foci, labeled by AtUBP1b, is induced by stress stimuli such as heat stress (Nguyen et al., 2016). Interestingly, dot-like localization of AtUBP1b was observable already under non-stress conditions in cells of transiently transformed *M. polymorpha* thalli (Fig. 70).

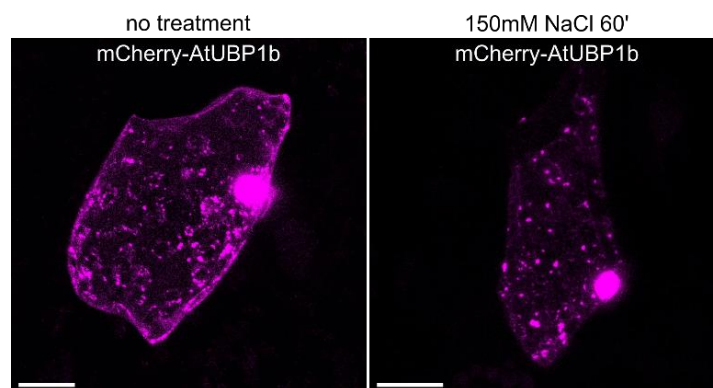


Figure 70: **The Arabidopsis stress granule marker AtUBP1b localizes to dot-like structures already under non-stress conditions in *M. polymorpha*.** Marchantia thallus fragments, transiently transformed with *35S::AtUBP1b*, were subjected to liquid Johnson's containing 150 mM NaCl for 60 min. Localization was observed before (left) and after (right) salt treatment.

3.2.5.6 MpSPIRRIG interacts with the ESCRT component MpLIP5 in yeast

In order to test if MpSPIRRIG not only co-localizes, but also physically interacts with ESCRT and P-body components, pairwise yeast two-hybrid assays were performed (Fig. 71).

| GAL4-AD \ GAL4-BD | MpSPI PBW | MpSPI PBWF | AtSPI PBW | MpDCP1 | MpSKD1 | MpLIP5 |
|-------------------|------------|------------|------------|-------------|---------------|-------------|
| MpSPI PBW | ND | ND | ND | - | - | - |
| MpSPI PBWF | ND | ND | ND | - | - | - |
| AtSPI PBW | ND | ND | ND | * 1-5 mM | - | * 3-5 mM |
| MpDCP1 | auto | auto | auto | ND | ND | ND |
| MpSKD1 | - | - | - | ND | ND | * 50 mM |
| MpLIP5 | * 50 mM | * 50 mM | * 50 mM | ND | * 30-50 mM | ND |

Figure 71: **Results of pairwise yeast-two hybrid assays of MpSPI with ESCRT and P-body components.** GAL4-AD=GAL4-activation domain, GAL4-BD=GAL4-binding domain, ND=not determined, auto=autoactive growth, - =no interaction, * =interaction on SD-LWH + indicated 3-AT concentration in at least three independent experiments without simultaneous growth of negative control (AD-protein of interest + BD-GFP).

Growth of yeast was considered as an interaction, when it was observed in at least three independent transformations and when the respective negative controls (AD-protein of interest + BD-GFP or BD-protein of interest + AD-GFP, respectively) did not show growth. If possible, both potential interaction partners were fused to the GAL4-AD/BD and were tested reciprocally. As BD-MpDCP1 caused activation of the *HISTIDINE* marker and growth of yeast, interactions were only tested with AD-MpDCP1.

The experiments revealed no interaction of MpSPI PBW/PBWF with MpDCP1 and MpSKD1 (Fig. 71). However, interestingly, the Marchantia DCP1 was able to interact with the Arabidopsis SPI-PBW. The integrity of MpSKD1 was confirmed by strong interaction with MpLIP5. MpLIP5 in turn was found to also interact with MpSPI PBW/PBWF as well as with AtSPI PBW (pictures of yeast and a detailed view on the interaction of the Marchantia proteins SPI and LIP5 can be found in fig. 85, appendix).

4 DISCUSSION

This two-tier study was set out to investigate SPIRRIG function using a variety of experimental approaches. One part of this study aimed to contribute to understanding the molecular function of SPIRRIG in salt stress response of *A. thaliana* by investigating a potential, so far unknown, interplay of the BDCP with TZF proteins. The other part of this work aimed to elucidate the basal functions of SPIRRIG in one of the first plants colonizing the land, *M. polymorpha*.

4.1 The interplay of TZF10 and 11 with the BDCP SPIRRIG in Arabidopsis salt stress response

Plant survival under unfavorable environmental conditions and abiotic stresses requires large-scale adaptations on the physiological, biochemical and molecular level. Research during the past decades addressed the stages of plants' salt stress response, such as signal perception (Yang and Guo, 2018) and signal transduction (Zhu, 2002) as well as ion homeostasis including ion uptake, transport and distribution (Isayenkov and Maathuis, 2019). The processes ultimately lead to growth alteration (Pierik and Testerink 2014; Julkowska and Testerink, 2015) and changes in gene expression (Kreps et al., 2002).

Gene expression regulates the abundance of transcripts. Transcript abundance however is not only modulated by transcriptional regulation, but is tightly controlled by post-transcriptional regulation as well. Upon export of mature mRNAs from the nucleus, mRNA metabolism is modulated by various mechanisms that trigger different fates of mRNAs in the cytoplasm. A number of mRNAs are directly translated at polysomes, while other mRNAs undergo quality control, are translationally stalled, stabilized or degraded upon sequestration to mRNP granules (Belostotsky and Sieburth, 2009; Kawa and Testerink, 2016). These destabilization and degradation processes strongly contribute to plants' stress response (Kawa and Testerink, 2016).

SPIRRIG, the so far best described BDCP in plants, was identified as a regulator of salt stress response of Arabidopsis (Steffens et al., 2015). The exact molecular function of SPIRRIG has not been fully elucidated yet. However, SPIRRIG was shown to be a positive regulator for P-body formation, as well as stabilization and localization of salt stress-related mRNAs (Steffens et al., 2015). To date, SPIRRIG is the first and only BDCP known to be involved in mRNA metabolism. Interestingly, SPIRRIG physically interacts with Arabidopsis TZF10 and 11 proteins (A. Steffens, unpublished data), of which mammalian homologs are known to regulate mRNA decay (Lykke-Andersen and Wagner, 2005).

4.1.1 TZF10 is associated with cytoplasmic mRNA granules and stress response

In humans, the mechanism by which TZF proteins induce mRNA decay is relatively well understood (Brooks and Blackshear, 2013). The most prominent and well described human

TZF, TTP, destabilizes mRNAs upon binding to AREs in 3'UTRs of target mRNAs and subsequent recruitment of the CCR4-NOT complex to induce deadenylation (Lykke-Andersen and Wagner, 2005). In plants however, evidence supporting connections of TZF proteins to mRNA metabolism accumulated more recently and exact molecular mechanisms remain elusive. Although association with cytoplasmic granules has already been shown for a subset of Arabidopsis TZF proteins (Pomeranz et al., 2010a; Qu et al., 2014; Maldonado-Bonilla, 2014; Tabassum et al., 2020), no reports that directly connect TZF10 to mRNA metabolism are available so far.

While Pomeranz et al. (2010b) already showed TZF10 to localize to cytoplasmic foci without identification of the nature of these granules, this work not only demonstrated TZF10 to co-localize with stress granules under stress-conditions (3.1.1), but also verified that both TZF protein and mRNA, co-localize with mRNPs already under non-stress conditions (3.1.2). The physical proximity of TZF10 protein and mRNA with P-body components supports the notion for a biological relevance of TZF10 for mRNA decay in *A. thaliana*. The fact that TZF10 protein relocates to stress granules under stress conditions (3.1.1) could further imply a function in stress response.

However, biological relevance of TZF10 and 11 in salt stress response could not be verified in this work, since thorough re-investigation of two *tzf10/tzf11* double mutants could not at all confirm that *tzf10/tzf11* double mutants exhibit a salt hypersensitivity phenotype (3.1.3; Sun et al., 2007b). Thus, a relevance of TZF10 and 11 for Arabidopsis salt stress response is questionable, but not fully excluded. As other Arabidopsis TZF proteins have been shown to be involved in salt stress response (Huang et al., 2011; Lee et al., 2012; Han et al., 2014), potential redundancies would be conceivable. Moreover, this study proved up-regulation of *TZF10* under salt stress conditions (3.1.4), hinting TZF10 to somewhat be associated with salt stress response.

4.1.2 The interplay between TZF10 and SPIRRIG is elusive

Extensive salt stress screening of newly generated *spirrig* lines stably expressing *TZF10* in this work confirmed TZF10 to rescue the salt hypersensitivity phenotype of *spirrig* (3.1.6, results from the respective experiment are further discussed in 4.1.3). It is disputable, if an interconnection of the BDCP and TZF10 mediates this rescue and if the two classes of proteins act in the same or in independent pathways of mRNA regulation.

An association is supported by direct protein-protein interaction and similar localization behavior of the proteins at P-bodies. Moreover, SPIRRIG and TZF proteins seem to share a function in regulating stress-related mRNA stability. Whereas TZF proteins have generally been shown to act in a destabilizing manner (Wells et al., 2017), SPIRRIG stabilizes salt stress-related mRNAs (Steffens et al., 2015). Nevertheless, the two antagonizing processes can be

unified in Arabidopsis salt stress response. In this hypothetical model, analogously to TTP function (according to Otsuka et al., 2019, fig. 4), TZF proteins are expressed upon stress stimuli; but are directly inactivated at the protein level by phosphorylation. During stress, proteins (e.g. Hu proteins in humans) execute antagonizing functions in stabilizing stress-related mRNAs. As soon as the stress level is ceasing, TZFs are dephosphorylated and activated to exert their function in inducing mRNA degradation and clearance of ARE containing, stress-related mRNAs.

Investigation of *TZF10* expression revealed expression levels to be on a similar level under non-stress as well as stress conditions in *spirrig* and Col-0. Furthermore, a moderate up-regulation of *TZF10* upon salt stress was similarly detectable in *spirrig* mutants and Col-0, indicating the *TZF10* salt stress response to be, if at all, only marginally affected in *spirrig* mutants (3.1.4). Hence, it is not likely that SPIRRIG has an effect on *TZF10* expression.

A more likely scenario explaining the interplay of SPIRRIG and *TZF10* is that *TZF10* might be affected in mRNA stability in *spirrig* mutants. This hypothesis is based on the knowledge that the mRNA of *TZF3* appeared to be strongly destabilized in *spirrig* under salt stress conditions (Steffens et al., 2015). However, thorough investigation of *TZF10* mRNA stability in Col-0 and *spirrig* yielded inconsistent results (3.1.5). The first impression that the stability of *TZF10* mRNA is more strongly affected in *spirrig* under non-stress and stress conditions than in Col-0, was not reproducible. The analysis was extended to determination of *TZF11* mRNA stability; but also here, no differences between the genotypes were detectable.

Destabilization of *TZF3* in *spirrig* was accompanied by altered localization behavior, as no salt stress-dependent recruitment of the *TZF3* mRNA to P-bodies took place. The finding suggested *TZF3* mRNAs to be stabilized in P-bodies upon salt stress in wild type cells (Steffens et al., 2015). Investigation of *TZF10* mRNA localization revealed a co-localization with DCP1 at already approximately 100% under control conditions in Col-0 and *spirrig* (3.1.2, fig. 6). The finding thus does not suggest a defect in guiding *TZF10* mRNA to P-bodies in *spirrig* mutants as it was described for *TZF3*, and therefore supports *TZF10* to be differentially regulated than *TZF3* and to not be affected in mRNA stability in *spirrig* mutants.

Taken together, the experiments performed in this work did not provide any indication hinting to a diminished *TZF10* function in *spirrig* mutants. The results indicate salt-stress induced *TZF10* mRNA expression and stability to not be affected in *spirrig* mutants. Even though slight effects were sporadically detectable in single experiments, it remains highly questionable if these marginal effects are ultimately reflected in altered protein levels and if they are biologically relevant for salt stress response defects in *spirrig* mutants.

4.1.3 *TZF10* function is not influenced by its UTRs in the context of *spirrig* salt hypersensitivity rescue

Mature mRNAs, exported from nuclei, consist of a 5'UTR, a coding sequence and a 3'UTR. Both UTRs play essential roles in post-transcriptional regulation: they affect the transport, translational efficiency, subcellular localization, and stability of mRNAs (Mignone et al., 2002; Jansen, 2001; Bashirullah et al., 2001; Srivastava et al., 2018). Respective mechanisms are for example exerted through stem-loop structures, UTR length modulated by alternative polyadenylation or alternative splicing, riboswitches, adenine methylation, upstream open reading frames and a variety of *cis*-acting elements serving as binding sites for RBPs (Mignone et al., 2002; Srivastava et al., 2018). The significance of UTRs is further emphasized by the fact that UTRs make up 18–19% of the total transcribed sequence in *A. thaliana* (Srivastava et al., 2018).

This work evaluated possible effects mediated by UTR sequences on TZF function. Therein, a special focus lay on the identification of biologically relevant roles of the *TZF10* UTRs in the context of salt hypersensitivity rescue of *spirrig*. The investigation ultimately aimed to establish a connection between regulatory functions exerted by TZF10 and the BDCP SPIRRIG.

The special importance of 3'UTRs to TZF function was demonstrated when mammalian TZF proteins were shown to induce mRNA decay upon binding to the *cis*-acting ARE in 3'UTRs of target mRNAs (Brooks and Blackshear, 2013). In accordance, an initial experiment showing TZF10 to rescue the salt hypersensitivity phenotype of *spirrig* mutants strongly pointed to a significant role of the 3'UTR also for TZF10 function, since the rescue effect was only visible in plants transformed with the *TZF10* CDS lacking the 3'UTR (A. Steffens, unpublished data).

Extensive salt stress screening of newly generated *spirrig* lines stably expressing *TZF10* did confirm TZF10 to rescue the salt hypersensitivity phenotype of *spirrig*. However, the effect was not abrogated in *spirrig* mutants transformed with *TZF10* including downstream 3'UTR (3.1.6). In contrast to previous results, this finding does not support a potential influence of the *TZF10* 3'UTR on *TZF10* function. Nonetheless, the result also does not yet fully exclude the 3'UTR to affect *TZF10* mRNA stability at all. Thus, this work examined potential direct and indirect effects of the 3'UTR on *TZF10* in the context of *spirrig* salt hypersensitivity rescue in different approaches.

The findings did not indicate an effect of the *TZF10* 3'UTR on *TZF10* mRNA expression in transgenic lines (3.1.6, fig. 25). Nevertheless, direct evaluation of 3'UTR-mediated effects on *TZF10* mRNA stability demonstrated the *TZF10* mRNA to indeed be more strongly destabilized under non-stress and stress conditions in transgenic lines transformed with the *TZF10* CDS+3'UTR compared to lines transformed with the *TZF10* CDS (3.1.6, fig. 26). This effect

can likely be ascribed to presence of the 3'UTR. However, it was not possible to correlate the degree of *TZF10* mRNA stability with the level of salt hypersensitivity rescue. Concomitantly, it is highly questionable, if observed increased mRNA destabilization induced by the 3'UTR would at all be reflected in TZF10 protein amounts. Unfortunately, it was not possible to detect TZF10 protein in non-stressed and salt-stressed *spi-4* lines transformed with *YFP-TZF10* CDS or *YFP-TZF10* CDS+3'UTR using an α -GFP-antibody (Fig. 80, appendix). Subsequent experiments detecting potential differences of protein levels in dependence of 3'UTR presence were thus not possible to conduct.

Finally, this study showed that the 3'UTR of *TZF10* is also not likely to affect the mRNA stability of other salt-induced mRNAs, which was assessed at the example of *RD29A* (3.1.6.4). All in all, a biological relevance of 3'UTR-mediated effects in the context of salt hypersensitivity rescue seems unlikely, since there are no indications that the 3'UTR mediates regulatory functions relevant to salt stress tolerance of *spirrig*. In support of this, an alternative approach in order to tackle the effect of the 3'UTR on the salt stress phenotype of *spirrig* revealed no influence of the 3'UTR on salt hypersensitivity of *spirrig*: the crossing of *TZF10* and 11 T-DNA alleles with *spirrig*, resulting in a stable introduction of disrupted *TZF10* and 11 3'UTRs, did not lead to a mitigation, or a rescue, of *spirrig* salt hypersensitivity (3.1.7).

In order to complement the analysis of UTR effects on *TZF10* function, this study moreover investigated a potential influence of the 5'UTR on salt hypersensitivity of *spirrig* mutants. The analysis revealed that no matter if the 5'UTR was present in *TZF10* constructs introduced into *spi-4* or not, salt hypersensitivity was clearly rescued (3.1.8).

Ultimately, it is highly remarkable that even weak overexpression of *TZF10*, and furthermore, instable *TZF10* mRNA is able to mediate the salt hypersensitivity rescue of *spirrig*. The mechanism behind this is elusive. It remains to be elucidated, if there is an actual interplay between the BDCP SPIRRIG and TZF10, or if *TZF10* just independently renders *spirrig* mutants more salt tolerant by an unknown mechanism.

Recent evidence suggested human TTP to not solely function in post-transcriptional regulation, but to exert regulatory functions in transcription, supported by nuclear-localization, as well (Tu et al., 2019). In a genome-wide approach, Sedlyarov et al. (2016) identified destabilizing, but also non-destabilizing TTP binding events and accordingly, demonstrated TTP binding events to be not sufficient to drive mRNA destabilization. In ensuing studies, Tu et al. (2019) proved TTP to regulate gene transcription and/or alternative splicing. TZFs in other organisms, such as in mice and *Caenorhabditis elegans*, were shown to activate and regulate transcription, respectively, as well (Murata et al., 2000; Ghosh and Seydoux, 2008). Among Arabidopsis TZFs, TZF6 and TZF1 are known to be nuclear-localized and to exhibit dsDNA-binding capacity (Li and Thomas, 1998; Pomeranz et al., 2011). In the light of these findings, and since

this study showed TZF10 to localize to the nucleus as well (3.1.1), it seems conceivable that TZF proteins in Arabidopsis could exert functions in transcriptional regulation as well. Consequently, a role of *TZF10* in salt stress response completely independent from SPIRRIG, and from UTR-mediated effects, could be possible.

4.1.4 The 3'UTR of *TZF10* mediates mRNA destabilizing effects independent from *spirrig*

Even though mRNA destabilizing effects induced by the *TZF10* 3'UTR could not be correlated to the salt hypersensitivity rescue of *spirrig*, the results nonetheless indicated the 3'UTR to negatively impact *TZF10* mRNA stability under non-stress and stress conditions. In order to support this notion, general mRNA destabilizing capacity of the *TZF10* 3'UTR was investigated in this work as well.

4.1.4.1 Localization behavior of the *TZF10* and *11* mRNA is not altered by the 3'UTR

First, it was reasoned that the 3'UTR might affect the subcellular localization of the mRNAs of *TZF10* and *TZF11*. As mRNPs are sites of mRNA storage and decay, a higher amount of mRNA was expected to co-localize with cytoplasmic granules when the CDS was fused to the 3'UTR. In accordance with the results of 3.1.2, demonstrating the mRNA of *TZF10* to locate to P-bodies, *TZF10* CDS mRNA was sporadically detectable at cytoplasmic granules (3.1.9.1). One experiment showed the *TZF10* CDS+3'UTR mRNA to be increasingly located at stress granules upon heat treatment. However, the results could not be confirmed in several repetitions of the experiment. Thus, it can be concluded that addition of the 3'UTR does not strikingly alter localization behavior of the *TZF10* or *TZF11* mRNA in cells of *A. thaliana* and *N. benthamiana*.

However, the assembly and disassembly of mRNP granules is a highly dynamic process. It was shown that association and disassociation of proteins to mRNP granules occur within seconds to minutes (Buchan and Parker, 2009; Lin et al., 2015). Moreover, the rapid process of liquid-liquid phase separation induced by intrinsically disordered regions (IDRs) in RBPs coupled with RNA-protein interactions was demonstrated to strongly contribute to mRNP assembly (Lin et al., 2015). Transcriptome sequencing of mammalian and yeast stress granule cores revealed that even though most of the mRNAs were targeted to stress granules, the targeting efficiency strongly varied between <1% to >95%. Furthermore, only a very low subset of these mRNAs was stably located in stress granules (Khong et al., 2017). In accordance, interactions between ribosome-free mRNAs and stress granules were described as short-lived (Moon et al., 2019; Lee and Seydoux et al., 2019).

In the light of these studies, it seems conceivable that potential effects of the 3'UTR on *TZF* mRNA localization might be highly dynamic and hard to detect in indirect mRNA visualization

studies. Even though the results on one hand do not support an effect, on the other hand they do not fully exclude it.

4.1.4.2 The 3'UTR of *TZF10* destabilizes the mRNA of *YFP*

A particularly exciting finding during the course of this work was the result that both the *TZF10* and *11* 3'UTRs were found to destabilize the mRNA of *YFP* (3.1.9.2). Consecutive fragmentation of both 3'UTRs moreover allowed the isolation of a conserved stretch with a length of 15 bp, **AUUUAUAUUGCUUUG**, presumably representing a motif inducing mRNA stabilization. Even though the sequence certainly can be classified as AU-rich as it contains an AUUUA pentamer (Barreau et al., 2005) and several Us, the sequence cannot be regarded as a classical ARE. The importance of this non-classical AU residue array however was emphasized by demonstrating *YFP* expression to be substantially enhanced when *YFP* was fused to mutated versions of the motif. The introduction of the motif into a foreign 3'UTR (*ABF3*) and subsequent fusion to *YFP* did not result in diminished *YFP* expression. The finding was not surprising as other factors coming along with the foreign 3'UTR such as different RBP binding motifs, 3'UTR folding structure or poly[A] tail length (Srivastava et al., 2018) could likely have a relevant and conceivably antagonizing impact on the process.

The experiments were complemented with subcellular localization analysis and revealed 3'UTR localization to not be substantially altered under stress conditions (3.1.9.3). Moreover, the parts of the 3'UTR, either shown to induce mRNA destabilization or not, did not exhibit differential localization behavior under non-stress and stress conditions. The dynamic nature of mRNA targeting to mRNP granules was already discussed above (4.1.4.1) and might be partially accountable for the lack of conclusive results in these experiments. Furthermore, in order to perform indirect mRNA visualization using the λ N22 system (Schönberger et al., 2012), the 3'UTR and parts of it were fused to Box-B elements, an array composed of several 15-nt RNA stem loops. Since the *TZF10* and *11* 3'UTRs were shown to affect and destabilize the mRNA of *YFP*, an effect on the Box-B elements cannot be fully excluded. Thus, it is conceivable that indirect visualization through binding of λ N22-mVenus did not efficiently occur in the conducted experiment.

4.1.5 *TZF10* and *11* interact with proteins of various functions in a yeast two-hybrid screen

Yeast two-hybrid screening with *TZF10* and *11* as the bait proteins yielded several interesting interactions with proteins of various classes, suggesting *TZF* proteins to be involved in several different pathways (3.1.10). In the course of this study, two different follow-up projects were initiated from two particularly interesting interactions. Both are summed up in the following.

4.1.5.1 TZF10 and 11 interact with RNA ligases

Strikingly, an interaction of TZF10 and 11 with the two proteins encoded by AT5G40190 and AT3G28140, sharing around 80% identity at the amino acid level, was represented with an unusually high number and more than 50% of all hits (in total 165) and was verified in pairwise yeast two-hybrid interaction assays (data not shown). The two proteins belong to the RNA ligase/cyclic nucleotide phosphodiesterase family, whose members are known to be involved in catalyzing tRNA processing in eukaryotes (Mazumder et al., 2002). AT3G28140 and AT5G40190 have not yet been described in Arabidopsis, but have been identified in a screen searching for calmodulin-binding proteins (Reddy et al., 2002). In this study, AT3G28140 was shown to co-localize with TZF10 already under non-stress conditions and with the SG marker UBP1b upon heat stress (Fig. 82, appendix), suggesting associated functions. Since no T-DNA insertion lines for both genes were available, a CRISPR/Cas9-based mutagenesis (Plasmid set *Streptococcus pyogenes*, provided by the working group of Prof. Dr. Holger Puchta, Karlsruher Institut für Technologie; Fauser et al., 2014) was conducted as a first step towards elucidating AT3G28140 and AT5G40190 function. While it was not possible to generate a mutant for AT3G28140, a homozygous mutant (single insertion 4 bp upstream of the protospacer adjacent motif (PAM)) for AT5G40190 was successfully isolated. No obvious phenotype of *at5g40190* could be identified. However, since AT5G40190 shares a high identity with AT3G28140, and both proteins showed similar interacting behavior in this work, redundant functions could be conceivable. Thus, a striking phenotype of single mutants would not be likely. Ultimately, the project was not further pursued in the course of this study.

4.1.5.2 TZF10 interacts with a MYB transcription factor involved in IG synthesis

Another interesting lead into a new project was an interaction, represented by five hits in the screen and confirmed in pairwise yeast two-hybrid interaction assays (data not shown), of TZF10 with MYB34, a well-described regulator of indolic glucosinolate (IG) biosynthesis (Celenza et al., 2005). Various transcription factors continually occurred in several yeast two-hybrid interaction screenings with bait proteins somewhat connected to PBs/SGs, performed in our group (personal communication, M. Jakoby). From this, the following question was derived: Can transcription factors be regulated by recruitment/trapping in stress granules and to thereby be separated from their target genes? Evidence for existence of this mechanism in *A. thaliana* was first reported by Koguchi et al. (2017), who demonstrated localization of VASCULAR PLANT ONE-ZINC FINGER 2 (VOZ2) to change from the cytoplasm to nuclei and cytoplasmic foci in cells of *A. thaliana* upon heat stress. They moreover showed that the VOZ2 protein is rapidly degraded via the ubiquitin/proteasome pathway under heat stress conditions. Furthermore, the authors showed that expression of *DEHYDRATION-RESPONSIVE ELEMENT BINDING PROTEIN 2A* (*DREB2A*) is strongly up-regulated in *voz1/voz2* mutants upon heat stress. Hence, they suggest VOZ2 to act as a transcriptional repressor of *DREB2A*

by its location in cytoplasmic foci and the nucleus followed by rapid degradation under heat stress conditions.

In this study, localization behavior under heat stress was examined for MYB34, MYB51 and MYB122, which act together and are indispensable for IG synthesis (Frerigmann and Gigolashvili, 2014). MYB34, MYB51 and MYB122 showed nuclear-cytoplasmic localization under non-stress conditions and indeed accumulated in dot-like structures with distinctive co-localization with the SG marker UBP1b upon heat treatment (exemplarily shown for MYB51, fig. 83A, appendix). However, a significant amount of fluorescence was still detectable in the nucleus upon heat stress. Subsequent analysis revealed MYB34 fluorescence to not decrease in the nuclei of transiently transformed *A. thaliana* cells upon heat stress (Fig. 83B, appendix), suggesting MYB34 to still be active in the nucleus. Nonetheless, a different approach, measuring *MYB34*, *MYB51* and *MYB122* transcript levels by qPCR analysis, revealed the expression of *MYB34*, *MYB51* and *MYB122* to be significantly down-regulated upon 1 h of heat treatment (Fig. 84, appendix). The expression of *MYB34* target genes, *CYTOCHROME P450 79B2* and *79B3* (*CYP79B2* and *CYP79B3*; Frerigmann et al., 2016), likewise was down-regulated after 3 h of heat treatment, indicating heat stress to render MYB34 inactive at later time points. Subsequent several attempts to prevent stress granule formation or dissolve stress granules in a transgenic *A. thaliana* SG marker overexpression line, failed so far. Treatment with known polysome-stabilizing agents such as cycloheximide (e.g. Mollet et al., 2008) and emetine (Kedersha et al., 2000) or integrated stress response inhibitor (ISRIB) shown to disassemble SGs (Sidrauski et al., 2015), did not cause any effect. Puromycine, which is known to destabilize polysomes and to thereby enhance formation of SGs (Kedersha et al., 2005), showed no effect as well. The underlying hypothesis for this strategy is that by blocking SG assembly, MYB34 would be prevented from being “trapped” in SGs, would thus still exert its function under stress conditions, and concomitantly, *MYB34* and *MYB34* target transcript levels would not decrease. In turn, by enhancing SG assembly, MYB34 protein would be permanently located in granules and thereby its function would be repressed irrespective of stress. In contrast to heat stress conditions, *MYB34* is supposed to be up-regulated under salt stress conditions (eFP Browser, AtGenExpress Abiotic Stress Series, Kilian et al., 2007). Moreover, *MYB34*, *51* and *122* transcripts differentially respond to hormone treatments such as to abscisic acid, methyl jasmonate or salicylic acid (Frerigmann and Gigolashvili, 2014). The identification of differential MYB stress responses, presumably reflected in different localization behavior, could support the potential connection of MYB recruitment to SGs with MYB inactivation. Furthermore, fusion of an intrinsically disordered region (IDR) shown to be sufficient to mediate recruitment to SGs (Zhu et al., 2020), could render MYB34 inactive by constitutive, stress-independent localization to SGs. The project was not further pursued in the

course of this work; however, several promising further leads, outlined above, could contribute to elucidating a not yet fully understood mechanism of transcription factor regulation.

4.1.6 Outlook

The experiments performed in this work proved TZF10 to rescue the salt hypersensitivity rescue of *spirrig* mutants. However, a connection between regulatory functions implemented by the *TZF10* 3'UTR and SPIRRIG in the context of salt hypersensitivity rescue was not identified. It is moreover still unclear, if the rescue induced by introduction of TZF10 can be explained by a direct interplay of TZF proteins with the BDCP, or if introduction of TZF10 as such renders the plant more tolerant to salt. More insight on this would be provided by examination of salt stress response in *TZF10* overexpression lines with wild type background.

Since the experiments performed in this study focused on post-transcriptional regulation, additional approaches aiming to connect SPIRRIG with TZF10 might address potential regulation of TZF10 at the protein level. Human TTP is regulated by MK2 phosphorylation at two conserved serine residues (Chrestensen et al., 2004) under stress conditions. Consequently, TTP is kept from inducing decay of target mRNAs upon sequestration by 14-3-3 proteins (Stoecklin et al., 2004). Interestingly, RNA-binding Arabidopsis TZF9 was reported to be phosphorylated and to thereby be modulated in its activity as well (Maldonado-Bonilla et al., 2014; Tabassum et al., 2020). Phosphosite mapping by mass spectrometry of *in vitro* MAPK-phosphorylated TZF9 identified the major phosphosites targeted by flg22-responsive MPK3 and MPK6. Moreover, TZF9 phosphorylation was linked with reduced *in vitro* RNA-binding and increased TZF9 protein destabilization (Tabassum et al., 2020). A study investigating Ca²⁺-dependent protein kinases (CPKs) interestingly identified TZF10 as a phosphorylation substrate as well (Kanchiswamy et al., 2010). In support of this, the Arabidopsis Protein Phosphorylation Site Database (PhosPhAt 4.0; Durek et al., 2010), which integrates *A. thaliana* mass spectrometry data from a variety of large-scale experiments, identifies several TZF10 phosphorylation sites. On the basis of these findings, on one hand, it would be highly exciting to investigate TZF10 phosphorylation in wild type versus *spirrig* plants. On the other hand, it would be possible to thereby broaden the knowledge on relevance of phosphorylation for TZF function in Arabidopsis in general.

On that note, other directions of future research on TZF10 and 11 independent of SPIRRIG are very promising since this study convincingly demonstrated the 3'UTRs of *TZF10* and *11* to exhibit mRNA destabilization capacity. Moreover, a motif, presumably responsible for mediating mRNA decay, was isolated. Performance of electrophoretic mobility shift assays (EMSA) investigating RNA-protein interactions could lead to the discovery of TZF10 binding to its own 3'UTR and thus could reveal a self-regulatory mechanism as it is known from TTP.

Moreover, it would be highly interesting to identify other proteins potentially binding to the motif using proteomics approaches.

So far, not only TZF-RNA interactions, but also TZF-protein interactions are scarcely explored in plants. To date, the mechanism by which TZF proteins might induce mRNA decay is not understood and interactions with NOT complexes have not yet been identified in Arabidopsis. Interestingly, Blackshear and Perera (2014) report absence of the C-terminal NOT1 binding domain in TZFs of almost all fungi and most of plants, including *A. thaliana*. Exploring potential TZF and NOT complex interactions in *A. thaliana* therefore is particularly interesting. Preliminary results in the course of this study gave a first indication that indeed TZF proteins, here tested at the example of TZF10 and 11, do interact with Arabidopsis NOT1 in yeast (data not shown). Expansion of these interaction studies could unravel if the mechanism known for human TTP, the recruitment of the CCR4-NOT complex to induce mRNA degradation, might also be applicable to plants.

4.2 SPIRRIG in *Marchantia polymorpha*

SPIRRIG executes a dual function in membrane dynamics and post-transcriptional regulation in *A. thaliana*. The unexpected finding of SPIRRIG playing a role in mRNA stability in the context of salt stress, has to date, not yet been ascribed to any other BDCP. Instead, BDCPs are known as facilitators of membrane dynamics controlling membrane fission and fusion events (De Lozanne, 2003; Cullinane et al., 2013). In accordance, SPIRRIG was found to be involved in MVB biogenesis as a positive regulator of SKD1, acting redundantly to LIP5 in Arabidopsis (Steffens et al., 2017).

This work implemented an evolutionary comparative approach and investigated SPIRRIG in the basal land plant *M. polymorpha*, aiming to identify the basal set of BDCP function required in land plants. An *Mpspirrig* mutant was characterized and interestingly, some communalities, but also differences to Arabidopsis *spirrig* were detected.

4.2.1 MpSPIRRIG contains a FYVE domain

Phylogenetic analysis identified MpSPIRRIG as the closest homolog to AtSPIRRIG. A striking difference between the two proteins is the presence of a FYVE domain downstream of the PH, BEACH and WD40 domains in MpSPIRRIG. Remarkably, no other BDCP of Marchantia or Arabidopsis (Teh et al., 2015) contains a FYVE domain.

A specific function of the FYVE domain in MpSPIRRIG remains to be unraveled. In localization and interaction studies performed in this study, constructs comprising C-terminal ends of MpSPIRRIG with and without FYVE domain were implemented in parallel. In accordance with Agudelo-Romero et al. (2020), who suggested the FYVE domain to have been lost during land plant evolution and to lack essential functions, no differences in MpSPIRRIG behavior with or

without FYVE domain were identified. However, functions of MpSPIRRIG in membrane trafficking or autophagy that might resemble functions of the closest human BDCP homolog containing a FYVE domain, HsWDFY3/ALFY, have not been investigated.

4.2.2 MpSPIRRIG is associated with cell proliferation and/or cell expansion processes

This work analyzed the short-rhizoid T-DNA mutant *Mpspirrig* isolated by Honkanen et al. (2016). A very pronounced phenotype of *Mpspirrig* became distinctively obvious during observation of gemmaling growth: gemmalings of *Mpspirrig* acquired larger size and concomitantly, more biomass during the early development. This was accompanied by overall faster vegetative development since emergence of gemmae cups was found to occur earlier on *Mpspirrig* than on Tak-1 wild type gemmalings (3.2.4).

Subsequent studies revealed the size phenotype of *Mpspirrig* to be associated with an increased amount of cells. Interestingly, at the same time, cells of *Mpspirrig* were found to be significantly smaller than cells of Tak-1. It seems likely that the *Mpspirrig* short rhizoid phenotype (Honkanen et al., 2016; confirmed in this study) is an expression of the same phenotype: the unicellular rooting structures are significantly smaller and they directly develop from ventral epidermal cells by polar growth in young gemmae (Cao et al., 2014; Shimamura et al., 2016).

While *Atspirrig* cell morphogenesis defects such as twisting of trichomes, less complexity of epidermal pavement cells and curled hypocotyl cells can be ascribed to irregular cell expansion (Saedler et al., 2009); an increased number of cells in *Mpspirrig* could probably more likely be ascribed to an increase in cell proliferation and/or reduced cell expansion.

Cell proliferation and cell expansion are two tightly linked developmental processes (Vercruysse et al., 2020; Gonzalez et al., 2012). The sites of cell proliferation in Marchantia are the apical notches, which are meristematic zones housing a single, cuneate apical cell with four cutting faces (compare fig. 54, Suzuki et al., 2020; Shimamura, 2016). Marchantia thalli growth occurs via continuous bifurcation of apical notches (Furuya et al., 2018; Shimamura, 2016). It could be conceivable that smaller cells in *Mpspirrig* are a result of an increased period of cell proliferation at apical notches and concomitant shortening of the cell expansion period. However, it could just as well be possible that cell size and cell number are genetically affected in *Mpspirrig* independently from each other (compare Usami et al., 2009).

Only a few BDCPs of other organisms have been connected to cell proliferation or alterations in cell size before. Human *LRBA* for example was shown to be strongly up-regulated in several cancer types. Consistently, *LRBA* overexpression was correlated to increased cell proliferation (Wang et al., 2004). Large volume sphere A (LvsA), a BDCP of *D. discoideum*, in turn was

shown to be essential for cytokinesis resulting in bloated, round cells (Kwak et al., 1999). The exact underlying function of LvsA required for cytokinesis is unknown, but participation in controlling endosome fusion and fission rate was postulated (De Lozanne, 2003).

Cell size in *Arabidopsis* was shown to generally correlate with endoreduplication in epidermal pavement cells and trichomes (Melaragno et al., 1993; Folkers et al., 1997; Hülkamp et al., 1994). Staining of nuclei with 4',6-diamidino-2-phenylindole (DAPI) enables quantification of DNA content and thus is frequently employed in order to discover endoreduplication (Schnittger and Hülkamp, 2007; Bramsiepe et al., 2010; Bhosale et al., 2018). However, nuclei in cells of *Marchantia* unfortunately cannot be readily stained with DAPI (Westermann et al., 2020). Nevertheless, gemmae are haploid, gametophytic tissue. Moreover, flow cytometry analyses suggested general absence of endoreduplication in liverworts (Bainard and Newmaster, 2010; Bainard et al., 2013). Thus, a correlation of altered cell size correlating to differences in ploidy level in *Mpspirrig* seems unlikely.

Leaf growth, shaped by cell proliferation and cell expansion, is immensely regulated by numerous different gene regulatory mechanisms (Vercruysse et al., 2020). In *Arabidopsis*, several prominent gene regulatory modules for cell proliferation such as the gibberellin (GA)-DELLA or GROWTH REGULATING FACTOR-GROWTH INTERACTING FACTOR (GRF-GIF) module, are well described and are connected to the cell cycle machinery (Vercruysse et al., 2020). It remains to be elucidated if and how gene regulatory mechanisms might be affected in *Mpspirrig*. Further exploration of the phenotype, which was not known from *Arabidopsis* before, depicts an outstanding opportunity to unravel new BDCP functions.

4.2.3 MpSPIRRIG is connected to P-body and ESCRT components

Arabidopsis SPIRRIG exerts a dual function in two presumably unrelated, independent pathways. Associations of AtSPIRRIG with membrane trafficking, connected to the ESCRT system (Steffens et al., 2017), and mRNA metabolism, connected to mRNA decay in P-bodies (Steffens et al., 2015), were uncovered. Prominent phenotypes of *Atspirrig* were linked to either functions and were analogously investigated in *Mpspirrig* in order to unravel the conserved set of BDCP functions in basal land plants. Subsequent co-localization and interaction studies aimed to support potential connections of MpSPIRRIG to the ESCRT system and P-bodies.

4.2.3.1 Vacuoles in rhizoids of *Mpspirrig* are not fragmented

Dictyostelium LvsA was found to belong to the same clade of BDCPs as SPIRRIG (Saedler et al., 2009). Defects in cytokinesis come along with strong fragmentation of contractile vacuoles in *lvsa* mutants (Kwak et al., 1999; Gerald et al., 2002; Wu et al., 2004; Du et al., 2008). The finding pointed to AtSPIRRIG exerting a related function and prompted investigation of vacuolar structure in root hairs of *Atspirrig* (Saedler et al., 2009). The following discovery of

the vacuole fragmentation phenotype in *Atspirrig* was the first indication for AtSPIRRIG to function in membrane dynamics (Saedler et al., 2009).

This study analogously investigated vacuole structure in unicellular rhizoids of *Mpspirrig*. However, unlike in root hairs of *Arabidopsis spirrig*, vacuoles in rhizoids of *Mpspirrig* did not exhibit a fragmentation phenotype (3.2.5.1). In the light of the finding that fragmented vacuoles are also absent in root hairs of *spirrig* mutants in *Arabis alpina* (Stephan, 2018; Stephan et al., 2021), a Brassicaceae closely related but also around 26 to 40 million years distant to *A. thaliana* (Beilstein et al., 2010; Koch et al., 2006), the result is not surprising. It seems likely that the precise function of SPIRRIG in maintaining vacuolar membrane integrity was acquired at later stages during land plant evolution and/or might be specific to *A. thaliana*.

Even though the result may exclude a specific function of MpSPIRRIG in regulating membrane dynamics in vacuoles of rhizoids, they clearly do not rule out general involvement in membrane trafficking processes of Marchantia.

4.2.3.2 MpSPIRRIG co-localizes and interacts with ESCRT components

In order to further elucidate association of MpSPIRRIG with membrane trafficking processes, co-localization with ESCRT components was investigated and revealed a strong and clear overlap with MpSKD1 and MpLIP5 (3.2.5.3). Towards supporting biological meaning of the co-localization, direct protein-protein interactions were analyzed. Yeast two-hybrid assays were conducted to gain a first impression on physical interactions (3.2.5.6).

While a direct interaction of MpSPI PBW with the ESCRT component MpSKD1 was not detectable in yeast two-hybrid assays, MpSPI PBW was found to interact with MpLIP5. MpLIP5 in turn strongly interacted with MpSKD1. Several studies proved the fundamental importance of AtLIP5 for MVB trafficking in the context of plant immunity (Wang et al., 2014) and stress tolerance (Wang et al., 2015) dependent on the interaction with AtSKD1. The fact that the SKD1-LIP5 interaction seems to be conserved in *M. polymorpha* further emphasizes the fundamental biological importance of the interaction for land plants.

Since AtLIP5 is a positive regulator of AtSKD1 function (Fujita et al., 2004; Haas et al., 2007), and AtSPIRRIG was shown to act redundantly to AtLIP5 in promoting AtSKD1 activity (Steffens et al., 2017), it could be conceivable that no direct interaction between MpSPIRRIG and MpSKD1 would be required in Marchantia. However, the results gained by yeast two-hybrid assays have to generally be regarded with caution as they can give rise to false positive results due to strong overexpression or bridging effects mediated by yeast proteins (Brückner et al., 2009). Therefore, the results have to be confirmed using at least one other protein-protein interaction method.

Confirmation of the interaction between MpSPI PBW and MpLIP5 is ongoing work. So far, the interaction was not detectable by thorough testing using bimolecular fluorescence complementation (BiFC) assays (data not shown). Due to technical limitations and the presumably highly dynamic interaction in even only slightly moving granules, Förster resonance energy transfer-acceptor photobleaching (FRET-AP) proved to not be an appropriate method as it would lead to false positive results (L. Stephan, personal communication). Moreover, co-immunoprecipitation of bacterially expressed proteins, so far, was not successful due to various technical reasons (e.g. theoretically specific antibodies non-specifically detected proteins fused to tags of any kind and moreover, MpLIP5 was non-specifically bound by any protein tag). It was furthermore not yet possible to detect MpSPI-PBW in protein extracts of a stably transformed *Marchantia* line (line presented in 3.2.2, fig. 49) by immunoblotting using α -GFP-antibody (data not shown). However, transient expression of the proteins fused to different tags in *N. benthamiana*, subsequent protein extraction and co-immunoprecipitation are still promising experiments in order to confirm the interaction of MpSPIRRIG and MpLIP5.

4.2.3.3 MpSPIRRIG has a function in *Marchantia* salt stress response and localizes to P-bodies

Atspirrig exhibits a salt hypersensitivity phenotype manifested in decreased primary root growth, strong cotyledon whitening and restricted overall growth under transpiring conditions when subjected to high salt concentrations (Steffens et al., 2015). This work demonstrated a salt hypersensitivity phenotype of *Mpspirrig* as well, since not only rhizoid length was significantly reduced, but also the overall *Mpspirrig* fresh weight was significantly lower compared to wild type plants after several days of growth on medium supplemented with NaCl (3.2.5.2). The results thus strongly point to SPIRRIG being biologically relevant for salt stress response in *Marchantia*. Since in *Arabidopsis*, the salt hypersensitivity phenotype of *Atspirrig* was connected to a role of AtSPIRRIG in regulating salt stress-related mRNA stability at P-bodies, a potential association of MpSPIRRIG with P-bodies was investigated in this work.

Subcellular localization analysis revealed strong and clear co-localization of MpSPI PBW with the P-body component MpDCP2 (3.2.5.3). Yeast two-hybrid assays however revealed no interaction between MpSPI PBW and MpDCP1 (3.2.5.6). Interestingly, MpDCP1 was found to interact with *Arabidopsis* SPI probably indicating MpDCP1 to be strongly conserved to AtDCP1. Subsequent alignment analysis revealed approximated 56% identity on the protein level (Clustal Omega). Nevertheless, as mentioned before, the nature of yeast two-hybrid assays does not allow the conclusion of definitive absence of an interaction between MpSPIRRIG and P-body components without confirmation in another, alternative protein-protein interaction method.

4.2.3.4 Processes relevant to ESCRT trafficking and mRNP granules might be associated in Marchantia

Subcellular localization analysis revealed strong and clear, granular co-localization of MpSPI PBW with P-body (MpDCP2) and ESCRT (MpSKD1 and MpLIP5) components. Even though co-localization was assessed qualitatively, the analysis allowed the observation that strikingly, fluorescent signals overlapped in a nearly complete manner. The result prompted successive investigations.

Due to the strong overlap of P-body and ESCRT components with SPIRRIG-labeled granules, it was asked if P-body and ESCRT components might locate to identical cytoplasmic foci independently from SPIRRIG (3.2.5.3). Recent studies in *A. thaliana* already demonstrated AtSKD1 and other ESCRTIII-associated proteins to partially associate with stress granules and P-bodies especially under stress conditions (Wolff, 2018). The molecular function behind co-localization of components of these assumingly unrelated pathways has not been elucidated yet. However, it was postulated that sequestration of SKD1 to mRNP granules could be an indirect mechanism to temporarily block ESCRT trafficking (Wolff, 2018). This study investigated transient co-expression of MpSKD1 or MpLIP5 with MpDCP2 in cells of *M. polymorpha*. The analysis indeed showed partial co-localization of the ESCRT members with the P-body component (Fig. 65) indicating that also in *M. polymorpha*, processes relevant to ESCRT trafficking in connection to mRNP granules might be somewhat associated.

4.2.4 Are mRNP granules continuously present in cells of *M. polymorpha*?

The salt hypersensitivity phenotype of *Mpspirrig* already demonstrated potential relevance of MpSPIRRIG to Marchantia salt stress response. Co-localization of MpSPI PBW with MpDCP2 further points to an association of MpSPIRRIG with P-bodies, similar to *A. thaliana*. In Arabidopsis, the salt stress-related connection of AtSPIRRIG to P-bodies was emphasized by demonstrating cytoplasmically localized, evenly distributed AtSPI to relocate to DCP1-labeled P-bodies only upon salt treatment.

In Marchantia, the situation however is strikingly different. MpSPI PBW localizes to cytoplasmic foci already under non-stress conditions. This study proved that this localization behavior is not affected by the position of the fluorescent tag, the method of transformation or the cellular environment in *M. polymorpha*, but instead is induced by the protein as such (3.2.2). Furthermore, salt treatment did not affect the number of granules and did not alter MpSPI PBW localization whether MpDCP2 was co-expressed or not (3.2.5.5).

The result raised the question if stress-induced subcellular localization changes generally occur in Marchantia. Towards this, the Arabidopsis stress granule marker UBP1b was transiently expressed and observed under non-stress and stress conditions. Surprisingly and unlike in Arabidopsis, also UBP1b localized to cytoplasmic dots already under non-stress

conditions. Qualitative assessment of UBP1b localization upon salt treatment suggests that the stress stimulus did not extensively influence UBP1b localization and granule number.

The here presented findings open up a lot of fundamental questions concerning stress responses in *Marchantia*. The results convey the highly speculative impression that mRNP granules are continually present in cells of *M. polymorpha*, irrespective of stress. Furthermore, it seems that stress-induced recruitment mechanisms to mRNP granules might not be present in *M. polymorpha* and potentially evolved at later stages during land plant development. This study so far is unprecedented in the *Marchantia* community as there are no other reports on the identification of P-bodies or stress granule components and mRNP granule dynamics in *Marchantia* available yet. In order to develop any kinds of conclusions on subcellular, molecular stress responses in *Marchantia*, further studies are needed. Thorough investigation on the impacts of different kinds of stresses such as heat or hypoxia on a variance of stress marker proteins and mRNP granule components that are yet to be identified and isolated in *M. polymorpha*, would be required. It would moreover be highly interesting to investigate presence of protein domains promoting recruitment to mRNP granules, such as prion-like, intrinsically disordered regions (IDRs, Lin et al., 2015) in *M. polymorpha* compared to the evolutionarily younger land plant *A. thaliana*.

4.2.5 Outlook

This work aimed to identify the basal functions of SPIRRIG in the ancient land plant *M. polymorpha*. Through the characterization of the *Mpspirrig* mutant as well as co-localization and interaction studies, several exciting insights on SPIRRIG in *Marchantia* were gathered.

The strongly pronounced *Mpspirrig* phenotype, comprising more and smaller cells, is particularly interesting as it was not known from *Arabidopsis* before and thus depicts an excellent opportunity to unravel and describe new functions exerted by BDCPs. Towards this, an RNAseq approach was chosen. In the course of this work, RNA samples were prepared and thereafter processed at the Cologne Center of Genomics (Illumina TruSeq). Subsequent data analysis performed by Dr. Markus Stetter (University of Cologne) is ongoing work and aims to identify differentially regulated genes somewhat connected to cell size regulation in *Mpspirrig* compared to wild type plants.

Importantly, the presented phenotypes yet refer to a single *Mpspirrig* mutant and certainly have to be confirmed in a second, independently generated mutant to ultimately prove phenotypes to be ascribed to the mutation in *MpSPIRRIG*. In the course of this study, a CRISPR/Cas9 mutagenesis by spore transformation using the *S. pyogenes* vector system, applicable to *M. polymorpha* (Sugano et al., 2014; Sugano et al., 2018), was prepared but not yet accomplished due to scarce spore production upon *Marchantia* crossings. Nevertheless, due to the fact that Honkanen et al. (2016) confirmed single-site insertion of the T-DNA and

Mpspirrig exhibits phenotypic overlap to *Atspirrig* (salt hypersensitivity) there is no substantial reason to expect phenotypes to not correlate with the mutation in *MpSPIRRIG*. An obvious alternative approach in order to support this would certainly be a rescue experiment. However, since *SPIRRIG* is an extraordinarily large gene, already full-length *AtSPIRRIG* was very hard, and so far, *AaSPIRRIG* even impossible to amplify (M. Jakoby, L. Stephan, personal communication). Accordingly, attempts to clone *MpSPIRRIG* failed in this work and a rescue experiment unfortunately cannot be conducted.

Co-localization and interaction studies strongly pointed to an association of *MpSPIRRIG* with the ESCRT trafficking pathway. Biological relevance of this association to *M. polymorpha* however has not been ascertained yet. Towards this, it would be highly interesting to investigate endosomal transport routes in *Mpspirrig*. As a defect in the endosomal transport route of soluble proteins to the lytic vacuole was detected in *Arabidopsis spirrig/lip5* double mutants, it would be especially appealing to analogously generate a mutant in *M. polymorpha*.

This study moreover indicated the function of *SPIRRIG* in salt stress response to be evolutionarily conserved and thus highlights the importance of BDCPs in stress responses to land plants. Similar to *Atspirrig*, *Mpspirrig* has a salt hypersensitivity phenotype. *MpSPI PBW* strongly co-localized with the P-body marker *MpDCP2* suggesting *MpSPIRRIG* to be connected to mRNA metabolism as well. Further studies however would be required to definitely link the role of *MpSPIRRIG* in salt stress response with functions in positive regulation of P-body formation and mRNA stability in the ancient plant *M. polymorpha*.

Finally, broader approaches to tackle *MpSPIRRIG* function would very well complement the presented studies. On that note, for example T-DNA screenings aiming to identify *MpSPIRRIG* suppressor proteins would be particularly feasible due to the general dominant, haploid gametophytic nature of *M. polymorpha*, as well as due to the easy-to-screen short rhizoid phenotype of *Mpspirrig*.

5 APPENDIX

Table 23: **Entry clones harboring *A. thaliana* genes/nucleic acids.** Primer pairs used to amplify nucleic acids of interest in this work are given. Entry clones were generated in BP reactions. The + indicates a clone with a stop codon, the - indicates a clone without stop codon. P=part.

| Nucleic acid | Gene ID | DONR | Clone ID | Primer pair used for amplification / origin |
|--|-----------|------|------------------------|---|
| Entry clones harboring the CDS of genes of interest | | | | |
| <i>MYB34</i> | AT5G60890 | 207 | EK064 (+) EK064 (-) | EP029 attB1 GGGGACAAGTTTGTACAAAAAAGCAGGCTCAATGGTGAGG ACACCATGTTGCAAAG EP030 attB2 GGGGACCACTTTGTACAAGAAAGCTGGGTATCMGACAAAG ACTCCAACCATATTGTC |
| <i>MYB51</i> | AT1G18570 | 207 | EK096 (+) EK092 (-) | EP052 attB1 GGGGACAAGTTTGTACAAAAAAGCAGGCTCAATGGTGCGG ACACCGTGTGCAAAG EP053 attB2 GGGGACCACTTTGTACAAGAAAGCTGGGTATCMTCCAAAAT AGTTATCAATTTCTGTC |
| <i>AT3G28140</i> | AT3G28140 | 207 | EK058 (-) | EP018 attB1 GGGGACAAGTTTGTACAAAAAAGCAGGCTCAATGTGCGCAAG GCTACGCAATCGAGC EP019 attB2 GGGGACCACTTTGTACAAGAAAGCTGGGTACTATCAAGATT CCAAATTGTTACCAAGA |
| TZF10, 11 and ABF3 entry clones harboring different UTR sequences | | | | |
| 5'UTR _{TZF11} +CDS _{TZF11} +3'UTR _{TZF11} | AT3G55980 | 201 | EK034 | EP008 attB1 GGGGACAAGTTTGTACAAAAAAGCAGGCTCACTCCTTCTTC ATTGCAAAGAA EP007 attB2 GGGGACCACTTTGTACAAGAAAGCTGGGTATACGGTTTGA TTGCTTAGCCATTCA |
| 5'UTR _{TZF10} (incl. intron) +CDS _{TZF10} +3'UTR _{TZF10} | AT2G40140 | 201 | AST666 | A. Steffens (<i>TZF10</i> 5'UTR contains intron sequence) |
| 5'UTR _{TZF10} +CDS _{TZF10} +3'UTR _{TZF10} | AT2G40140 | 201 | EK035 | Primer pair for site-directed mutagenesis on AST666 EP025 GTTATCTTCTTTTCTAGGAAGAGATATGTGCGGTGCAAAGA GC EP026 GCTCTTTCACCGCACATATCTCTTCTAGAAAAGAAGATAA C |
| CDS _{TZF11} +3'UTR _{TZF11} | AT3G55980 | 201 | EK021 | J1073 attB1 GGGGACAAGTTTGTACAAAAAAGCAGGCTCAATGTGCAGTG GACCAAAGAGCAATCTCTGC EP007 attB2 GGGGACCACTTTGTACAAGAAAGCTGGGTATACGGTTTGA TTGCTTAGCCATTCA |

| | | | | |
|---|------------------------|-----|------------|---|
| 3'UTR _{TZF11} | AT3G55980 | 207 | EK061 | EP033 attB1 GGGGACAAGTTTGTACAAAAAAGCAGGCTCAACACACACAA AGATGGTTTCTTATA EP007 attB2 GGGGACCACTTTGTACAAGAAAGCTGGGTATACGGTTTGGGA TTGCTTAGCCATTCA |
| 3'UTR _{TZF10} | AT2G40140 | 201 | AST664 | A. Steffens |
| 3'UTR _{ABF3} | AT4G34000 | 207 | EK153 | EP077 attB1 GGGGACAAGTTTGTACAAAAAAGCAGGCTCAAGCTTATAAT GGCGTCTAAGGAACC AP512 attB2 GGGGACCACTTTGTACAAGAAAGCTGGGTTTAACCGTTTGA AAGCATCTT |
| CDS _{ABF3+} 3'UTR _{ABF3} | AT4G34000 | 207 | EK032 | EP013 attB1 GGGGACAAGTTTGTACAAAAAAGCAGGCTCAATGGGGTCTA GATTAACTTCAAGA AP512 attB2 GGGGACCACTTTGTACAAGAAAGCTGGGTTTAACCGTTTGA AAGCATCTT |
| 3'UTR _{TZF10} (P1) | AT2G40140 | 207 | EK165 | AP0411 attB1 GGGGACAAGTTTGTACAAAAAAGCAGGCTTAGAAGCAGAAA GAAAGATGTG EP083 attB2 GGGGACCACTTTGTACAAGAAAGCTGGGTATCMCAAAGAAA AAAAGAACATAAAAAAA |
| 3'UTR _{TZF10} (P2) | AT2G40140 | 207 | EK166 | EP084 attB1 GGGGACAAGTTTGTACAAAAAAGCAGGCTCATCATTCTCTT GTCCTTCGTGACACT AP0410 attB2 GGGGACCACTTTGTACAAGAAAGCTGGGTTCCCCAAAATCT CTTAGGCC |
| 3'UTR _{TZF11} (P1) | AT3G55980 | 207 | EK167 | EP033 attB1 GGGGACAAGTTTGTACAAAAAAGCAGGCTCAACACACACAA AGATGGTTTCTTATA EP081 attB2 GGGGACCACTTTGTACAAGAAAGCTGGGTATCMATACTACT AATAACAGTAACAATA |
| 3'UTR _{TZF11} (P2) | AT3G55980 | 207 | EK168 | EP082 attB1 GGGGACAAGTTTGTACAAAAAAGCAGGCTCAATGGTTTGT GTCACTACGAGTCTA EP007 attB2 GGGGACCACTTTGTACAAGAAAGCTGGGTATACGGTTTGGGA TTGCTTAGCCATTCA |
| CDS _{TZF10} +3'UTR _{35SCaMV} | AT2G40140 | 201 | MJ1172 (+) | M. Jakoby |
| CDS _{TZF10} +3'UTR _{TZF10} | AT2G40140 | 201 | AST664 | A. Steffens |
| CDS _{TZF11} +3'UTR _{35SCaMV} | AT3G55980 | 201 | MJ1173 (+) | M. Jakoby |
| 5'UTR _{TZF10} +CDS _{ABF3} | AT2G40140 AT4G34000 | 207 | AST1338 | A. Steffens |

| | | | | |
|---|------------------------|-----|---------|--|
| +3'UTR _{ABF3} | | | | |
| 5'UTR _{ABF3} +CDS _{TZF10} +3'UTR _{TZF10} | AT2G40140 AT4G34000 | 207 | AST1339 | A. Steffens |
| 5'UTR _{ABF3} +CDS _{ABF3} +3'UTR _{TZF10} | AT2G40140 AT4G34000 | 207 | AST1340 | A. Steffens |
| CDS _{ABF3} +3'UTR _{TZF10} | AT2G40140 AT4G34000 | 207 | EK030 | EP013 attB1 GGGGACAAGTTTGTACAAAAAAGCAGGCTCAATGGGGTCTA GATTAAACTTCAAGA AP0410 attB2 GGGGACCACTTTGTACAAGAAAGCTGGGTTCCCAAAATCT CTTAGGCC |
| CDS _{TZF10} +3'UTR _{ABF3} | AT2G40140 AT4G34000 | 207 | EK031 | J1069 attB1 GGGGACAAGTTTGTACAAAAAAGCAGGCTCAATGTGCGGT GCAAAGAGCAACCTTTG AP512 attB2 GGGGACCACTTTGTACAAGAAAGCTGGGTTTAACCGTTTGA AAGCATCTT |
| 5'UTR _{TZF10} +CDS _{TZF10} +3'UTR _{ABF3} | AT2G40140 AT4G34000 | 207 | EK051 | Primer pairs for overlapping PCRs on EK035 and AST1338 AP0412 attB1 GGGGACAAGTTTGTACAAAAAAGCAGGCTTAGACGAAAGAA AGAGCGTACC J1070 attB2 GGGGACCACTTTGTACAAGAAAGCTGGGTATCMTGCCACA ATCTGCTGCTCATGGTCTATA AP0527 F CAGCAGATTGTGGCATAAAGCTTATAATGGCGTCTA AP512 attB2 GGGGACCACTTTGTACAAGAAAGCTGGGTTTAACCGTTTGA AAGCATCTT |

Table 24: **Expression clones harboring *A. thaliana* genes/nucleic acids.** Expression clones were generated with respective entry clones (Table 23) in LR reactions. *These constructs were generated by LR reactions in EK016, EK017, EK045, respectively, in which 5'UTR sequences were integrated upstream of *YFP* using a *XhoI/SalI* restriction digest. Primers, with which 5'UTRs including restriction sites were amplified, are given.

| Gene/Nucleic acid | Plasmid | Clone ID | Reference/Origin |
|---|------------|----------|------------------|
| Expression clones harboring the CDS of genes of interest | | | |
| <i>UBP1b</i> | pAMARENA | EK077 | A. Steffens |
| | pENSG-CFP | EK078 | A. Steffens |
| <i>DCP1</i> | pAUBERGINE | AST248 | A. Steffens |
| <i>SKL</i> | pENSG-CFP | MJ1417 | M. Jakoby |
| <i>SPIRRIG</i> | pACT | AST169 | A. Steffens |
| | pAS | AST177 | A. Steffens |
| <i>AT3G28140</i> | pEXSG-YFP | EK067 | This study |
| <i>MYB51</i> | pENSG-YFP | EK099 | This study |
| <i>MYB34</i> | pENSG-YFP | EK074 | This study |
| <i>TZF10</i> | pENSG-YFP | AST1274 | A. Steffens |
| | pAMARENA | AST1078 | A. Steffens |

| | | | |
|---|-----------------|---------|---|
| | pSCJ232 | AST1285 | A. Steffens |
| | pAS | L106 | L. Stephan |
| <i>TZF11</i> | pAS | L107 | L. Stephan |
| <i>TZF10, 11</i> and <i>ABF3</i> expression clones harboring different UTR sequences | | | |
| 5'UTR _{<i>TZF10</i>} + CDS _{<i>TZF10</i>} + 3'UTR _{<i>TZF10</i>} | pSCJ232 | AST1285 | A. Steffens |
| CDS _{<i>TZF10</i>} + 3'UTR _{<i>TZF10</i>} | pSCJ232 | EK145 | This study |
| CDS _{<i>TZF10</i>} + 3'UTR _{OCS} | pSCJ232 | EK148 | This study |
| CDS _{<i>TZF11</i>} + 3'UTR _{<i>TZF11</i>} | pSCJ232 | EK147 | This study |
| CDS _{<i>TZF11</i>} + 3'UTR _{OCS} | pSCJ232 | EK151 | This study |
| 3'UTR _{<i>TZF10</i>} | pSCJ232 | EK174 | This study |
| 3'UTR _{<i>TZF10</i>} (P1) | pSCJ232 | EK170 | This study |
| 3'UTR _{<i>TZF10</i>} (P2) | pSCJ232 | EK171 | This study |
| 3'UTR _{<i>TZF10</i>} (P1) | UBQ pENSG-YFP | EK175 | This study |
| 3'UTR _{<i>TZF10</i>} (P2) | UBQ pENSG-YFP | EK176 | This study |
| 3'UTR _{<i>TZF11</i>} (P1) | UBQ pENSG-YFP | EK177 | This study |
| 3'UTR _{<i>TZF11</i>} (P2) | UBQ pENSG-YFP | EK178 | This study |
| 3'UTR _{<i>TZF10</i>} (P1-1) | UBQ pENSG-YFP | EK184 | This study |
| 3'UTR _{<i>TZF10</i>} (P1-2) | UBQ pENSG-YFP | EK181 | This study |
| 3'UTR _{<i>TZF11</i>} (P1-1) | UBQ pENSG-YFP | EK182 | This study |
| 3'UTR _{<i>TZF11</i>} (P1-2) | UBQ pENSG-YFP | EK183 | This study |
| 3'UTR _{<i>TZF10</i>} (P1-1-1) | UBQ pENSG-YFP | EK185 | This study |
| 3'UTR _{<i>TZF10</i>} (P1-1-2) | UBQ pENSG-YFP | EK186 | This study |
| 3'UTR _{<i>TZF10</i>} (P1-1-C) | UBQ pENSG-YFP | EK187 | This study |
| 3'UTR _{<i>TZF11</i>} (P1-1-1) | UBQ pENSG-YFP | EK188 | This study |
| 3'UTR _{<i>TZF11</i>} (P1-1-C) | UBQ pENSG-YFP | EK189 | This study |
| 3'UTR _{<i>TZF10</i>} (P1-1-C) MUT1 | UBQ pENSG-YFP | EK190 | This study |
| 3'UTR _{<i>TZF10</i>} (P1-1-C) MUT2 | UBQ pENSG-YFP | EK191 | This study |
| 3'UTR _{<i>ABF3</i>} MUT | UBQ pENSG-YFP | EK192 | This study |
| 3'UTR _{<i>TZF10</i>} | UBQ pENSG-YFP | EK143 | This study |
| 3'UTR _{<i>TZF11</i>} | UBQ pENSG-YFP | EK076 | This study |
| 5'UTR _{<i>TZF10</i>} -YFP-GW | UBQ pENSG-YFP | EK016 | EP001 F CCCCCTCGAGGACGAAAGAAAGAGCGTA EP002 R CCCCGTCGACATCTCTTCTAGAAAAGA |
| 5'UTR _{<i>TZF11</i>} -YFP-GW | UBQ pENSG-YFP | EK045 | EP009 F CCCCCTCGAGCTCCTTCTTATTGCAAA EP010 R CCCCGTCGACAATACTATCTGGAATGA |
| 5'UTR _{<i>ABF3</i>} -YFP-GW | UBQ pENSG-YFP | EK017 | EP011 F CCCCCTCGAGGGTTTGTGAATCGATTT EP012 R CCCCGTCGACTACTCAAGCTTTCGTACA |
| 5'UTR _{<i>TZF10</i>} +CDS _{<i>TZF10</i>} +3'UTR _{<i>TZF10</i>} | UBQ pAM-PAT | EK042 | This study |
| | UBQ pENSG-YFP * | EK018 | This study |
| CDS _{<i>TZF10</i>} +3'UTR _{35SCaMV} | UBQ pAM-PAT | EK003 | This study |
| | UBQ pENSG-YFP | AST1022 | A. Steffens |
| CDS _{<i>TZF10</i>} +3'UTR _{<i>TZF10</i>} | UBQ pAM-PAT | EK004 | This study |
| | UBQ pENSG-YFP | AST1300 | A. Steffens |
| 5'UTR _{<i>TZF11</i>} +CDS _{<i>TZF11</i>} +3'UTR _{<i>TZF11</i>} | UBQ pAM-PAT | EK043 | This study |

| | | | |
|---|-----------------|---------|-------------|
| | UBQ pENSG-YFP * | EK057 | This study |
| CDS _{TZF11} +3'UTR _{35SCaMV} | UBQ pAM-PAT | EK044 | This study |
| | UBQ pENSG-YFP | AST1014 | A. Steffens |
| CDS _{TZF11} +3'UTR _{TZF11} | UBQ pAM-PAT | EK053 | This study |
| | UBQ pENSG-YFP | EK046 | This study |
| 5'UTR _{TZF10} +CDS _{ABF3} +3'UTR _{ABF3} | UBQ pAM-PAT | EK005 | This study |
| | UBQ pENSG-YFP * | EK055 | This study |
| 5'UTR _{ABF3} +CDS _{ABF3} +3'UTR _{TZF10} | UBQ pAM-PAT | EK007 | This study |
| | UBQ pENSG-YFP * | EK052 | This study |
| 5'UTR _{ABF3} +CDS _{TZF10} +3'UTR _{TZF10} | UBQ pAM-PAT | EK006 | This study |
| | UBQ pENSG-YFP * | EK019 | This study |
| 5'UTR _{TZF10} +CDS _{TZF10} +3'UTR _{ABF3} | UBQ pAM-PAT | EK056 | This study |
| | UBQ pENSG-YFP * | EK047 | This study |

Table 25: Entry clones harboring *M. polymorpha* genes generated in this work.

| Gene | Gene ID | DONR | Clone ID | Primer pair used for amplification |
|-----------------------|-----------|------|------------------------|--|
| MpSPI PBW | Mp2g15800 | 201 | EK204 (-) EK206 (+) | EP160 attB1 GGGGACAAGTTTGTACAAAAAAGCAGGCTCAATGGTACCCG GCGAGAAGATTAG EP149 attB2 GGGGACCACTTTGTACAAGAAAGCTGGGTATCMCGAGCAT GACTCCAACGGGC |
| MpSPI PBWF | Mp2g15800 | 201 | EK205 (+) | EP160 attB1 GGGGACAAGTTTGTACAAAAAAGCAGGCTCAATGGTACCCG GCGAGAAGATTAG EP150 attB2 GGGGACCACTTTGTACAAGAAAGCTGGGTATCMGGATTTTC TAGAGTCAAAGC |
| MpDCP2 | Mp8g16420 | 201 | EK256 (+) EK215 (-) | EP168 attB1 GGGGACAAGTTTGTACAAAAAAGCAGGCTCAATGTCCGGCA ACGCGCGTGC EP169 attB2 GGGGACCACTTTGTACAAGAAAGCTGGGTATCMGACTTCCA ACTTTTGTATTATGCTT |
| MpDCP1 | Mp1g25660 | 201 | EK275 (+) EK218 (-) | EP166 attB1 GGGGACAAGTTTGTACAAAAAAGCAGGCTCAATGGCACAAA ATGGCAAGCCGATGC EP167 attB2 GGGGACCACTTTGTACAAGAAAGCTGGGTATCMTGTTGAAT GTGCATTGAGCATCTCC |
| MpLIP5 | Mp1g06880 | 201 | EK226 (+) EK216 (-) | EP162 attB1 GGGGACAAGTTTGTACAAAAAAGCAGGCTCAATGGGGGAG ACTGCGGATCCGAAGA EP163 attB2 GGGGACCACTTTGTACAAGAAAGCTGGGTATCMGTGAGCT TGTGATGAAGAAGAGGTC |
| MpSKD1 | Mp8g01610 | 201 | EK217 (+) EK227 (-) | EP164 attB1 GGGGACAAGTTTGTACAAAAAAGCAGGCTCAATGTACAGCA ATTTCAAGGA |

| | | | | |
|---------------|-----------|-----|------------|--|
| | | | | EP165 attB2 GGGGACCACTTTGTACAAGAAAGCTGGGTATCMACCCTCCT CACCAAATTCAC |
| MpARA6 | Mp8g00450 | 201 | EK 224 (-) | EP172 attB1 GGGGACAAGTTTGTACAAAAAAGCAGGCTCAATGGGTTGTG CTGCCTCAGC EP173 attB2 GGGGACCACTTTGTACAAGAAAGCTGGGTATCMAGGCTTCT GGGTTGGCTGTC |
| MpRAB5 | Mp1g08940 | 201 | EK 246 (+) | EP174 attB1 GGGGACAAGTTTGTACAAAAAAGCAGGCTCAATGGCCACC GCGGGAACGAA EP175 attB2 GGGGACCACTTTGTACAAGAAAGCTGGGTATCMGACGCAG CACATGCTTGATT |

Table 26: **Expression clones harboring *M. polymorpha* genes.** The clones were generated in LR reactions with respective entry clones (Table 25).

| Gene | Plasmid | Clone ID | Reference/Origin |
|-------------------|------------|----------|-------------------------------------|
| MpSPI PBW | pEXSG-CFP | EK211 | This study |
| | pENSG-CFP | EK318 | This study |
| | pAS | EK236 | This study |
| | pACT | EK242 | This study |
| | pMpGWB406 | EK257 | This study |
| MpSPI PBWF | pENSG-CFP | EK213 | This study |
| | pAS | EK237 | This study |
| | pACT | EK243 | This study |
| MpDCP2 | pAUBERGINE | EK219 | This study |
| | pEXSG-YFP | EK230 | This study; Westermann et al., 2020 |
| | pMpGWB335 | EK266 | This study |
| MpDCP1 | pEXSG-YFP | EK228 | This study; Westermann et al., 2020 |
| | pAS | EK233 | This study |
| | pACT | EK239 | This study |
| MpLIP5 | pEXSG-YFP | EK220 | This study |
| | pMpGWB335 | EK316 | This study |
| | pAS | EK232 | This study |
| | pACT | EK238 | This study |
| MpSKD1 | pAMARENA | EK222 | This study |
| | pMpGWB335 | EK270 | This study |
| | pAS | EK235 | This study |
| | pACT | EK241 | This study |
| MpARA6 | pEXSG YFP | EK250 | This study; Westermann et al., 2020 |
| | pAUBERGINE | EK251 | This study |
| MpRAB5 | pAMARENA | EK255 | This study; Westermann et al., 2020 |

Table 27: **Genotyping-primer for *A. thaliana* T-DNA insertion lines.** The table gives the sequences for T-DNA left border primers and for primer pairs used to amplify wild type alleles in respective T-DNA mutants.

| SIGnAL SALK Identifier(s) | Primer ID | Sequence | Origin/Reference |
|---------------------------|------------------|--|----------------------------|
| SALK | LBa1 | T-DNA left border primer TGGTTCACGTAGTGGGCCATCG | signal.salk.edu |
| SAIL | LB1 | T-DNA left border primer GCCTTTTCAGAAATGGATAAATAGCCTTGCTTCC | signal.salk.edu |
| GABI-Kat (GK) | o8409 | T-DNA left border primer ATATTGACCATCATACTCATTGC | Kleinboelting et al., 2012 |
| GK_158E10 | AP0419 AP0541 | F CCGTTTAGCAGCTTGGAGATGATGCC R GAAGCTCATTGAGGTGGCGTTG | A. Steffens |
| SALK_024800 | EP004 J1069 | F ATGATCCCAGCGTCAAAGGA R GGGGACAAGTTTGTACAAAAAGCAGGCTCAATGTGCGGTGCAAAGAGCAACCTTTG | This study/ M. Jakoby |
| SALK_141550 | J1596 AP0239 | F CCACCACAACACAATCCCCTTG R TGTTAAGGTTCTTGAAGAGCAGAG | M. Jakoby/ A. Steffens |
| SAIL_207G08 | AP0388 AP0410 | F TGTCTCCGATTGGGGATCACCAATG R GGGGACCACTTTGTACAAGAAAGCTGGGTTCCCAAAATCTCTTAGGCC | A. Steffens |
| SAIL_191G05 | AP0419 AP0541 | F CCGTTTAGCAGCTTGGAGATGATGCC R GAAGCTCATTGAGGTGGCGTTG | A. Steffens |
| GK_420D09 | J1130 J1131 | F CCGGTTGTTGCACTTGCATCCTGGCTAGGCTCC R CATCAGTAGCTGGATTCGGAGATGGCCTCTCT | M. Jakoby |
| SALK_065311 | J1586 J1585 | F GCAGCACAAGCTTCTTATTGG R CGTCATGATGGACCTAGTTGG | M. Jakoby |

Table 28: **Genotyping-primer pairs for *M. polymorpha*.**

| Primer ID | Gene | Purpose | Sequence | Origin/Reference |
|---------------------|----------------|---|--|--------------------------------------|
| JW45 JW46 | <i>rbm27</i> | Male-specific primer pair, sex determination | F CCAAGTGCGGGCAGAATCAAGT R TTCATCGCCCGCTATCACCTTC | J. Westermann, Fujisawa et al., 2001 |
| JW47 JW48 | <i>rhf73</i> | Female-specific primer pair, sex determination | F TGACGACGAAGATGTGGATGAC R GAAACTTGGCCGTGTGACTGA | J. Westermann, Fujisawa et al., 2001 |
| JW61 (LB1) EP145 | <i>spirrig</i> | Genotyping <i>Mpspirrig</i> (<i>Mpspi-2</i> , ST17-11) | F CAGATAAGGGAATTAGGGTTCCTATAGG R CGAGCCGACTTACCCCTAAT | J. Westermann, this study |

Table 29: **Primer pairs used for qPCR analysis.**

| Primer ID | Gene | Gene ID | Sequence | Origin/Reference |
|------------------|---|-----------|--|----------------------------|
| AP0344 AP0345 | 18S rRNA | AT3G41768 | F AAACGGCTACCACATCCAAG R GACTCGAAAGAGCCCGGTAT | Steffens et al., 2015 |
| AP0110 AP0111 | <i>RD29A</i> | AT5G52310 | F CCGATAACGTTGGAGGAAGAGTCG R TTTCCAGCTCAGCTCCTGACTCGTCACC | A. Steffens |
| AP0236 AP0237 | <i>TZF10</i> | AT2G40140 | F CATGGTTCCGGTTATGGAAGAA R TGCATCAGCTGGATACTTAGTCA | A. Steffens |
| EP095 EP096 | <i>TZF10</i> (construct in transgenic lines, 3.1.6) | AT2G40140 | F CTGCAGCCATCACAAAGTTT R TCCGTCTTCTGATTTCTGCCT | This study |
| EP131 EP132 | <i>TZF11</i> | AT3G55980 | F CGGTGAGACAACCGCATCT R TCGACTGTGGTGCTGCTTGA | This study |
| EP154 EP155 | Mp <i>SPIRRIG</i> | Mp2g15880 | F AGTGGAGACGGTGCAGGACA R GCACGACGAGCATGACTCCA | This study |
| EP156 EP157 | Mp <i>APT3</i> | Mp3g25140 | F CGAAAGCCCAAGAAGCTACC R GTACCCCGGTTGCAATAAG | Saint-Marcoux et al., 2015 |
| EP158 EP159 | Mp <i>ACT7</i> | Mp6g11010 | F AGGCATCTGGTATCCACGAG R ACATGGTCTTCTCCAGAC | Saint-Marcoux et al., 2015 |
| EP046 EP047 | <i>MYB34</i> | AT5G60890 | F CACGACTGTGCATAATTTGGGTT R CATATTGTCATCTTCTGTTCCAGGA | Frerigmann et al., 2016 |
| EP048 | <i>MYB51</i> | AT1G18570 | F CTACAAGTGTTCGGTTGACTCTGAA | Frerigmann et al., 2016 |

| | | | | |
|--------------|----------------|-----------|--------------------------------------|-------------------------|
| EP049 | | | R ACGAAATTATCGCAGTACATTAGAGGA | |
| EP050 | <i>MYB122</i> | AT1G18570 | F ACCTCTTCGAATCTCCCATC | Frerigmann et al., 2016 |
| EP051 | | | R AACTTCATTGATCGGCGTCAC | |
| EP042 | <i>CYP79B2</i> | AT4G39950 | F AACAAAAAGAACCCTATCTGCCAC | Frerigmann et al., 2016 |
| EP043 | | | R TCCTAACTTCACGCATGCTATCTC | |
| EP044 | <i>CYP79B3</i> | AT2G22330 | F CTCCTTCTTCTTGCAAATGGA | Frerigmann et al., 2016 |
| EP045 | | | R GAGAATCATCAAGAAGCAAAGGG | |
| EP040 | <i>PP2A</i> | AT1G69960 | F CAAGAGTTCCACACGAAGGA | Frerigmann et al., 2016 |
| EP041 | | | R TGTAACCAGCACCACGAGGA | |

Table 30: Other primer pairs used in this work.

| Primer ID | Gene | Gene ID | Purpose | Sequence | Origin/Reference |
|--------------------------------|--|-----------|---|---|----------------------------|
| ANS167 ANS168 | <i>EF1α</i> | AT5G60390 | cDNA testing | F ATGCCCCAGGACATCGTGATTCAT R TTGGCGGCACCCTTAGCTGGATCA | A. Schrader |
| AP0388 J611 | <i>TZF10</i> (construct in transgenic lines, 3.1.6) | AT2G40140 | Genotyping | F TGTCTCCGATTGGGGATCACCAAATG R GGGGACCACTTTGTACAAGAAAGCTGGGT | A. Steffens / M. Jakoby |
| EP101 EP102 | <i>CFP</i> | | Amplification of CFP with BbsI recognition sites | attB1 GGGGACAAGTTTGTACAAAAAGCAGGCT CAGGGTCTTCATGGTGAGCAAGGGCGAGGA attB2 GGGGACCACTTTGTACAAGAAAGCTGGGT ACTAAGTCTTCTTACTTGTACAGCTCGTCCA | This study |
| AD5XXL | | | Yeast colony PCR, 5'end | GGACGGACCAAAGTGCATATAACGCG TTTGAATCACTACAGGGATG | |
| AD3XL | | | Yeast colony PCR, 3'end | GCGACCTCATGTATACCTGAGAAA GCAACCTGACCTACAGGAAAGAG | |
| SeIA | | | Sequencing | TCGCGTTAACGCTAGCATGGATCTC | |
| SeIB | | | Sequencing | GTAACATCAGAGATTTTGAGACAC | |
| EP186 EP187 | <i>MpSPIRRIG</i> | Mp2g15800 | Spanning the T-DNA insertion site in <i>Mpspirrig</i> | F TGAGGGCAGCGTCTTCTTTA R TATCTCCGCAAGCAAGTCCA | This study |

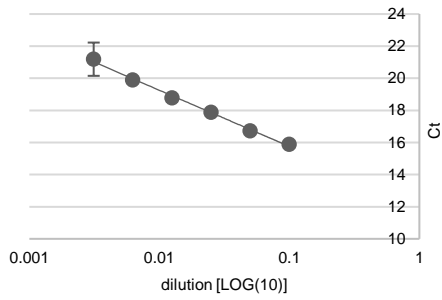
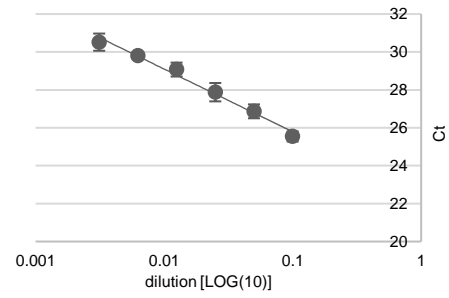
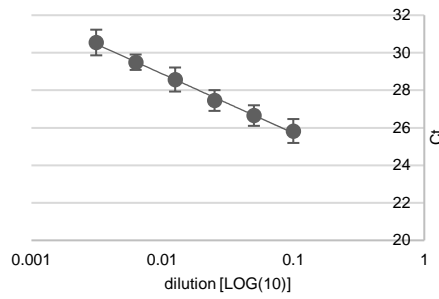
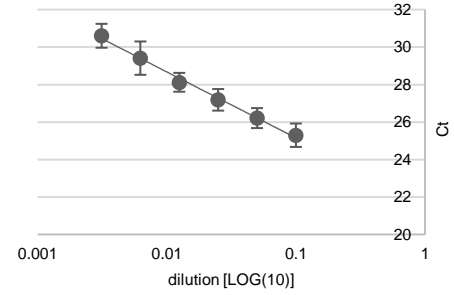
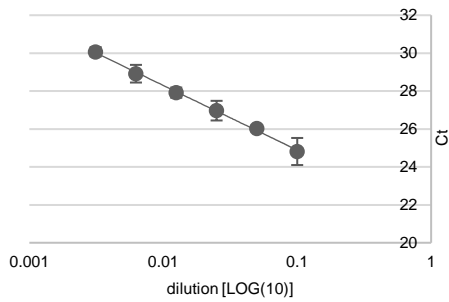
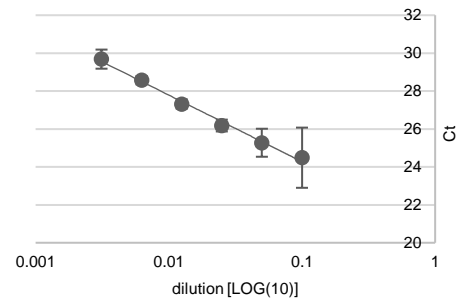
A 18S rRNA (ID: AP0344+0345)**B** MpSPIRRIG (ID:EP154+155)**C** TZF10 (ID: AP0236+0237)**D** TZF10 (ID: EP096+095)**E** TZF11 (ID: EP131+132)**F** RD29A (ID: AP0110+0111)

Figure 72: qPCR efficiency test standard curves of primer pairs used in this study. Ct values were determined in two technical and three biological replicates. Error bars represent standard deviation.

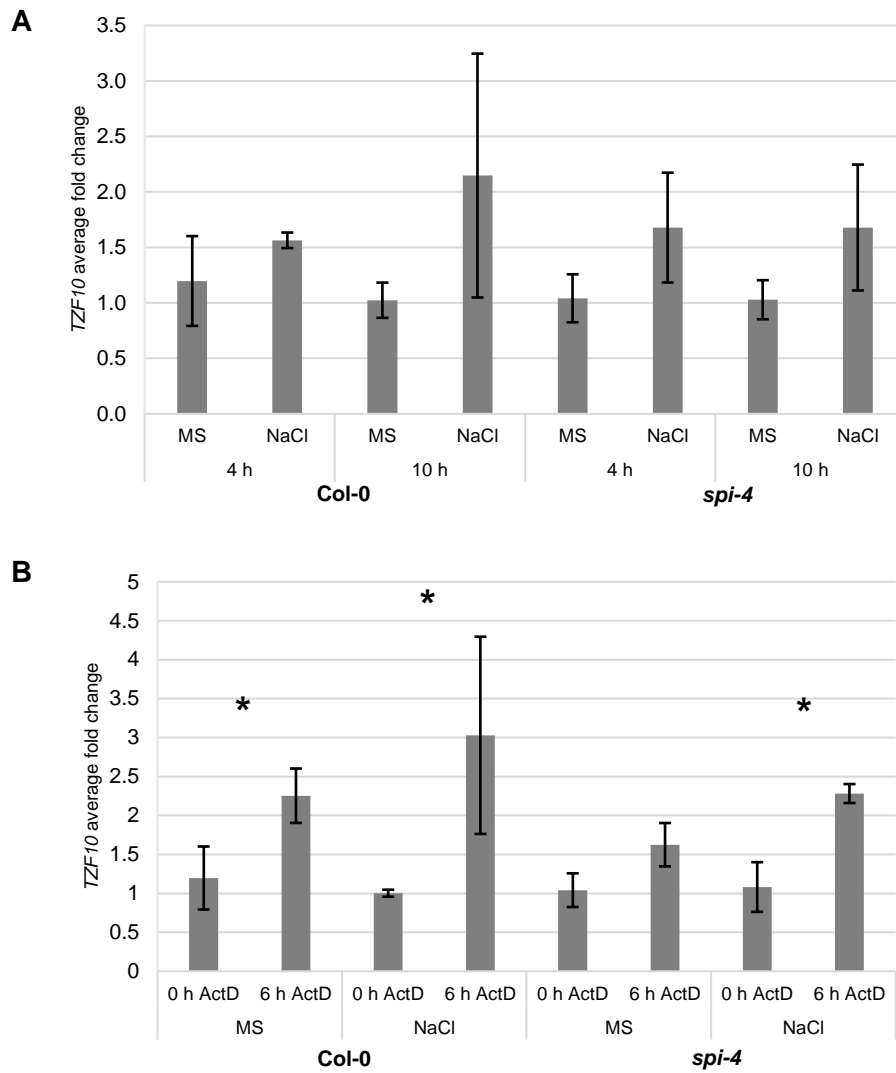


Figure 73: ***TZF10* expression levels.** The effect of salt treatment (**A**) and transcriptional block induced by ActD (**B**) was tested in *Col-0* and *spi-4*. **A** Relative expression of *TZF10* in samples incubated in liquid $\frac{1}{2}$ MS containing 125 mM NaCl compared to control samples incubated in liquid $\frac{1}{2}$ MS only for designated time periods, normalized to reference gene 18S rRNA. $n=3$. **B** Relative expression of *TZF10* in samples incubated in liquid $\frac{1}{2}$ MS with or without 150 mM NaCl and treated with 150 μ g/ml ActD for designated time periods compared to respective control samples, normalized to reference gene 18S rRNA. $n=3$. Error bars indicate the standard error. Significance, indicated by the asterisk, was tested with a Mann-Whitney-U test ($p<0.10$).

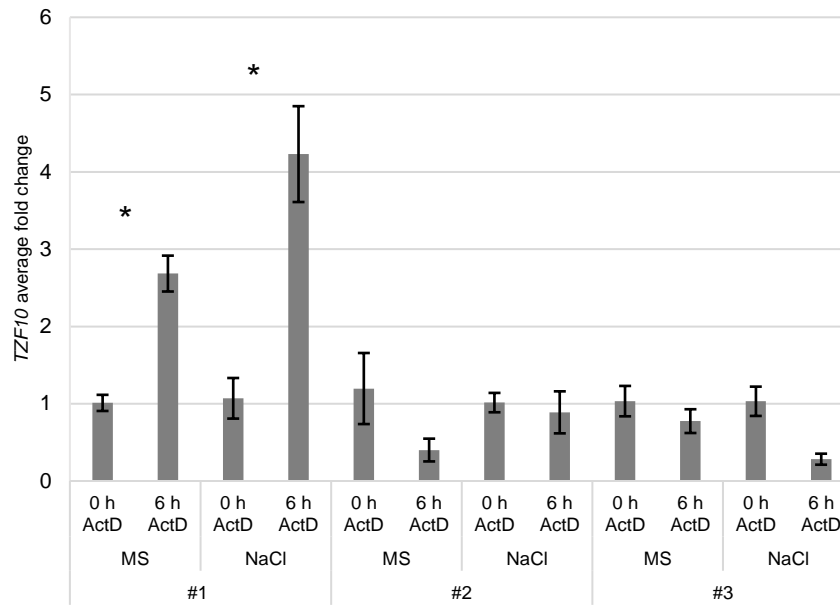
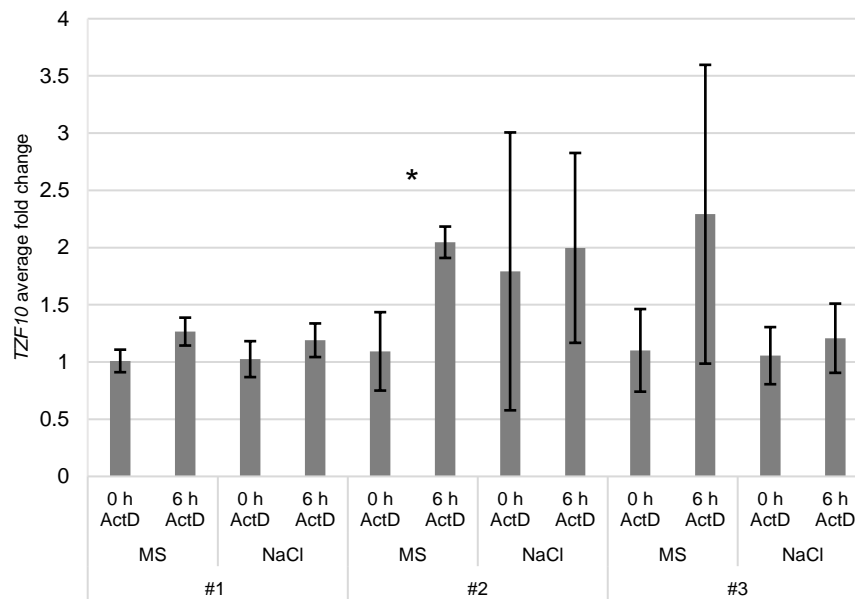
A #1-3 *TZF10* CDS in *spi-4***B #1-3 *TZF10* CDS+3'UTR in *spi-4***

Figure 74: **The effect of ActD on *TZF10* expression in different transgenic lines.** The effect of transcriptional block induced by ActD is displayed by relative expression of *TZF10* in three different transgenic *spi-4* lines either transformed with the *TZF10* CDS (A) or the *TZF10* CDS+3'UTR (B). Samples were incubated in liquid ½ MS with or without 125 mM NaCl and treated with 150 µg/ml ActD for designated time periods, compared to control samples incubated in liquid ½ MS with or without 125 mM NaCl only, and normalized to reference gene 18S rRNA. $n=3$. Error bars indicate the standard error. Significance was tested with a Mann-Whitney-U test ($p < 0.10$).

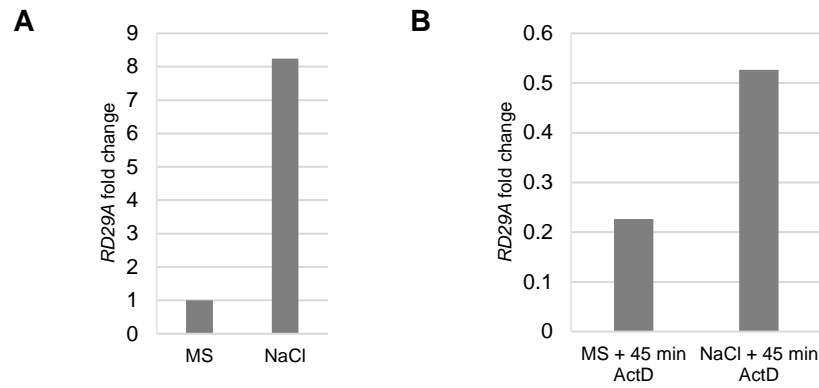


Figure 75: **RD29A expression levels.** The effect of salt treatment (**A**) and transcriptional block induced by ActD (**B**) was exemplarily tested in single Col-0 replicates. **A** Relative expression of *RD29A* in samples incubated in liquid $\frac{1}{2}$ MS containing 200 mM NaCl for 90 min, compared to control samples incubated in liquid $\frac{1}{2}$ MS only, normalized to reference gene 18S rRNA. $n=1$. **B** Relative expression of *RD29A* in samples incubated in liquid $\frac{1}{2}$ MS with or without 200 mM NaCl for 90 min and treated with 150 μ g/ml ActD for 45 min compared to respective control samples, normalized to reference gene 18S rRNA. $n=1$.

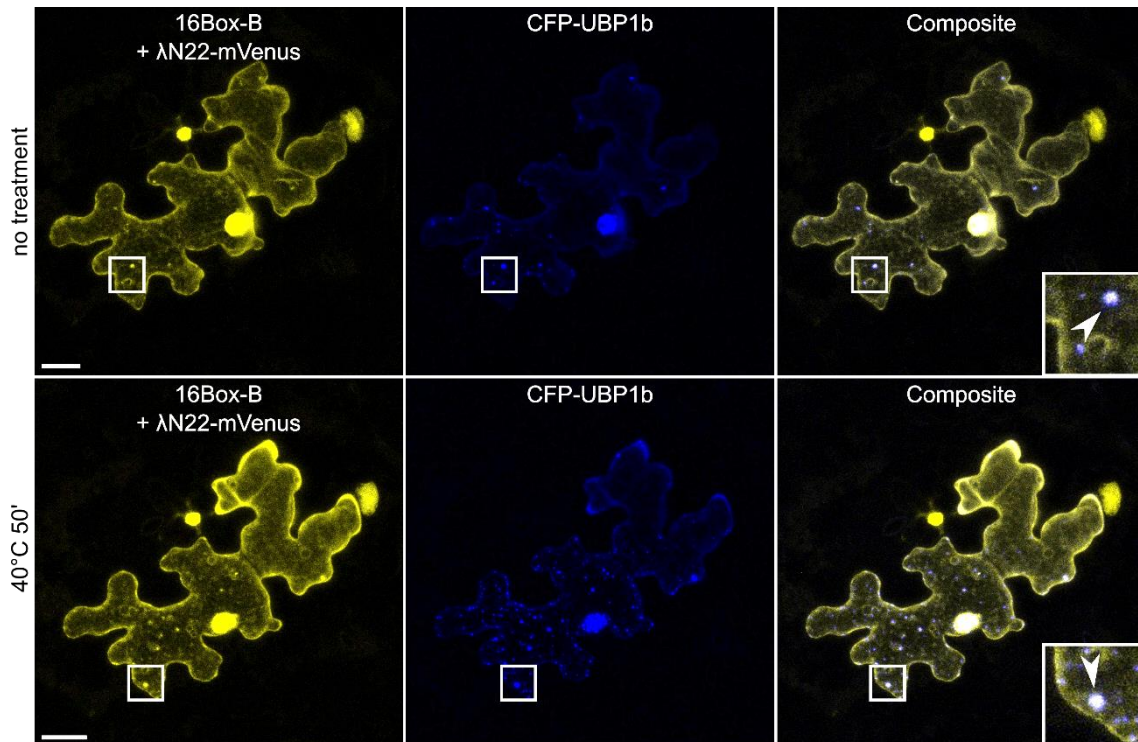


Figure 76: **The λ N22-mVENUS reporter co-expressed with Box-B repeats without an mRNA target localizes in cytoplasmic granules.** The λ N22 reporter construct was co-expressed with Box-B repeats and *35S::CFP-UBP1b* via particle bombardment in *A. thaliana* epidermal leaf cells. Exemplary pictures of cells under non-stress and stress (40°C, 50 min) conditions are shown. The arrows highlight overlapping mVenus signals with the stress granule marker CFP-UBP1b. Scale bars indicate 20 μ m.

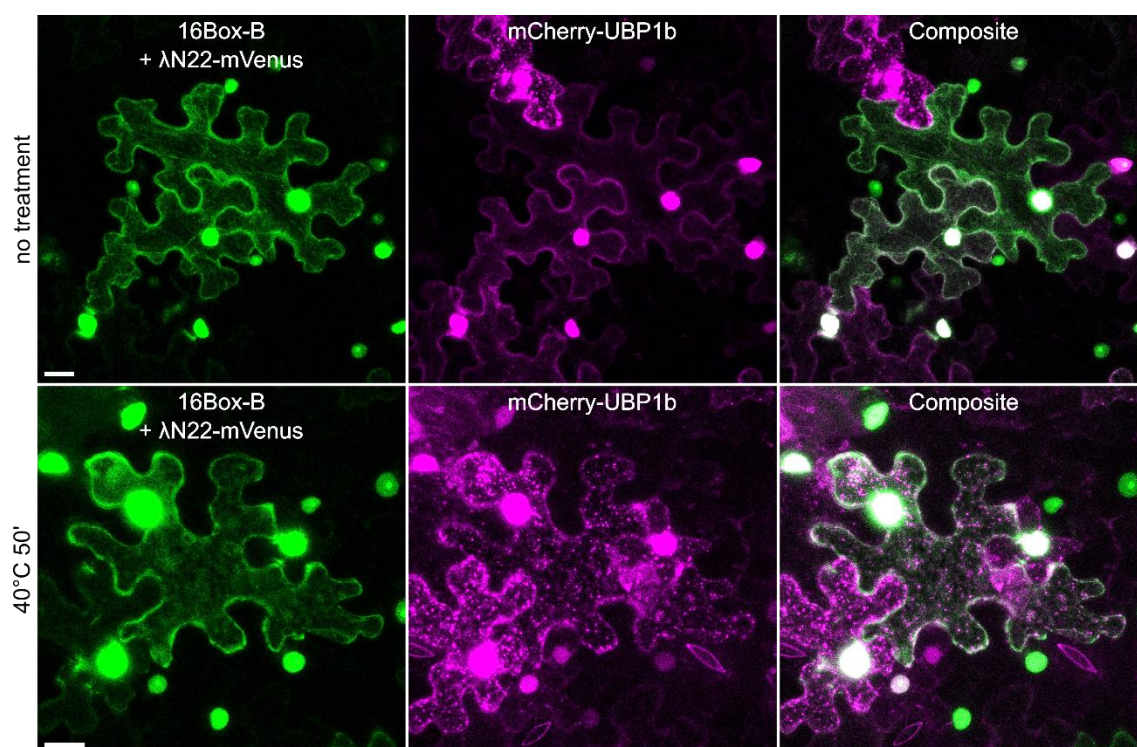


Figure 77: The λ N22-mVENUS reporter co-expressed with Box-B repeats without an mRNA target does not localize in cytoplasmic granules in *N. benthamiana*. The λ N22 reporter construct was co-expressed with Box-B repeats and *35S::mCherry-UBP1b* via infiltration of *N. benthamiana* leaves. Exemplary pictures of cells under non-stress and stress (40°C, 50 min) conditions are shown. Scale bars indicate 20 μ m.

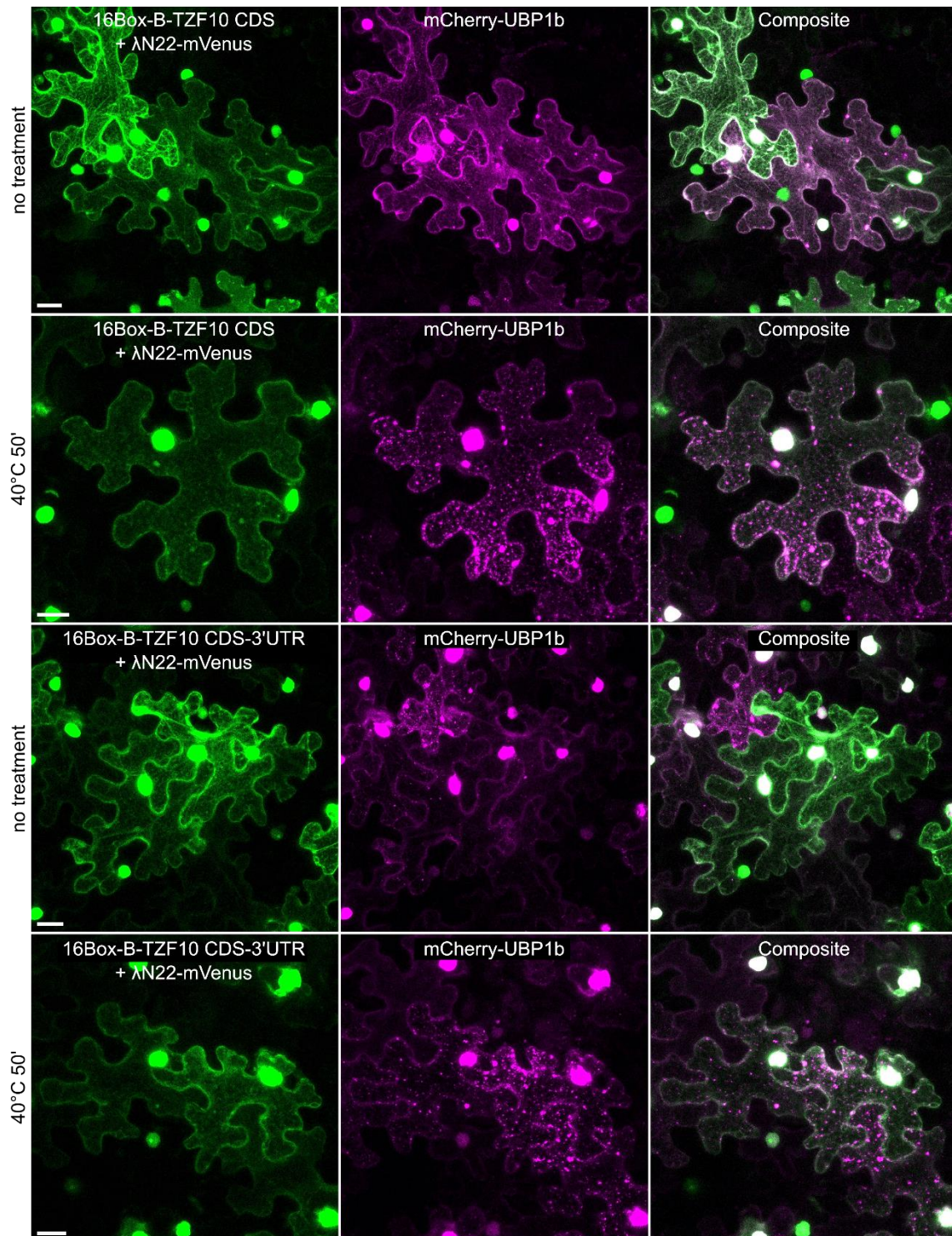


Figure 78: **The mRNA of *TZF10* sporadically localizes to stress granules.** The λN22-system was applied to transiently visualize the mRNA of *TZF10* CDS with or without the addition of the 3'UTR via infiltration of *N. benthamiana* leaves. Exemplary pictures of epidermal cells under non-stress and stress (40°C, 50 min) conditions are shown. Scale bars indicate 20 μm.

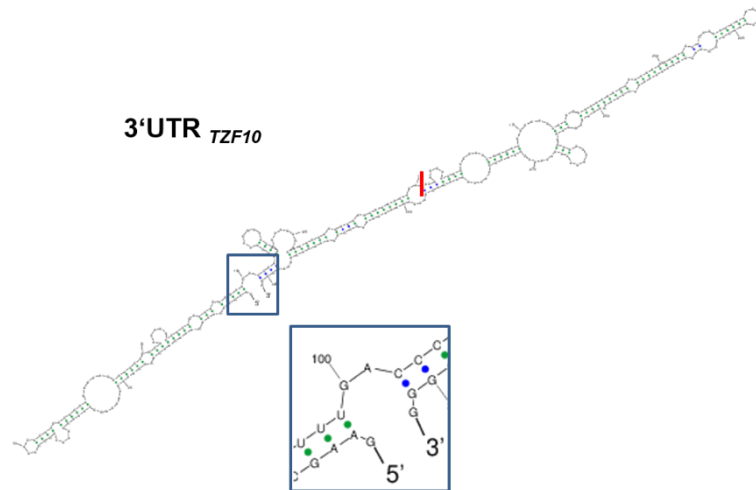


Figure 79: ***TZF10* 3'UTR structure prediction.** The model was obtained from the Software for Statistical Folding of Nucleic Acids and Studies of Regulatory RNAs (Sfold, <http://sfold.wadsworth.org>; job mode: batch; minimum free energy structure diagram). The blue box highlights the 5' and 3' end of the 3'UTR in order to allow better overview. The red line indicates the location at which the 3'UTR was split into fragments.

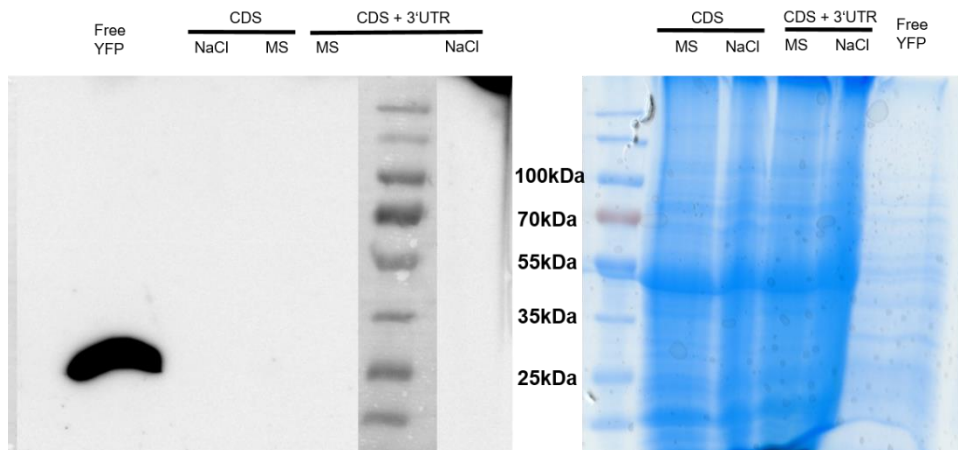


Figure 80: ***TZF10* protein cannot be detected in transgenic *TZF10* overexpression lines (*spi-4* background).** Total protein extracts derived from salt hypersensitivity rescue lines, stably expressing either a construct harboring *YFP-TZF10* CDS or *YFP-TZF10* CDS+3'UTR, treated or not treated with 125 mM NaCl, were subjected to SDS-PAGE followed by Coomassie staining (right) and α -GFP immunoprecipitation (left). Free YFP (26 kDa) from a control protein extract (kindly provided by Jessica Pietsch) was successfully detected, while *YFP-TZF10* (88 kDa) fusions were not detectable. Protein ladder: PageRuler™ Prestained (Thermo Scientific).

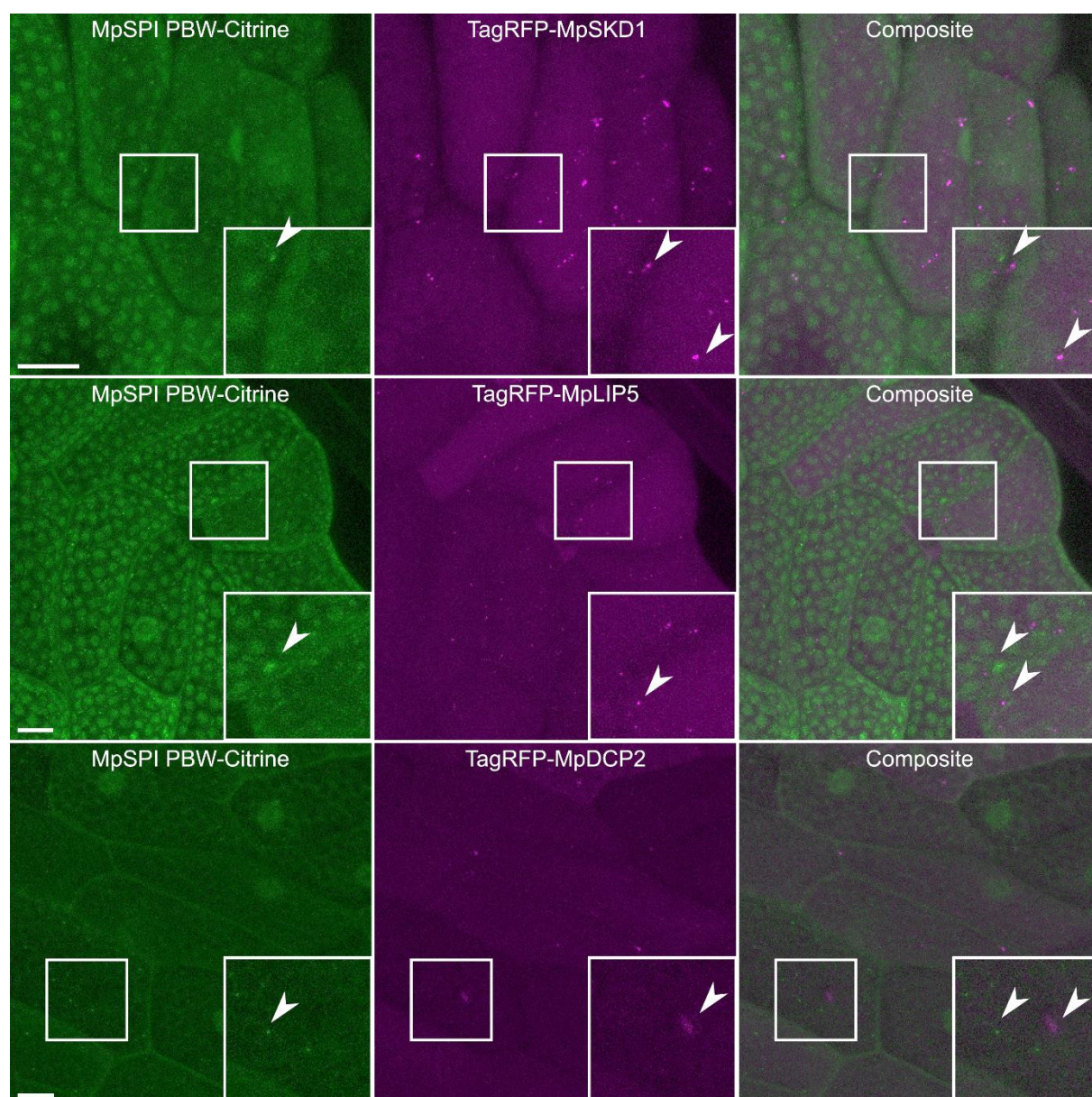


Figure 81: *M. polymorpha*, stably co-transformed with **35S::MpSPI PBW-Citrine** and **35S::TagRFP-MpSKD1**, **-MpLIP5**, **-MpDCP2**, respectively. Exemplary pictures of epidermal cells of five-day-old gemmae, derived from the stable lines, are shown. Fluorescence of MpSPI PBW-Citrine and marker proteins was hardly detectable (Laser intensities set to: 514 nm (Citrine): 70% at 20% argon laser intensity, 561 nm (TagRFP): 85%; line accumulation: 3). Zoom-ins highlight occasional occurrence of dot-like structures. The scale bars indicate 20 μ m.

Table 31: List of interacting proteins identified in the yeast two-hybrid screenings with TZF10 and 11 as bait proteins. The descriptions were extracted from The Arabidopsis Information Resource (TAIR).

| Mating | Hits | Gene ID | Description |
|---|------|-----------|---|
| SNARE proteins or ESCRT/ESCRT associated components | | | |
| TZF10xFlag+ | 2 | AT1G03260 | SNARE associated Golgi protein family |
| TZF10xETIO | 2 | AT1G32410 | Vacuolar protein sorting 55 (VPS55) family protein |
| TZF10xFlag+ | 1 | AT2G45200 | GOS12, ATGOS12 golgi snare 12 |
| TZF10xCLON | 1 | AT4G17790 | SNARE associated Golgi protein family |
| TZF10xSAL | 1 | AT4G26550 | Got1/Sft2-like vesicle transport protein family |
| Calcium/calmodulin-binding/associated proteins | | | |
| TZF10xSAL | 1 | AT1G18210 | Calcium-binding EF-hand family protein |
| TZF10xFlag+ | 1 | AT1G76180 | ERD14 Dehydrin family protein |
| TZF10xETIO | 1 | AT3G28140 | RNA ligase/cyclic nucleotide phosphodiesterase family |
| TZF11xETIO | 21 | AT3G28140 | RNA ligase/cyclic nucleotide phosphodiesterase family |
| TZF11xSAL | 11 | AT3G28140 | RNA ligase/cyclic nucleotide phosphodiesterase family |
| TZF10xSAL | 6 | AT3G28140 | RNA ligase/cyclic nucleotide phosphodiesterase family |
| TZF11xFlag+ | 23 | AT3G28140 | RNA ligase/cyclic nucleotide phosphodiesterase family |
| TZF10xFlag+ | 3 | AT3G28140 | RNA ligase/cyclic nucleotide phosphodiesterase family |
| TZF10xETIO | 1 | AT5G04170 | Calcium-binding EF-hand family protein |
| TZF10xETIO | 4 | AT5G40190 | RNA ligase/cyclic nucleotide phosphodiesterase family |
| TZF10xFlag+ | 3 | AT5G40190 | RNA ligase/cyclic nucleotide phosphodiesterase family |
| TZF11xETIO | 30 | AT5G40190 | RNA ligase/cyclic nucleotide phosphodiesterase family |
| TZF11xSAL | 19 | AT5G40190 | RNA ligase/cyclic nucleotide phosphodiesterase family |
| TZF11xCLON | 10 | AT5G40190 | RNA ligase/cyclic nucleotide phosphodiesterase family |
| TZF10xSAL | 16 | AT5G40190 | RNA ligase/cyclic nucleotide phosphodiesterase family |
| TZF11xFlag+ | 23 | AT5G40190 | RNA ligase/cyclic nucleotide phosphodiesterase family |
| NAD(P)-binding or NADPH-producing / -associated proteins | | | |
| TZF10xETIO | 1 | AT1G65930 | cCDH cytosolic NADP+-dependent isocitrate dehydrogenase |
| TZF10xETIO | 3 | AT3G29250 | NAD(P)-binding Rossmann-fold superfamily protein |
| TZF10xETIO | 1 | AT3G44190 | FAD/NAD(P)-binding oxidoreductase family protein |
| TZF10xCLON | 1 | AT4G00570 | NAD-ME2 NAD-dependent malic enzyme 2 |
| TZF10xETIO | 1 | AT5G27150 | NHX1, ATNHX, AT-NHX1, ATNHX1 Na+/H+ exchanger 1 |
| TZF10xCLON | 1 | AT5G37510 | EMB1467, CI76 NADH-ubiquinone dehydrogenase, mitochondrial, putative |
| Lipid droplet- or lipid transfer-associated proteins | | | |
| TZF10xSAL | 1 | AT2G26250 | FDH, KCS10 3-ketoacyl-CoA synthase 10 |
| TZF10xSAL | 1 | AT2G29980 | FAD3 fatty acid desaturase 3 |
| TZF10xETIO | 1 | AT2G38530 | LTP2, LP2, cdf3 lipid transfer protein 2 |
| TZF10xETIO | 4 | AT2G47780 | Rubber elongation factor protein (REF) |
| TZF10xCLON | 1 | AT3G24460 | Serinc-domain containing serine and sphingolipid biosynthesis protein |
| Other proteins | | | |
| TZF10xETIO | 5 | AT5G60890 | ATMYB34, ATR1, MYB34 myb domain protein 34 |
| TZF10xETIO | 1 | AT2G32460 | MYB101, ATMYB101, ATM1 myb domain protein 101 |
| TZF10xETIO | 1 | AT2G21660 | ATGRP7, CCR2, GR-RBP7, GRP7 cold, circadian rhythm, and rna binding 2 |
| TZF10xETIO | 1 | AT1G01380 | ETC1 Homeodomain-like superfamily protein |
| TZF10xSAL | 1 | AT1G04410 | Lactate/malate dehydrogenase family protein |
| TZF10xETIO | 1 | AT1G09690 | Translation protein SH3-like family protein |
| TZF10xSAL | 1 | AT1G09840 | ATSK41, SK41 shaggy-like protein kinase 41 |

| | | | |
|--------------------|---|-----------|---|
| TZF10xCLON | 1 | AT1G15690 | AVP1, ATAVP3, AVP-3, AtVHP1;1 Inorganic Hpyrophosphatase family protein |
| TZF10xSAL | 2 | AT1G17480 | IQD7 IQ-domain 7 |
| TZF10xETIO | 1 | AT1G20340 | DRT112, PETE2 Cupredoxin superfamily protein |
| TZF11xETIO | 1 | AT1G29090 | Cysteine proteinases superfamily protein |
| TZF10xCLON | 1 | AT1G45130 | BGAL5 beta-galactosidase 5 |
| TZF10xSAL | 1 | AT1G47420 | SDH5 succinate dehydrogenase 5 |
| TZF10xFlag+ | 1 | AT1G51980 | Insulinase (Peptidase family M16) protein |
| TZF10xETIO | 1 | AT1G54010 | GDSL-like Lipase/Acylhydrolase superfamily protein |
| TZF10xCLON | 1 | AT1G54410 | dehydrin family protein |
| TZF10xSAL | 1 | AT1G58080 | ATATP-PRT1, HISN1A, ATP-PRT1 ATP phosphoribosyl transferase 1 |
| TZF10xFlag+ | 1 | AT1G61250 | SC3 secretory carrier 3 |
| TZF10xCLON | 1 | AT1G63970 | ISPF, MECPS isoprenoid F |
| TZF10xFlag+ | 1 | AT1G64810 | APO1 <i>Arabidopsis thaliana</i> protein of unknown function (DUF794) |
| TZF10xCLON | 1 | AT1G67870 | glycine-rich protein |
| TZF10xCLON | 1 | AT1G70760 | CRR23 inorganic carbon transport protein-related |
| TZF10xSAL | 2 | AT1G75380 | ATBBD1, BBD1 bifunctional nuclease in basal defense response 1 |
| TZF10xETIO | 2 | AT1G78300 | GRF2, 14-3-3OMEGA, GF14 OMEGA |
| TZF10xSAL | 1 | AT1G78920 | AVP2, AVPL1, AtVHP2;1, VHP2;1, VP2 vacuolar H ⁺ -pyrophosphatase 2 |
| TZF10xCLON | 1 | AT2G04030 | CR88, Hsp88.1, AtHsp90.5 Chaperone protein htpG family |
| TZF10xETIO | 1 | AT2G05380 | GRP3S glycine-rich protein 3 short isoform |
| TZF10xSAL | 1 | AT2G07050 | CAS1 cycloartenol synthase 1 |
| TZF11xFlag+ | 1 | AT2G21240 | Symbols: BPC4, BBR, ATBPC4 basic pentacysteine 4 |
| TZF10xFlag+ | 1 | AT2G26210 | Ankyrin repeat family protein |
| TZF10xETIO | 1 | AT2G30870 | ATGSTF10, ERD13, ATGSTF4, GSTF10 glutathione S-transferase PHI 10 |
| TZF10xCLON | 1 | AT2G38170 | CAX1, ATCAX1, RCI4 cation exchanger 1 |
| TZF10xCLON | 5 | AT2G39700 | ATEXPA4, ATEXP4, ATHEXP ALPHA 1.6, EXPA4 expansin A4 |
| TZF10xCLON | 1 | AT2G42220 | Rhodanese/Cell cycle control phosphatase superfamily |
| TZF10xETIO | 1 | AT2G45180 | Bifunctional inhibitor/lipid-transfer protein/seed storage 2S albumin superfamily protein |
| TZF10xETIO | 1 | AT2G47110 | UBQ6 ubiquitin 6 |
| TZF10xSAL | 2 | AT2G47710 | Adenine nucleotide alpha hydrolases-like superfamily protein |
| TZF10xSAL | 1 | AT3G03270 | Adenine nucleotide alpha hydrolases-like superfamily protein |
| TZF10xCLON | 1 | AT3G04740 | SWP, MED14, ATMED14 RNA polymerase II transcription mediators |
| TZF11xCLON | 1 | AT3G05030 | NHX2, ATNHX2 sodium hydrogen exchanger 2 |
| TZF11xFlag+ | 1 | AT3G05070 | CONTAINS InterPro DOMAIN/s: mRNA splicing factor Cwf18 |
| TZF10xSAL | 2 | AT3G10985 | SAG20, WI12, ATWI-12 senescence associated gene 20 |
| TZF11xFlag+ | 1 | AT3G11700 | FLA18 FASCICLIN-like arabinogalactan protein 18 precursor |
| TZF10xFlag+ | 1 | AT3G11930 | Adenine nucleotide alpha hydrolases-like superfamily |
| TZF10xSAL | 1 | AT3G16760 | Tetratricopeptide repeat (TPR)-like superfamily protein |
| TZF10xCLON | 1 | AT3G24190 | Protein kinase superfamily protein |
| TZF10xETIO | 2 | AT3G29037 | Pseudogene of AT5G35760; beta-galactosidase |
| TZF10xSAL | 1 | AT3G29360 | UDP-glucose 6-dehydrogenase family protein |
| TZF10xFlag+ | 1 | AT3G48140 | B12D protein |
| TZF10xSAL | 1 | AT3G48670 | IDN2, RDM12 XH/XS domain-containing protein |
| TZF10xETIO | 1 | AT3G52300 | ATPQ ATP synthase D chain, mitochondrial |

| | | | |
|--------------------|---|-----------|---|
| TZF10xSAL | 1 | AT3G52470 | Late embryogenesis abundant (LEA) hydroxyproline-rich glycoprotein family |
| TZF10xSAL | 1 | AT3G53740 | Ribosomal protein L36e family protein |
| TZF10xFlag+ | 3 | AT3G56310 | Melibiose family protein |
| TZF10xCLON | 1 | AT3G58990 | IPMI1 isopropylmalate isomerase 1 |
| TZF10xSAL | 1 | AT3G60210 | GroES-like family protein |
| TZF10xETIO | 1 | AT4G01750 | RGXT2 rhamnogalacturonan xylosyltransferase 2 |
| TZF10xETIO | 2 | AT4G03210 | XTH9 xyloglucan endotransglucosylase/hydrolase 9 |
| TZF10xFlag+ | 2 | AT4G12060 | Double Clp-N motif protein |
| TZF10xSAL | 1 | AT4G13930 | SHM4 serine hydroxymethyltransferase 4 |
| TZF10xSAL | 1 | AT4G20320 | CTP synthase family protein |
| TZF11xCLON | 1 | AT4G20380 | LSD1 LSD1 zinc finger family protein |
| TZF10xCLON | 1 | AT4G21960 | PRXR1 Peroxidase superfamily protein |
| TZF10xSAL | 1 | AT4G25100 | FSD1 Fe superoxide dismutase 1 |
| TZF10xCLON | 1 | AT4G25210 | DNA-binding storekeeper protein-related transcriptional regulator |
| TZF10xETIO | 1 | AT4G27450 | Aluminium induced protein with YGL and LRDR motifs |
| TZF10xSAL | 1 | AT4G30440 | GAE1 UDP-D-glucuronate 4-epimerase 1 |
| TZF11xCLON | 3 | AT4G32190 | Myosin heavy chain-related protein |
| TZF10xETIO | 1 | AT4G35100 | PIP3, PIP3A, PIP2;7, SIMIP plasma membrane intrinsic protein 3 |
| TZF10xETIO | 1 | AT4G36800 | RCE1 RUB1 conjugating enzyme 1 |
| TZF10xSAL | 1 | AT4G37180 | Homeodomain-like superfamily protein |
| TZF10xSAL | 1 | AT5G01542 | Potential natural antisense gene, locus overlaps with AT5G01540 |
| TZF10xSAL | 1 | AT5G01542 | Potential natural antisense gene, locus overlaps with AT5G01540 |
| TZF10xETIO | 1 | AT5G03860 | MLS malate synthase |
| TZF10xFlag+ | 1 | AT5G07610 | F-box family protein |
| TZF10xFlag+ | 1 | AT5G10980 | Histone superfamily protein |
| TZF10xSAL | 1 | AT5G13280 | AK-LYS1, AK1, AK aspartate kinase 1 |
| TZF10xFlag+ | 1 | AT5G13490 | AAC2 ADP/ATP carrier 2 |
| TZF10xSAL | 1 | AT5G20150 | ATSPX1, SPX1 SPX domain gene 1 |
| TZF10xCLON | 1 | AT5G22800 | EMB86, EMB1030, EMB263 Alanine-tRNA synthetase |
| TZF10xSAL | 1 | AT5G23575 | Transmembrane CLPTM1 family protein |
| TZF10xSAL | 2 | AT5G24318 | O-Glycosyl hydrolases family 17 protein |
| TZF10xCLON | 1 | AT5G25980 | TGG2, BGLU37 glucoside glucohydrolase 2 |
| TZF10xCLON | 1 | AT5G26667 | PYR6 P-loop containing nucleoside triphosphate hydrolases superfamily protein |
| TZF11xSAL | 2 | AT5G39340 | AHP3, ATHP2 histidine-containing phosphotransmitter 3 |
| TZF10xETIO | 1 | AT5G39730 | AIG2-like (avirulence induced gene) family protein |
| TZF11xFlag+ | 1 | AT5G52470 | Symbols: FIB1, FBR1, ATFIB1, ATFBR1, SKIP7 |
| TZF11xETIO | 1 | AT5G52552 | CPuORF14 conserved peptide upstream open reading frame |
| TZF10xFlag+ | 1 | AT5G53560 | ATB5-A, B5 #2, ATCB5-E, CB5-E cytochrome B5 isoform E |
| TZF10xFlag+ | 2 | AT5G53640 | CONTAINS InterPro DOMAIN/s: F-box domain, cyclin-like |
| TZF10xCLON | 1 | AT5G55220 | trigger factor type chaperone family protein |
| TZF10xETIO | 1 | AT5G59690 | Histone superfamily protein |
| TZF10xETIO | 1 | AT5G60660 | PIP2F, PIP2;4 plasma membrane intrinsic protein 2;4 |
| TZF10xFlag+ | 1 | AT5G61590 | Integrase-type DNA-binding superfamily protein |

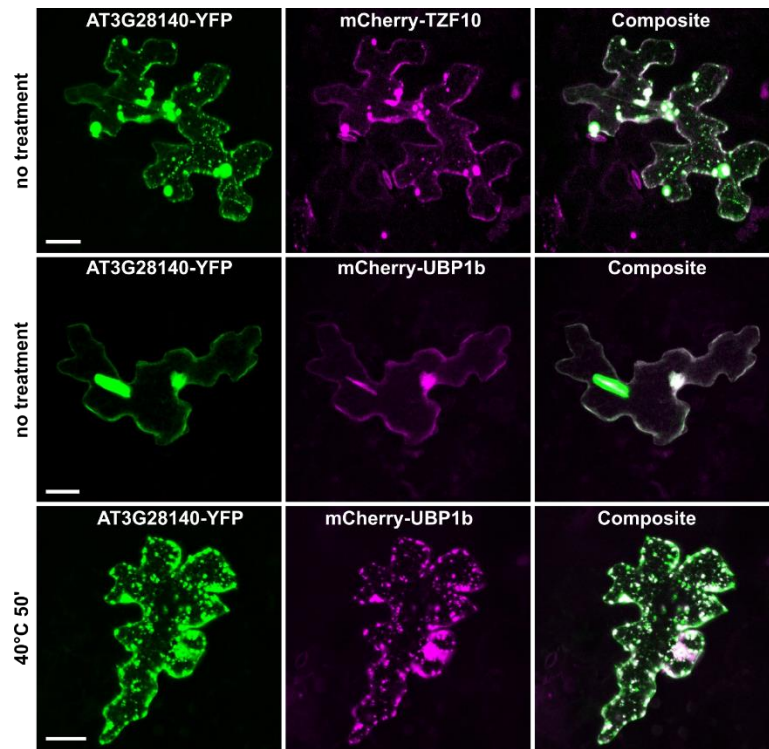


Figure 82: **The RNA ligase AT3G28140 co-localizes with TZF10 and UBP1b.** *35S::AT3G28140-YFP* was transiently co-expressed with *35S::mCherry-TZF10* and *35S::mCherry-UBP1b*, respectively, in *A. thaliana* epidermal cells via particle bombardment. Whereas AT3G28140 already co-localized with TZF10 under non-stress conditions; localization in distinct granules labeled by UBP1b was detectable after heat stress. The scale bars depict 20 µm.

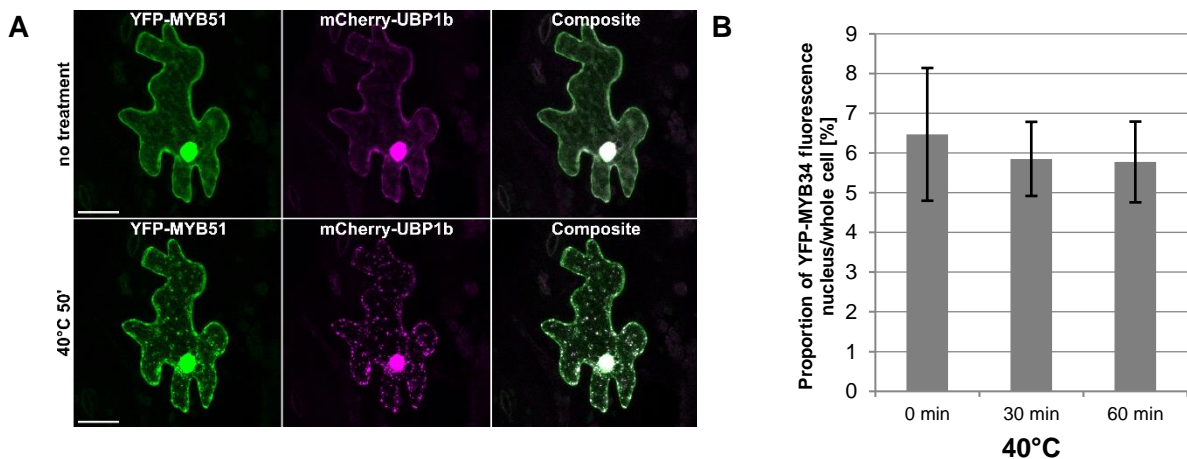


Figure 83: **MYB51 localizes to stress granules under heat stress conditions.** **A** *35S::YFP-MYB51* was transiently co-expressed in *A. thaliana* epidermal cells via particle bombardment. The scale bars depict 20 µm. **B** The proportion of YFP-MYB34 fluorescence in the nucleus relative to total fluorescence does not decrease during 1h of heat treatment at 40°C. *35S::YFP-MYB34* was transiently expressed in *N. benthamiana* via leaf infiltration. $n=12-24$. Fluorescence intensities were calculated with cell/nuclei areas multiplied with mean gray intensity values using ImageJ. Error bars show standard deviation. Two-tailed, unpaired Student's *t*-testing revealed no significant differences.

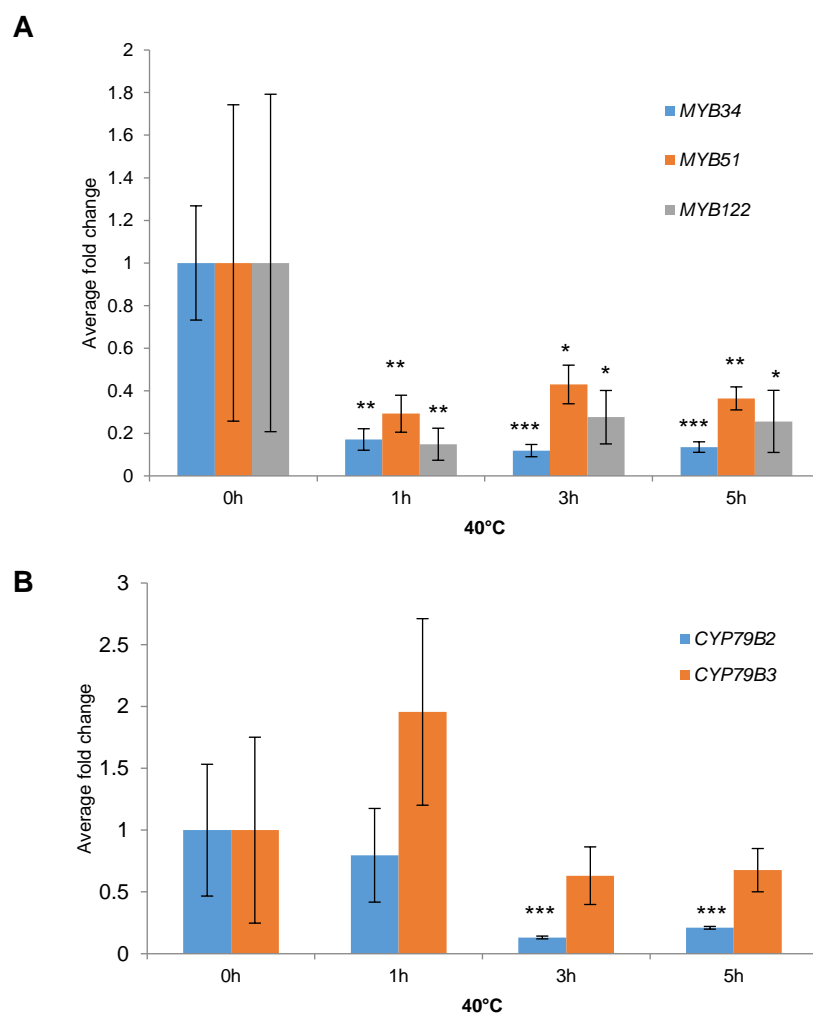


Figure 84: **The transcripts of *MYB34*, *51* and *122* and target genes are down-regulated upon heat stress.** Relative expression of *MYB34*, *51*, and *122* (A) and target genes *CYP79B2* and *CYP79B3* (B) in heat-stressed (1 h-5 h) compared to control samples (0h), normalized to reference gene *PP2A*. Expression levels were determined in Col-0 ($n=3$) samples, treated or not treated with 40°C for designated time periods. Error bars indicate the standard error. Significance was tested with unpaired, two-tailed, Student's *t*-test.

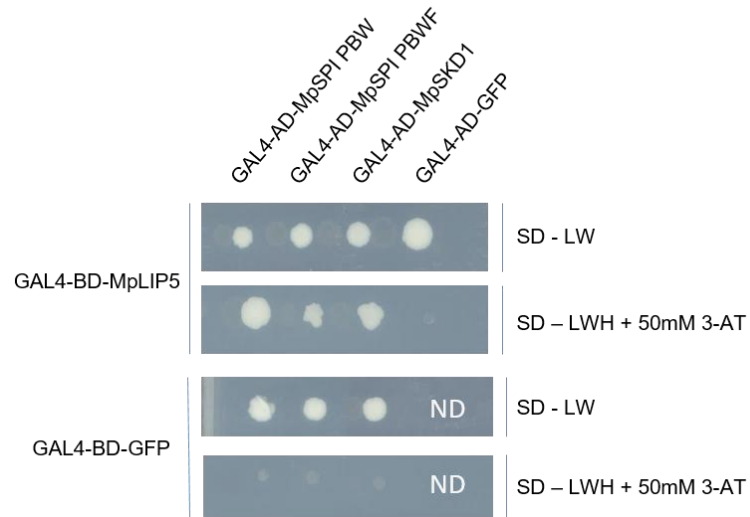


Figure 85: **MpSPI PBW/PBWF interacts with MpLIP5 in yeast.** GAL4-AD=GAL4-activation domain, GAL4-BD=GAL4-binding domain, ND=not determined.

6 REFERENCES

- Abdel Latef, A. A.** (2010). Changes of antioxidative enzymes in salinity tolerance among different wheat cultivars. *Cereal Res. Commun.* **38**, 43–55.
- Agudelo-Romero, P., Fortes, A. M., Suárez, T., Lascano, H. R. and Saavedra, L.** (2020). Evolutionary insights into FYVE and PHOX effector proteins from the moss *Physcomitrella patens*. *Planta* **251**, 1–20.
- Altenbach, D. and Robatzek, S.** (2007). Pattern recognition receptors: From the cell surface to intracellular dynamics. *Mol. Plant-Microbe Interact.* **20**, 1031–1039.
- Anderson, P. and Kedersha, N.** (2008). Stress granules: The Tao of RNA triage. *Trends Biochem. Sci.* **33**, 141–150.
- Arae, T., Morita, K., Imahori, R., Suzuki, Y., Yasuda, S., Sato, T., Yamaguchi, J. and Chiba, Y.** (2019). Identification of Arabidopsis CCR4-NOT Complexes with Pumilio RNA-Binding Proteins, APUM5 and APUM2. *Plant Cell Physiol.* **60**, 2015–2025.
- Babst, M., Katzmann, D. J., Estepa-Sabal, E. J., Meerloo, T. and Emr, S. D.** (2002a). ESCRT-III: An endosome-associated heterooligomeric protein complex required for MVB sorting. *Dev. Cell* **3**, 271–282.
- Babst, M., Katzmann, D. J., Snyder, W. B., Wendland, B. and Emr, S. D.** (2002b). Endosome-associated complex, ESCRT-II, recruits transport machinery for protein sorting at the multivesicular body. *Dev. Cell* **3**, 283–289.
- Bailey-Serres, J., Sorenson, R. and Juntawong, P.** (2009). Getting the message across: cytoplasmic ribonucleoprotein complexes. *Trends Plant Sci.* **14**, 443–453.
- Bainard, J. D. and Newmaster, S. G.** (2010). Endopolyploidy in Bryophytes: Widespread in Mosses and Absent in Liverworts. *J. Bot.* **2010**, 1–7.
- Bainard, J. D., Forrest, L. L., Goffinet, B. and Newmaster, S. G.** (2013). Nuclear DNA content variation and evolution in liverworts. *Mol. Phylogenet. Evol.* **68**, 619–627.
- Barbosa, M. D., Nguyen, Q. A., Tchernev, V. T., Ashley, J. A., Detter, J. C., Blaydes, S. M., Brandt, S. J., Chotai, D., Hodgman, C., Solari, R. C., Lovett, M. and Kingsmore, S. F.** (1996). Identification of the homologous beige and Chediak-Higashi syndrome genes. *Nature* **382**: 262–265.
- Barreau, C., Paillard, L. and Osborne, H. B.** (2005). AU-rich elements and associated factors: Are there unifying principles? *Nucleic Acids Res.* **33**, 7138–7150.
- Bashirullah, A., Cooperstock, R. L. and Lipshitz, H. D.** (2001). Spatial and temporal control of RNA stability. *Proc. Natl. Acad. Sci. U. S. A.* **98**, 7025–7028.
- Beilstein, M. A., Nagalingum, N. S., Clements, M. D., Manchester, S. R. and Mathews, S.** (2010). Dated molecular phylogenies indicate a Miocene origin for *Arabidopsis thaliana*. *Proc. Natl. Acad. Sci. USA* **107**, 18724–18728.
- Belostotsky, D. A. and Sieburth, L. E.** (2009). Kill the messenger: mRNA decay and plant development. *Curr. Opin. Plant Biol.* **12**, 96–102.
- Bernard, P. and Couturier, M.** (1992). Cell killing by the F plasmid CcdB protein involves poisoning of DNA-topoisomerase II complexes. *J. Mol. Biol.* **226**, 735–745.
- Bhosale, R., Boudolf, V., Cuevas, F., Lu, R., Eekhout, T., Hu, Z., Van Isterdael, G., Lambert, G. M., Xu, F., Nowack, M. K., et al.** (2018). A spatiotemporal DNA endploidy map of the Arabidopsis root reveals roles for the endocycle in root development and stress adaptation. *Plant Cell* **30**, 2330–2351.
- Bilodeau, P. S., Urbanowski, J. L., Winistorfer, S. C. and Piper, R. C.** (2002). The Vps27p-Hse1p complex binds ubiquitin and mediates endosomal protein sorting. *Nat. Cell Biol.* **4**, 534–539.
- Bischler, H.** (1989). Marchantia L. The Asiatic and Oceanic taxa. *Bryophyt. Bibl.* **38**: 1–124.
- Blackshear, P. J. and Perera, L.** (2014). Phylogenetic distribution and evolution of the linked RNA-binding and NOT1-binding domains in the tristetraprolin family of tandem CCCH zinc finger proteins. *J. Interf. Cytokine Res.* **34**, 297–306.

- Blackshear, P. J., Phillips, R. S., Lai, W. S.** (2005). Tandem CCCH zinc finger proteins in mRNA binding. In: Iuchi, S., and Kuldell, N. (Eds.), *Zinc Finger Proteins: From Atomic Contact to Cellular Function*. *Kluwer Academic/Plenum Publishers* **13**: 80–90.
- Blanvillain, R., Wei, S., Wei, P., Kim, J. H. and Ow, D. W.** (2011). Stress tolerance to stress escape in plants: role of the OXS2 zinc-finger transcription factor family. *EMBO J.* **30**, 3812–3822.
- Blaydes, S. M., Brandt, S. J., Chotai, D., Hodgman, C., Solari, C. E., Lovett, M. and Kingsmore, S. F.** (2010). Identification of the homologous beige and Chediak-Higashi syndrome genes. *Nature* **382**, 262–265.
- Bogamuwa, S. P. and Jang, J.** (2016). Plant Tandem CCCH Zinc Finger Proteins Interact with ABA, Drought and Stress Response Regulators in Processing-Bodies and Stress Granules. *PLOS ONE* **11**, e0151574.
- Bogamuwa, S. P. and Jang, J.** (2014). Tandem CCCH Zinc Finger Proteins in Plant Growth, Development and Stress Response. *Plant Cell Physiol.* **55**, 1367–1375.
- Bogdanović, M. D., Dragičević, M. B., Tanić, N. T., Todorović, S. I., Mišić, D. M., Živković, S. T., Tissier, A. and Simonović, A. D.** (2013). Reverse Transcription of 18S rRNA with Poly(dT)18 and Other Homopolymers. *Plant Mol. Biol. Report.* **31**, 55–63.
- Bolognesi, B. and Lehner, B.** (2018). Reaching the limit: How many copies of a protein can be made before it becomes toxic to the cell? *eLife* **7**, e39804.
- Bowman, J. L.** (2016). A brief history of Marchantia from Greece to genomics. *Plant Cell Physiol.* **57**, 210–229.
- Bowman, J. L., Araki, T., Arteaga-Vazquez, M. A., Berger, F., Dolan, L., Haseloff, J., Ishizaki, K., Kyozyuka, J., Lin, S. S., Nagasaki, H., et al.** (2016). The naming of names: Guidelines for gene nomenclature in Marchantia. *Plant Cell Physiol.* **57**, 257–261.
- Bowman, J. L., Floyd, S. K. and Sakakibara, K.** (2007). Green Genes - Comparative Genomics of the Green Branch of Life. *Cell* **129**, 229–234.
- Bowman, J. L., Kohchi, T., Yamato, K. T., Jenkins, J., Shu, S., Ishizaki, K., Yamaoka, S., Nishihama, R., Nakamura, Y., Berger, F., et al.** (2017). Insights into Land Plant Evolution Garnered from the *Marchantia polymorpha* Genome. *Cell* **171**, 287–304.e15.
- Bramsiepe, J., Wester, K., Weinl, C., Roodbarkelari, F., Kasili, R., Larkin, J. C., Hülskamp, M. and Schnittger, A.** (2010). Endoreplication controls cell fate maintenance. *PLOS Genet.* **6**, 1–14.
- Brooks, S. A. and Blackshear, P. J.** (2013). Tristetraprolin (TTP): Interactions with mRNA and proteins, and current thoughts on mechanisms of action. *Biochim Biophys Acta.* **1829**, 666–679.
- Brooks, S. A., Connolly, J. E. and Rigby, W. F. C.** (2004). The Role of mRNA Turnover in the Regulation of Tristetraprolin Expression: Evidence for an Extracellular Signal-Regulated Kinase-Specific, AU-Rich Element-Dependent, Autoregulatory Pathway. *J. Immunol.* **172**, 7263–7271.
- Brückner, A., Polge, C., Lentze, N., Auerbach, D. and Schlattner, U.** (2009). Yeast two-hybrid, a powerful tool for systems biology. *Int. J. Mol. Sci.* **10**, 2763–2788.
- Buchan, J. R. and Parker, R.** (2009). Eukaryotic Stress Granules: The Ins and Out of Translation. *Mol. Cell* **36**, 932.
- Bulbrook, D., Brazier, H., Mahajan, P., Kliszczak, M., Fedorov, O., Marchese, F. P., Aubareda, A., Chalk, R., Picaud, S., Strain-Damerell, C., et al.** (2018). Tryptophan-Mediated Interactions between Tristetraprolin and the CNOT9 Subunit Are Required for CCR4-NOT Deadenylation Complex Recruitment. *J. Mol. Biol.* **430**, 722–736.
- Burgeff, H.** (1943). *Genetische Studien an Marchantia*. Gustav Fischer, Jena.
- Bustin, S. A., Benes, V., Garson, J. A., Hellems, J., Huggett, J., Kubista, M., Mueller, R., Nolan, T., Pfaffl, M. W., Shipley, G. L., et al.** (2009). The MIQE guidelines: Minimum information for publication of quantitative real-time PCR experiments. *Clin. Chem.* **55**, 611–622.
- Cao, H., Deterding, L. J. and Blackshear, P. J.** (2007). Phosphorylation site analysis of the anti-inflammatory and mRNA destabilizing protein tristetraprolin. *Expert Rev Proteomics* **4**, 711–726.
- Cao, J., Dai, X., Zou, H. and Wang, Q.** (2014). Formation and development of rhizoids of the liverwort *Marchantia polymorpha*. *The Journal of the Torrey Botanical Society* **141**, 126–134.

- Caput, D., Beutler, B., Hartog, K., Thayer, R., Brown-Shimer, S. and Cerami, A.** (1986). Identification of a common nucleotide sequence in the 3'-untranslated region of mRNA molecules specifying inflammatory mediators. *Proc. Natl. Acad. Sci. U. S. A.* **83**, 1670–1674.
- Carballo, E.** (1998). Feedback Inhibition of Macrophage Tumor Necrosis Factor - Production by Tristetraprolin. *Science* **281**, 1001–1005.
- Celenza, J. L., Quiel, J. A., Smolen, G. A., Merrikh, H., Silvestro, A. R., Normanly, J. and Bender, J.** (2005). The Arabidopsis ATR1 Myb Transcription Factor Controls Indolic Glucosinolate Homeostasis. *Plant Physiol.* **137**, 253–262.
- Chang, T. H., Huang, H. Y., Hsu, J. B. K., Weng, S. L., Horng, J. T. and Huang, H. Da** (2013). An enhanced computational platform for investigating the roles of regulatory RNA and for identifying functional RNA motifs. *BMC Bioinformatics* **14**, S4.
- Chantarachot, T. and Bailey-Serres, J.** (2018). Polysomes, Stress Granules, and Processing Bodies: A Dynamic Triumvirate Controlling Cytoplasmic mRNA Fate and Function. *Plant Physiol.* **176**, 254-269.
- Chen, C. A. and Shyu, A.** (1995). AU-rich elements: characterization and importance in mRNA degradation. *Trends Biochem Sci.* **20**, 465–470.
- Chen, C. A. and Shyu, A.** (2011). Mechanisms of deadenylation-dependent decay. *Wiley Interdiscip. Rev. RNA* **2**, 167–183.
- Chen, J., Chiang, Y. C. and Denis, C. L.** (2002). CCR4, a 3'-5' poly(A) RNA and ssDNA exonuclease, is the catalytic component of the cytoplasmic deadenylase. *EMBO J.* **21**, 1414–1426.
- Chrestensen, C. A., Schroeder, M. J., Shabanowitz, J., Hunt, D. F., Pelo, J. W., Worthington, M. T. and Sturgill, T. W.** (2004). MAPKAP Kinase 2 Phosphorylates Tristetraprolin on in Vivo Sites Including Ser178, a Site Required for 14-3-3 Binding. *J. Biol. Chem.* **279**, 10176–10184.
- Chung, B. Y. W., Simons, C., Firth, A. E., Brown, C. M. and Hellens, R. P.** (2006). Effect of 5'UTR introns on gene expression in *Arabidopsis thaliana*. *BMC Genomics* **7**, 1–13.
- Clark, A., Dean, J., Tudor, C. and Saklatvala, J.** (2009). Post-transcriptional gene regulation by MAP kinases via AU-rich elements. *Front. Biosci.* **14**, 847–871.
- Clement, S. L., Scheckel, C., Stoecklin, G. and Lykke-Andersen, J.** (2011). Phosphorylation of Tristetraprolin by MK2 Impairs AU-Rich Element mRNA Decay by Preventing Deadenylation Recruitment. *Mol. Cell. Biol.* **31**, 256–266.
- Collier, N. C., Heuser, J., Levy, M. A. and Schlesinger, M. J.** (1988). Ultrastructural and biochemical analysis of the stress granule in chicken embryo fibroblasts. *J. Cell Biol.* **106**, 1131–1139.
- Coonrod, E. M. and Stevens, T.H.** (2010). The Yeast *vps* Class E Mutants: The Beginning of the Molecular Genetic Analysis of Multivesicular Body Biogenesis. *Mol. Biol. Cell* **21**, 4057-4060.
- Corvera, S., D'Arrigo, A. and Stenmark, H.** (1999). Phosphoinositides in membrane traffic. *Curr. Opin. Cell Biol.* **11**, 460–465.
- Cullinane, A. R., Schäffer, A. A. and Huizing, M.** (2013). The BEACH Is Hot: A LYST of Emerging Roles for BEACH-Domain Containing Proteins in Human Disease. *Traffic* **14**, 749–766.
- Daigle, N. and Ellenberg, J.** (2007). λ N-GFP: An RNA reporter system for live-cell imaging. *Nat. Methods* **4**, 633–636.
- Datta, S., Biswas, R., Novotny, M., Pavicic, P. G., Herjan, T., Mandal, P. and Hamilton, T. A.** (2008). Tristetraprolin Regulates CXCL1 (KC) mRNA Stability. *J. Immunol.* **180**, 2545–2552.
- De Lozanne, A.** (2003). The role of BEACH proteins in Dictyostelium. *Traffic* **4**, 6–12.
- Du, F., Edwards, K., Shen, Z., Sun, B., De Lozanne, A., Briggs, S. and Firtel, R. A.** (2008). Regulation of contractile vacuole formation and activity in Dictyostelium. *EMBO J.* **27**, 2064–2076.
- Durek, P., Schmidt, R., Heazlewood, J. L., Jones, A., MacLean, D., Nagel, A., Kersten, B. and Schulze, W. X.** (2009). PhosPhAt: The *Arabidopsis thaliana* phosphorylation site database. An update. *Nucleic Acids Res.* **38**, 828–834.

- Fabian, M. R., Frank, F., Rouya, C., Siddiqui, N., Lai, W. S., Karetnikov, A., Blackshear, P. J., Nagar, B. and Sonenberg, N.** (2013). Structural basis for the recruitment of the human CCR4-NOT deadenylase complex by tristetraprolin. *Nat. Struct. Mol. Biol.* **20**, 735-739.
- Fausser, F., Schimi, S. and Puchta, H.** (2014). Both CRISPR/Cas-based nucleases and nickases can be used efficiently for genome engineering in *Arabidopsis thaliana*. *Plant J.* **79**, 348–359.
- Feys, B. J., Wiermer, M., Bhat, R. A., Moisan, L. J., Medina-Escobar, N., Neu, C., Cabral, A. and Parker, J. E.** (2005). Arabidopsis SENESCENCE-ASSOCIATED GENE101 stabilizes and signals within an ENHANCED DISEASE SUSCEPTIBILITY1 complex in plant innate immunity. *Plant Cell* **17**, 2601–2613.
- Fields, S. and Song, O. K.** (1989). A novel genetic system to detect protein-protein interactions. *Nature* **340**, 245–246.
- Flowers, T. J., Galal, H. K. and Bromham, L.** (2010). Evolution of halophytes: Multiple origins of salt tolerance in land plants. *Funct. Plant Biol.* **37**, 604–612.
- Folkers, U., Berger, J. and Hülskamp, M.** (1997). Cell morphogenesis of trichomes in Arabidopsis: Differential control of primary and secondary branching by branch initiation regulators and cell growth. *Development* **124**, 3779–3786.
- Frerigmann, H. and Gigolashvili, T.** (2014). MYB34, MYB51, and MYB122 distinctly regulate indolic glucosinolate biosynthesis in *Arabidopsis thaliana*. *Mol. Plant* **7**, 814–828.
- Frerigmann, H., Piślewska-Bednarek, M., Sánchez-Vallet, A., Molina, A., Glawischnig, E., Gigolashvili, T. and Bednarek, P.** (2016). Regulation of Pathogen-Triggered Tryptophan Metabolism in *Arabidopsis thaliana* by MYB Transcription Factors and Indole Glucosinolate Conversion Products. *Mol. Plant* **9**, 682–695.
- Fujisawa, M., Hayashi, K., Nishio, T., Bando, T., Okada, S., Yamato, K. T., Fukuzawa, H. and Ohyania, K.** (2001). Isolation of X and Y chromosome-specific DNA markers from a liverwort, *Marchantia polymorpha*, by representational difference analysis. *Genetics* **159**, 981–985.
- Fujita, H., Umezaki, Y., Imamura, K., Ishikawa, D., Uchimura, S., Nara, A., Yoshimori, T., Hayashizaki, Y., Kawai, J., Ishidoh, K., et al.** (2004). Mammalian class E Vps proteins, SBP1 and mVps2/CHMP2A, interact with and regulate the function of an AAA-ATPase SKD1/Vps4B. *J. Cell Sci.* **117**, 2997–3009.
- Fujita, H., Yamanaka, M., Imamura, K., Tanaka, Y., Nara, A., Yoshimori, T., Yokota, S. and Himeno, M.** (2003). A dominant negative form of the AAA ATPase SKD1/VPS4 impairs membrane trafficking out of endosomal/lysosomal compartments: Class E vps phenotype in mammalian cells. *J. Cell Sci.* **116**, 401–414.
- Fukao, A., Mishima, Y., Takizawa, N., Oka, S., Imataka, H., Pelletier, J., Sonenberg, N., Thoma, C. and Fujiwara, T.** (2014). MicroRNAs trigger dissociation of eIF4A1 and eIF4AII from target mRNAs in humans. *Mol. Cell* **56**, 79–89.
- Furuya, T., Hattori, K., Kimori, Y., Ishida, S., Nishihama, R., Kohchi, T. and Tsukaya, H.** (2018). ANGUSTIFOLIA contributes to the regulation of three-dimensional morphogenesis in the liverwort *Marchantia polymorpha*. *Dev.* **145**, 1–10.
- Gao, C., Zhuang, X., Shen, J. and Jiang, L.** (2017). Plant ESCRT Complexes: Moving Beyond Endosomal Sorting. *Trends Plant Sci.* **22**, 986–998.
- García-Mauriño, S. M., Rivero-Rodríguez, F., Velázquez-Cruz, A., Hernández-Vellisca, M., Díaz-Quintana, A., De la Rosa, M. A. and Díaz-Moreno, I.** (2017). RNA binding protein regulation and cross-talk in the control of AU-rich mRNA Fate. *Front. Mol. Biosci.* **4**, 1–9.
- Gaullier, J.-M., Simonsen, A., D'Arrigo, A., Bremnes, B. and Stenmark, H.** (1998). FYVE finger proteins as effectors of phosphatidylinositol 3-phosphate. *Chem. Phys. Lipids* **98**, 87-94.
- Gerald, N. J., Siano, M. and De Lozanne, A.** (2002). The Dictyostelium LvsA protein is localized on the contractile vacuole and is required for osmoregulation. *Traffic* **3**, 50–60.
- Gilks, N., Kedersha, N., Ayodele, M., Shen, L., Stoecklin, G., Dember, L. M. and Anderson, P.** (2004). Stress granule assembly is mediated by prion-like aggregation of TIA-1. *Mol. Biol. Cell.* **15**, 5383-5398.
- Ghosh, D. and Seydoux, G.** (2008). Inhibition of transcription by the *Caenorhabditis elegans* germline protein PIE-1: Genetic evidence for distinct mechanisms targeting initiation and elongation. *Genetics* **178**, 235-243.
- Gonzalez, N., Vanhaeren, H. and Inzé, D.** (2012). Leaf size control: Complex coordination of cell division and expansion. *Trends Plant Sci.* **17**, 332–340.

- Haas, T. J., Sliwinski, M. K., Martínez, D. E., Preuss, M., Ebine, K., Ueda, T., Nielsen, E., Odorizzi, G. and Otegui, M. S.** (2007). The Arabidopsis AAA ATPase SKD1 is involved in multivesicular endosome function and interacts with its positive regulator LYST-INTERACTING PROTEIN5. *Plant Cell* **19**, 1295–1312.
- Han, G., Wang, M., Yuan, F. and Sui, N.** (2014). The CCCH zinc finger protein gene AtZFP1 improves salt resistance in *Arabidopsis thaliana*. *Plant Mol. Biol.* **86**, 237–253.
- Han, J. W., Zheng, H. F., Cui, Y., Sun, L. D., Ye, D. Q., Hu, Z., Xu, J. H., Cai, Z. M., Huang, W., Zhao, G. P., et al.** (2009). Genome-wide association study in a Chinese Han population identifies nine new susceptibility loci for systemic lupus erythematosus. *Nat. Genet.* **41**, 1234–1237.
- Hanahan, D.** (1983). Studies on transformation of *Escherichia coli* with plasmids. *J. Mol. Biol.* **166**, 557–580.
- Hartley, J. L., Temple, G. F. and Brasch, M. A.** (2000). DNA Cloning Using In Vitro Site-Specific Recombination *Genome Research* **10**, 1788–1795.
- Henne, W. M., Buchkovich, N. J. and Emr, S. D.** (2011). The ESCRT Pathway. *Dev. Cell* **21**, 77–91.
- Hentze, M. W., Castello, A., Schwarzl, T. and Preiss, T.** (2018). A brave new world of RNA-binding proteins. *Nat. Rev. Mol. Cell Biol.* **19**, 327–341.
- Honkanen, S.** (2015). Genetic basis of rhizoid development in the liverwort *Marchantia polymorpha* (Dissertation, University of Oxford).
- Honkanen, S., Jones, V. A. S., Morieri, G., Champion, C., Hetherington, A. J., Kelly, S., Proust, H., Saint-Marcoux, D., Prescott, H. and Dolan, L.** (2016). The Mechanism Forming the Cell Surface of Tip-Growing Rooting Cells Is Conserved among Land Plants. *Curr. Biol.* **26**, 3238–3244.
- Horvathova, I., Voigt, F., Kotrys, A. V., Zhan, Y., Artus-Revel, C. G., Eglinger, J., Stadler, M. B., Giorgetti, L. and Chao, J. A.** (2017). The Dynamics of mRNA Turnover Revealed by Single-Molecule Imaging in Single Cells. *Mol. Cell* **68**, 615–625.
- Houseley, J. and Tollervey, D.** (2009). Review The Many Pathways of RNA Degradation. *Cell* **136**, 763–776.
- Hoyle, N. P., Castelli, L. M., Campbell, S. G., Holmes, L. E. A. and Ashe, M. P.** (2007). Stress-dependent relocalization of translationally primed mRNPs to cytoplasmic granules that are kinetically and spatially distinct from P-bodies. *J. Cell Biol.* **179**, 65–74.
- Huang, P., Ju, H. W., Min, J. H., Zhang, X., Chung, J. S., Cheong, H. S. and Kim, C. S.** (2012). Molecular and physiological characterization of the *Arabidopsis thaliana* oxidation-related zinc finger 2, a plasma membrane protein involved in ABA and salt stress response through the ABI2-mediated signaling pathway. *Plant Cell Physiol.* **53**, 193–203.
- Hudson, B. P., Martinez-Yamout, M. A., Dyson, H. J. and Wright, P. E.** (2004). Recognition of the mRNA AU-rich element by the zinc finger domain of TIS11d. *Nat. Struct. Mol. Biol.* **11**, 257–264.
- Hülkamp, M., Misra, S., and Jürgens, G.** (1994). Genetic dissection of trichome cell development in Arabidopsis. *Cell* **76**, 555–566.
- Hurley, J. H. and Hanson, P. I.** (2010). Membrane budding and scission by the ESCRT machinery: It's all in the neck. *Nat. Rev. Mol. Cell Biol.* **11**, 556–566.
- Hurley, J.H.** (2010). The ESCRT Complexes. *Crit. Rev. Biochem. Mol. Biol.* **45**, 463–487.
- Intergovernmental Panel on Climate Change** (2014). *IPCC, 2014: Climate Change 2014: Synthesis Report.*
- Iqbal, M. B., Johns, M., Cao, J., Liu, Y., Yu, S. C., Hyde, G. D., Laffan, M. A., Marchese, F. P., Cho, S. H., Clark, A. R., et al.** (2014). PARP-14 combines with tristetruprolin in the selective posttranscriptional control of macrophage tissue factor expression. *Blood* **124**, 3646–3655.
- Isayenkov, S. V. and Maathuis, F. J. M.** (2019). Plant salinity stress: Many unanswered questions remain. *Front. Plant Sci.* **10**, 80.
- Ishizaki, K., Chiyoda, S., Yamato, K. T. and Kohchi, T.** (2008). Agrobacterium-mediated transformation of the haploid liverwort *Marchantia polymorpha* L., an emerging model for plant biology. *Plant Cell Physiol.* **49**, 1084–1091.
- Ishizaki, K., Johzuka-Hisatomi, Y., Ishida, S., Iida, S. and Kohchi, T.** (2013). Homologous recombination-mediated gene targeting in the liverwort *Marchantia polymorpha* L. *Sci. Rep.* **3**, 1–6.

- Ishizaki, K., Nishihama, R., Ueda, M., Inoue, K., Ishida, S., Nishimura, Y., Shikanai, T. and Kohchi, T. (2015). Development of gateway binary vector series with four different selection markers for the liverwort *Marchantia polymorpha*. *PLOS ONE* **10**, 1–13.
- Ishizaki, K., Nishihama, R., Yamato, K. T. and Kohchi, T. (2016). Molecular genetic tools and techniques for *Marchantia polymorpha* research. *Plant Cell Physiol.* **57**, 262–270.
- James, P., Halladay, J. and Craig, E. A. (2002). Genomic Libraries and a Host Strain Designed for Highly Efficient Two-Hybrid Selection in Yeast. *Genetics* **144**, 1425–1436.
- Jang, J.-C. (2016). Arginine-rich motif-tandem CCCH zinc finger proteins in plant stress responses and post-transcriptional regulation of gene expression. *Plant Sci.* **252**, 118–124.
- Jansen, R. P. (2001). mRNA localization: Message on the move. *Nat. Rev. Mol. Cell Biol.* **2**, 247–256.
- Jogl, G., Shen, Y., Gebauer, D., Li, J., Wiegmann, K., Kashkar, H., Krönke, M. and Tong, L. (2002). Crystal structure of the BEACH domain reveals an unusual fold and extensive association with a novel PH domain. *EMBO J.* **21**, 4785–4795.
- Johnson, B. A., Stehn, J. R., Yaffe, M. B. and Keith Blackwell, T. (2002). Cytoplasmic localization of tristetraprolin involves 14-3-3-dependent and -independent mechanisms. *J. Biol. Chem.* **277**, 18029–18036.
- Johnson, C. M., Stout, P. R., Broyer, T. C. and Carlton, A. B. (1957). Comparative chlorine requirements of different plant species. *Plant Soil* **8**, 337–353.
- Julkowska, M. M. and Testerink, C. (2015). Tuning plant signaling and growth to survive salt. *Trends Plant Sci.* **20**, 586–594.
- Kamran, M., Parveen, A., Ahmar, S., Malik, Z., Hussain, S., Chattha, M. S., Saleem, M. H., Adil, M., Heidari, P. and Chen, J. T. (2020). An overview of hazardous impacts of soil salinity in crops, tolerance mechanisms, and amelioration through selenium supplementation. *Int. J. Mol. Sci.* **21**, 1–27.
- Kanazawa, M., Ikeda, Y., Nishihama, R., Yamaoka, S., Lee, N. H., Yamato, K. T., Kohchi, T. and Hirayama, T. (2020). Regulation of the poly(A) status of mitochondrial mRNA by poly(A)-specific ribonuclease is conserved among land plants. *Plant Cell Physiol.* **61**, 470–480.
- Kanchiswamy, C. N., Takahashi, H., Quadro, S., Maffei, M. E., Bossi, S., Berthea, C., Zebelo, S. A., Muroi, A., Ishihama, N., Yoshioka, H., et al. (2010). Regulation of Arabidopsis defense responses against *Spodoptera littoralis* by CPK-mediated calcium signaling. *BMC Plant Biol.* **10**, 97.
- Kaplan, J., Domenico, I. D. and McVey Ward, D. (2008). Chediak-Higashi syndrome. *Curr. Opin. Hematol.* **15**, 22–29.
- Katzmann, D. J., Stefan, C. J., Babst, M. and Emr, S. D. (2003). Vps27 recruits ESCRT machinery to endosomes during MVB sorting. *J. Cell Biol.* **162**, 413–423.
- Kawa, D. and Testerink, C. (2017). Regulation of mRNA decay in plant responses to salt and osmotic stress. *Cell. Mol. Life Sci.* **74**, 1165–1176.
- Kedersha, N., Cho, M. R., Li, W., Yacono, P. W., Chen, S., Gilks, N., Golan, D. E. and Anderson, P. (2000). Dynamic shuttling of TIA-1 accompanies the recruitment of mRNA to mammalian stress granules. *J. Cell Biol.* **151**, 1257–1268.
- Kedersha, N., Gupta, M., Li, W., Miller, I. and Anderson, P. (1999) RNA-binding Proteins TIA-1 and TIAR Link the Phosphorylation of eIF-2a to the Assembly of Mammalian Stress Granules. *J. Cell Biol.* **147**, 1431–1441.
- Kedersha, N., Stoecklin, G., Ayodele, M., Yacono, P., Lykke-Andersen, J., Fitzler, M. J., Scheuner, D., Kaufman, R. J., Golan, D. E. and Anderson, P. (2005). Stress granules and processing bodies are dynamically linked sites of mRNP remodeling. *J. Cell Biol.* **169**, 871–884.
- Khong, A., Matheny, T., Jain, S., Mitchell, S. F., Wheeler, J. R. and Parker, R. (2017). The Stress Granule Transcriptome Reveals Principles of mRNA Accumulation in Stress Granules. *Mol. Cell* **68**, 808–820.e5.
- Kilian, J., Whitehead, D., Horak, J., Wanke, D., Weinl, S., Batistic, O., D'Angelo, C., Bornberg-Bauer, E., Kudla, J. and Harter, K. (2007). The AtGenExpress global stress expression data set: Protocols, evaluation and model data analysis of UV-B light, drought and cold stress responses. *Plant J.* **50**, 347–363.

- Kim, J. S., Jung, H. J., Lee, H. J., Kim, K. A., Goh, C. H., Woo, Y., Oh, S. H., Han, Y. S. and Kang, H.** (2008). Glycine-rich RNA-binding protein7 affects abiotic stress responses by regulating stomata opening and closing in *Arabidopsis thaliana*. *Plant J.* **55**, 455–466.
- Kim, W., Kim, J., Ko, J., Kang, H., Kim, J. and Han, K.** (2014). AtC3H14, a plant-specific tandem CCCH zinc-finger protein, binds to its target mRNAs in a sequence-specific manner and affects cell elongation in *Arabidopsis thaliana*. *Plant J.* **80**, 772–784.
- Kleinboelting, N., Huel, G., Kloetgen, A., Viehoveer, P. and Weisshaar, B.** (2012). GABI-Kat Simple Search: New features of the *Arabidopsis thaliana* T-DNA mutant database. *Nucleic Acids Res.* **40**, 1211–1215.
- Kloppfleisch, K., Phan, N., Augustin, K., Bayne, R. S., Booker, K. S., Botella, J. R., Carpita, N. C., Carr, T., Chen, J. G., Cooke, T. R., et al.** (2011). Arabidopsis G-protein interactome reveals connections to cell wall carbohydrates and morphogenesis. *Mol. Syst. Biol.* **7**, 1–7.
- Koba, M., and Konopa, J.** (2005). Actinomycin D and its mechanisms of action. *Postepy Hig Med Dosw.* **59**, 290-298.
- Koch, M. A., Kiefer, C., Ehrich, D., Vogel, J., Brochmann, C. and Mummenhoff, K.** (2006). Three times out of Asia Minor: The phylogeography of *Arabis alpina* L. (Brassicaceae). *Mol. Ecol.* **15**, 825–839.
- Koguchi, M., Yamasaki, K., Hirano, T. and Sato, M. H.** (2017). Vascular plant one-zinc-finger protein 2 is localized both to the nucleus and stress granules under heat stress in *Arabidopsis*. *Plant Signal. Behav.* **3**, e1295907.
- Koncz, C., Martini, N., Mayerhofer, R., Koncz-Kalman, Z., Körber, H., Redei, G. P. and Schell, J.** (1989). High-frequency T-DNA-mediated gene tagging in plants. *Proc. Natl. Acad. Sci. U. S. A.* **86**, 8467–8471.
- Korbei, B., Moulinier-Anzola, J., De-Araujo, L., Lucyshyn, D., Retzer, K., Khan, M. A. and Luschnig, C.** (2013). Arabidopsis TOL proteins act as gatekeepers for vacuolar sorting of PIN2 plasma membrane protein. *Curr. Biol.* **23**, 2500-2505.
- Köster, T., Meyer, K., Weinholdt, C., Smith, L. M., Lummer, M., Speth, C., Grosse, I., Weigel, D. and Staiger, D.** (2014). Regulation of pri-miRNA processing by the hnRNP-like protein AtGRP7 in Arabidopsis. *Nucleic Acids Res.* **42**, 9925-9936.
- Kozak, M.** (1986). Point mutations define a sequence flanking the AUG initiator codon that modulates translation by eukaryotic ribosomes. *Cell* **44**, 283-292.
- Kreps, J. A., Wu, Y., Chang, H. S., Zhu, T., Wang, X. and Harper, J. F.** (2002). Transcriptome changes for Arabidopsis in response to salt, osmotic, and cold stress. *Plant Physiol.* **130**, 2129-2141.
- Kubota, A., Ishizaki, K., Hosaka, M. and Kohchi, T.** (2013). Efficient Agrobacterium-mediated transformation of the liverwort *Marchantia polymorpha* using regenerating thalli. *Biosci. Biotechnol. Biochem.* **77**, 167–172.
- Kwak, E., Gerald, N., Larochelle, D. A., Vithalani, K. K., Niswonger, M. L., Maready, M. and De Lozanne, A.** (1999). LvsA, a protein related to the mouse beige protein, is required for cytokinesis in Dictyostelium. *Mol. Biol. Cell* **10**, 4429-4439.
- Lagnado, C. A., Brown, C. Y. and Goodall, G. J.** (1994). AUUUA is not sufficient to promote poly(A) shortening and degradation of an mRNA: the functional sequence within AU-rich elements may be UUAUUUA(U/A)(U/A). *Mol. Cell. Biol.* **14**, 7984-7995.
- Lai, W. S., Carballo, E., Thorn, J. M., Kennington, E. A. and Blackshear, P. J.** (2000). Interactions of CCCH zinc finger proteins with mRNA. Binding of tristetraprolin-related zinc finger proteins to AU-rich elements and destabilization of mRNA. *J. Biol. Chem.* **275**, 17827-17837.
- Laity, J. H., Lee, B. M. and Wright, P. E.** (2001). Zinc finger proteins: new insights into structural and functional diversity. *Curr. Opin. Struct. Biol.* **11**, 39-46.
- Lamaoui, M., Jemo, M., Datla, R. and Bekkaoui, F.** (2018). Heat and drought stresses in crops and approaches for their mitigation. *Front. Chem.* **6**, 1-14.
- Landy, A.** (1989). Dynamic, structural, and regulatory aspects of λ site-specific recombination. *Annual Review of Biochemistry* **58**, 913-941
- Lau, N. C., Kolkman, A., van Schaik, F. M. A., Mulder, K. W., Pijnappel, W. W. P., Heck, A. J. R. and Timmers, H. T. M.** (2009). Human Ccr4-Not complexes contain variable deadenylase subunits. *Biochem. J.* **422**, 443-453.

- Layat, E., Probst, A. V. and Tourmente, S.** (2013). Structure, function and regulation of Transcription Factor IIIA: From *Xenopus* to *Arabidopsis*. *Biochim. Biophys. Acta - Gene Regul. Mech.* **1829**, 274-282.
- Lee, S. J. and Michel, S. L.** (2014). Structural metal sites in nonclassical zinc finger proteins involved in transcriptional and translational regulation. *Acc. Chem. Res.* **47**, 2643-2650.
- Lee, C. Y. and Seydoux, G.** (2019). Dynamics of mRNA entry into stress granules. *Nat. Cell Biol.* **21**, 116-117.
- Lee, S. J., Jung, H. J., Kang, H. and Kim, S. Y.** (2012). *Arabidopsis* zinc finger proteins AtC3H49/AtTZF3 and AtC3H20/AtTZF2 are involved in ABA and JA responses. *Plant Cell Physiol.* **53**, 673-686.
- Lee, S. Y., Boon, N. J., Webb, A. A. R. and Tanaka, R. J.** (2016). Synergistic activation of RD29A via integration of salinity stress and abscisic acid in *Arabidopsis thaliana*. *Plant Cell Physiol.* **57**, 2147-2160.
- Lemmom, M. A.** (1999). Structural basis for high-affinity phosphoinositide binding by pleckstrin homology domains. *Biochem. Soc. Trans.* **27**, 617-624.
- Leppek, K., Das, R. and Barna, M.** (2018). Functional 5' UTR mRNA structures in eukaryotic translation regulation and how to find them. *Nat. Rev. Mol. Cell Biol.* **19**, 158-174.
- Li, B., Wang, Y., Zhang, Y., Tian, W., Chong, K., Jang, J. C. and Wang, L.** (2019). PRR5, 7 and 9 positively modulate TOR signaling-mediated root cell proliferation by repressing TANDEM ZINC FINGER 1 in *Arabidopsis*. *Nucleic Acids Res.* **47**, 5001-5015.
- Li, Z. and Thomas, T. L.** (1998). PE11, an embryo-specific zinc finger protein gene required for heart-stage embryo formation in *Arabidopsis*. *Plant Cell* **10**, 383-98.
- Liang, W., Li, C., Liu, F., Jiang, H., Li, S., Sun, J., Wu, X. and Li, C.** (2009). The *Arabidopsis* homologs of CCR4-associated factor 1 show mRNA deadenylation activity and play a role in plant defence responses. *Cell Res.* **19**, 307-316.
- Lin, P. C., Pomeranz, M. C., Jikumaru, Y., Kang, S. G., Hah, C., Fujioka, S., Kamiya, Y. and Jang, J. C.** (2011). The *Arabidopsis* tandem zinc finger protein AtTZF1 affects ABA- and GA-mediated growth, stress and gene expression responses. *Plant J.* **65**, 253-268.
- Lin, Y., May, G. E., Kready, H., Nazzaro, L., Mao, M., Spealman, P., Creeger, Y. and McManus, J. C.** (2019). Impacts of uORF codon identity and position on translation regulation. *Nucleic Acids Res.* **47**, 9358-9367.
- Lin, Y., Protter, D. S. W., Rosen, M. K. and Parker, R.** (2015). Formation and Maturation of Phase-Separated Liquid Droplets by RNA-Binding Proteins. *Mol. Cell* **60**, 208-219.
- Livak, K. J. and Schmittgen, T. D.** (2001). Analysis of relative gene expression data using real-time quantitative PCR and the 2- $\Delta\Delta$ CT method. *Methods* **25**, 402-408.
- Lopez-Herrera, G., Tampella, G., Pan-Hammarström, Q., Herholz, P., Trujillo-Vargas, C. M., Phadwal, K., Simon, A. K., Moutschen, M., Etzioni, A., Mory, A., et al.** (2012). Deleterious mutations in LRBA are associated with a syndrome of immune deficiency and autoimmunity. *Am. J. Hum. Genet.* **90**, 986-1001.
- Lykke-Andersen, J. and Wagner, E.** (2005). Recruitment and activation of mRNA decay enzymes by two ARE-mediated decay activation domains in the proteins TTP and BRF-1. *Genes Dev.* **19**, 351-361.
- Mahtani, K. R., Mahtani, K. R., Brook, M., Brook, M., Dean, J. L., Dean, J. L., Sully, G., Sully, G., Saklatvala, J., Saklatvala, J., et al.** (2001). Mitogen-activated protein kinase p38 controls the expression and posttranslational modification of tristetraprolin, a regulator of tumor necrosis factor alpha mRNA stability. *Mol. Cell Biol.* **21**, 6461-9.
- Maldonado-Bonilla, L. D.** (2014). Composition and function of P bodies in *Arabidopsis thaliana*. *Front. Plant Sci.* **5**, 1-11.
- Maronedze, C., Thomas, L., Serrano, N. L., Lilley, K. S. and Gehring, C.** (2016). The RNA-binding protein repertoire of *Arabidopsis thaliana*. *Sci. Rep.* **6**, 1-13.
- Mazumder, R., Iyer, L. M., Vasudevan, S. and Aravind, L.** (2002). Detection of novel members, structure-function analysis and evolutionary classification of the 2H phosphoesterase superfamily. *Nucleic Acids Res.* **30**, 5229-5243.
- McVey Ward, D., Griffiths, G. M., Stinchcombe, J. C. and Kaplan, J.** (2000). Analysis of the lysosomal storage disease Chediak-Higashi syndrome. *Traffic* **1**, 816-822.
- Melaragno, J. E., Mehrotra, B. and Coleman, A. W.** (1993). Relationship between endopolyploidy and cell size in epidermal tissue of *Arabidopsis*. *Plant Cell* **5**, 1661-1668.

- Merchante, C., Brumos, J., Yun, J., Hu, Q., Spencer, K. R., Enríquez, P., Binder, B. M., Heber, S., Stepanova, A. N. and Alonso, J. M.** (2015). Gene-Specific Translation Regulation Mediated by the Hormone-Signaling Molecule EIN2. *Cell* **163**, 684–697.
- Merret, R., Carpenier, M.-C., Favory, J.-J., Picart, C., Descombin, J., Bousquet-Antonelli, C., Tillard, P., Lejay, L., Deragon, J.-M. and Charny, Y.** (2017). Heat-shock protein HSP101 affects the release of ribosomal protein mRNAs for recovery after heat shock. *Plant Physiol.* **174**, 1216–1225.
- Mignone, F., Gissi, C., Liuni, S. and Pesole, G.** (2002). Untranslated regions of mRNAs. *Genome Biol.* **3**, 1–10.
- Miller, J., McLachlan, A. D. and Klug, A.** (1985). Repetitive zinc-binding domains in the protein transcription factor IIIA from *Xenopus* oocytes. *EMBO J.* **4**, 1609–1614.
- Minamino, N., Kanazawa, T., Era, A., Ebine, K., Nakano, A. and Ueda, T.** (2018). RAB GTPases in the Basal Land Plant *Marchantia polymorpha*. *Plant Cell Physiol.* **59**, 845–856.
- Mishiba, K. I., Nagashima, Y., Suzukia, E., Hayashi, N., Ogata, Y., Shimada, Y. and Koizumi, N.** (2013). Defects in IRE1 enhance cell death and fail to degrade mRNAs encoding secretory pathway proteins in the Arabidopsis unfolded protein response. *Proc. Natl. Acad. Sci. U. S. A.* **110**, 5713–5718.
- Mishler, B.D. and Churchill, S.P.** (1984). A cladistic approach to the phylogeny of the bryophytes. *Brittonia* **36**: 406–424.
- Mollet, S., Cougot, N., Wilczynska, A., Dautry, F., Kress, M., Bertrand, E. and Weil, D.** (2008). Translationally repressed mRNA transiently cycles through stress granules during stress. *Mol. Biol. Cell.* **19**, 4469–4479.
- Moon, S. L., Morisaki, T., Khong, A., Lyon, K., Parker, R. and Stasevich, T. J.** (2019). Multicolour single-molecule tracking of mRNA interactions with RNP granules. *Nat. Cell Biol.* **21**, 162–168.
- Motomura, K., Le, Q. T. N., Hamada, T., Kutsuna, N., Mano, S., Nishimura, M. and Watanabe, Y.** (2015). Diffuse decapping enzyme DCP2 accumulates in DCP1 foci under heat stress in *Arabidopsis thaliana*. *Plant Cell Physiol.* **56**, 107–115.
- Msanne, J., Lin, J., Stone, J. M. and Awada, T.** (2011). Characterization of abiotic stress-responsive *Arabidopsis thaliana* RD29A and RD29B genes and evaluation of transgenes. *Planta* **234**, 97–107.
- Murashige, T. and Skoog, F.** (1962). A Revised Medium for Rapid Growth and Bio Assays with Tobacco Tissue Cultures. *Physiol. Plant.* **15**, 473–497.
- Murata, T., Hikita, K., Kaneda, N.** (2000). Transcriptional activation function of zinc finger protein TIS11 and its negative regulation by phorbol ester. *Biochem. Biophys. Res. Commun.* **274**, 526–532.
- Nagle, D. L., Karim, M. A., Woolf, E. A., Holmgren, L., Bork, P., Misumi, D. J., Mcgrail, S. H., Barry, J., Perou, C. M., Raymond, E., et al.** (1996). Identification and mutation analysis of the complete gene for Chediak-Higashi syndrome. *Nature Genetics* **14**, 307–311.
- Narsai, R., Howell, K. A., Millar, A. H., O’Toole, N., Small, I. and Whelan, J.** (2007). Genome-wide analysis of mRNA decay rates and their determinants in *Arabidopsis thaliana*. *Plant Cell* **19**, 3418–3436.
- Németh, K., Salchert, K., Putnoky, P., Bhalerao, R., Koncz-Kálmán, Z., Stankovic-Stangeland, B., Bakó, L., Mathur, J., Ökrész, L., Stabel, S., et al.** (1998). Pleiotropic control of glucose and hormone responses by PRL1, a nuclear WD protein, in *Arabidopsis*. *Genes Dev.* **12**, 3059–3073.
- Nguyen, C. C., Nakaminami, K., Matsui, A., Kobayashi, S., Kurihara, Y., Toyooka, K., Tanaka, M. and Seki, M.** (2016). Oligouridylate Binding Protein 1b Plays an Integral Role in Plant Heat Stress Tolerance. *Front. Plant Sci.* **7**, 853.
- Nover, L., Scharf, K. D. and Neumann, D.** (1983). Formation of cytoplasmic heat shock granules in tomato cell cultures and leaves. *Mol. Cell. Biol.* **3**, 1648–1655.
- Okada, S., Fujisawa, M., Sone, T., Nakayama, S., Nishiyama, R., Takenaka, M., Yamaoka, S., Sakaida, M., Kono, K., Takahama, M., et al.** (2000). Construction of male and female PAC genomic libraries suitable for identification of Y-chromosome-specific clones from the liverwort, *Marchantia polymorpha*. *Plant J.* **24**, 421–428.
- Ono, K., Ohyama, K., & Gamborg, O. L.** (1979). Regeneration of the liverwort *Marchantia polymorpha* L. from protoplasts isolated from cell suspension culture. *Plant Science Letters* **14**, 225–229.
- Otsuka, H., Fukao, A., Funakami, Y., Duncan, K. E. and Fujiwara, T.** (2019). Emerging evidence of translational control by AU-rich element-binding proteins. *Front. Genet.* **10**, 1–10.

- Parker, R. and Song, H.** (2004). The enzymes and control of eukaryotic mRNA turnover. *Nat. Struct. Mol. Biol.* **11**, 121–127.
- Pfaffl, M. W., Tichopad, A., Prgomet, C. and Neuvians, T. P.** (2004). Determination of stable housekeeping genes, differentially regulated target genes and sample integrity: BestKeeper - Excel-based tool using pair-wise correlations. *Biotechnol. Lett.* **26**, 509–515.
- Pierik, R. and Testerink, C.** (2014). The Art of Being Flexible: How to Escape from Shade, Salt, and Drought. *Plant Physiol.* **166**, 5–22.
- Pomeranz, M. C., Hah, C., Lin, P., Kang, S. G., Finer, J. J., Blackshear, P. J. and Jang, J.** (2010a). The Arabidopsis Tandem Zinc Finger Protein AtTZF1 Traffics between the Nucleus and Cytoplasmic Foci and binds both DNA and RNA. *Plant Physiol.* **152**, 151–165.
- Pomeranz, M. C., Lin, P., Finer, J. and Jang, J.** (2010b). AtTZF gene family localizes to cytoplasmic foci. *Plant Signaling & Behavior.* **5:2**, 190-192.
- Pomeranz, M. C., Zhang, L., Finer, J. J., Jang, J.C.** (2011). Can AtTZF1 act as a transcriptional activator or repressor in plants? *Plant Signal. Behav.* **6**, 719-722.
- Popovitchenko, T., Thompson, K., Viljetic, B., Jiao, X., Kontonyiannis, D. L., Kiledjian, M., Hart, R. P. and Rasin, M. R.** (2016). The RNA binding protein HuR determines the differential translation of autism-associated FoxP subfamily members in the developing neocortex. *Sci. Rep.* **6**, 1–9.
- Protter, D. S. W. and Parker, R.** (2016). Principles and Properties of Stress Granules. *Trends Cell Biol.* **26**, 668–679.
- Qiu, Y. L., Li, L., Wang, B., Chen, Z., Knoop, V., Groth-Maloney, M., Dombrowska, O., Lee, J., Kent, L., Rest, J., et al.** (2006). The deepest divergences in land plants inferred from phylogenomic evidence. *Proc. Natl. Acad. Sci. U. S. A.* **103**, 15511–15516.
- Qu, J., Kang, S. G., Wang, W., Musier-Forsyth, K. and Jang, J. C.** (2014). The *Arabidopsis thaliana* tandem zinc finger 1 (AtTZF1) protein in RNA binding and decay. *Plant J.* **78**, 452-467.
- Raymond, C. K., Howald-Stevenson, I., Vater, C. A. and Stevens, T. H.** (1992). Morphological classification of the yeast vacuolar protein sorting mutants: Evidence for a prevacuolar compartment in class E vps mutants. *Mol. Biol. Cell* **3**, 1389–1402.
- Reddy, V. S., Ali, G. S. and Reddy, A. S. N.** (2002). Genes encoding calmodulin-binding proteins in the Arabidopsis genome. *J. Biol. Chem.* **277**, 9840–9852.
- Reverdatto, S. V., Dutko, J. A., Chekanova, J. A., Hamilton, D. A. and Belostotsky, D. A.** (2004). mRNA deadenylation by PARN is essential for embryogenesis in higher plants. *RNA* **10**, 1200–1214.
- Rigby, W. F. C., Roy, K., Collins, J., Rigby, S., Connolly, J. E., Bloch, D. B. and Brooks, S. A.** (2005). Structure/Function Analysis of Tristetraprolin (TTP): p38 Stress-Activated Protein Kinase and Lipopolysaccharide Stimulation Do Not Alter TTP Function. *J. Immunol.* **174**, 7883–7893.
- Rotman, B. and Papermaster, B. W.** (1966). Membrane properties of living mammalian cells as studied by enzymatic hydrolysis of fluorogenic esters. *Proc. Natl. Acad. Sci. USA* **55**, 134–141.
- Rozen, F., Edery, I., Meerovitch, K., Dever, T. E., Merrick, W. C. and Sonenberg, N.** (1990). Bidirectional RNA helicase activity of eucaryotic translation initiation factors 4A and 4F. *Mol. Cell. Biol.* **10**, 1134–1144.
- Saedler, R., Jakoby, M., Marin, B., Galiana-Jaime, E. and Hülskamp, M.** (2009). The cell morphogenesis gene SPIRRIG in Arabidopsis encodes a WD / BEACH domain protein. *Plant J.* **59**: 612-621.
- Saint-Marcoux, D., Proust, H., Dolan, L. and Langdale, J. A.** (2015). Identification of reference genes for real-time quantitative PCR experiments in the liverwort *Marchantia polymorpha*. *PLOS ONE* **10**, 1-14.
- Sandler, H., Kreth, J., Timmers, H. T. and Stoecklin, G.** (2011). Not1 mediates recruitment of the deadenylase Caf1 to mRNAs targeted for degradation by tristetraprolin. *Nucleic Acids Res.* **39**, 4373-4386.
- Sanduja, S., Blanco, F. F. and Dixon, D. A.** (2011). The roles of TTP and BRF proteins in regulated mRNA decay. *Wiley Interdiscip. Rev. RNA.* **2**, 42-57.
- Scarpin, M. R., Sigaut, L., Temprana, S. G., Boccaccio, G. L., Pietrasanta, L. I. and Muschietti, J. P.** (2017). Two Arabidopsis late pollen transcripts are detected in cytoplasmic granules. *Plant Direct* **00**, 1-10.

- Schimi, S., Fauser, F. and Puchta, H.** (2016). CRISPR/Cas-Mediated Site-Specific Mutagenesis in *Arabidopsis thaliana* Using Cas9 Nucleases and Paired Nickases Chromosome and Genomic Engineering in Plants. *Methods and Protocols, Methods in Molecular Biology* **1469**.
- Schmidt, O. and Teis, D.** (2012). The ESCRT machinery. *Curr. Biol.* **22**, 116–120.
- Schnittger, A., and Hülskamp, M.** (2007). Whole-Mount DAPI Staining and Measurement of DNA Content in Plant Cells. *CSH Protoc.* pdb, prot4684.
- Schönberger, J., Hammes, U. Z. and Dresselhaus, T.** (2012). In vivo visualization of RNA in plants cells using the Δ N 22 system and a GATEWAY-compatible vector series for candidate RNAs. *Plant J.* **71**, 173–181.
- Sedlyarov, V., Fallmann, J., Ebner, F., Huemer, J., Sneezum, L., Ivin, M., Kreiner, K., Tanzer, A., Vogl, C., Hofacker, I., and Kovarik, P.** (2016) Tristetraprolin binding site atlas in the macrophage transcriptome reveals a switch for inflammation resolution. *Mol Syst Biol.* **12**, 868.
- Shen, L., Liang, Z., Gu, X., Chen, Y., Teo, Z. W. N., Hou, X., Cai, W. M., Dedon, P. C., Liu, L. and Yu, H.** (2016). N6-Methyladenosine RNA Modification Regulates Shoot Stem Cell Fate in Arabidopsis. *Dev. Cell* **38**, 186–200.
- Sheth, U. and Parker, R.** (2003). Decapping and decay of messenger RNA occur in cytoplasmic processing bodies. *Science* **300**, 805–808.
- Shi, H., Xiong, L., Stevenson, B., Lu, T. and Zhu, J.** (2002). The Arabidopsis *salt overly sensitive 4* Mutants Uncover a Critical Role for Vitamin B6 in Plant Salt Tolerance. *Plant Cell* **14**, 575–588.
- Shimamura, M.** (2016). *Marchantia polymorpha*: Taxonomy, phylogeny and morphology of a model system. *Plant Cell Physiol.* **57**, 230–256.
- Sidrauski, C., McGeachy, A. M., Ingolia, N. T. and Walter, P.** (2015). The small molecule ISRIB reverses the effects of eIF2 α phosphorylation on translation and stress granule assembly. *eLife* **4**, 1–16.
- Sim, J., Osborne, K. A., Argudo García, I., Matysik, A. S. and Kraut, R.** (2019). The BEACH Domain Is Critical for Blue Cheese Function in a Spatial and Epistatic Autophagy Hierarchy. *Front. Cell Dev. Biol.* **7**.
- Simonsen, A., Birkeland, H. C. G., Gillooly, D. J., Mizushima, N., Kuma, A., Yoshimori, T., Slagsvold, T., Brech, A. and Stenmark, H.** (2004). Alfy, a novel FYVE-domain-containing protein associated with protein granules and autophagic membranes. *J. Cell Sci.* **117**, 4239–4251.
- Sobell, H. M.** (1985). Actinomycin and DNA transcription. *Proc. Natl. Acad. Sci. USA* **82**, 5328–5331.
- Sorenson, R. and Bailey-Serres, J.** (2014). Selective mRNA sequestration by OLIGOURIDYLATEBINDING PROTEIN 1 contributes to translational control during hypoxia in Arabidopsis. *Proc. Natl. Acad. Sci. USA* **111**, 2373–2378.
- Srivastava, A. K., Lu, Y., Zinta, G. Lang, Z. and Zhu, J.-K.** (2018). UTR dependent control of gene expression in plants. *Trends Plant. Sci.* **23**, 248–259.
- Steffens, A.** (2014). Molecular Characterization of the BEACH Domain Containing Protein SPIRRIG in *Arabidopsis thaliana* (Dissertation, University of Cologne).
- Steffens, A., Bräutigam, A., Jakoby, M. and Hülskamp, M.** (2015). The BEACH Domain Protein SPIRRIG Is Essential for Arabidopsis Salt Stress Tolerance and Functions as a Regulator of Transcript Stabilization and Localization. *PLOS Biol.* **13**, e1002188.
- Steffens, A., Jakoby, M. and Hülskamp, M.** (2017). Physical, Functional and Genetic Interactions between the Beach Domain Protein SPIRRIG and LIP5 and SKD1 and its Role in Endosomal Trafficking to the Vacuole in Arabidopsis. *Front. Plant Sci.* **8**, 1–13.
- Stephan, L.** (2018). Cell morphogenesis in Brassicaceae: Analysis of myosin functions and the BEACH domain protein SPIRRIG (Dissertation, University of Cologne).
- Stephan, L., Jakoby, M. and Hülskamp, M.** (2021). Evolutionary comparison of the developmental/physiological phenotype and the molecular behavior of SPIRRIG between *Arabidopsis thaliana* and *Arabis alpina*. *Front. Plant Sci.* **11**, 596065.
- Stephan, L., Tilmes, V. and Hülskamp, M.** (2019). Selection and validation of reference genes for quantitative Real-Time PCR in *Arabis alpina*. *PLOS ONE* **14**, 1–13.

- Stirnemann, C. U., Petsalaki, E., Russell, R. B. and Müller, C. W.** (2010). WD40 proteins propel cellular networks. *Trends Biochem. Sci.* **35**, 565–574.
- Stoecklin, G., Mayo, T. and Anderson, P.** (2006). ARE-mRNA degradation requires the 5' - 3' decay pathway. *EMBO Rep.* **7**, 72–77.
- Stoecklin, G., Stubbs, T., Kedersha, N., Wax, S., Rigby, W. F. C., Blackwell, T. K. and Anderson, P.** (2004). MK2-induced tristetraprolin:14-3-3 Complexes prevent stress granule association and ARE-mRNA decay. *EMBO J.* **23**, 1313–1324.
- Stoecklin, G., Tenenbaum, S. A., Mayo, T., Chittur, S. V., George, A. D., Baroni, T. E., Blackshear, P. J. and Anderson, P.** (2008). Genome-wide analysis identifies interleukin-10 mRNA as target of tristetraprolin. *J. Biol. Chem.* **283**, 11689–11699.
- Sugano, S. S., Nishihama, R., Shirakawa, M., Takagi, J., Matsuda, Y., Ishida, S., Shimada, T., Hara-Nishimura, I., Osakabe, K. and Kohchi, T.** (2018). Efficient CRISPR/Cas9-based genome editing and its application to conditional genetic analysis in *Marchantia polymorpha*. *PLOS ONE* **13**, 1–22.
- Sugano, S. S., Shirakawa, M., Takagi, J., Matsuda, Y., Shimada, T., Hara-Nishimura, I. and Kohchi, T.** (2014). CRISPR/Cas9-mediated targeted mutagenesis in the liverwort *Marchantia polymorpha* L. *Plant Cell Physiol.* **55**, 475–481.
- Sun, J., Jiang, H., Xu, Y., Li, H., Wu, X., Xie, Q. and Li, C.** (2007b). The CCCH-Type Zinc Finger Proteins AtSZF1 and AtSZF2 Regulate Salt Stress Responses in Arabidopsis. **48**, 1148–1158.
- Sun, L., Stoecklin, G., Van Way, S., Hinkovska-Galcheva, V., Guo, R. F., Anderson, P. and Shanley, T. P.** (2007a). Tristetraprolin (TTP)-14-3-3 complex formation protects TTP from dephosphorylation by protein phosphatase 2a and stabilizes tumor necrosis factor- α mRNA. *J. Biol. Chem.* **282**, 3766–3777.
- Suzuki, H., Harrison, C. J., Shimamura, M., Kohchi, T. and Nishihama, R.** (2020). Positional cues regulate dorsal organ formation in the liverwort *Marchantia polymorpha*. *J. Plant Res.* **133**, 311–321.
- Suzuki, T., Kikuguchi, C., Sharma, S., Sasaki, T., Tokumasu, M., Adachi, S., Natsume, T., Kanegae, Y. and Yamamoto, T.** (2015). CNOT3 suppression promotes necroptosis by stabilizing mRNAs for cell death-inducing proteins. *Sci. Rep.* **5**, 1–14.
- Tabassum, N., Eschen-Lippold, L., Athmer, B., Baruah, M., Brode, M., Maldonado-Bonilla, L. D., Hoehenwarter, W., Hause, G., Scheel, D. and Lee, J.** (2020). Phosphorylation-dependent control of an RNA granule-localized protein that fine-tunes defence gene expression at a post-transcriptional level. *Plant J.* **101**, 1023–1039.
- Tanaka, H., Suzuki, R., Okabe, N., Suzuki, T. and Kodama, Y.** (2018). Salinity stress-responsive transcription factors in the liverwort *Marchantia polymorpha*. *Plant Biotechnol.* **35**, 281–284.
- Taylor, G. A., Carballo, E., Lee, D. M., Lai, W. S., Thompson, M. J., Patel, D. D., Schenkman, D. I., Gilkeson, G. S., Broxmeyer, H. E., Haynes, B. F., et al.** (1996). A pathogenetic role for TNF α in the syndrome of cachexia, arthritis, and autoimmunity resulting from tristetraprolin (TTP) deficiency. *Immunity* **4**, 445–454.
- Tchen, C. R., Brook, M., Saklatvala, J. and Clark, A. R.** (2004). The stability of tristetraprolin mRNA is regulated by mitogen-activated protein kinase p38 and by tristetraprolin itself. *J. Biol. Chem.* **279**, 32393–32400.
- Tchernev, V. T., Mansfield, T. A., Giot, L., Kumar, A. M., Nandabalan, K., Li, Y., Mishra, V. S., Detter, J. C., Rothberg, J. M., Wallace, M. R., et al.** (2002). The Chediak-Higashi Protein Interacts with SNARE Complex and Signal Transduction Proteins. *Mol. Med.* **8**, 56–64.
- Teh, O. K., Hatsugai, N., Tamura, K., Fuji, K., Tabata, R., Yamaguchi, K., Shingenobu, S., Yamada, M., Hasebe, M., Sawa, S., et al.** (2015). BEACH-domain proteins act together in a cascade to mediate vacuolar protein trafficking and disease resistance in Arabidopsis. *Mol. Plant* **8**, 389–398.
- Tu, Y., Wu, X., Yu, F., Dang, J., Wang, J., Wei, Y., Cai, Z., Zhou, Z., Liao, W., Li, L. and Zhang, Y.** (2019). Tristetraprolin specifically regulates the expression and alternative splicing of immune response genes in HeLa cells. *BMC Immunol.* **20**, 13.
- Tucker, M., Valencia-Sanchez, M. A., Staples, R. R., Chen, J., Denis, C. L. and Parker, R.** (2001). The transcription factor associated Ccr4 and Caf1 proteins are components of the major cytoplasmic mRNA deadenylase in *Saccharomyces cerevisiae*. *Cell* **104**, 377–386.

- Uchida, Y., Chiba, T., Kurimoto, R. and Asahara, H.** (2019). Post-transcriptional regulation of inflammation by RNA-binding proteins via cis-elements of mRNAs. *J. Biochem.* **166**, 375–382.
- Usami, T., Horiguchi, G., Yano, S. and Tsukaya, H.** (2009). The more and smaller cells mutants of *Arabidopsis thaliana* identify novel roles for SQUAMOSA PROMOTER BINDING PROTEIN-LIKE genes in the control of heteroblasty. *Development* **136**, 955–964.
- Vandesompele, J., De Preter, K., Pattyn, F., Poppe, B., Van Roy, N., De Paepe, A., Speleman, F., Åman, P., Semb, H., Powers, D., et al.** (2002). The multifunctional FUS, EWS and TAF15 proto-oncoproteins show cell type-specific expression patterns and involvement in cell spreading and stress response. *Genome Biol.* **3**, research0034.1.
- Vercruyse, J., Baekelandt, A., Gonzalez, N. and Inzé, D.** (2020). Molecular networks regulating cell division during Arabidopsis leaf growth. *J. Exp. Bot.* **71**, 2365–2378.
- Volders, K., Nuytens, K. and W.M. Creemers, J.** (2011). The Autism Candidate Gene Neurobeachin Encodes a Scaffolding Protein Implicated in Membrane Trafficking and Signaling. *Curr. Mol. Med.* **11**, 204–217.
- Walley, J. W., Kelley, D. R., Savchenko, T. and Dehesh, K.** (2010). Investigating the function of CAF1 deadenylases during plant stress responses. *Plant Signal. Behav.* **5**, 802–805.
- Wang, D., Guo, Y., Wu, C., Yang, G., Li, Y. and Zheng, C.** (2008). Genome-wide analysis of CCCH zinc finger family in Arabidopsis and rice. *BMC Genomics* **20**, 1–20.
- Wang, F., Shang, Y., Fan, B., Yu, J. Q. and Chen, Z.** (2014). Arabidopsis LIP5, a Positive Regulator of Multivesicular Body Biogenesis, Is a Critical Target of Pathogen-Responsive MAPK Cascade in Plant Basal Defense. *PLOS Pathog.* **10**.
- Wang, F., Yang, Y., Wang, Z., Zhou, J., Fan, B. and Chen, Z.** (2015). A critical role of Lyst-interacting Protein 5, a positive regulator of multivesicular body biogenesis, in plant responses to heat and salt stresses. *Plant Physiol.* **169**, 497–511.
- Wang, J. W., Gamsby, J. J., Highfill, S. L., Mora, L. B., Bloom, G. C., Yeatman, T. J., Pan, T. C., Ramne, A. L., Chodosh, L. A., Cress, W. D., et al.** (2004). Deregulated expression of LRBA facilitates cancer cell growth. *Oncogene* **23**, 4089–4097.
- Waris, S., Wilce, M. C. J. and Wilce, J. A.** (2014). RNA recognition and stress granule formation by TIA proteins. *Int. J. Mol. Sci.* **15**, 23377–23388.
- Weber, C., Nover, L. and Fauth, M.** (2008). Plant stress granules and mRNA processing bodies are distinct from heat stress granules. *Plant J.* **56**, 517–530.
- Wells, M. L., Perera, L. and Blackshear, P. J.** (2017). An ancient family of RNA-binding proteins: Still important! *Trends Biochem Sci.* **42**, 285–296.
- Westbroek, W., Adams, D., Huizing, M., Koshoffer, A., Dorward, H., Tinloy, B., Parkes, J., Helip-Wooley, A., Kleta, R., Tsilou, E., et al.** (2007). Cellular defects in Chediak-Higashi syndrome correlate with the molecular genotype and clinical phenotype. *J. Invest. Dermatol.* **127**, 2674–2677.
- Westermann, J.** (2018). Unraveling novel and evolutionarily conserved regulators of cell wall integrity signaling in tip-growing plant cells (*Dissertation, University of Cologne*).
- Westermann, J., Koebeke, E., Lentz, R., Hülkamp, M. and Boisson-Dernier, A.** (2020). A comprehensive toolkit for quick and easy visualization of marker proteins, protein-protein interactions and cell morphology in *Marchantia polymorpha*. *Front. Plant Sci.* **11**, 569194.
- Wilkie, G. S., Dickson, K. S. and Gray, N. K.** (2003). Regulation of mRNA translation by 5'- and 3'-UTR-binding factors. *Trends Biochem. Sci.* **28**, 182–188.
- Wolff, H.** (2018). Analysis of heat-induced localization of ESCRTIII core and associated proteins to mRNP granules in *A. thaliana* (*Dissertation, University of Cologne*).
- Wollert, T. and Hurley, J.H.** (2010). Molecular Mechanism of Multivesicular Body Biogenesis by ESCRT Complexes. *Nature* **464**, 864–869.
- Worthington, M. T., Pelo, J. W., Sachedina, M. A., Applegate, J. L., Arseneau, K. O. and Pizarro, T. T.** (2002). RNA binding properties of the AU-rich element-binding recombinant Nup475/TIS11/tristetraprolin protein. *J. Biol. Chem.* **277**, 48558–48564.

- Wortman, J. R., Haas, B. J., Hannick, L. I., Smith, R. K., Maiti, R., Ronning, C. M., Chan, A. P., Yu, C., Ayele, M., Whitelaw, C. A., et al.** (2003). Annotation of the Arabidopsis Genome. *Plant Physiol.* **132**, 461–468.
- Wu, S. J., Ding, L. and Zhu, J. K.** (1996). SOS1, a genetic locus essential for salt tolerance and potassium acquisition. *Plant Cell* **8**, 617–627.
- Wu, W. I., Yajnik, J., Siano, M. and De Lozanne, A.** (2004). Structure-function analysis of the BEACH protein LvsA. *Traffic* **5**, 346–355.
- Xu, J. and Chua, N. H.** (2009). Arabidopsis DECAPPING 5 is required for mRNA decapping, P-body formation, and translational repression during postembryonic development. *Plant Cell* **21**, 3270–3279.
- Xu, J. and Chua, N. H.** (2012). Dehydration stress activates Arabidopsis MPK6 to signal DCP1 phosphorylation. *EMBO J.* **31**, 1975–1984.
- Xu, J., Yang, J. Y., Niu, Q. W. and Chua, N. H.** (2006). Arabidopsis DCP2, DCP1, and VARICOSE form a decapping complex required for postembryonic development. *Plant Cell* **18**, 3386–3398.
- Yamasaki, S.** (2018). Recent advances in the role of RNA-binding protein, tristetraprolin, in arthritis. *Immunol. Med.* **41**, 98–102.
- Yanagisawa, M., Zhang, C. and Szymanski, D. B.** (2013). ARP2/3-dependent growth in the plant kingdom: SCARs for life. *Front. Plant Sci.* **4**, 1–12.
- Yang, Y. and Guo, Y.** (2018). Unraveling salt stress signaling in plants. *J. Integr. Plant Biol.* **60**, 796–804.
- Zhang, H., Deng, X., Miki, D., Cutler, S., La, H., Hou, Y. J., Oh, J. E. and Zhu, J. K.** (2012). Sulfamethazine suppresses epigenetic silencing in Arabidopsis by impairing folate synthesis. *Plant Cell* **24**, 1230–1241.
- Zhang, S., Zeng, Y., Yi, X. and Zhang, Y.** (2016). Selection of suitable reference genes for quantitative RT-PCR normalization in the halophyte *Halostachys caspica* under salt and drought stress. *Sci. Rep.* **6**, 30363.
- Zheng, D., Chen, C. Y. A. and Shyu, A. Bin** (2011). Unraveling regulation and new components of human P-bodies through a protein interaction framework and experimental validation. *RNA* **17**, 1619–1634.
- Zhu, J.** (2000). Update on Stress Signaling Genetic Analysis of Plant Salt Tolerance Using Arabidopsis. *Society* **124**, 941–948.
- Zhu, J. K.** (2002). Salt and drought stress signal transduction in plants. *Annual Review of Plant Biology* **53**, 247-273.
- Zhu, M., Kuechler, E. R., Zhang, J., Matalon, O., Dubreuil, B., Hofmann, A., Loewen, C., Levy, E. D., Gsponer, J. and Mayor, T.** (2020). Proteomic analysis reveals the direct recruitment of intrinsically disordered regions to stress granules in *S. cerevisiae*. *J. Cell. Sci.* **133**, jcs244657.

7 ACKNOWLEDGEMENTS

First and foremost, I would like to thank my supervisor **Prof. Dr. Martin Hülskamp** for allowing me to work on my doctoral thesis and to pursue not only one, but two different, highly interesting, projects in his lab. Thank you for your perpetual encouragement, motivation and lots of ideas and discussions, especially in times of a challenging project that was marked by several ups and downs.

I cordially thank **Prof. Dr. Ute Höcker** and **Prof. Dr. Siegfried Roth** for agreeing to be part of my examination committee.

I thank **Prof. Dr. Liam Dolan** (University of Oxford) for provision of the *Marchantia spirrig* mutant line.

I am very grateful to **Dr. Marc Jakoby**. Discussions with you, and your continuous great ideas during the whole time have helped me a lot and advanced my projects in content and practice. Moreover, thank you for critically proof-reading this manuscript. Working with you not only is a pleasure from a scientific point of view - daily jokes and interesting conversations contribute a lot to that.

A huge 'thank you' goes out to **Dr. Lisa Stephan**. You are always there for me - not only with lots of scientific advice and help. I am grateful for having a blast with you during back to back lab work, talking about anything and everything, and laughing a lot. Not least, I thank you for critically proof-reading this manuscript.

I thank **Dr. Alexandra Steffens**, who did all preceding experiments that paved the way for my TZF studies and provided lots of material.

A great thanks goes out to my 'Marchantia community': **Dr. Aurélien Boisson-Dernier**, **Dr. Jens Westermann** and **Roswitha Lentz**. Jens and Roswitha, your help regarding theoretical and experimental issues concerning Marchantia was not only enormously helpful in learning to work with a new model organism, but is continuously supporting me in the daily work on my project. Aurélien and Jens, thank you for your initiative and awesome ideas: working together on a manuscript has been a pleasure and was very motivating.

Dr. Markus Stetter, thank you for collaborating with us on an RNAseq experiment and your work on the data analysis. I am very much looking forward to further discussions.

Thank you, **Jessica Pietsch**. I am happy that we are able to experience our whole PhD time together. Thank you for always 'having an open ear' - it is awesome to have you as an office member. Thanks a lot for your accuracy in reading this manuscript and all the help that you provided during the whole time.

Dr. Heike Wolff, as my former direct office neighbor, you made 'onboarding' to AG Hülskamp easy in scientific but also private manners. I enjoyed lots of deep conversations, as well as joking around with you.

Hanna Bechtel, thank you for taking over lab work for me during your time as a student helper. I am happy to have you as a fellow PhD student and lab member now. I would not want to have missed all our scientific as well as non-scientific conversations during lab work together.

Thank you, dear **ABC(D) Club: Lisa, Jessi, Hanna and Barbara**. I love our fun times in the lab, office and kitchen, or Corona-induced digital meetings from home. I could not have imagined my PhD time without you all.

Thank you **Sabine, Roswitha, Birgit, Irene, Uschi, Bastian** and **all former and present members of the AG Hülskamp**. I highly appreciate your exceptional helpfulness, reliability and positivity. I currently miss our ever so entertaining and funny lunches in the kitchen a lot!

Thank you **Mori, Mimi, my family** and **friends**.

8 DECLARATION OF ACADEMIC INTEGRITY

Ich versichere, dass ich die von mir vorgelegte Dissertation selbständig angefertigt, die benutzten Quellen und Hilfsmittel vollständig angegeben und die Stellen der Arbeit – einschließlich Tabellen, Karten und Abbildungen –, die anderen Werken im Wortlaut oder dem Sinn nach entnommen sind, in jedem Einzelfall als Entlehnung kenntlich gemacht habe; dass diese Dissertation noch keiner anderen Fakultät oder Universität zur Prüfung vorgelegen hat; dass sie – abgesehen von unten angegebenen Teilpublikationen – noch nicht veröffentlicht worden ist, sowie, dass ich eine solche Veröffentlichung vor Abschluss des Promotionsverfahrens nicht vornehmen werde. Die Bestimmungen der Promotionsordnung sind mir bekannt. Die von mir vorgelegte Dissertation ist von Prof. Dr. Martin Hülskamp betreut worden.

Teilpublikationen:

A comprehensive toolkit for quick and easy visualization of marker proteins, protein-protein interactions and cell morphology in Marchantia polymorpha

Westermann, Jens*, Koebke, Eva*, Lentz, Roswitha, Hülskamp, Martin, Boisson-Dernier, Aurélien

*The authors contributed equally.

2020, Frontiers in Plant Science 11, 569194, <https://doi.org/10.3389/fpls.2020.569194>

Köln, den

Eva Koebke